BULLETIN OF THE EARTHQUAKE RESEARCH INSTITUTE,
UNIVERSITY OF TOKYO. Vol. 37, Part 3. September, 1959.

東京大學
地震研究所彙報

第 37 號　第 3 冊

昭和 34 年 9 月

目　次

論文及報告

頁

26. 最大振巾と震央距離との関係について
—実験式の波動論的考察—(英文) ..... 吉山良一 389
27. 地球核内の熱電磁流体振動（英文） ..... 力武常次 405
28. 20° 不連続と電気的性質（英文） ..... 力武常次 423
29. 諏訪湖周辺の火山岩類の古地磁気学的および地質学的研究
—中部地方における鮮新世火山岩の古地磁気学的研究 (2)—(英文) .. 百瀬寛一・小林国夫・山田哲雄 433
30. 多くの観測点の資料に基づく脈動の研究（その二）
—脈動源に関する前推論への再検討—(英文) ..... 三東哲夫 483
31. 第 2 回鉾田爆破地震動の観測（英文） ..... 爆破地震動研究グループ 495
32. 第 2 回鉾田爆破観測から得られた地殻構造について（英文） ..... 松沢武雄・松本利松・浅野周三 509
33. 地震計用トランジスター前置増幅器(邦文) ..... 松本英照 525
34. 1959 年 1 月 31 日北海道弟子屈地震の余震観測報告（邦文） ..... 松本利松 531

(The titles in occidental languages are given on the back cover.)

地震研究所彙報は，年4回定期に（ただし，第1号より第6号までは不定期に，第7号は3冊として刊行された），彙報別冊は不定期に刊行される．

この彙報に載せられた論文及び報告についての責任は，すべてその著者のみにある．

この彙報についての照会通信は，すべて東京大学地震研究所長にあてられたい．

The Bulletin is published quarterly. (Vols. 1–6 were published at irregular intervals and Vol. 7 consisted of three parts.)
Supplementary Volume is published at irregular interval.

The authors of the papers alone are responsible for the statements and opinions contained in their respective papers.

All communications relating to this Bulletin should be addressed to the Director of the Earthquake Research Institute, University of Tokyo, Japan.

Earthquake Research Institute, University of Tokyo
Address:
No. 1, Motofuji-cho, Bunkyo-ku
Tokyo Metropolis, Japan.
Telephone: 92-3161-Extension 6506
Cable address: ZISINKEN, TOKYO.

東京大学地震研究所
所在地
東京都文京区本富士町一番地
電話 小石川 92—3161 (代) 構内 6506
電略 ブンケウ トウダイ ヂシン

BULLETIN OF THE EARTHQUAKE
RESEARCH INSTITUTE
Vol. 37 (1959), pp. 389-404

26. *Maximum Amplitude and Epicentral Distance. —Proposed a Theoretical Elucidation of Empirical Formulas and Some Development.—*

By Ryoichi YOSHIYAMA,

Earthquake Research Institute.

(Read March 25, 1958; Oct. 29, 1958; April 28, 1959;
May 26, 1959.—Received June 30, 1959.)

1. Introduction and some remarks.

Various empirical formulas of the maximum amplitude of an earthquake wave as a function of the epicentral distance are presented by many authors, but a generally accepted one has not yet been found. Difficult points in these studies originate clearly in the fact that the seismograph is not sufficiently completed for the analysis of earthquake waves with complicated feature. Moreover, something has been left unstudied to give to these various formulas a lucid elucidation by the well known theory of wave attenuation: and, in this paper, this point is studied. This is, in short, a new, but perhaps already tacitly understood in general, interpretation of the "observations of maximum amplitude." The writer assumes therein that the observations give the amplitude of the maximum component of the spectrum of what is recorded in the seismogram, whereas the seismogram itself shows the resultant of waves of various period and phase differences. Therefore, it is to be noted that the above stated interpretation does not refer to the "maximum amplitude" itself, but to the "observations or measurements of maximum amplitude," obtained by a certain process.

From the seismometrical stand point, it seems to the writer such an interpretation should have already been accepted as a matter of course, at least in the first approximation, because, after a manual of seismometry published from the Central Meteorological Observatory of Japan, maximum amplitude (A) and its period (T) are measured, either smoothing out the higher harmonics, or picking up a short period oscillation on which is superposed long period and small amplitude oscillation, and a half of total amplitude is measured without reference to the zero line: this method of observation is clearly a rough spectral analysis.

And it is to be pointed out also that, even though the "maximum amplitude" in the seismogram is corrected by the response curve of the seismograph to get a corresponding "displacement amplitude," it is doubtful if it is a true maximum displacement amplitude, because the maximum amplitude is assigned in the seismogram previous to the correction. So that the results of study of the "maximum amplitude" versus epicentral distances based on such observations are naturally affected by the characteristics of the seismograph; practically, if we emphasize the "maximum," the maximum amplitude "A" in the results of study in some cases naturally stands none the less, for example, for the "maximum acceleration amplitude" according to the characteristics of the seismograph, in spite of the procedure to get a displacement amplitude by the response curve of the seismograph. The question as to which interpretation of the two or any other is more suitable will be utterly determined by the characteristics of the seismograph. And, in some cases, the procedure of the correction by the response curve after the "rough spectral analysis" on the seismogram, generally adopted as it is, gives but an ambiguous quantity in the study of the "maximum amplitude" vs. "epicentral distances" relation.

2. Some discussions of various formulas.

Various expressions of the empirical formula of $A \sim \Delta$ relation hitherto presented[1] are classified as follows;

$$\log A = a - m \log \Delta \,, \tag{1}$$

$$\log A = a - m \log \Delta - k\Delta \,, \tag{2}$$

$$\log A = a - m \log \Delta - f(T)\Delta \,, \tag{3}$$

(A: obs. of max. amplitude, Δ: epicentral distance)

where a, m and k are certain constants, m and k being positive, T period of waves of the "maximum amplitude" concerned. Of the three the first, being free from any theoretical foresight, perhaps appears most empirical-formula-like, and is adopted by Richter, by Tsuboi and later by several authors in Japan. Richter in his studies of earthquakes in America obtained $m=3$, whereas Tsuboi $m=1.73$ based on the observations of earthquakes in Japan after a careful computation. As shown later, according to the writer's interpretation of the "observations of maximum amplitude," the difference of the m-value by the two authors

1) C. TSUBOI, "On the Magnitudes of Earthquakes." (*Reviews*), *Zisin* **10** (1957), 6-23.

is caused by the different response of the seismographs used in the two countries.

As to the expression of (2), the latest results of Kawasumi's studies of 80 earthquakes in Japan are as follows:

$$m=1/2, \quad k=0.00305\,\mathrm{km}^{-1}, \quad 100\,\mathrm{km}<\Delta<750\,\mathrm{km},$$
$$m=1/2, \quad k=0.00183\,\mathrm{km}^{-1}, \quad 750\,\mathrm{km}<\Delta<2000\,\mathrm{km}.$$

In his earliest paper of the seismic intensity, if "A" represents "maximum acceleration," m is as large as 2.3, while $k=0.002\,\mathrm{km}^{-1}$. Each of these results by the two authors is based on the observations of many earthquakes in Japan extending over many years. So that the understanding seems reasonable that these formulas respectively give us the observations of some, if not general, earthquakes in Japan, though there are some different opinions against it and also against the procedure by which these formulas were derived, and though even Tsuboi himself seems to acknowledge little significance in the functional form of his formula, perhaps because there was no practical method to presume the most probable function for the empirical formula.

The expression (3), $n=1/2$ for surface wave and $n=1$ for bodily wave, is familiar in the theory of wave attenuation, and was used by Wadati and later by the present writer in a theoretical calculation, in which the period of the "maximum amplitude" is presumed to be fixed by the magnitude of the earthquake and constant for all epicentral distance. As regards the study of the writer, statistical computation to deduce any empirical formula was not a project of his. The results of study of those presumptions are not yet conclusive in Japan, chiefly because, according to an informal opinion of several authors, of a response defect of the seismograph. Since the results are closely related to the present study, observations of the period vs. Δ are illustrated in this paper concerning several remarkable earthquakes in Japan.

According to Tsuboi, differences between the two values of "A" computed by the two formulas, one by Tsuboi himself and the other by Kawasumi, are practically negligible considering the accuracy of observations. It is true, and what is worse, we have so far scarcely any theoretical reason or method to assign *a priori* a certain function to the empirical formula. But the study of those differences will give some means to solve these ambiguous circumstances; some means to find out the most reasonable expression of the empirical formula for the improvement of the theory of earthquake waves in future. The writer, therefore, first tries to reveal the differences among the formulas by pure mathematics,

and, at the same time, presents the observations of several destructive earthquakes in Japan for an illustration of his procedure of mathematical treatment and, also, for an examination of those formulas.

3. Mathematical study of the empirical formulas already presented.

So far as $\log A \sim \Delta$ relation is concerned, the difference between those various formulas derived from (1) or (2) may be apparently indistinct, because, as regards both of the expressions (1) and (2), not only $\log A$ but also $\partial \log A/\partial \Delta$ are decreasing functions of Δ. However, $\log \Delta^n A \sim \Delta$ relation, when n is sufficiently large, is quite different. So long as n is small and $n<m$, $\log \Delta^n A$ remains a decreasing function of Δ, but if $n>m$ and $k \neq 0$, $\log \Delta^n A$ has a maximum value at a certain epicentral distance, Δ_m. And the epicentral distance Δ_m increases with the assigned value of n. If $k=0$, i.e. the empirical formula is expressed by (1), used by Tsuboi and Richter, $\log \Delta^n A$ is always monotonous for any value of n, or constant particularly when $n=m$; ever decreasing when $n<m$, and ever increasing when $n>m$. Mathematically speaking, it follows that

$$\Delta_m = \frac{n-m}{k}, \quad \frac{\partial \Delta_m}{\partial n} = \frac{1}{k}. \qquad (4)$$

By these formulas, the most probable

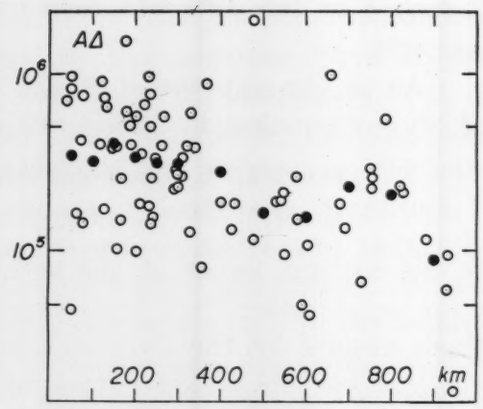

Fig. 1. $\log \Delta A \sim \Delta$ relation of the Shizuoka earthquake.

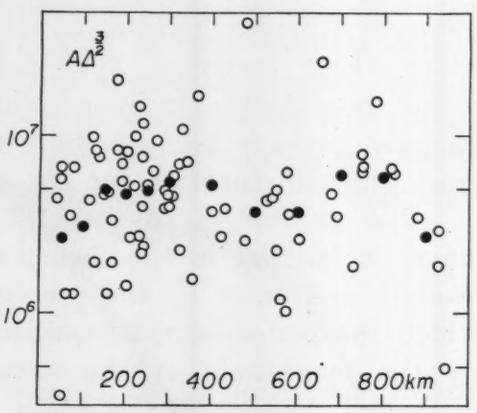

Fig. 2. $\log \Delta^{3/2} A \sim \Delta$ relation of the Shizuoka earthquake.

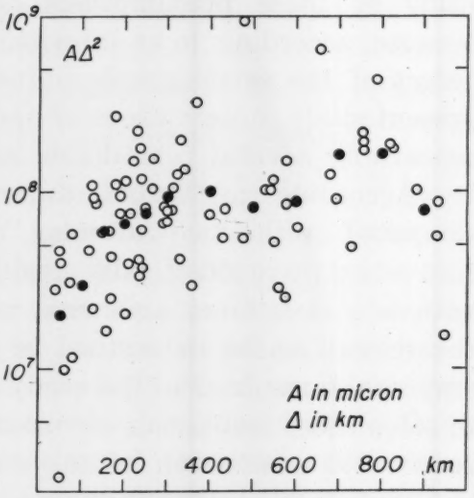

Fig. 3. $\log \Delta^2 A \sim \Delta$ relation of the Shizuoka earthquake.

value of m and k, when the expression (2) is adopted, will be computed graphically from the observations, though as yet in the present accuracy of observation the practical location of Δ_m is difficult for a large value of n, since as Δ increases the accuracy of observations of A and therefore $\log \Delta^n A$ falls. Propriety of an empirical formula to the observations of an earthquakes is also examined closely by these formulas: in the case of Kawasumi's formula, Δ_m is 163 km, 326 km and 488 km when n is equal to 1, 3/2 and 2 respectively. And, in the following, examples are computed with the observations of some destructive earthquakes in Japan.

Figs. 1–3 are the relation of $\log \Delta^n A$ vs. Δ of the Shizuoka earthquake in 1935, putting $n=1$, 3/2 and 2 respectively. Logarithmic mean for every 50 km or for 100 km are given by filled-up circles in each figures. Perhaps, without an objection, nothing conclusive will be obtained from these mean values, because the observations are extremely dispersive. However, for the range of epicentral distance less than 600 km or so, a maximum is likely near the distance expected from Kawasumi's formula in each of those figures. Therefore, in this case, Kawasumi's formula is probably appropriate; at least $n<1.5$ is reasonable for the most probable empirical formula, rejecting Tsuboi's, because we can see clearly a maximum already in Fig. 2 of $\log \Delta^{3/2} A$ vs. Δ.

Table 1.

Earthquake	Date (J.S.T.)	Epicentre	M
1. North-Izu	Nov. 26, 1930	35.1 N 139.0 E	7.0
2. Saitama	Sept. 21, 1931	36.1 N 139.2 E	7.0
3. Shizuoka	July 11, 1935	35.1 N 138.4 E	6.3
4. Kawachi-Yamato	Feb. 21, 1936	34.5 N 135.7 E	6.4
5. Shionomisaki	April 18, 1948	33.1 N 135.6 E	7.2
6. Fukui	June 28, 1948	36.1 N 136.2 E	7.3
7. Imaichi	Dec. 26, 1949	36.7 N 139.7 E	6.7

From Seism. Bull. J. M. A. Suppl. Vol. (1958).

Observations of six more earthquakes in Table 1 are taken up: mean maximum amplitudes (A_m) are calculated for every 50 km ($\Delta \leq 300$ km) or for every 100 km ($\Delta \geq 400$ km): and, in Figs. 4–6, $\log \Delta^n A_m$ are illustrated together with the two curves, K—K and T—T expected respectively from Kawasumi's and Tsuboi's formulas, ordinates of which are arbitrary and to be determined according to the magnitude of each earthquake. As regards the Imaichi earthquake, two shocks occured only about eight minutes apart: maximum amplitude of the second shock (A_2) is estimated

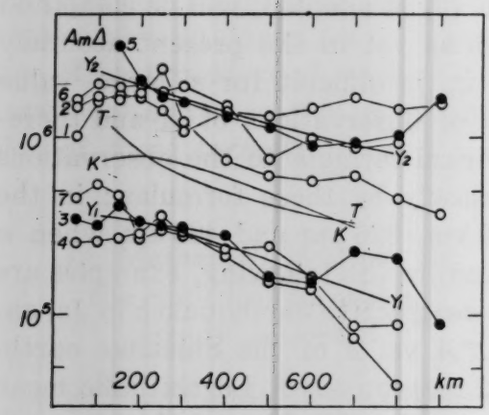

Fig. 4. Mean $\log \Delta A \sim \Delta$ relation of seven earthquakes in the table.

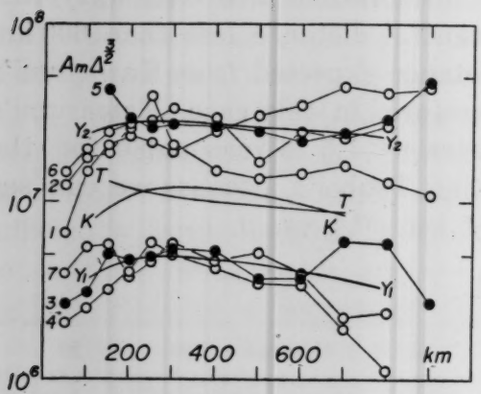

Fig. 5. Mean $\log \Delta^{3/2} A \sim \Delta$ relation of seven earthquakes in the table.

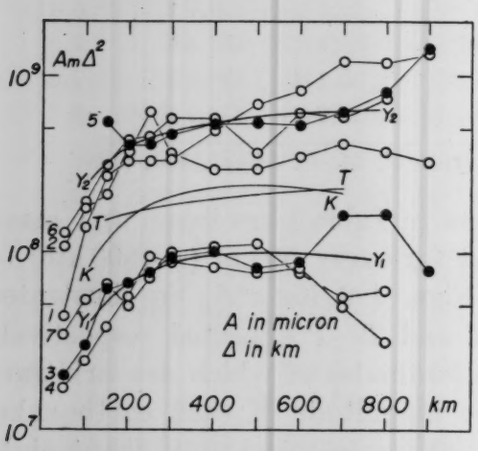

Fig. 6. Mean $\log \Delta^2 A \sim \Delta$ relation of seven earthquakes in the table.

everywhere as large as 1.3 times that of the first one (A_1) by a correlation diagram: to reduce the observational error, mean maximum amplitudes (A) of the two shocks are calculated by $\log A = (1/2)[\log A_1 + \log (A_1 \times 1.3)]$ and are used for the maximum amplitudes of the "Imaichi earthquake."

To discuss the propriety of each formula for these earthquakes is not the main subject of study in this paper; it is sufficient to see that in some cases Kawasumi's formula is applicable and in other cases Tsuboi's or some others: and expression of the formula by a function different from those already given seems necessary, too. Characteristic aspect of $A \sim \Delta$ relation of each earthquake will come out still more clearly in future observations of high accuracy: then it must be one of the important problems to distinguish among those formulas the most appropriate expression for each earthquake by the method above studied.

In the following, an idea is first presented to deduce those various formulas from a presumed fundamental law of wave attenuation on a certain assumption, the appropriateness of which will be examined by observations in future. Though, in the course of the studies, it will be evident that it does not matter if the presumed fundamental law above stated is any particular one or not the classical one is adopted,

for the present, to explain the idea as concretely as possible.

4. Fundamental assumptions and illustration of the procedure.

The assumptions were made in three respects as follows:

1) Earthquake waves are built up by a superposition of monochromatic waves of amplitude A_i and period T_i. Theoretically the period T_i remains constant on the way of propagation of the wave. In some cases the spectrum may be of course continuous and unbounded. However, the idea is explained for simplicity by waves of several line spectrum.

2) Amplitude A_i of the monochromatic wave decays with Δ according to the above said fundamental law of wave attenuation, and it is assumed, as can readily be understood theoretically,

$$A_i=\frac{B_i(T_i)}{\Delta^{n_0}}\exp\{-f(T_i)\Delta\}\ . \qquad (5)$$

By the well-known classical theory, $n_0=1$ for bodily wave or $n_0=1/2$ for surface wave, and $f(T)\propto 1/T^2$. If the last postulate is not the case, $f(T)$ will be at least a function such that $f(T_1)>f(T_2)$ when $T_1<T_2$. Now, it makes no difference in our discussion whether the above said amplitude stands for displacement or acceleration or something else, if it is only used for a definite one throughout the studies. And we can neglect the effect of the characteristics of the seismograph in our discussion for the present, because the response curve of the seismograph in general is flat over a considerable range of the period of wave at least for some one among the displacement, the velocity and the acceleration. If not, it will be of no consequence as to the point of the discussion: it is only hoped to simplify the mathematical expression at present. Then the amplitude, $\boldsymbol{A}$, in the seismogram will be expressed as a function of time and epicentral distance as follows:

$$\boldsymbol{A}(t,\Delta)=\sum_i \boldsymbol{A}_i\ ,\quad \boldsymbol{A}_i=A_i\sin\left\{\frac{2\pi}{T_i}\left(\frac{\Delta}{V_i}-t\right)+\varepsilon_i\right\}\ , \qquad (6)$$

where t is time coordinate, ε_i phase angle, T_i ($i=1, 2, 3, \cdots$ and $T_1<T_2<T_3<\cdots$) period of the component wave, and V_i velocity of propagation, possibly a function of T; A_i is given by (5) and $B_i(T_i)$ is determined from the spectrum of the earthquake wave at its origin.

It is quite natural to consider that the maximum amplitude in the seismogram at some station where $\Delta=\Delta_0$ is given by the maximum of

$\boldsymbol{A}(t, \Delta_0)$. However, since $\boldsymbol{A}$ is affected by the phase angle ε_i, functional form of $f(T)$ and $V(T)$, we can never expect a simple relation between the maximum of $\boldsymbol{A}$ and Δ.

3) The third assumption is that A, the "observations of the maximum amplitude" is not the maximum of $\boldsymbol{A}$, but is equal to the amplitude, A_i, of one of component waves which is the largest at $\Delta=\Delta_0$. Practically, the observations are not the results of a complete harmonic analysis; the wave whose period and amplitude are measured in the seismogram apparently as a monochromatic wave is in some cases composed of many monochromatic waves. Therefore, in a future study of higher accuracy than that in this paper, an application of a theory of propagation of a wave packet will be necessary, too. From the theoretical standpoint, it is desirable that the observations would be given by the results of a complete harmonic analysis to avoid an ambiguity in the course of reasoning.

Then the $A\sim\Delta$ relation, especially when $\log \Delta^{n_0}A\sim\Delta$ relation is considered, is much simplified as follows: $\log \Delta^{n_0}A_i\sim\Delta$ relation is linear, its gradient $\partial \log \Delta^{n_0}A_i/\partial\Delta=-f(T_i)$, and magnitude of $\log \Delta^{n_0}A_i$ at $\Delta=0$ is equal to $\log B_i$. In the diagram to show the $\log \Delta^{n_0}A\sim\Delta$ relation, we have first straight lines, which give $\log \Delta^{n_0}A_i\sim\Delta$ relation, as many as the number of A_i. And then by the third assumption, we can trace the curve of $\log \Delta^{n_0}A\sim\Delta$ relation from those straight lines; it is, in some cases, a bent line built up by several segments of these lines; the bent line tends to a smooth curve of envelope when the spectrum of the earthquake wave is continuous; it is, in some other cases, built up by a few segments. An example is illustrated in Figs. 7–9 when the number of A_i is only three, A_1, A_2 and A_3, explaining none the less satisfactorily the important point of the process of the reasoning. The relative position of the three lines, A_1, A_2 and A_3, depends on the relative magnitude of B_1 B_2 and B_3; the slope of the lines are $f(T_1)$, $f(T_2)$ and $f(T_3)$, where $T_1<T_2<T_3$ and therefore $f(T_1)>f(T_2)>f(T_3)$.

If $B_1<B_2<B_3$, the three lines A_1, A_2 and A_3 will be such as shown in Fig. 7, and then by the third assumption the $\log \Delta^{n_0}A\sim\Delta$ relation is clearly given by the A_3-line itself. When B_1 is largest and B_2 is almost equal to B_3, the lines will be such as shown in Fig. 8, and the relation will be given by the two segments of the two lines, A_1 and A_3, i.e. by PQR. When $B_1>B_2>B_3$, the relation will be given by the three segments of the three lines, A_1, A_2 and A_3, as shown in Fig. 9 by $PQRS$.

Perhaps we can easily associate Fig. 7 with Kawasumi's formula, and Fig. 8 or 9 with Tsuboi's or with Richter's. Moreover, it is to be noted that $|\partial \boldsymbol{A}_i/\partial t|=2\pi|\boldsymbol{A}_i|/T_i$. So that, even if the $\log \Delta^{n_0}A \sim \Delta$ relation of an earthquake is such as shown in Fig. 7 when it is observed by displacement seismograph, the same relation may be such as shown in Fig. 8 or 9 when it is observed by velocity seismograph or acceleration seismograph. Of course, the different appearance of the $A \sim \Delta$ relation when the seismographs used are different is originally quite natural, but, to give a reasonable explanation of a presumed remarkable difference, the third assumption here mentioned will be most effective. And from the difference of the characteristics of the seismographs used in two countries, it seems quite natural that Richter's formula was obtained on the observations in America, and Tsuboi's on those in Japan. Another important point is that $B_i(T_i)$, spectrum of the earthquake wave at its origin, is estimated by extending back the segments of each line, A_1, A_2, A_3, observable in Fig. 9, to the ordinate axis $\Delta=0$. We can not estimate B_2 and B_3 from the $\log \Delta^{n_0}A \sim \Delta$ relation such as shown in Fig. 7, because two lines A_2 and A_3 are not observable there. And in some cases, the estimation of all B_i is possible only when the $\log \Delta^{n_0}A \sim \Delta$ relation such as shown in Fig. 9 is obtained by the observation with seismograph which records velocity or acceleration or still higher time-derivatives of the displacement.

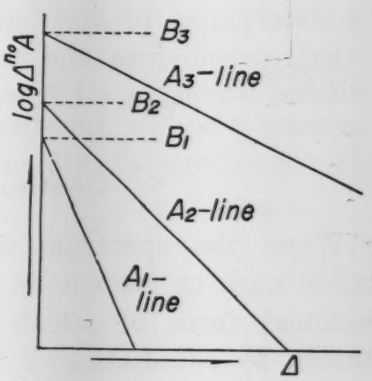

Fig. 7.

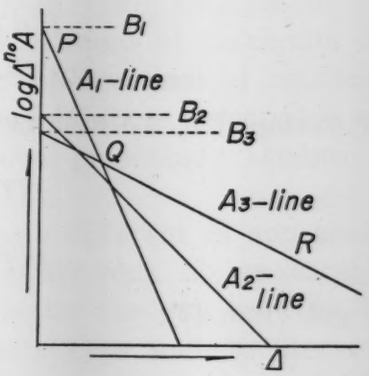

Fig. 8.

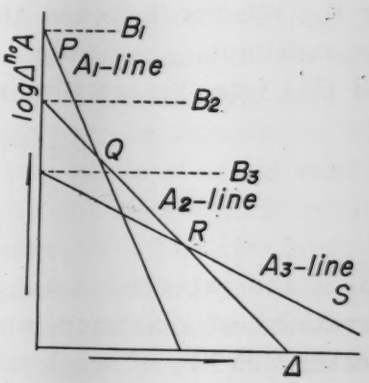

Fig. 9.

How to determine the n_0-value and functional form of $f(T)$ from the observations is a difficult problem. However, clearly, for the application of the present idea, n_0 should not be larger than the smallest value

of n determined by the formulas (4) from the observed $A\sim\Delta$ relation. So that, considering the result of studies by Kawasumi and the theory of elastic waves, $n_0=1/2$ seems most probable at present.

5. Continuous spectrum and envelope.

When the spectrum of the wave is continuous, the $\log \Delta^{n_0}A\sim\Delta$ relation such as shown in Fig. 9 tends to an envelope of A_i-lines, functional form of which depends on those of $B(T)$ and $f(T)$, and is obtained by eliminating T from the following two equations,

$$\frac{1}{B}\frac{dB}{dT}=\Delta\frac{df}{dT}\,, \tag{7}$$

$$\log \Delta^{n_0}A=\log B(T)-f(T)\Delta\,. \tag{8}$$

For example, if we assume that

$$f(T)=\frac{k}{T^2}\,, \tag{9}$$

$$B(T)=C\exp(-sT^2)\,, \tag{10}$$

we get from (7),

$$T^4=\frac{k}{s}\Delta\,, \tag{11}$$

for the relation between the epicentral distance Δ and the "period of the maximum amplitude" to be observed there. Substituting (9), (10) and (11) into (8), we obtain

$$\log \Delta^{n_0}A=\log C-2\sqrt{ks}\sqrt{\Delta}\,, \tag{12}$$

or

$$A=\frac{C}{\Delta^{n_0}}\exp(-2\sqrt{ks}\sqrt{\Delta})\,, \tag{13}$$

(13) is the expected $A\sim\Delta$ relation, in which A is, of course, the "observations of maximum amplitude" of what is assigned by (10) to the spectrum $B(T)$; of acceleration, of displacement or of some others. Now following the result of a laboratory experiment if we assume $f(T)=k/T$ instead of (9),

$$T^3=\frac{k}{2s}\Delta\,, \tag{14}$$

$$A=\frac{C}{\Delta^{n_0}}\exp\left\{-3s\left(\frac{k}{2s}\Delta\right)^{2/3}\right\}\,. \tag{15}$$

Suppose instead of (10) the spectrum is given by

$$B(T)=CT^2\exp(-sT^2)\,, \tag{16}$$

which, if (10) is an acceleration amplitude spectrum, will be a reasonable assumption as a corresponding displacement amplitude spectrum. Then we have, putting $f(T)=k/T^2$,

$$T^2=\frac{1+\sqrt{1+4ks\Delta}}{2s}\,, \tag{17}$$

$$A=\frac{C}{\Delta^{n_0}}\frac{1+\sqrt{1+4ks\Delta}}{2s}\exp(-\sqrt{1+4ks\Delta})\,, \tag{18}$$

in place of (11) and (13) respectively. "A" in (18), formula of the expected $A\sim\Delta$ relation, represents the "observations of maximum displacement amplitude," corresponding to the "observations of maximum acceleration amplitude A" in (13). There may be more reasonable and plausible expressions of $B(T)$ than those above presented; studies on that point are left for the future.

The formulas (13), (15) and (18) are quite different in appearance from what we know well, but as it will be easily seen if we consider $d\log\Delta^{n_0}A/d\Delta$, these formulas fill up conveniently the gap between the two formulas, (1) and (2), or say, Kawasumi's type and Richter's or Tsuboi's type. Therefore, in future studies when observations of high accuracy are obtained these formulas will do much. As regards (11), (13), (17) and (18), the following points are to be noted especially.

As already stated, two kinds of amplitude spectrum of the same earthquake wave at its origin are expressed by (10) and (16), the one is of acceleration and the other of displacement. In accordance with that, the two formulas, (13) and (18), are the two kinds of $A\sim\Delta$ relation of the same earthquake wave, the former by the acceleration seismograph and the latter by the displacement seismograph. The two formulas are so different that perhaps we can never presume the one from the other, to say nothing of that the one can not be obtained from the other by mere amplitude correction, following the response curve.

For a small epicentral distance, mathematical behaviour of (13) is somewhat similar to Tsuboi's or Richter's formula, while that of (18) to Kawasumi's. It is also remarkable that the smallest value of T given by (11) is zero, while that by (17) is $\sqrt{1/s}$. The reason from which these circumstances arise is illustrated already in the last paragraph: in this case we can not obtain the complete spectrum from the $A\sim\Delta$ relation based on the observations by the displacement seismograph,

because the component waves of short period do not join in the relation.

6. Calculation from the observations.

On the other hand, by the following procedure, from the observed $A\sim\Delta$ relation, if we assume a fundamental law of attenuation, for which (5) being adopted for the present, we can determine $B(T)$, the spectrum of the earthquake wave at its origin, and also predict the "period T of the maximum amplitude," which will be examined comparing with the observations.

From the observations of A, $\log \Delta^{n_0}A\sim\Delta$ relation is first calculated, and put $\log \Delta^{n_0}A=F(\Delta)$. Then,

$$f(T)=-\frac{dF}{d\Delta}, \qquad (19)$$

which predicts $T\sim\Delta$ relation if $f(T)$ is known theoretically. And, if $A\sim\Delta$ and $T\sim\Delta$ relation are given, we can determine the function $f(T)$.

From (8),

$$\log B(T)=F(\Delta)+f(T)\Delta \qquad (20)$$

in which, Δ of the right hand member being substituted by T from the $T\sim\Delta$ relation above obtained. For example, suppose the observed $A\sim\Delta$ relation is Richter's type,

$$A=C/\Delta^{n},$$

$$F(\Delta)=\log C-(n-n_0)\log\Delta;$$

then, if

$$f(T)=k/T^{2},$$

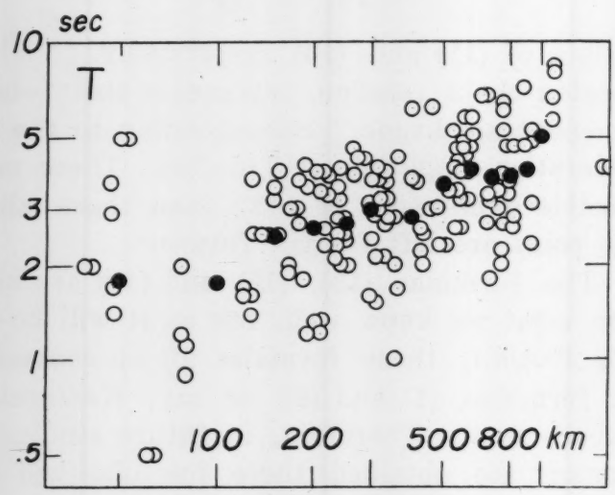

Fig. 10. $T\sim\Delta$ relation of the Shizuoka earthquake, in logarithmic scale.

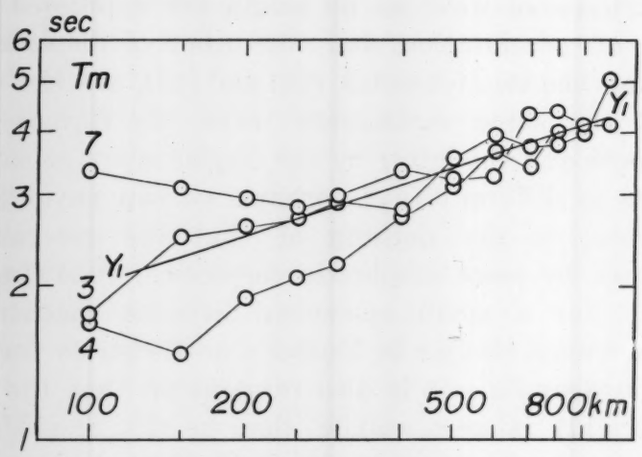

Fig. 11. Mean $T\sim\Delta$ relation of three earthquakes, (3) Shizuoka, (4) Kawachi-Yamato and (7) Imaichi earthquake.

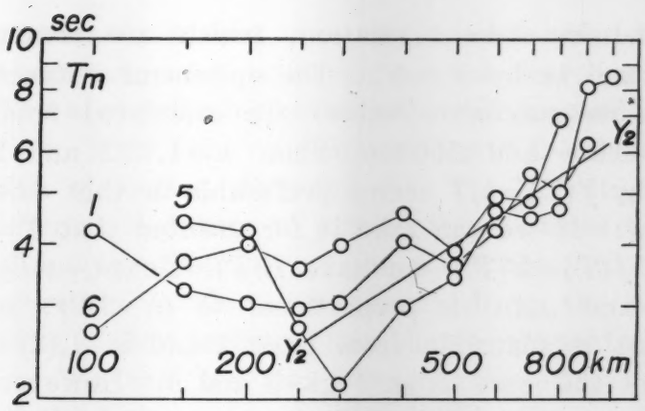

Fig. 12. Mean $T\sim\Delta$ relation of three earthquakes, (1) North-Izu, (5) Shionomisaki and (6) Fukui earthquake.

$$T=\sqrt{k\Delta/(n-n_0)}$$

and

$$B(T)=C'/T^{2(n-n_0)}\,.$$

If $T\sim\Delta$ relation from the observations and the functional form of $f(T)$ are given, we can compare the prediction curve of $A\sim\Delta$ relation with its observation : in that case, the following formula is used, being obtained from (7) and (8),

$$\log \Delta^{n_0}A=\text{const.}-\int f(T)d\Delta\,. \qquad (21)$$

The writer does not know what is the result of study of the $T\sim\Delta$ relation with the observations from which Richter and Tsuboi derived their formulas. So that observations of T versus Δ of the Shizuoka earthquake are shown in Fig. 10, and mean values of the observations of the six earthquakes in the Table 1 in Figs. 11 and 12. For the Shizuoka earthquake, the exponent 1/2 in the above obtained result, which gives $T=a\sqrt{\Delta}$, seems a little too large. Of course, propriety of the present idea will be examined in future from such points of discordancy between the prediction and the observations. However, as far as this earthquake is concerned, the discordancy above stated seems, to have some correlation with the fact that the observations of $A\sim\Delta$ relation of this earthquake are not satisfactorily represented by their formulas. There is also an opinion by some authors, including Kawasumi, that observations of T at almost all observatories in Japan are utterly affected by undesirable resonance of seismograph, Wiechert type seismograph being used, and are found constant over whole epicentral distance : Kawasumi's opinion in this point is concordant with his formula of $A\sim\Delta$ relation, and, at present, will not be a check on the way of thinking in this paper. However, to the writer, it seems not the case, too, at least in several destructive earthquakes ; in any case observations of high accuracy in the immediate future are desired.

For an example of calculation, taking up the Shizuoka earthquake, and putting in the formulas (14) and (15) $n_0=1/2$, $k/2s=0.08\,\text{sec}^3\text{km}^{-1}$, $s=0.06\,\text{sec}^{-2}$, so that $k=0.0096\,\text{sec km}^{-1}$, and $C=7.25\cdot10^4\,\mu\,\text{km}^{1/2}$, we have

curves of $T\sim\Delta$ relation and $\log \Delta^n A\sim\Delta$ relation, which are shown respectively in Figs. 4∼6, and 11 by Y_1-Y_1. The epicentral distance $\Delta_m(n)$, where $\log \Delta^n A$ attains its maximum value, are calculated from these constants 105 km, 300 km and 550 km when $n=1$, 3/2 and 2 respectively. The reason why $f(T)=k/T$ seems preferable in this case to $f(T)=k'/T^2$ is as follows: If we can take it for granted that $T=\alpha\Delta^{1/3}$ from Fig. 10 and put $f(T)=k'/T^2$, we have $B(T)=C\exp(-s'T)$, instead of (10), from (7), and $\Delta_m(n)$ is proportional to $(n-1/2)^3$, so that if $\Delta_m(3/2)=300$ km, that is plausible from Figs. 2 and 5, $\Delta_m(2)=1000$ km that is perhaps not the case from Figs. 3 and 6. However, accuracies of observations are not sufficient for any conclusion. If accuracies of observations are sufficient, k-value is to be compared with those obtained from experimental studies; s-value gives the spectrum of this earthquake waves, which also is to be compared with the observations.

The k-value, where $f(T)=k/T$, is related to a dimensionless and generally used quantity $1/Q$ by $1/Q=kc/\pi$, where c is the velocity of the wave; for some reference, putting $c=2\sim3$ km/sec, we have $1/Q=0.007\sim0.009$, which is not so much different from the result of laboratory experiment by Born. Born's result[2] is, though it is for compressional waves, $kc=0.02\sim0.03$.

In the next place, let us see if the above obtained k-value is applicable to the observations of another earthquakes. We will take up the largest earthquakes in the Table 1, the Fukui- and Shionomisaki earthquake, $A\sim\Delta$ relations of which are similar to each other for $\Delta>200$ km. As regards $T\sim\Delta$ relation, some differences are apparent between the two, and that of the North-Izu earthquake gives a mean tendency of the two. $A\sim\Delta$ and $T\sim\Delta$ relation of the Saitama earthquake are utterly different from those of the three, and are rather similar to those of minor earthquakes, but for its large amplitudes.

Putting $n_0=1/2$, $f(T)=k/T$, where $k=0.0096$ sec km^{-1}, and $T=\alpha\Delta^\beta$ in (21), we get,

$$\log \Delta^n A=C+(n-1/2)\log\Delta-k\Delta^{1-\beta}/(1-\beta)\alpha\ . \qquad (22)$$

From the observations, it is assumed that $T=4$ sec at $\Delta=500$ km, $\Delta_m(3/2)=250\sim300$ km, and $\Delta_m(2)\lesssim800$ km. Then the following constants are obtained for one of possible solutions; $\beta=2/3$, $\alpha=4/63$ sec km$^{-2/3}$, $C=2\cdot10^6\,\mu$ km$^{-1/2}$, $\sqrt{\Delta}\cdot A=C\exp(-3k\Delta^{1/3}/\alpha)$, $B(T)=C\exp(-2k\sqrt{T}/\alpha^{3/2})$, $\log_{10}\Delta^n A=6.290+(n-1/2)\log_{10}\Delta-0.197\Delta^{1/3}$; Δ in km, A in μ. It seems

2) W. T. BORN, "The attenuation constant of earth materials," *Geophysics*, **6** (1941), 132-148.

preferable to put β a little larger than 2/3 for 300 km$<\Delta<$1000 km; observations for $\Delta<200$ km are not clear, because of too large amplitudes. The above obtained constants will be used for $\Delta>200$ km, and, therefore, $T>2.5$ sec. Calculated $\log \Delta^n A \sim \Delta$ and $T \sim \Delta$ curves are shown in the respective diagrams by $Y_2 - Y_2$. It will be a problem of some interest in future to extend those curves to a large distance and examine the propriety of the above obtained constants, especially, of $B(T)$, when the k-value is re-examined on the observations of, at least, a little higher accuracy than herein presented.

We can see also a reasonable difference in the expression of $B(T)$ of the two earthquakes, the Shizuoka- and the Shionomisaki-, in accordance with the difference of their magnitudes: for the former $B(T) = C \exp(-sT^2)$, while for the latter $B(T) = C' \exp(-s'\sqrt{T})$.

7. Concluding remarks and acknowledgement.

Though partial success is apparent, it is impossible to deduce a conclusive finding, for or against the writer's idea, from those scanty and dispersive observations so far obtained. At present, they are presented as data for future studies, expecting still more observations of high accuracy. The dispersive appearance of observations seems at present, apart from the geological condition of observatory and instrumental defects in observation, partly due to a want of clear definition of the "maximum amplitude" and a shortness of a guiding principle for observation. It is hoped that the way of thinking proposed here will give some indications in that respect.

The writer is grateful to the members of Observatories of Japan Meteorological Agency for their kind and speedy information to his troublesome inquiries. He is much obliged to Miss E. Tsutsui for her laborious calculation and preparation of many figures; and also to Miss S. Murata who prepared the data in the first stage of these studies.

Financial support for these studies was partly granted from the Research Fund for Science of the Ministry of Education.

26. 最大振巾と震央距離との関係について
—実験式の波動論的考察—

地震研究所　吉　山　良　一

所謂最大振巾と震央距離との関係について種々の実験式が提出されている．それ等の間の理論的結び付きとその実験式を地震波の理論のためどのように使つていくかについて考察を試みた．このような理論的考察は複雑な地震記象を与えるいわゆる破壊的地震の波動論的解明に必要である．まず“最大振巾”の定義，すなわちその計測方法が確立していなければならないのであるが，諸家の実験式の資料となつている過去の観測報告はこの点において必ずしも満足すべきものとは思われない．しかし気象庁の“地震観測法”によつて判断するに，いつの頃からか振巾の計測には高調波を均らして測定し，全振巾を測つてその半をとり，また“最大振巾”の“周期”もあわせ測定する習慣が生れ，最近はこの方法に一定されたようである．この方法に落ちついたことから考えれば過去の資料も大体の傾向としてはこの方法によつたものと考えてよいであろう．このような観測方法の基調をなすものは調和解析の考え方である．したがつて“最大振巾とその周期”の“報告値”の本質はどちらかといえば最大振巾をもつ成分波の振巾とその周期を与えるものと考えてよい．今後この計測方針を一層明確にすることが“振巾”といい“周期”といい理論的にもすつきりするし，地震波理論の基礎資料としても有効である．厳密にいえば現在の目の子的調和解析による“最大振巾”の処理には波のむれの理論を必要とするが，それを使うことは未知量を増し数学形式を複雑にして，数学的興味を別とすれば，実効がないように思う．将来若し“最大振巾”の厳密な定義が問題となるようなことがあるならば，調和解析を完全にして複雑な波のむれの理論を必要としないような方向に観測資料の整理を考えることが理論的には望ましい．“最大振巾”の“報告値”をこのように成分波の観測値と解釈すれば“最大振巾”と“震央距離”との関係についてすでに提出された，あるいは将来提出されるであろう多くの実験式も唯一つの基本則から比較的簡単に誘導される．その過程が簡単であるから逆に多くの関係式から一つの基本則を帰納することもできる．この理論の裏付けにはいままで兎角注目されなかつた“最大振巾の周期”と震央距離との関係を調査することが必要である．日本の過去に数多い破壊的地震の観測資料もこのような観点からすればはなはだ数少いものとなつてしまう．計算例のため比較的観測精度が高いと思われる地震7個をとつたが，偶然大きさによつて二分される結果となつた．特にその中からそれぞれの大きさを代表して静岡地震(昭和10年)と汐岬地震(昭和23年)について数値計算を行なつた．“最大振巾”と“震央距離”の関係から震央におけるスペクトルを推定し数学式で表わすことができる．静岡地震では $\exp(-sT^2)$，汐岬地震では $\exp(-s'\sqrt{T})$ となり地震の大きさによる違いが予想通り現われたことは筆者の考え方が将来理論的に役立つことを示すものではないかと思う．地震波に対する地殻の内部摩擦係数も $1/Q=0.007\sim0.009$ と計算され，Born が実験的に，Ewing, Press 等が表面波の観測から推定しているものとほぼ同程度の値を得たが，少しく大きすぎると思われるので今後さらに検討の予定である．なおここにいう“最大振巾”は“変位振巾”だけに限らず“速度振巾,”“加速度振巾”あるいはもつと高次の微係数の振巾であることも，または逆に時間的積分の振巾であることも考えられる．いずれであるかはその観測網に用いられた地震計の特性で定まることで，この点についても筆者の解釈は従来のものと少しく異るのではないかと思う．すなわち地震記象であらかじめ“最大振巾”を測定してから地震計の特性による補正を施しては“最大”の意味が曖昧となり，理論的研究の資料としては混迷を招く．この見地からすれば同一観測網に属する地震計の特性を揃えることが必要であり，かつスペクトルを完全に求めるためには種々特性の異つた地震計を同一観測点にあわせ置くことが必要である．

BULLETIN OF THE EARTHQUAKE
RESEARCH INSTITUTE
Vol. 37 (1959), pp. 405-422

27. *Thermo-magneto-hydrodynamic Oscillations in the Earth's Core.*

By Tsuneji RIKITAKE,

Earthquake Research Institute.

(Read June 23, 1959.—Received June 23, 1959.)

Summary

A linearized treatment of the simultaneous equations of electromagnetism, hydrodynamics and heat transfer in a conducting fluid sphere is described. It turns out that a sort of thermo-magneto-hydrodynamic oscillations seems likely to occur through the couplings between magnetic fields, fluid motions and thermal fields. With some drastic simplifications, the eigen-period of the oscillation, which superposes on the steady state of the earth's dynamo is estimated at 20 *years*.

1. Introduction

The writer[1)~8)] has been studying magneto-hydrodynamic oscillations in the earth's core in relation to the theory of the earth's magnetism and its secular variation. One of the most important results obtained through those studies is the fact that, when the influence of the Coriolis force due to the earth's rotation is taken into account, geomagnetic secular variations would not be explained as magneto-hydrodynamic free oscillations in the earth's core. It has been further shown that the buoyancy force due to a time-dependent thermal field, the amplitude of which amounts to $10^{-4}°C$, may give rise to the secular variations observed. As to the cause of such a time-dependent thermal field, no account has been taken of it in the previous paper.

1) T. RIKITAKE, *Bull. Earthq. Res. Inst.*, **33** (1955), 1.
2) T. RIKITAKE, *Bull. Earthq. Res. Inst.*, **33** (1955), 175.
3) T. RIKITAKE, *Bull. Earthq. Res. Inst.*, **33** (1955), 571.
4) T. RIKITAKE, *Bull. Earthq. Res. Inst.*, **33** (1955), 583.
5) T. RIKITAKE, *Bull. Earthq. Res. Inst.*, **34** (1956), 139.
6) T. RIKITAKE, *Bull. Earthq. Res. Inst.*, **34** (1956), 283.
7) T. RIKITAKE, *Journ. Phys. Soc. Japan*, **13** (1958), 1224.
8) T. RIKITAKE, *Bull. Earthq. Res. Inst.*, **37** (1959), 245.

It has been suggested, however, that a sort of thermo-magneto-hydrodynamic oscillations might be excited through couplings between magnetic fields, fluid motions and thermal fields in the earth's core. It is no easy matter to obtain simultaneous solutions of the equations of electromagnetism, hydrodynamics and heat transfer in a complete form because these equations are essentially non-linear. A linearized treatment of these equations will be attempted here by considering small disturbances superposing on Bullard's dynamo which may be regarded as steady or nearly steady. Even in such a treatment some drastic simplifications are required in order to obtain eigen-values as will be seen in the following.

2. Equations to be solved

Maxwell's equations are written as

$$\vec{I}=\sigma(\vec{E}+\vec{V}\wedge\vec{H})\,, \tag{1}$$

$$\text{curl}\,\vec{E}=-\partial\vec{H}/\partial t\,, \tag{2}$$

$$\text{curl}\,\vec{H}=4\pi\vec{I}\,, \tag{3}$$

where $\vec{I}$, $\vec{E}$, $\vec{H}$, σ and $\vec{V}$ denote respectively the electric current density, electric field, magnetic field, electrical conductivity and velocity of fluid motion. The magnetic permeability is assumed as unity in electromagnetic unit.

Meanwhile the equation of motion can be written as

$$\rho\partial\vec{V}/\partial t+\rho(\vec{V}\cdot\text{grad})\vec{V}+2\rho(\vec{\omega}_0\wedge\vec{V})=\vec{I}\wedge\vec{H}-\text{grad}\,P+\vec{G}\,, \tag{4}$$

where ρ, $\vec{\omega}_0$, P and $\vec{G}$ denote respectively the density, rotation vector of uniform rotation about $\theta=0$ axis, pressure and non-electromagnetic force.

In addition to the equations from (1) to (4), we have to write down the equation for temperature. Following Chandrasekhar[9),10)] and Namikawa[11)], it may be written as

$$\partial\Theta/\partial t=\kappa\nabla^2\Theta+\varepsilon\,, \tag{5}$$

where Θ, κ and ε denote respectively the temperature, thermometric conductivity and rate of heat generation.

Let us put

9) S. CHANDRASEKHAR, *Phil. Mag.*, (vii), **43** (1952), 1317.
10) S. CHANDRASEKHAR, *Phil. Mag.*, (vii), **2** (1957), 845.
11) T. NAMIKAWA, *Journ. Geomagn. Geoelectr.*, **9** (1957), 182.

$$\left.\begin{aligned} &\vec{I}=\vec{I}_0+\vec{i}\ , \quad \vec{E}=\vec{E}_0+\vec{e}\ , \quad \vec{H}=\vec{H}_0+\vec{h}\ , \\ &\vec{V}=\vec{V}_0+\vec{v}\ , \quad P=P_0+p\ , \quad \vec{G}=\vec{G}_0+\vec{g}\ , \\ &\Theta=\Theta_0+u\ , \end{aligned}\right\} \tag{6}$$

in which the quantities with subscript 0 specify the steady state, while those denoted with small letters are the departures from the steady state and are regarded as the first order small quantities. One more relation related to thermal expansion is given as

$$\rho=\rho_0(1+\alpha\Theta)^{-1}\ ,$$

where α denotes the coefficient of volume expansion which is estimated at $4.5\times10^{-6}{}^{\circ}C^{-1}$ by Bullard and Gellman[12]. Since $\alpha\Theta\ll1$ for the earth's core, the above relation can be rewritten as

$$\rho=\rho_0(1-\alpha\Theta)\ . \tag{7}$$

Putting (6) and (7) into the equations from (1) to (5), we have a system of linear differential equations as follows;

$$\vec{i}=\sigma(\vec{e}+\vec{v}\wedge\vec{H}_0+\vec{V}_0\wedge\vec{h})\ , \tag{8}$$

$$\operatorname{curl}\vec{e}=-\partial\vec{h}/\partial t\ , \tag{9}$$

$$\operatorname{curl}\vec{h}=4\pi\vec{i}\ , \tag{10}$$

$$\rho_0(\partial\vec{v}/\partial t)+2\rho_0(\vec{\omega}_0\wedge\vec{v})=\vec{i}\wedge\vec{H}_0+\vec{I}_0\wedge\vec{h}-\operatorname{grad}p+\vec{g}\ , \tag{11}$$

$$\partial u/\partial t=\kappa\nabla^2u-(\vec{v}\cdot\operatorname{grad})\Theta_0\ , \tag{12}$$

provided the second order small quantities are ignored. In the right-hand-side of (11), we write ρ_0 in place of $\rho_0(1-\alpha\Theta)$. As has usually been done in theories of thermal convection, this means that the thermal expansion contributes only to the buoyancy force, the fluid being assumed as incompressible for motion. Since $\alpha\Theta\ll1$, the assumption may be acceptable.

$\vec{g}$, that appears in (11), can be obtained from the following consideration. Since the only non-electromagnetic force arises from gravitation, the acceleration of gravity at a point, of which the distance from the centre is r, is due to the gravitation of the mass within the spherical surface passing the point. Since the said mass amounts to $(4/3)\pi\rho_m r^3$, $\vec{G}$, which has only the radial component, is given by

12) E. C. BULLARD and H. GELLMAN, *Phil. Trans. Roy. Soc. London A*, **247** (1954), 213.

$$\vec{G}=-(4/3)\pi\rho\rho_m k^2\vec{r}\ , \tag{13}$$

where ρ_m and k^2 are the mean density and the gravitational constant. Putting (7) into (13) and taking the sixth equation of (6) into account, we can deduce

$$\left.\begin{aligned}\vec{G}_0&=-\rho_0(1-\alpha\Theta_0)\gamma\alpha^{-1}\vec{r}\ ,\\ \vec{g}&=\rho_0\gamma u\vec{r}\ ,\end{aligned}\right\} \tag{14}$$

where

$$\gamma=(4/3)\pi\rho_m k^2\alpha\ . \tag{15}$$

In the next place, we may assume the steady state of temperature as

$$\Theta_0=\beta(a^2-r^2)\ , \tag{16}$$

which leads to $\Theta_0=0$ at the core-mantle boundary ($r=a$). This entails no loss of generality.

Putting (14) and (16) respectively into (11) and (12), we obtain

$$\rho_0(\partial\vec{v}/\partial t)+2\rho_0(\vec{\omega}_0\wedge\vec{v})=\vec{i}\wedge\vec{H}_0+\vec{I}_0\wedge\vec{h}-\text{grad}\ p+\rho_0\gamma u\vec{r}\ , \tag{17}$$

$$\partial u/\partial t=\kappa\nabla^2 u+2\beta(\vec{v}\cdot\vec{r})\ , \tag{18}$$

which govern small departures from the steady state together with (8), (9) and (10).

If we eliminate $\vec{i}$ and $\vec{e}$ from the above equations and write D in place of $\partial/\partial t$, we obtain

$$\{D-(4\pi\sigma)^{-1}\nabla^2\}\vec{h}=\text{curl}\,(\vec{V}_0\wedge\vec{h})+\text{curl}\,(\vec{v}\wedge\vec{H}_0)\ , \tag{19}$$

$$\rho_0 D\vec{v}+2\rho_0(\vec{\omega}_0\wedge\vec{v})=(4\pi)^{-1}\{(\text{curl}\,\vec{h}\wedge\vec{H}_0)+(\text{curl}\,\vec{H}_0\wedge\vec{h})\}-\text{grad}\ p+\rho_0\gamma u\vec{r}\ , \tag{20}$$

$$Du=\kappa\nabla^2 u+2\beta(\vec{v}\cdot\vec{r})\ . \tag{21}$$

If these three equations are solved under suitable boundary conditions, we may investigate the couplings between electromagnetism, fluid motion and thermal field which are prevailing in the earth's core. $\vec{V}_0$ and $\vec{H}_0$, that appear in the above equations, are the steady components of the velocity and magnetic field in the earth's core.

3. Solution for pressure

The condition that the fluid is incompressible for motion implies

$$\text{div}\,\vec{v}=0\ , \tag{22}$$

so that, by taking div of (20), we obtain

$$\nabla^2 p=-(4\pi)^{-1}(\vec{H}_0\cdot\nabla^2\vec{h}+\vec{h}\cdot\nabla^2\vec{H}_0+2\,\mathrm{curl}\,\vec{h}\cdot\mathrm{curl}\,\vec{H}_0)+2\rho_0\vec{\omega}_0\cdot\mathrm{curl}\,\vec{v}$$
$$+\rho_0\gamma r^{-2}\frac{d(r^3u)}{dr}\,. \tag{23}$$

$\mathrm{curl}\,\vec{\omega}_0=0$ which is derived from the condition of uniform rotation is also taken into account in deducing (23).

In general, $\vec{h}$ is to be expressed with the sum of poloidal and toroidal magnetic fields of various degree. As has been done in the previous papers, however, we shall take only the S_1^0-type field ignoring magnetic fields of other types that appear in the righthand-side of (19). Through such a simplification, the problem becomes tractable because it is possible to pick up the specified field among many fields of various types which come out through the induction processes.

If we take only the S_1^0 field, we may write the r, θ and ϕ components of the field and associated vectors as

$$\left.\begin{aligned}
\vec{h}&=\begin{cases}-2s(r)P_1\\ -\left(r\dfrac{ds}{dr}+2s\right)\dfrac{dP_1}{d\theta}\\ 0\end{cases},\\
\mathrm{curl}\,\vec{h}&=\begin{cases}0\\ 0\\ -\left(r\dfrac{d^2s}{dr^2}+4\dfrac{ds}{dr}\right)\dfrac{dP_1}{d\theta}\end{cases},\\
\nabla^2\vec{h}&=\begin{cases}-2\left(\dfrac{d^2s}{dr^2}+\dfrac{4}{r}\dfrac{ds}{dr}\right)P_1\\ -\left(r\dfrac{d^3s}{dr^3}+6\dfrac{d^2s}{dr^2}+\dfrac{4}{r}\dfrac{ds}{dr}\right)\dfrac{dP_1}{d\theta}\\ 0\end{cases}.
\end{aligned}\right\} \tag{24}$$

As for the steady magnetic fields and fluid motions, we take the simplest combination of Bullard's dynamo[12], so that the motion consists of the T_1^0 and S_2^{2c} types while the magnetic fields contain the S_1^0, T_2^0, T_2^{2c} and T_2^{2s} types. It then follows that

$$\left.\begin{aligned}
\vec{H}_0&=\vec{H}_1+\vec{H}_2+\vec{H}_3+\vec{H}_4\,,\\
\vec{V}_0&=\vec{V}_1+\vec{V}_2\,,
\end{aligned}\right\} \tag{25}$$

where

$$\left.\begin{aligned}
\vec{H}_1&=\begin{cases}-2S_1(r)P_1\\ -\left(r\dfrac{dS_1}{dr}+2S_1\right)\dfrac{dP_1}{d\theta}\\ 0\end{cases},\\
\operatorname{curl}\vec{H}_1&=\begin{cases}0\\0\\ -\left(r\dfrac{d^2S_1}{dr^2}+4\dfrac{dS_1}{dr}\right)\dfrac{dP_1}{d\theta}\end{cases},\\
\nabla^2\vec{H}_1&=\begin{cases}-2\left(\dfrac{d^2S_1}{dr^2}+\dfrac{4}{r}\dfrac{dS_1}{dr}\right)P_1\\ -\left(r\dfrac{d^3S_1}{dr^3}+6\dfrac{d^2S_1}{dr^2}+\dfrac{4}{r}\dfrac{dS_1}{dr}\right)\dfrac{dP_1}{d\theta}\\ 0\end{cases},
\end{aligned}\right\}\qquad(26)$$

$$\left.\begin{aligned}
\vec{H}_2&=\begin{cases}0\\0\\ (r/a)^2T_2(r)\dfrac{dP_2}{d\theta}\end{cases},\\
\operatorname{curl}\vec{H}_2&=\begin{cases}-6a^{-2}rT_2P_2\\ -a^{-2}\left(r\dfrac{dT_2}{dr}+3T_2\right)r\dfrac{dP_2}{d\theta}\\ 0\end{cases},\\
\nabla^2\vec{H}_2&=\begin{cases}0\\0\\ a^{-2}\left(\dfrac{d^2T_2}{dr^2}+\dfrac{6}{r}\dfrac{dT_2}{dr}\right)r^2\dfrac{dP_2}{d\theta}\end{cases},
\end{aligned}\right\}\qquad(27)$$

$$\vec{H}_3=\begin{cases}0\\ -(r/a)^2T_3(r)\dfrac{\partial(P_2^2\cos 2\phi)}{\sin\theta\partial\phi}\\ (r/a)^2T_3(r)\dfrac{\partial(P_2^2\cos 2\phi)}{\partial\theta}\end{cases},$$

$$\left.\begin{aligned}
\operatorname{curl}\vec{H}_3 &= \begin{cases} -6a^{-2}rT_3P_2^2\cos 2\phi \\ -a^{-2}\left(r\dfrac{dT_3}{dr}+3T_3\right)r\dfrac{\partial(P_2^2\cos 2\phi)}{\partial\theta} \\ -a^{-2}\left(r\dfrac{dT_3}{dr}+3T_3\right)r\dfrac{\partial(P_2^2\cos 2\phi)}{\sin\theta\partial\phi}\,, \end{cases} \\
\nabla^2\vec{H}_3 &= \begin{cases} 0 \\ -a^{-2}\left(\dfrac{d^2T_3}{dr^2}+\dfrac{6}{r}\dfrac{dT_3}{dr}\right)r^2\dfrac{\partial(P_2^2\cos 2\phi)}{\sin\theta\partial\phi} \\ a^{-2}\left(\dfrac{d^2T_3}{dr^2}+\dfrac{6}{r}\dfrac{dT_3}{dr}\right)r^2\dfrac{\partial(P_2^2\cos 2\phi)}{\partial\theta}\,, \end{cases}
\end{aligned}\right\} \tag{28}$$

$$\left.\begin{aligned}
\vec{H}_4 &= \begin{cases} 0 \\ -(r/a)^2T_4(r)\dfrac{\partial(P_2^2\sin 2\phi)}{\sin\theta\partial\phi} \\ (r/a)^2T_4(r)\dfrac{\partial(P_2^2\sin 2\phi)}{\partial\theta}\,, \end{cases} \\
\operatorname{curl}\vec{H}_4 &= \begin{cases} -6a^{-2}rT_4P_2^2\sin 2\phi \\ -a^{-2}\left(r\dfrac{dT_4}{dr}+3T_4\right)r\dfrac{\partial(P_2^2\sin 2\phi)}{\partial\theta} \\ -a^{-2}\left(r\dfrac{dT_4}{dr}+3T_4\right)r\dfrac{\partial(P_2^2\sin 2\phi)}{\sin\theta\partial\phi}\,, \end{cases} \\
\nabla^2\vec{H}_4 &= \begin{cases} 0 \\ -a^{-2}\left(\dfrac{d^2T_4}{dr^2}+\dfrac{6}{r}\dfrac{dT_4}{dr}\right)r^2\dfrac{\partial(P_2^2\sin 2\phi)}{\sin\theta\partial\phi} \\ a^{-2}\left(\dfrac{d^2T_4}{dr^2}+\dfrac{6}{r}\dfrac{dT_4}{dr}\right)r^2\dfrac{\partial(P_2^2\sin 2\phi)}{\partial\theta}\,, \end{cases}
\end{aligned}\right\} \tag{29}$$

$$\vec{V}_1 = \begin{cases} 0 \\ 0 \\ (r/a)V_1(r)\dfrac{dP_1}{d\theta}\,, \end{cases} \tag{30}$$

$$\vec{V}_2=\begin{cases}-6(r/a)V_2(r)P_2^2\cos 2\phi \\ -(r/a)\left(r\dfrac{dV_2}{dr}+3V_2\right)\dfrac{\partial(P_2^2\cos 2\phi)}{\partial\theta} \\ -(r/a)\left(r\dfrac{dV_2}{dr}+3V_2\right)\dfrac{\partial(P_2^2\cos 2\phi)}{\sin\theta\partial\phi}\end{cases}. \tag{31}$$

With the above expressions, the first three terms of the righthand-side of (23) are calculated as follows;

$$\begin{aligned}\vec{H}_0\cdot\nabla^2\vec{h}=&\frac{2}{3}\left\{2S_1\left(\frac{d^2s}{dr^2}+\frac{4}{r}\frac{ds}{dr}\right)+\left(r\frac{dS_1}{dr}+2S_1\right)\left(r\frac{d^3s}{dr^3}+6\frac{d^2s}{dr^2}+\frac{4}{r}\frac{ds}{dr}\right)\right\}\\&+\frac{2}{3}\left\{4S_1\left(\frac{d^2s}{dr^2}+\frac{4}{r}\frac{ds}{dr}\right)-\left(r\frac{dS_1}{dr}+2S_1\right)\left(r\frac{d^3s}{dr^3}+6\frac{d^2s}{dr^2}+\frac{4}{r}\frac{ds}{dr}\right)\right\}P_2\\&+2a^{-2}T_3r^2\left(r\frac{d^3s}{dr^3}+6\frac{d^2s}{dr^2}+\frac{4}{r}\frac{ds}{dr}\right)P_2^2\sin 2\phi\\&-2a^{-2}T_4r^2\left(r\frac{d^3s}{dr^3}+6\frac{d^2s}{dr^2}+\frac{4}{r}\frac{ds}{dr}\right)P_2^2\cos 2\phi\,,\end{aligned} \tag{32}$$

$$\begin{aligned}\vec{h}\cdot\nabla^2\vec{H}_0=&\frac{2}{3}\left\{2\left(\frac{d^2S_1}{dr^2}+\frac{4}{r}\frac{dS_1}{dr}\right)s+\left(r\frac{d^3S_1}{dr^3}+6\frac{d^2S_1}{dr^2}+\frac{4}{r}\frac{dS_1}{dr}\right)\left(r\frac{ds}{dr}+2s\right)\right\}\\&+\frac{2}{3}\left\{4\left(\frac{d^2S_1}{dr^2}+\frac{4}{r}\frac{dS_1}{dr}\right)s-\left(r\frac{d^3S_1}{dr^3}+6\frac{d^2S_1}{dr^2}+\frac{4}{r}\frac{dS_1}{dr}\right)\left(r\frac{ds}{dr}+2s\right)\right\}P_2\\&+2a^{-2}\left(r^2\frac{d^2T_3}{dr^2}+6r\frac{dT_3}{dr}\right)\left(r\frac{ds}{dr}+2s\right)P_2^2\sin 2\phi\\&-2a^{-2}\left(r^2\frac{d^2T_4}{dr^2}+6r\frac{dT_4}{dr}\right)\left(r\frac{ds}{dr}+2s\right)P_2^2\cos 2\phi\,,\end{aligned} \tag{33}$$

$$\begin{aligned}\operatorname{curl}\vec{h}\cdot\operatorname{curl}\vec{H}_0=&\frac{2}{3}\left(r\frac{d^2S_1}{dr^2}+4\frac{dS_1}{dr}\right)\left(r\frac{d^2s}{dr^2}+4\frac{ds}{dr}\right)\\&-\frac{2}{3}\left(r\frac{d^2S_1}{dr^2}+4\frac{dS_1}{dr}\right)\left(r\frac{d^2s}{dr^2}+4\frac{ds}{dr}\right)P_2\\&+2a^{-2}\left(r^2\frac{dT_3}{dr}+3rT_3\right)\left(r\frac{d^2s}{dr^2}+4\frac{ds}{dr}\right)P_2^2\sin 2\phi\\&-2a^{-2}\left(r^2\frac{dT_4}{dr}+3rT_4\right)\left(r\frac{d^2s}{dr^2}+4\frac{ds}{dr}\right)P_2^2\cos 2\phi\,.\end{aligned} \tag{34}$$

We thus see that the electromagnetic force considered gives rise to pressure of which the distribution is described with spherical surface harmonics P_0, P_2, $P_2^2\cos 2\phi$ and $P_2^2\sin 2\phi$.

In the next place, we have to examine the role of $\vec{\omega}_0\cdot\operatorname{curl}\vec{v}$. Since

the velocities that give rise to the S_1^0 magnetic field through curl $(\vec{v}\wedge\vec{H}_0)$ in (19) are only the S_2^0, S_2^{2c} and S_2^{2s} types, it is sufficient to consider the following velocities:

$$\vec{v}=\vec{v}_1+\vec{v}_2+\vec{v}_3\,, \tag{35}$$

where

$$\vec{v}_1=\begin{cases}-6\xi_2(r)rP_2\\ -\left(r\dfrac{d\xi_2}{dr}+3\xi_2\right)r\dfrac{dP_2}{d\theta}\\ 0\end{cases}, \tag{36}$$

$$\vec{v}_2=\begin{cases}-6\xi_2^{2c}(r)rP_2^2\cos 2\phi\\ -\left(r\dfrac{d\xi_2^{2c}}{dr}+3\xi_2^{2c}\right)r\dfrac{\partial(P_2^2\cos 2\phi)}{\partial\theta}\\ -\left(r\dfrac{d\xi_2^{2c}}{dr}+3\xi_2^{2c}\right)r\dfrac{\partial(P_2^2\cos 2\phi)}{\sin\theta\partial\phi}\end{cases}, \tag{37}$$

$$\vec{v}_3=\begin{cases}-6\xi_2^{2s}(r)rP_2^2\sin 2\phi\\ -\left(r\dfrac{d\xi_2^{2s}}{dr}+3\xi_2^{2s}\right)r\dfrac{\partial(P_2^2\sin 2\phi)}{\partial\theta}\\ -\left(r\dfrac{d\xi_2^{2s}}{dr}+3\xi_2^{2s}\right)r\dfrac{\partial(P_2^2\sin 2\phi)}{\sin\theta\partial\phi}\end{cases}. \tag{38}$$

In that case, we obtain

$$\left.\begin{aligned}&\vec{\omega}_0\cdot\mathrm{curl}\,\vec{v}_1=0\,,\\ &\vec{\omega}_0\cdot\mathrm{curl}\,\vec{v}_2=2\omega r^2\left(\frac{d^2\xi_2^{2c}}{dr^2}+\frac{6}{r}\frac{d\xi_2^{2c}}{dr}\right)P_2^2\sin 2\phi\,,\\ &\vec{\omega}_0\cdot\mathrm{curl}\,\vec{v}_3=-2\omega r^2\left(\frac{d^2\xi_2^{2s}}{dr^2}+\frac{6}{r}\frac{d\xi_2^{2s}}{dr}\right)P_2^2\cos 2\phi\,.\end{aligned}\right\} \tag{39}$$

Finally, u may be assumed as

$$u=\theta_2P_2+\theta_2^{2c}P_2^2\cos 2\phi+\theta_2^{2s}P_2^2\sin 2\phi\,, \tag{40}$$

while thermal fields of other types have nothing to do with the present problem as can be easily seen from (20).

Introducing (32), (33), (34), (39) and (40) to the righthand-side of (23), we obtain the differential equation for the pressure as follows;

$$\nabla^2p=f_0+f_2P_2+f_2^{2c}P_2^2\cos 2\phi+f_2^{2s}P_2^2\sin 2\phi\,, \tag{41}$$

where

$$\left.\begin{aligned}
f_0&=-(4\pi)^{-1}\frac{4}{3}S_1\left(r\frac{d^3s}{dr^3}+7\frac{d^2s}{dr^2}+\frac{8}{r}\frac{ds}{dr}\right),\\
f_2&=-(4\pi)^{-1}\frac{4}{3}S_1\left(r\frac{d^3s}{dr^3}+4\frac{d^2s}{dr^2}-\frac{4}{r}\frac{ds}{dr}\right)+\rho_0\gamma\frac{d(r^3\theta_2)}{r^2dr},\\
\begin{pmatrix}f_2^{2c}\\ f_2^{2s}\end{pmatrix}&=\pm(4\pi)^{-1}2\left(\frac{r}{a}\right)^2\begin{pmatrix}T_4\\ T_3\end{pmatrix}\left(r\frac{d^3s}{dr^3}+12\frac{d^2s}{dr^2}+\frac{28}{r}\frac{ds}{dr}\right)\\
&\quad\mp 4\rho_0\omega\begin{pmatrix}\dfrac{d^2\xi_2^{2s}}{dr^2}+\dfrac{6}{r}\dfrac{d\xi_2^{2s}}{dr}\\ \dfrac{d^2\xi_2^{2c}}{dr^2}+\dfrac{6}{r}\dfrac{d\xi_2^{2c}}{dr}\end{pmatrix}+\rho_0\gamma\begin{pmatrix}\dfrac{d(r^3\theta_2^{2c})}{r^2dr}\\ \dfrac{d(r^3\theta_2^{2s})}{r^2dr}\end{pmatrix},
\end{aligned}\right\}\qquad(42)$$

in which it is assumed, for the sake of simplicity, that S_1, T_3 and T_4 are independent of r.

The solution of (41) can be expressed as

$$p=\sum_{n,m}q_n^m(r)\,Y_n^m\,,\qquad(43)$$

where

$$Y_n^m=P_n^m(\cos\theta)\begin{matrix}\cos\\ \sin\end{matrix}m\phi\,.$$

Since $\nabla^2 p$ can be written as

$$\nabla^2 p=\sum_{n,m}\left\{\frac{1}{r^2}\frac{d}{dr}\left(r^2\frac{d}{dr}\right)-\frac{n(n+1)}{r^2}\right\}q_n^m(r)\,Y_n^m\,,$$

we have a set of ordinary differential equations such as

$$\left.\begin{aligned}
&\frac{1}{r}\frac{d}{dr}\left(r^2\frac{d}{dr}\right)q_0^0=f_0\,,\\
&\left\{\frac{1}{r}\frac{d}{dr}\left(r^2\frac{d}{dr}\right)-\frac{6}{r^2}\right\}\begin{pmatrix}q_2^0\\ q_2^{2c}\\ q_2^{2s}\end{pmatrix}=\begin{pmatrix}f_2\\ f_2^{2c}\\ f_2^{2s}\end{pmatrix}.
\end{aligned}\right\}\qquad(44)$$

The solutions of (44) which remain finite at $r=0$ are given as

$$\left.\begin{aligned}
q_0^0&=(4\pi)^{-1}\left\{L_0^0-\frac{4}{3}S_1\left(r\frac{ds}{dr}+3s\right)\right\},\\
q_2^0&=(4\pi)^{-1}\left\{\left(\frac{r}{a}\right)^2L_2^0+\frac{4}{3}S_1r\frac{ds}{dr}\right\}+\frac{1}{5}\rho_0\gamma\left\{3r^2\int r^{-1}\theta_2dr+2r^{-3}\int r^4\theta_2dr\right\},\\
\begin{pmatrix}q_2^{2c}\\ q_2^{2s}\end{pmatrix}&=(4\pi)^{-1}\left\{\left(\frac{r}{a}\right)^2\begin{pmatrix}L_2^{2c}\\ L_2^{2s}\end{pmatrix}\pm\begin{pmatrix}T_4\\ T_3\end{pmatrix}\left(r^3\frac{ds}{dr}+4r^2s-2r^{-3}\int r^4sdr\right)\right\}\\
&\quad\mp 4\rho_0\omega r^2\begin{pmatrix}\xi_2^{2s}\\ \xi_2^{2c}\end{pmatrix}+\frac{1}{5}\rho_0\gamma\left\{3r^2\int r^{-1}\begin{pmatrix}\theta_2^{2c}\\ \theta_2^{2s}\end{pmatrix}dr+2r^{-3}\int r^4\begin{pmatrix}\theta_2^{2c}\\ \theta_2^{2s}\end{pmatrix}dr\right\},
\end{aligned}\right\}\qquad(45)$$

where L_0^0, L_2^0, L_2^{2c} and L_2^{2s} are constants which shall be determined by the boundary conditions.

4. Velocity, magnetic field and temperature

Since the solutions for pressure are given by (43) together with (45), we can easily calculate grad p that appears in (20). If we ignore the T_1^0, T_2^0, T_3^{2c} and T_3^{2s} velocities which are derived from curl $\vec{H}_0 \wedge \vec{h}$, (20) leads to the equations for the T_2^0, T_2^{2c} and T_2^{2s} velocities which are readily obtained as follows;

$$D\rho_0\xi_2=(4\pi a^2)^{-1}\left(\frac{1}{3}L_2^0-\frac{2}{3}a^2S_1r^{-1}\frac{ds}{dr}\right)+\frac{\rho_0\gamma}{5}\left(\int r^{-1}\theta_2 dr-r^{-5}\int r^4\theta_2 dr\right), \tag{46}$$

$$D\rho_0\xi_2^{2c}=(4\pi a^2)^{-1}\left(\frac{1}{3}L_2^{2c}+2T_4r^{-5}\int r^4 s dr\right)-\frac{2}{3}\rho_0\omega\left(r\frac{d\xi_2^{2s}}{dr}+3\xi_2^{2s}\right)$$
$$+\frac{\rho_0\gamma}{5}\left(\int r^{-1}\theta_2^{2c}dr-r^{-5}\int r^4\theta_2^{2c}dr\right), \tag{47}$$

$$D\rho_0\xi_2^{2s}=(4\pi a^2)^{-1}\left(\frac{1}{3}L_2^{2s}-2T_3r^{-5}\int r^4 s dr\right)+\frac{2}{3}\rho_0\omega\left(r\frac{d\xi_2^{2c}}{dr}+3\xi_2^{2c}\right)$$
$$+\frac{\rho_0\gamma}{5}\left(\int r^{-1}\theta_2^{2s}dr-r^{-5}\int r^4\theta_2^{2s}dr\right). \tag{48}$$

It is also easily seen that the pressure gradient which does not depend on θ and ϕ is cancelled by the electromagnetic force derived from curl $\vec{h} \wedge \vec{H}_1$. L_2^0, L_2^{2c} and L_2^{2s} are to be determined by the conditions that the normal component of the velocities should vanish at $r=a$.

In the next place, the equation for the magnetic field will be deduced by calculating curl $(\vec{V}_0 \wedge \vec{h})$ and curl $(\vec{v} \wedge \vec{H}_0)$ in (19) and picking up only the S_1^0 magnetic field. We obtain

$$Ds-(4\pi\sigma)^{-1}\left(\frac{d^2s}{dr^2}+\frac{4}{r}\frac{ds}{dr}\right)=-\frac{6}{5}S_1\left(r\frac{d\xi_2}{dr}+5\xi_2\right)-\frac{216}{5}a^{-2}r^2(T_4\xi_2^{2c}-T_3\xi_2^{2s}). \tag{49}$$

Furthermore, by taking (35) and (40) into account, (21) leads to

$$D\theta_2=\kappa\left(\frac{d^2\theta_2}{dr^2}+\frac{2}{r}\frac{d\theta_2}{dr}-\frac{6}{r^2}\theta_2\right)-12\beta r^2\xi_2, \tag{50}$$

$$D\theta_2^{2c}=\kappa\left(\frac{d^2\theta_2^{2c}}{dr^2}+\frac{2}{r}\frac{d\theta_2^{2c}}{dr}-\frac{6}{r^2}\theta_2^{2c}\right)-12\beta r^2\xi_2^{2c}, \tag{51}$$

$$D\theta_2^{2s}=\kappa\left(\frac{d^2\theta_2^{2s}}{dr^2}+\frac{2}{r}\frac{d\theta_2^{2s}}{dr}-\frac{6}{r^2}\theta_2^{2s}\right)-12\beta r^2\xi_2^{2s}\,. \tag{52}$$

The equations from (46) to (52) can be regarded as the simultaneous integro-differential equations for ξ_2, ξ_2^{2c}, ξ_2^{2s}, s, θ_2, θ_2^{2c} and θ_2^{2s}.

5. Approximate solution of the integro-differential equations

The equations to be solved are so complicated that it seems unlikely that exact solutions can be obtained. As has been done in the previous papers, let us assume

$$\left.\begin{aligned} &s=\sum_n a_n(r/a)^n\,,\quad \xi_2^{2c}=\sum_n A_n(r/a)^n\,,\quad \xi_2^{2s}=\sum_n B_n(r/a)^n\,,\quad \xi_2=\sum_n C_n(r/a)^n\,,\\ &\theta_2^{2c}=\sum_n \lambda_n(r/a)^n\,,\quad \theta_2^{2s}=\sum_n \mu_n(r/a)^n\,,\quad \theta_2=\sum_n \nu_n(r/a)^n\,. \end{aligned}\right\} \tag{53}$$

Introducing (53) to the equations from (46) to (52), we obtain

$$D\rho_0\sum C_n\left(\frac{r}{a}\right)^n=(4\pi a^2)^{-1}\left(\frac{1}{3}L_2^0-\frac{2}{3}S_1\sum n a_n\left(\frac{r}{a}\right)^{n-2}\right)$$
$$+\rho_0\gamma\sum\frac{\nu_n}{n(n+5)}\left(\frac{r}{a}\right)^n\,, \tag{54}$$

$$D\rho_0\sum A_n\left(\frac{r}{a}\right)^n=(4\pi a^2)^{-1}\left(\frac{1}{3}L_2^{2c}+2T_4\sum\frac{a_n}{n+5}\left(\frac{r}{a}\right)^n\right)$$
$$-\frac{2}{3}\rho_0\omega\sum(n+3)B_n\left(\frac{r}{a}\right)^n+\rho_0\gamma\sum\frac{\lambda_n}{n(n+5)}\left(\frac{r}{a}\right)^n\,, \tag{55}$$

$$D\rho_0\sum B_n\left(\frac{r}{a}\right)^n=(4\pi a^2)^{-1}\left(\frac{1}{3}L_2^{2s}-2T_3\sum\frac{a_n}{n+5}\left(\frac{r}{a}\right)^n\right)$$
$$+\frac{2}{3}\rho_0\omega\sum(n+3)A_n\left(\frac{r}{a}\right)^n+\rho_0\gamma\sum\frac{\mu_n}{n(n+5)}\left(\frac{r}{a}\right)^n\,, \tag{56}$$

$$D\sum a_n\left(\frac{r}{a}\right)^n-(4\pi\sigma a^2)^{-1}\sum n(n+3)a_n\left(\frac{r}{a}\right)^{n-2}=-\frac{6}{5}S_1\sum(n+5)C_n\left(\frac{r}{a}\right)^n$$
$$-\frac{216}{5}\left(T_4\sum A_n\left(\frac{r}{a}\right)^{n+2}-T_3\sum B_n\left(\frac{r}{a}\right)^{n+2}\right)\,, \tag{57}$$

$$Da^2\sum\nu_n\left(\frac{r}{a}\right)^n=\kappa\sum(n-2)(n+3)\nu_n\left(\frac{r}{a}\right)^{n-2}-12\beta a^4\sum C_n\left(\frac{r}{a}\right)^{n+2}\,, \tag{58}$$

$$Da^2\sum\lambda_n\left(\frac{r}{a}\right)^n=\kappa\sum(n-2)(n+3)\lambda_n\left(\frac{r}{a}\right)^{n-2}-12\beta a^4\sum A_n\left(\frac{r}{a}\right)^{n+2}\,, \tag{59}$$

$$Da^2\sum\mu_n\left(\frac{r}{a}\right)^n=\kappa\sum(n-2)(n+3)\mu_n\left(\frac{r}{a}\right)^{n-2}-12\beta a^4\sum B_n\left(\frac{r}{a}\right)^{n+2}, \tag{60}$$

in which we can write L_2^0, L_2^{2c} and L_2^{2s} in a form of series by applying the boundary conditions that $\xi_2=\xi_2^{2c}=\xi_2^{2s}=0$ at $r=a$. Eliminating L_2^0, L_2^{2c} and L_2^{2s} from (54), (55) and (56), they become

$$D\rho_0\sum C_n\left(\frac{r}{a}\right)^n=(4\pi a^2)^{-1}\frac{2}{3}S_1\sum na_n\left(1-\left(\frac{r}{a}\right)^{n-2}\right)+\rho_0\gamma\sum\frac{\nu_n}{n(n+5)}\left(\left(\frac{r}{a}\right)^n-1\right), \tag{61}$$

$$D\rho_0\sum A_n\left(\frac{r}{a}\right)^n=(4\pi a^2)^{-1}2T_4\sum\frac{a_n}{n+5}\left(\left(\frac{r}{a}\right)^n-1\right)-\frac{2}{3}\rho_0\omega\sum B_n\left((n+3)\left(\frac{r}{a}\right)^n-n\right)+\rho_0\gamma\sum\frac{\lambda_n}{n(n+5)}\left(\left(\frac{r}{a}\right)^n-1\right), \tag{62}$$

$$D\rho_0\sum B_n\left(\frac{r}{a}\right)^n=-(4\pi a^2)^{-1}2T_3\sum\frac{a_n}{n+5}\left(\left(\frac{r}{a}\right)^n-1\right)+\frac{2}{3}\rho_0\omega\sum A_n\left((n+3)\left(\frac{r}{a}\right)^n-n\right)+\rho_0\gamma\sum\frac{\mu_n}{n(n+5)}\left(\left(\frac{r}{a}\right)^n-1\right). \tag{63}$$

By equating the coefficients of the corresponding terms of both the sides of (57), (58), (59), (60), (61), (62) and (63), we obtain

$$Da_0-10(4\pi\sigma a^2)^{-1}a_2=-6S_1C_0, \tag{64}$$

$$Da_2-28(4\pi\sigma a^2)^{-1}a_4=-\frac{42}{5}S_1C_2-\frac{216}{5}(T_4A_0-T_3B_0), \tag{65}$$

$$\nu_0=0, \tag{66}$$

$$Da^2\nu_2=14\kappa\nu_4-12\beta a^4C_0, \tag{67}$$

$$\lambda_0=0, \tag{68}$$

$$Da^2\lambda_2=14\kappa\lambda_4-12\beta a^4A_0, \tag{69}$$

$$\mu_0=0, \tag{70}$$

$$Da^2\mu_2=14\kappa\mu_4-12\beta a^4B_0, \tag{71}$$

$$D\rho_0C_0=\frac{8}{3}(4\pi a^2)^{-1}S_1a_4-\rho_0\gamma\left(\frac{\nu_2}{14}+\frac{\nu_4}{36}\right), \tag{72}$$

$$D\rho_0C_2=-\frac{8}{3}(4\pi a^2)^{-1}S_1a_4+\rho_0\gamma\frac{\nu_2}{14}, \tag{73}$$

$$D\rho_0 C_4=\rho_0\gamma\frac{\nu_4}{36}\ , \tag{74}$$

$$D\rho_0 A_0=-2(4\pi a^2)^{-1}T_4\left(\frac{a_2}{7}+\frac{a_4}{9}\right)-\frac{2}{3}\rho_0\omega(3B_0-2B_2-4B_4)$$
$$-\rho_0\gamma\left(\frac{\lambda_2}{14}+\frac{\lambda_4}{36}\right)\ , \tag{75}$$

$$D\rho_0 A_2=2(4\pi a^2)^{-1}T_4\frac{a_2}{7}-\frac{10}{3}\rho_0\omega B_2+\rho_0\gamma\frac{\lambda_2}{14}\ , \tag{76}$$

$$D\rho_0 A_4=2(4\pi a^2)^{-1}T_4\frac{a_4}{9}-\frac{14}{3}\rho_0\omega B_4+\rho_0\gamma\frac{\lambda_4}{36}\ , \tag{77}$$

$$D\rho_0 B_0=2(4\pi a^2)^{-1}T_3\left(\frac{a_2}{7}+\frac{a_4}{9}\right)+\frac{2}{3}\rho_0\omega(3A_0-2A_2-4A_4)-\rho_0\gamma\left(\frac{\mu_2}{14}+\frac{\mu_4}{36}\right)\ , \tag{78}$$

$$D\rho_0 B_2=-2(4\pi a^2)^{-1}T_3\frac{a_2}{7}+\frac{10}{3}\rho_0\omega A_2+\rho_0\gamma\frac{\mu_2}{14}\ , \tag{79}$$

$$D\rho_0 B_4=-2(4\pi a^2)^{-1}T_3\frac{a_4}{9}+\frac{14}{3}\rho_0\omega A_4+\rho_0\gamma\frac{\mu_4}{36}\ , \tag{80}$$

where the coefficients whose subscripts are larger than 4 are ignored. It is easily seen that the coefficients with odd n vanish.

In addition to the above equations, we have

$$3a_0+5a_2+7a_4=0\ , \tag{81}$$

which is deduced from the condition that the magnetic field is continuous at $r=a$. Zero conductivity is assumed outside the core.

At $r=a$, $u=0$ is also required, so that we have

$$\lambda_0+\lambda_2+\lambda_4=0\ , \tag{82}$$
$$\mu_0+\mu_2+\mu_4=0\ , \tag{83}$$
$$\nu_0+\nu_2+\nu_4=0\ . \tag{84}$$

The equations from (64) to (84) are regarded as the simultaneous equations for a_0, a_2, a_4, A_0, A_2, A_4, B_0, B_2, B_4, C_0, C_2, C_4, λ_0, λ_2, λ_4, μ_0, μ_2, μ_4, ν_0, ν_2 and ν_4.

Since these equations are too complicated, we shall make some simplifications on the basis of the following physical considerations.

According to Bullard and Gellman[12], the T_2^0 magnetic field would be very large in the earth's core amounting to some 400 *gauss*, while the S_1^0 field would amount to only a few *gauss*. The T_2^{2c} and T_2^{2s} fields would be of intermediate intensity, probably amounting to the

order of 10 *gauss*.

For an order-of-magnitude estimate, we may therefore put

$$\left.\begin{aligned} &T_3=T_4=T\ , \\ &S_1=0\ . \end{aligned}\right\} \tag{85}$$

In that case, the simultaneous equations can be devided into the systems for C_n's and ν_n's and for a_n's, A_n's, B_n's, λ_n's and μ_n's. Only the latter should be considered here. We thus see that there is no coupling between the time-dependent S_1^0 magnetic field and the S_2^0 motion, though a coupling still exists between the S_2^0 motion and the θ_2 thermal field.

If we assume $\sigma=10^{-6}\ e.m.u.$ which is usually taken for the electrical conductivity in the earth's core, $(4\pi\sigma a^2)^{-1}$ amounts to $6.5\times10^{-13}\ sec^{-1}$. Meanwhile, supposing a 100-*year* period variation which may be regarded as one of the typical periods of secular variations, the modulus of D becomes $2.0\times10^{-9}\ sec^{-1}$. We therefore see that, for usual secular variations, the first term of the lefthand-side of (65) is much larger than the second term. We may disregard the second term in this case. This conclusion is based on the fact that the decay of magnetic field due to Joule loss in a conductor of large dimension such as the earth's core is very slow, so that we may treat the core as a perfect conductor.

A similar discussion can be applied to equations (67), (69) and (71). In the earth's core, the thermometric conductivity has been estimated at $0.06\ cm^2sec^{-1}$ from the supposed specific heat ($0.16\ cal/gm°C$) and the thermal conductivity ($0.10\ cal/cm°C\ sec$). Hence we have $\kappa a^{-2}=5\times10^{-19}\ sec^{-1}$ which is much smaller than the modulus of D for usual secular variations. We thus see that the rate of thermal conduction is extremely small in the earth's core. The first terms of the righthand-sides of (67), (69) and (71) can be safely ignored.

In the light of the above discussion, the equations from (64) to (84) can be simplified as

$$\left.\begin{aligned} &a_0=0\ , \\ &5a_2+7a_4=0\ , \\ &Da_2=-\frac{216}{5}T(A_0-B_0)\ , \\ &D\rho_0A_0=-2(4\pi a^2)^{-1}T\left(\frac{a_2}{7}+\frac{a_4}{9}\right)-\frac{2}{3}\rho_0\omega(3B_0-2B_2-4B_4)-\rho_0\gamma\left(\frac{\lambda_2}{14}+\frac{\lambda_4}{36}\right), \\ &D\rho_0A_2=2(4\pi a^2)^{-1}T\frac{a_2}{7}-\frac{10}{3}\rho_0\omega B_2+\rho_0\gamma\frac{\lambda_2}{14}\ , \end{aligned}\right\}$$

$$
\left.\begin{aligned}
&D\rho_0 A_4=2(4\pi a^2)^{-1}T\frac{a_4}{9}-\frac{14}{3}\rho_0\omega B_4+\rho_0\gamma\frac{\lambda_4}{36}\ ,\\
&D\rho_0 B_0=2(4\pi a^2)^{-1}T\left(\frac{a_2}{7}+\frac{a_4}{9}\right)+\frac{2}{3}\rho_0\omega(3A_0-2A_2-4A_4)-\rho_0\gamma\left(\frac{\mu_2}{14}+\frac{\mu_4}{36}\right)\ ,\\
&D\rho_0 B_2=-2(4\pi a^2)^{-1}T\frac{a_2}{7}+\frac{10}{3}\rho_0\omega A_2+\rho_0\gamma\frac{\mu_2}{14}\ ,\\
&D\rho_0 B_4=-2(4\pi a^2)^{-1}T\frac{a_4}{9}+\frac{14}{3}\rho_0\omega A_4+\rho_0\gamma\frac{\mu_4}{36}\ ,\\
&\lambda_0=0\ ,\\
&\lambda_2+\lambda_4=0\ ,\\
&D\lambda_2=-12\beta a^2 A_0\ ,\\
&\mu_0=0\ ,\\
&\mu_2+\mu_4=0\ ,\\
&D\mu_2=-12\beta a^2 B_0\ .
\end{aligned}\right\}
\tag{86}
$$

Since (86) is a set of homogeneous equations, by eliminating a_0, a_2, a_4, A_0, A_2, A_4, B_0, B_2, B_4, λ_0, λ_2, λ_4, μ_0, μ_2 and μ_4, we can obtain the characteristic equation for D as follows;

$$
\begin{vmatrix}
D\left\{\frac{5}{216}-\frac{4}{7}\tau_1^{-2}\left(\frac{1}{D^2+\{(10/3)\omega\}^2}-\frac{5/9}{D^2+\{(14/3)\omega\}^2}\right)\right\} & \tau_2^{-2}\left(\frac{1}{14}\frac{D-(10/3)\omega}{D^2+\{(10/3)\omega\}^2}-\frac{1}{36}\frac{D-(14/3)\omega}{D^2+\{(14/3)\omega\}^2}\right) & -\tau_2^{-2}\left(\frac{1}{14}\frac{D+(10/3)\omega}{D^2+\{(10/3)\omega\}^2}-\frac{1}{36}\frac{D+(14/3)\omega}{D^2+\{(14/3)\omega\}^2}\right)\\
-\frac{2}{7}\tau_1^{-2}\left(\frac{D+(10/3)\omega}{D^2+\{(10/3)\omega\}^2}-\frac{5}{9}\frac{D+(14/3)\omega}{D^2+\{(14/3)\omega\}^2}\right) & D\left\{12-\tau_2^{-2}\left(\frac{1}{14}\frac{1}{D^2+\{(10/3)\omega\}^2}-\frac{1}{36}\frac{1}{D^2+\{(14/3)\omega\}^2}\right)\right\} & \omega\tau_2^{-2}\left(\frac{1}{14}\frac{10/3}{D^2+\{(10/3)\omega\}^2}-\frac{1}{36}\frac{14/3}{D^2+\{(14/3)\omega\}^2}\right)\\
\frac{2}{7}\tau_1^{-2}\left(\frac{D-(10/3)\omega}{D^2+\{(10/3)\omega\}^2}-\frac{5}{9}\frac{D-(14/3)\omega}{D^2+\{(14/3)\omega\}^2}\right) & -\omega\tau_2^{-2}\left(\frac{1}{14}\frac{10/3}{D^2+\{(10/3)\omega\}^2}-\frac{1}{36}\frac{14/3}{D^2+\{(14/3)\omega\}^2}\right) & D\left\{12-\tau_2^{-2}\left(\frac{1}{14}\frac{1}{D^2+\{(10/3)\omega\}^2}-\frac{1}{36}\frac{1}{D^2+\{(14/3)\omega\}^2}\right)\right\}
\end{vmatrix}=0\ ,
\tag{87}
$$

where

$$
\left.\begin{aligned}
&\tau_1=\frac{a}{V_H}\ , \qquad V_H=\frac{T}{\sqrt{4\pi\rho_0}}\ ,\\
&\tau_2=\frac{a}{V_T}\ , \qquad V_T=\sqrt{\beta\gamma}\,a^2\ ,
\end{aligned}\right\}
\tag{88}
$$

V_H, the velocity of the Alfvén wave, amounts to only $0.9\,cm/sec$, so that τ_1, the time required for the wave to be propagated over a distance equal to the core's radius, becomes $3.9\times10^8\,sec$. From (15), γ is estimated at $1.3\times10^{-12}\,sec^{-2}{}^\circ C^{-1}$ provided $\alpha=4.5\times10^{-6}{}^\circ C^{-1}$ as given by Bullard and Gellman[12] is taken for granted. If the temperature difference between the top and bottom of the core is taken at $450^\circ C$ as has been also given by Bullard and Gellman[12], we obtain $\beta a^2=450^\circ C$ from which we see $V_T=8.4\times10^3\,cm/sec$ and $\tau_2=4.2\times10^4\,sec$.

Since $\tau_1 \gg \tau_2$ and $\tau_1 \gg \omega^{-1}$ ($\omega = 7.5 \times 10^{-5}\, sec^{-1}$), we see that the terms of the second and third columns in the second row of the determinant are very much larger than the term of the first column so long as the modulus of D is assumed to be smaller than $10^{-5}\, sec^{-1}$, that is, the period of variation is larger than a few tens of days. The situation is the same for the third row. We may therefore assume, for a crude approximation, that the first terms in the second and third rows are zero. In that case, the characteristic equation becomes

$$\frac{5}{216} - \frac{4}{7}\tau_1^{-2}\left(\frac{1}{D^2+\{(10/3)\omega\}^2} - \frac{5/9}{D^2+\{(14/3)\omega\}^2}\right) = 0 \qquad (89)$$

or

$$D^2\left\{12 - \tau_2^{-2}\left(\frac{1}{14}\frac{1}{D^2+\{(10/3)\omega\}^2} - \frac{1}{36}\frac{1}{D^2+\{(14/3)\omega\}^2}\right)\right\}^2$$
$$+\omega^2\tau_2^{-4}\left(\frac{1}{14}\frac{10/3}{D^2+\{(10/3)\omega\}^2} - \frac{1}{36}\frac{14/3}{D^2+\{(14/3)\omega\}^2}\right)^2 = 0\,. \qquad (90)$$

Equation (89), that has been already obtained in one of the previous papers[6], gives eigen-periods of several *hours*. We see that the oscillation is mainly caused by the coupling between the S_2^{2c} and S_2^{2s} motions through the rotation, the existence of steady magnetic field and temperature gradient being not important in this case. In the above, however, we have been looking for eigen-periods larger than scores of days, so that the solutions of (89) are not important here.

On the assumption that the modulus of D is much smaller than ω, the eigen-values of (90) are obtained as

$$D^2 = -0.97 \times 10^{-16}\, sec^{-2} \text{ or } D = \pm i 0.98 \times 10^{-8}\, sec^{-1}\,,$$

which results in an eigen-period of 20 *years*. It is of interest that a period which does not differ much from those of actual secular variations is obtained, though the way of solving the equations is extremely crude. Attention should be paid, however, to the fact that no steady magnetic field appears in (90), so that the oscillation of this sort is caused by the coupling between fluid motion and heat transfer only. The time-dependent magnetic field is caused by the induction by the fluid motion thus excited in the presence of the steady magnetic field.

No detailed study of the eigen-functions for s, ξ_2^{2c}, ξ_2^{2s}, θ_2^{2c} and θ_2^{2s} is worked out. However, the discussion in the previous paper[8] can be applied to such a study. In order to have a secular variation of the S_1^0 magnetic field, 1000 *gammas* in amplitude at the pole, the amplitude

of the thermal fields would be of the order of $10^{-4}°C$.

6. Concluding remarks

It is found that an oscillation having a period of 20 *years* is caused by the coupling between fluid motions and thermal fields in the earth's core. The oscillation accompanies a time-dependent magnetic field of the S_1^0 type. Since the eigen-period is derived from a crude treatment of the simultaneous equations for electromagnetism, hydrodynamics and heat transfer, its value may be likely to be subjected to a large change provided a more exact solution can be obtained. It would be possible to make a more rigorous study with help of an automatic computor.

In spite of an extremely crude treatment, however, the point that the possibility of thermo-magneto-hydrodynamic oscillations is proved in the earth's core seems of interest and importance. We might be able to believe that some parts of the geomagnetic secular variations, which cannot be explained as free oscillations of magneto-hydrodynamic origin, are caused by the free oscillations considered in this paper.

---

27. 地球核内の熱電磁流体振動

地震研究所　力　武　常　次

地磁気ダイナモに重畳する微小振幅の磁場，流体運動および温度場の相互結合を近似的に調べた．その結果，S_1^0 磁場については周期約 20 年程度の振動が起る可能性が見出された．地磁気永年変化の一部はこのようなメカニズムで発生することが可能であると推測される．

BULLETIN OF THE EARTHQUAKE
RESEARCH INSTITUTE
Vol. 37 (1959), pp. 423-431

28. *Geophysical Evidence of the Olivine-spinel Transition Hypothesis in the Earth's Mantle.*

By Tsuneji RIKITAKE,

Earthquake Research Institute.

(Read June 23, 1959.—Received June 23, 1959.)

Summary

Assuming olivine-spinel transition of Mg_2SiO_4 at the depth of 400 *km* in the earth, the difference in free energy between substances composing the upper and lower mantle is estimated. The difference obtained here is approximately the same as that deduced by Ringwood from experimental results.

The influence of the transition on the electrical conductivity is also studied. The steep increase of the electrical conductivity at the depth as inferred from the studies of geomagnetic variations seems to be justified by the transition hypothesis.

1. Introduction

A discontinuity of seismic wave velocities, density and electrical conductivity has been suggested through geophysical investigations at a depth of about 400 *km* in the earth's mantle. One of the possible causes of such a discontinuity might be a polymorphic inversion in olivine as has been suggested by Bernal[1] and Jeffreys[2]. On the basis of the fact that Mg_2GeO_4, which is closely related to Mg_2SiO_4, has both olivine and spinel structures, Bernal suggested that olivine-spinel transition of Mg_2SiO_4 might occur at high pressures. In that case, an increase in the density would be necessarily expected.

No direct proof of Bernal's hypothesis has been given. It is also not possible to produce spinel-type Mg_2SiO_4 artificially. However, a method of calculating the pressure required to cause Mg_2SiO_4 invert from the olivine to the spinel structure has been recently advanced by Ringwood[3]. He studied experimentally Ni_2GeO_4—Mg_2SiO_4 spinel solid

1) J. D. BERNAL, *Observatory*, **59** (1936), 268.
2) H. JEFFREYS, *The Earth* 3rd ed., (1952), Cambridge Univ. Press.
3) A. E. RINGWOOD, *Geochimica et Cosmochimica*, **13** (1958), 303.

solutions. It was found that Ni_2GeO_4, which has a spinel structure, dissolves 9 per cent of Mg_2SiO_4. A thermodynamical theory of the relationship between the amount of solid solution between Mg_2SiO_4 and Ni_2GeO_4 and the free energy of transition between olivine and spinel Mg_2SiO_4 was also developed. Combining the experimental results with the theory, Ringwood found that the molar free energy of transition between olivine and spinel Mg_2SiO_4 amounts to $70,000 \pm 10,000$ *Joule/mole* at 1500° *C*. The lattice constant of spinel-type Mg_2SiO_4 was also estimated at 7.99 $\mathring{A}$ by extraporation.

It seems to the writer that Ringwood's study has an important bearing on various geophysical problems in the earth's mantle because the energy of the transition and the lattice constant of Mg_2SiO_4 spinel deduced by Ringwood may give some clue to check the physical quantities inferred from other geophysical methods. The purpose of this paper is to estimate the internal energies and electrical conductivities of the substances composing the upper and lower mantle. These quantities will be examined from the results obtained by Ringwood.

In Section 1, the difference in Gibbs free energy between the substances composing the upper and lower mantle is estimated with the aid of appropriate thermodynamical relations together with the density and pressure distributions. The difference in internal energy between both the substances at zero pressure and temperature is also obtained. These values will be criticized by Ringwood's result. On assuming the lattice constant for the spinel Mg_2SiO_4 which was obtained by Ringwood, the difference in the activation energy for electrical conduction between olivine and spinel Mg_2SiO_4 is estimated in Section 2 and is discussed in relation to the distribution of electrical conductivity which has been obtained by the writer from analyses of geomagnetic variations.

Wada[4] has published a paper in which it is concluded by comparing the lattice energies for both the structures that the transition between olivine and spinel Mg_2SiO_4 would not be possible. Since the difference in lattice energy is much smaller than the lattice energies themselves, small errors in the estimation of lattice energies would seriously affect the conculsion, though it has been successful to discuss the stability of certain structures in this way for a number of simple crystals such as AgCl, CuCl and so forth. Accurate estimate of lattice energies of complicated crystals such as Mg_2SiO_4 will be therefore of great difficulty, so that it might not be impossible to suppose that Wada's conclusion is

4) T. WADA, *Zisin*, **11** (1958), 55. (in Japanese)

a little modified. All through this paper, the olivine-spinel transition in the earth's mantle is taken for granted. The advantage of admitting the hypothesis is discussed from the two points mentioned in the last paragraph.

2. Gibbs free energies in the upper and lower mantle

On the assumption that the olivine and spinel Mg_2SiO_4, which compose respectively the upper and lower mantle, are at equilibrium at the depth of 400 *km*, the difference in free energy will be estimated from the distributions of density and pressure and their extraporations.

Gibbs free energy at temperature (absolute) T and pressure P can be written as

$$\Psi(T, P)=\int_0^P V(T, P)dP+\Psi(T, 0)\ , \qquad (1)$$

where V denotes the volume. V is given by

$$V(T, P)=V(0, P)(1+\alpha T)\ . \qquad (2)$$

The volume expansion coefficient α is in general dependent on pressure amounting to some $10^{-5}/°C$. For an order-of-magnitude estimate, however, we may assume that the term αT can be ignored for the reason mentioned below. If we assume $\alpha=2.5\times10^{-5}/°C$ as has been given by Birch[5] for olivine and $T=1{,}800°\ K$ which has been suggested by many geophysicists for the part of mantle 400$\sim$500 *km* deep, αT amounts to only 0.05 which may be ignored for the present estimate. Even if the possible ranges of α and T are taken into account, it does not seem likely that αT exceeds 0.1, so that the following estimate would be safely taken within a range of accuracy of 10 per cent.

For the part of the mantle above the 20° discontinuity, the density and pressure which have been obtained by Bullen[6] can be applied directly. In so far as we assume $V(T, P)=V(0, P)$ as stated above, the integral term of the righthand-side of (1) can be numerically calculated on the basis of Bullen's distribution. The upper limit of the integral is to be taken at the pressure just above the discontinuity.

For the substance composing the mantle deeper than the discontinuity, however, it is not possible to apply Bullen's distribution. In this case, in order to carry out the integration in (1), we have to

5) F. BIRCH, *Journ. Geophys. Res.*, **57** (1952), 227.
6) K. E. BULLEN, *An Introduction to the Theory of Seismology*, (1947).

know the hypothetical distributions of density and pressure which should have been observed in the upper part of the mantle if the transition did not occur. For the purpose of a crude estimate, we may extraporate the approximately linear distribution of the density as has been shown by Bullen below the depth of 800～900 *km*. In that case, the densities at depths of 0, 100, 200, 300 and 400 *km* are obtained to be 4.00, 4.08, 4.16, 4.24 and 4.32 gm/cm^3 respectively.

The density at zero pressure obtained by extraporation is almost 20 per cent larger than that of olivine Mg_2SiO_4. Ringwood[3] has suggested that the increase in density caused by the olivine-spinel transition would be 11 ± 3 per cent. The difference might be caused by the simple extraporation. The influence of the difference will be discussed later.

It is not exactly known what the hypothetical distribution of pressure will be. For the sake of simplicity, the pressure distribution for this case is assumed to be the same as Bullen's one above the discontinuity. In any case, the upper limit of the integration is to be the same as that for the upper mantle. Since the distribution of pressure is almost linear, no large error will be introduced by the procedure.

Since the two phases are assumed to be at equilibrium at the level of the discontinuity, we have

$$\int_0^P V_1(T, P)dP+\Psi_1(T, 0)=\int_0^P V_2(T, P)dP+\Psi_2(T, 0) ,$$

which can be rewritten as

$$\Psi_2(T, 0)-\Psi_1(T, 0)=\int_0^P V_1(T, P)dP-\int_0^P V_2(T, P)dP , \qquad (3)$$

where subscripts 1 and 2 denote respectively the upper and lower mantle. Actual calculation based on the assumptions in the above gives

$$\Psi_2(T, 0)-\Psi_1(T, 0)=0.65\times10^{10}\ erg/gm.$$

By taking into account the fact that the molecular weight of Mg_2SiO_4 amounts to 140.7, the difference in the Gibbs free energy becomes

$$\Psi_2(T, 0)-\Psi_1(T, 0)=90{,}000\ Joule/mole \qquad (4)$$

at zero pressure. The figure becomes a little smaller by taking into consideration the fact that the extraporated density is slightly higher than that supposed by experimental results.

This value should be compared to the one which has been estimated

by Ringwood on the basis of experimental results. He gave $70,000 \pm 10,000$ *Joule/mole* for olivine-spinel transition of Mg_2SiO_4 at $1,500°C$. Although the estimate attempted here is very crude, it is interesting that the present and Ringwood's values are about the same. It might be therefore said that the olivine-spinel transition hypothesis is supported by thermodynamical theory based on the distributions of density and pressure deduced from seismology.

In the next place, the difference in internal energy between spinel and olivine Mg_2SiO_4 at zero pressure and temperature can be estimated from the above result. At zero pressure, Helmholtz free energy is defined by

$$F=\int_0^T C_v dT - T\int_0^T \frac{C_v}{T} dT + U_0 , \qquad (5)$$

where C_v and U_0 denote respectively specific heat at constant volume and internal energy at zero temperature. With subscripts 1 and 2, by which we designate olivine and spinel, the equilibrium condition leads to

$$U_{0,2} - U_{0,1} = F_2 - F_1 = -\int_0^T (C_{v,2} - C_{v,1}) dT + T\int_0^T \frac{C_{v,2} - C_{v,1}}{T} dT . \qquad (6)$$

As has been pointed out by Birch[5], C_v approaches 0.3 *cal/deg gm* for most of the rock-forming silicates at temperatures of the order of $1,000°C$. Although it is not possible to know exact values of C_v for both the olivine and spinel Mg_2SiO_4, it seems hardly likely that $C_{v,2} - C_{v,1}$ exceeds 0.03 *cal/deg gm* for a temperature range between several hundred degrees in centigrade and $1,500°C$. Below the Debye temperature, which is a few hundred degrees in centigrade, $C_{v,2} - C_{v,1}$ takes much smaller values. For an order-of-magnitude estimate, we may assume $C_{v,2} - C_{v,1} = 0.03 cal/deg\ gm$ between $0° \sim 1,800°K$. In that case, by assuming that the equilibrium is attained at $1,800°K$, the integral terms of (6) can be calculated as 6,000 *Joule/mole*.

Since $F_2 - F_1$ has been estimated by Ringwood at 70,000 *Joule/mole* and 90,000 *Joule/mole* by the present writer, the influence of the integral terms is less than 10 per cent. For a crude estimation of the difference in internal energy at zero pressure and temperature, therefore, we may take $U_{0,2} - U_{0,1} = 70,000$ *Joule/mole*.

3. Activation energies for electric conduction in the upper and lower mantle

It has been shown by Chapman[7], Price[7),8)], Lahiri[8)] and Rikitake[9)] that the electrical conductivity increases enormously at a depth of several hundred kilometers within the earth. According to Rikitake, the electrical conductivity increases discontinuously at the depth of 400 *km* from 10^{-15} *e.m.u.* to 10^{-12} *e.m.u.*

Applying the theory of ionic crystals to the electric conduction in the mantle, the conductivity σ is described by

$$\sigma=\sigma_0 e^{-\epsilon/kT} \qquad (7)$$

where ϵ, k and T denote respectively the activation energy, Boltzmann's constant and absolute temperature. With suitable considerations concerning the effect of pressure, the distribution of temperature can be approximately obtained from the distribution of the electrical conductivity. Rikitake[10)] has made this sort of estimate of temperature distribution in the earth down to a depth of 1,500 *km*. In that study, it is required that the activation energy of the substance composing the layer between the top of the mantle and a depth of 400 *km* is different from that below this level, otherwise a discontinuity must occur in the temperature distribution. The activation energy for the upper part amounts to 2.3 *eV* at zero pressure and temperature, while that below the depth of 400 *km* amounts to 1.8 *eV*.

Runcorn and Tozer[11)] have also concluded that a considerable decrease in the activation energy would be necessary in some region of the mantle on the basis of their study on the electrical conductivity of olivine at high temperatures and pressures.

The purpose of this section is to estimate to what extent the activation energy will be affected by the olivine-spinel transition by applying the theory of lattice defect of ionic crystals.

Let us consider a Schottky-type lattice defect due to vacancies of Mg^{++} and O^{--}. The activation energy is then given by

$$\epsilon=\tfrac{1}{2}W+U \qquad (8)$$

where W and U are respectively the energy required to make a lattice

7) S. CHAPMAN and A. T. PRICE, *Phil. Trans. Roy. Soc. London A*, **229** (1930), 427.
8) B. N. LAHIRI and A. T. PRICE, *Phil. Trans. Roy. Soc. London A*, **237** (1939), 509.
9) T. RIKITAKE, *Bull. Earthq. Res. Inst.*, **28** (1950), 45, 219, 263; **29** (1951), 61.
10) T. RIKITAKE, *Bull. Earthq. Res. Inst.*, **30** (1952), 13.
11) S. K. RUNCORN and D. C. TOZER, *Ann. Géophys.*, **11** (1955), 98.

defect and the potential energy which must be exceeded by thermal energy of ions in motion. The energy required to make a lattice defect in ionic crystals is given by

$$W=U^{+}+U^{-}-E \tag{9}$$

in which U^{+}, U^{-} and E denote respectively the energies required to take off a positive ion, to take off a negative one and to make a pair of ions.

By taking into account the polarization energy due to the electric field in ion vacancies, U^{+} and U^{-} are approximately given as

$$U^{+}=E-\frac{Z_{Mg}e^{2}}{q^{+}r}(1-1/\kappa)\,, \tag{10}$$

$$U^{-}=E-\frac{Z_{O}e^{2}}{q^{-}r}(1-1/\kappa)\,, \tag{11}$$

in which Z_{Mg}, Z_{O}, e and κ denote respectively number of electric charge of Mg^{++}, that of O^{--}, charge of electron and dielectric constant, while $q^{+}r$ and $q^{-}r$ denote the effective radii of vacancies of positive and negative ions. If r denotes the interionic distance, it is known that $q^{+}\sim 0.6$ and $q^{-}\sim 0.9$.

It is not possible to estimate U in (8) exactly. Since positive ions seem likely to contribute in the main to the conductivity of rocks as experimentally shown by Coster[12], however, we may assume $U=U^{+}$ for a crude approximation. In that case, putting $Z_{Mg}=Z_{O}=2$, the activation energies for olivine and spinel may be written as

$$\text{olivine:}\quad \epsilon_{1}=\tfrac{3}{2}E_{1}-\left(\frac{3}{q^{+}}+\frac{1}{q^{-}}\right)\frac{e^{2}}{2r_{1}}(1-1/\kappa_{1})\,, \tag{12}$$

$$\text{spinel:}\quad \epsilon_{2}=\tfrac{3}{2}E_{2}-\left(\frac{3}{q^{+}}+\frac{1}{q^{-}}\right)\frac{e^{2}}{2r_{2}}(1-1/\kappa_{2})\,. \tag{13}$$

We further assume $\kappa_{1}=\kappa_{2}=5$, $q^{+}=0.6$ and $q^{-}=0.9$. As to the distance between Mg and O atoms, it has been known that $r_{1}=2.078$ Å for olivine $Mg_{2}SiO_{4}$, while, for spinel $Mg_{2}SiO_{4}$ which is cubic, the lattice constant obtained by Ringwood, 7.99 Å say, leads to $r_{2}=1.998$ Å. Using these values, the difference in the activation energy becomes

$$\epsilon_{2}-\epsilon_{1}=1.5(E_{2}-E_{1})-0.7 \tag{14}$$

in units of eV.

In the next place, we have to calculate $E_{2}-E_{1}$. According to

12) H. P. Coster, *Mon. Not. R. Astron. Soc. Geophys. Suppl.*, **5** (1949), 193.

Wada's calculation[4] of lattice energy of spinel Mg_2SiO_4, the total lattice energy amounts to 168 eV at zero pressure and zero temperature. Meanwhile, it is also shown that the energy required to make a pair of Mg^{++} and O^{--} ions amounts approximately to 35.8 eV. We therefore see that the energy required to make an ion pair amounts to 21 per cent of the total lattice energy. For an order-of-magnitude estimate, the same proportion may be applied to olivine Mg_2SiO_4. The difference in internal energy between Mg_2SiO_4 of both the types has been thoroughly discussed in the last section. The difference in energy required to make an ion pair may be obtained by taking 21 per cent of 70,000 *Joule/mole*. This consideration leads to

$$E_2 - E_1 = 0.15 \ eV \ , \tag{15}$$

whence, from (14), we see

$$\epsilon_2 - \epsilon_1 = -0.5 \ eV \ . \tag{16}$$

Although the above estimate is based on various approximations, it is of interest that the activation energy would decrease by the transition from olivine to spinel. The amount of decrease estimated is in good agreement with the value supposed by the present writer previously. It may be said, then, that the steep increase in electrical conductivity below the depth of 400 *km* as inferred from studies of geomagnetic variations is in harmony with the hypothetical olivine-spinel transition in the mantle.

4. Discussion and concluding remarks

It has been shown in Section 2 that, so long as we admit the olivine-spinel transition of Mg_2SiO_4 in the earth's mantle, the difference in free energy between the two phases can be estimated from physical quantities such as density and pressure, though some extraporations are required to make actual calculation. Since the extraporations are not very reliable, the difference in free energy obtained here is not accurate. However, it is of interest that the energy difference thus deduced is about the same as that obtained by Ringwood on an experimental basis.

In the real earth, the chemical composition is likely to change gradually with depth. Especially, it is widely believed that such a change is highly likely at the depths between 400 and 900 *km*. The effect of Fe_2SiO_4 would be specially important in that part of the mantle, though no account has been taken of such an effect in this paper.

This point should be improved in the future.

It is highly important to see whether or not the olivine-spinel transition hypothesis accounts for the increase in the electrical conductivity at the depth of 400 *km*. The calculation of the conductivity, based on the theory of ionic crystals, has proved that the hypothesis approximately harmonizes with the electrical state. Although the calculation seems not very accurate, it is of interest and importance that the mechanical and electrical properties of the earth's mantle can be interpreted from a unified view-point provided the olivine-spinel transition of Mg_2SiO_4 is assumed at the depth of 400 *km*.

In conclusion the writer thanks Dr. S. Akimoto for his kind help in the estimation of interionic distance.

---

28. 20° 不連続と電気的性質

地震研究所　力武常次

最近 Ringwood は，Ni_2GeO_4—Mg_2SiO_4 固溶体を調べ，地球中間層内に於て Mg_2SiO_4 がオリビンスピネル転移を起すことが可能であることを推論した．彼の研究によれば，転移に伴なう自由エネルギーの変化は 1,500°*C* に於て 70,000 ± 10,000 *Joule/mole*，密度変化は約 11%，スピネル Mg_2SiO_4 の格子常数は 7.99 *Å* となる．

本論文に於ては，深さ 400 *km* に於ける不連続面が，多方転移によつてできたものとして，その上部および下部を構成する物質の自由エネルギーの差を地震波速度分布による知識をもとにして，近似的に求め，90,000 *Joule/mole* という値を得た．計算の精度を考慮するならば，この値は Ringwood の値とよく一致しているといえよう．

つぎに，オリビンスピネル転移が電気的性質にどのような寄与をするかを，イオン結晶理論により，近似的に調べた。その結果電気伝導度に対する活性化エネルギーは 0.5 *eV* の減少をきたし，地磁気変化観測結果より推定されるように，電気伝導度がスピネル構造の発生に伴なつて，いちじるしく増大することがわかつた．したがつてオリビンスピネル転移仮説によつて，地下 400 *km* に於ける力学的および電気的不連続を統一的に解釈することができることになる．

BULLETIN OF THE EARTHQUAKE
RESEARCH INSTITUTE
Vol. 37 (1959), pp. 433-481

29. *Palaeomagnetic and Geologic Researches for the Volcanic Rocks around Lake Suwa. —Palaeomagnetic Researches for the Pliocene Volcanic Rocks in Central Japan (2)—*

By Kan'ichi MOMOSE,
Earthquake Research Institute;
and
Kunio KOBAYASHI and Tetsuo YAMADA,
Department of Geology, Shinshu University.

(Read April 22, 1958.—Received June 30, 1959.)

Summary

Palaeomagnetic research for Pliocene lava-flows of the Enrei formation in Central Japan supplied a lot of reliable evidence concerning palaeomagnetic variations in geologic times. It seems likely that the pole position might have migrated westward encircling the present position of the Earth's rotation axis through the whole time range of the Enrei formation.

The geomagnetic field might rather be stable only in the case when the dipole axis was close to the rotation axis, and the geomagnetic reversal might have taken place in an way unconnect with the rotation axis through the span of time when geomagnetic unstability was introduced by some causes.

It has become possible to infer the geologic age of various volcanic rocks of late Cenozoic times by means of palaeomagnetic considerations.

1. Introduction

In his preceding paper[1] the senior author presented his opinions about the geomagnetic variation in Younger Tertiary times based upon his rock-magnetic studies of various volcanic rocks in Central Japan. In that discussion, the results obtained from the Enrei formations were an important part of the available data for the confirmation of his conclusion. This is the second paper in which the authors are to refer to some more evidences found in the Enrei formations.

1) K. MOMOSE, *Jour. Geomagn. Geoelectr.*, **10** (1958), 12.

As was formerly reported, the senior author[2a, b] made for the first time in 1954 a notable finding that the magnetic polarization of the so-called "*Teppeiseki*" from a famous quarry at Fukuzawa-yama was reversed. Since that time, the two junior authors have been co-operating with the senior author in his field work and geologic considerations.

Lake Suwa (36°2′N. Lat.; 138°5′E. Long.) which is situated in the mountainous district of Central Japan, is thought to have originated from structural depression which might have taken during the Pleistocene. In the earliest days of geological research, Harada[3] expressed his opinion that Lake Suwa might originate from a huge crater perhaps of *Maar*. Apart from this sort of problematic opinion, we can find around Lake Suwa a complex of pyroclastic formations consisting of an enormous quantity of tuff-breccias and associate lava-flows over a wide extent perhaps of 200 Km^2. or more[4),5),6)]. It is a well-known fact that some lava-flows in the Enrei formation are markedly platy-jointed and are called "*Hira-ishi*" or "*Teppeiseki*" (the name signifies "*Iron-flagstone*"). Both features of jointed structures and remarkable lateral extension of lava-flows are dominant characteristics of andesites of the Enrei formation. Another peculiar feature of the Enrei formation is that water-deposited signs of tuffaceous parts are recognized lithologically in many places and especially in the upper part of the formation. The summit level of the upland consisting of the Enrei formation is therefore thought to be a depositional surface.

In the light of the results obtained from rock-magnetic researches, the traditional and conventional methods of interpretation which are concerned with the sequence of volcanism in this area need several revisions.

Leading articles which will be mentioned in the text are expressed briefly as following:

(1) According to observed magnetic polarization of rock samples, the age of the Enrei formation may be assigned to the Younger Pliocene.

(2) Calculated pole positions seem accordingly to record the feature

2a) T. NAGATA, S. AKIMOTO, S. UYEDA, K. MOMOSE, & E. ASAMI, *Jour. Geomagn. Geoelectr.*, **6** (1954), 182.

2b) K. MOMOSE, *Science* (*Kagaku*), **25** (1954), 257.

3) T. HARADA, (1888); *See Maumann, E.* (1893) *Pethermanns Mitt.*, **108**. Ergänzungsheft, 26.

4) N. YAMAZAKI, *Shinsai Yobo Chosakai Hokoku*, **20** (1898).

5) F. HOMMA, *Geology of Central Shinano, Kokon Shoin, Tokyo* (1931).

6) K. SAWAMURA & E. OWA, *Geological Map and its Explanatory Text* (1: 50,000), *Suwa sheet*; *Geol. Survey Japan* (1953).

of secular variations of geomagnetic field during the Younger Pliocene.

(3) The feature of secular variation of the geomagnetic field, may also afford a valid base of correlation for Pliocene chronology.

(4) The traditional method in which we have attempted to make correlations of various volcanic rocks based mainly upon their lithological characteristics, was recognized not to be a decisive one.

(5) By means of *AC*—demagnetization and some other treatments, it has been proved that a series of rock samples which maintains anomalously strong magnetism might have been given by lightning.

(6) Based upon geologic field evidences, no significant hiatus was recognized as intervening between Kirigamine Volcano and the Enrei formation. Although a slight transitional feature of lithology might be recognized among these volcanic rocks, the volcanic activity which have built Kirigamine Volcano should be referred to that of the final or later stage of the Enrei Volcanism.

(7) Kirigamine Volcano which has long been assigned as an example of shield volcanoes[7] may be a member of the Enrei formation and accordingly the necessity of origination of such a flat type of volcanic cone may easily be understood.

(8) Considering that the Enrei formation is to be Younger Pliocene in age and that the base level is averagely at an altitude less than 1,500 m, the following conclusion which offers a serious bearing on geomorphology of this area, may be introduced. The highest erosion surfaces which truncate the mountain ranges bordering the outer margin of the Enrei formation and which are at the level higher than 1,500 m might have originated since late Tertiary times or perhaps the late Miocene.

2. Labolatory Tests

1. *Examination of stabilities of rock magnetism*

In order to carry out reliable studies of palaeomagnetism, it is required to conduct close examinations[8] related to the stabilities of rock magnetism. Since the samples which the authors have treated were so many, it was hardly possible to test their stabilities by applying the full procedures proposed. Most samples have therefore been tested by making use of a slightly simplified method as described in the following.

(1) First, it is highly likely that the *R.N.R.M* (*Reverse N.R.M.*)

7) H. KUNO, *Volcano and Volcanic Rocks* (Tokyo 1954), *Iwanami, Tokyo.*

8) K. MOMOSE, *loc. cit.*, 1).

retained in rocks has long been under the influence of the geomagnetic field which is nearly opposite to it in direction. The fact that we still observe reversed magnetizations seems to indicate the stableness of the *R.N.R.M.* retained in rocks.

Secondly, it should be examined whether or not the *R.N.R.M.* is caused by self-reverse magnetization[9),10),11),12)]. For this purpose, several samples were heated up to 600°C in a non-magnetic electric oven and cooled in the geomagnetic field in order to observe the nature of *T.R.M.* All the samples thus treated show that their *T.R.M.* are of normal type indicating that their magnetic directions agree in every case with that of the geomagnetic field.

There still remains a slight possibility that the self-reversal mechanism of magnetization might once have affected the magnetism of our samples as was suggested by Kawai and others[13)], who have detected the existence of self-reversal mechanism originated from exsolution of magnetic rock-forming minerals. In this respect, however, the authors are unable to offer any plausible proof.

(2) The authors found in Central Japan many examples which might have been influenced by peculiar magnetizations due to thunderbolts. In order to recognize magnetizations of this kind, some of the samples were demagnetized by *AC*-demagnetization assay. This way of demagnetization is also useful for the detection of occurrence of any unstable component (i.e. *I.R.M.*).

(3) The value of Jn/JTc

On the assumption that the intensities of geomagnetic field in the past is roughly comparable with that of the present, the samples of which the values of Jn/JTc are within a range from 0.2 to 1.0 are treated here.

From the above-mentioned standpoint, the tests made on rock samples from various localities will be discussed in the following. The following notations are adopted in the figures and tables.

Jn ·····intensity of natural remanent magnetism.
JTc ·····intensity of thermo-remanent magnetism.
Jn-T ·····mode of thermal demagnetization of Jn by heating up to T and cooling down to T_0 in non-magnetic space (T_0: room temperature).

9) T. NAGATA, S. UYEDA, and S. AKIMOTO, *Jour. Geomagn. Geoelectr.*, **4** (1952), 22.
10) T. NAGATA, S. UYEDA, and S. AKIMOTO, and N. KAWAI, *ibid.*, **4** (1952), 102.
11) T. NAGATA, S. AKIMOTO, and S. UYEDA, *ibid.*, **5** (1953), 168.
12) S. UYEDA, *Jap. Jour. Geophys.*, **2** (1958), 1.
13) N. KAWAI, S. KUME, and S. SASAJIMA, *Proc. Jap. Acad.*, **30** (1954), 588.

JTc-T ····mode of thermal demagnetization of JTc by heating up to T and cooling down to T_0 in non-magnetic space (T_0 : room temperature)

Js-T ·····mode of saturation magnetization with respect to change of temperature T.

$(Jn)\tilde{H}$ ····mode of demagnetization of Jn by alternating magnetic field whose maximal intensity is H.

$(JTc)\tilde{H}$ ···mode of demagnetization of JTc by alternating magnetic field whose maximal intensity is H.

2. *Basic test applied to the samples taken from Fukuzawa-yama near Suwa.*

As the samples taken from Fukuzawa-yama have offered a standard

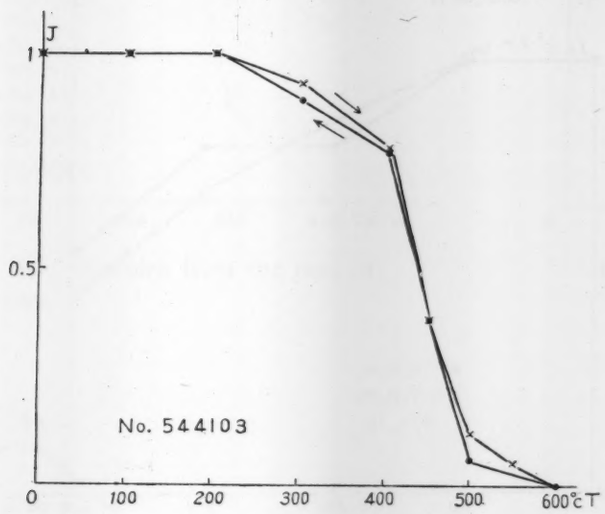

Fig. 1. Modes of variation of JTc through heating and cooling processes (andesite at Fukuzawa-yama).

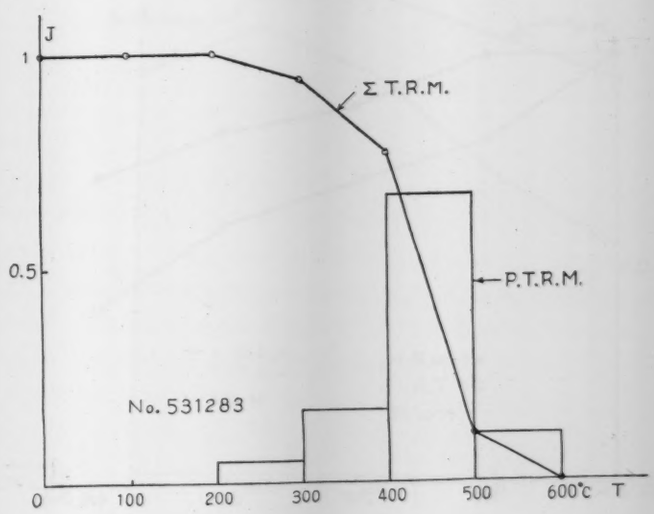

Fig. 2. The thermo-remanent magnetization curve showing that it coincides with the total sum Σ of partial thermo-remanent magnetism (*P.T.R.M.*) produced by cooling in the present geomagnetic field. (andesite at Fukuzawa-yama).

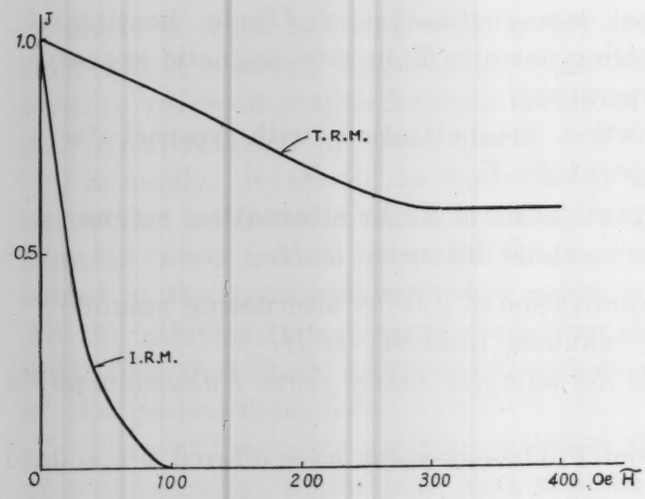

Fig. 3A-3G. Curves of *AC*-demagnetization applied to *N.R.M.* $(Jn)\tilde{H}$ and to *T.R.M.* $(Jtc)\ \tilde{H}$.

Fig. 3A. Samples from Mt. Utsukushi-ga-hara (Upper lava).

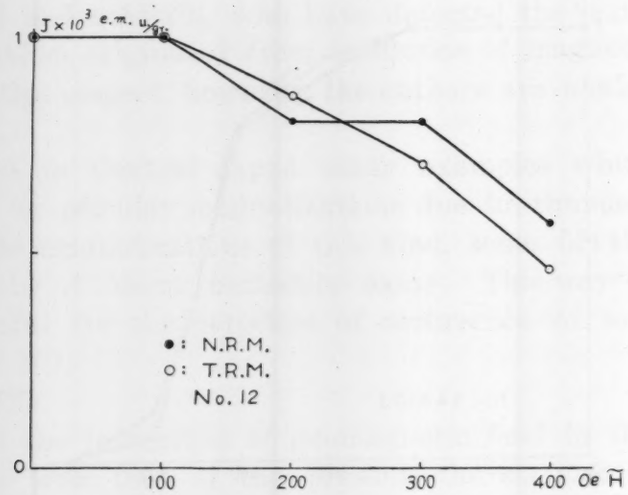

Fig. 3B 1. Samples from Mt. Takao-san.

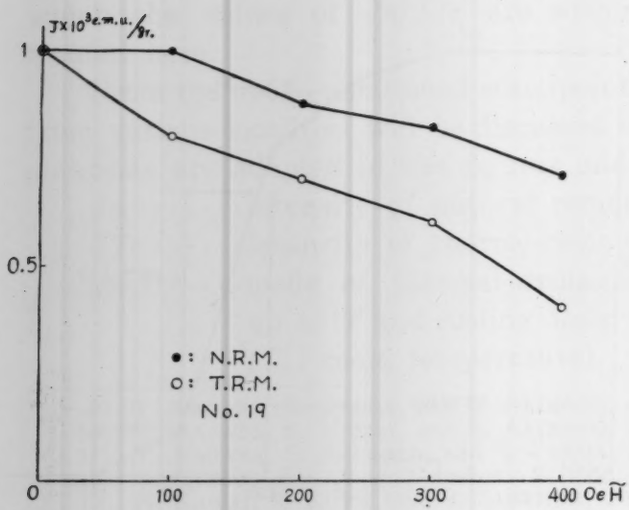

Fig. 3B 2. Samples from Mt. Takao-san.

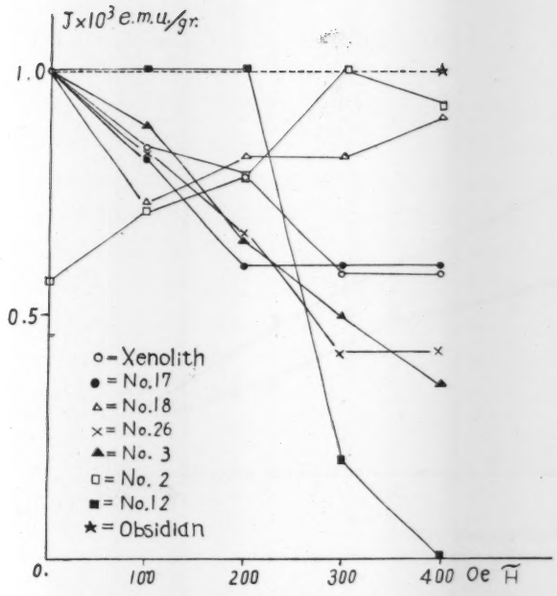

Fig. 3 C. Samples from the pass of Wada-toge.

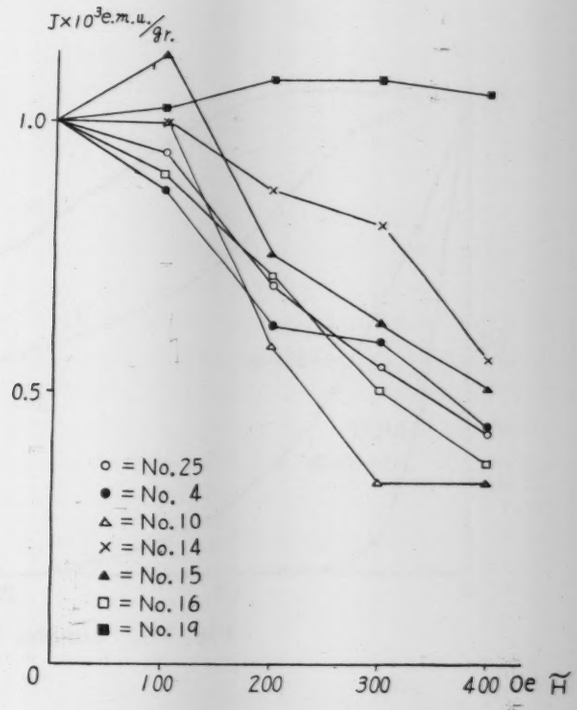

Fig. 3 D. Samples from Kawagishi.

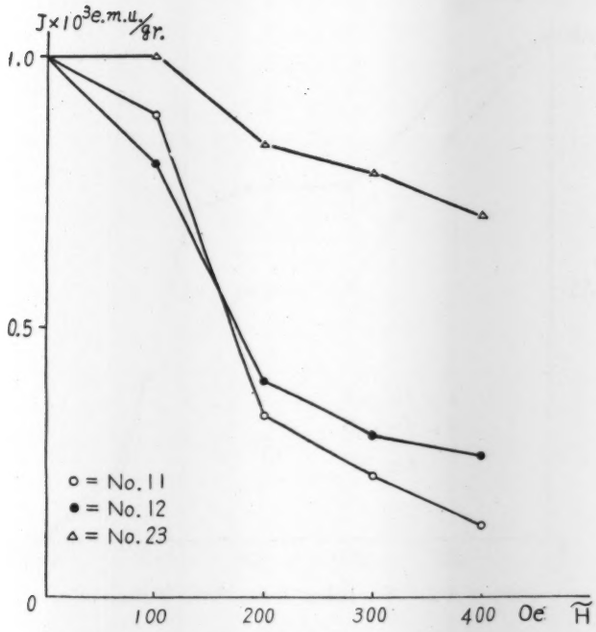

Fig. 3 E. Samples from Mt. Mitsu-mine.

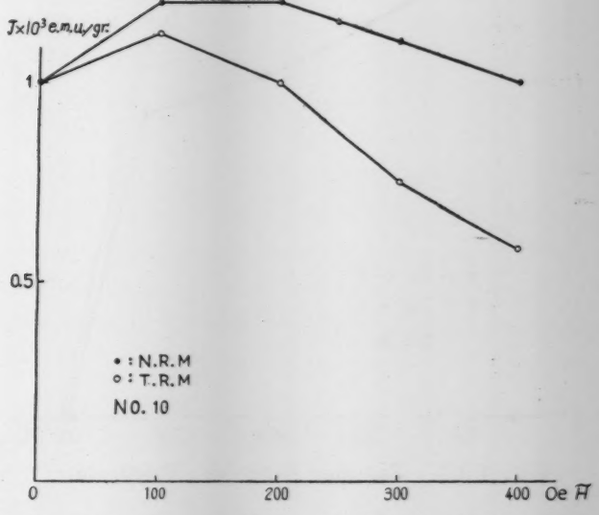

Fig. 3 F. Samples from Mt. Utsukushi-ga-hara.

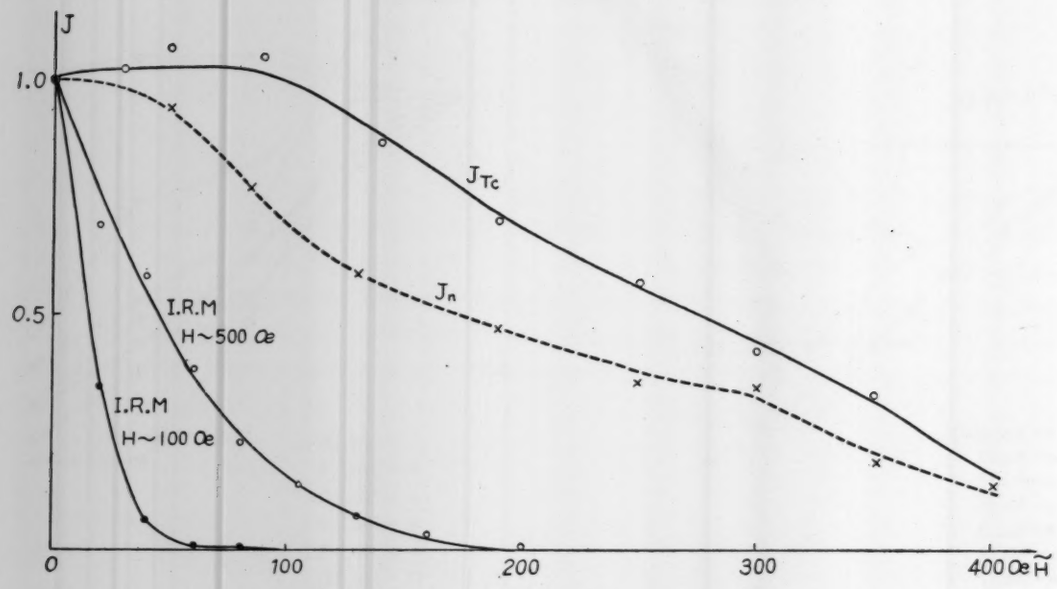

Fig. 3 G. Samples from Fukuzawa-yama.

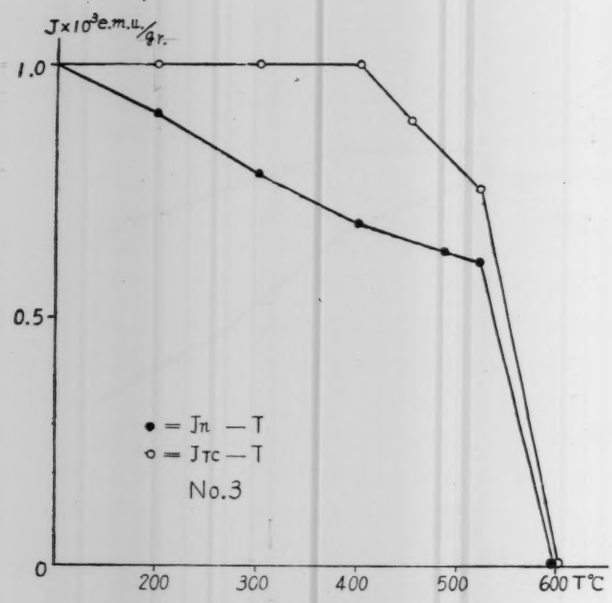

Fig. 4 A 1. Samples from Mt. Takao-san.

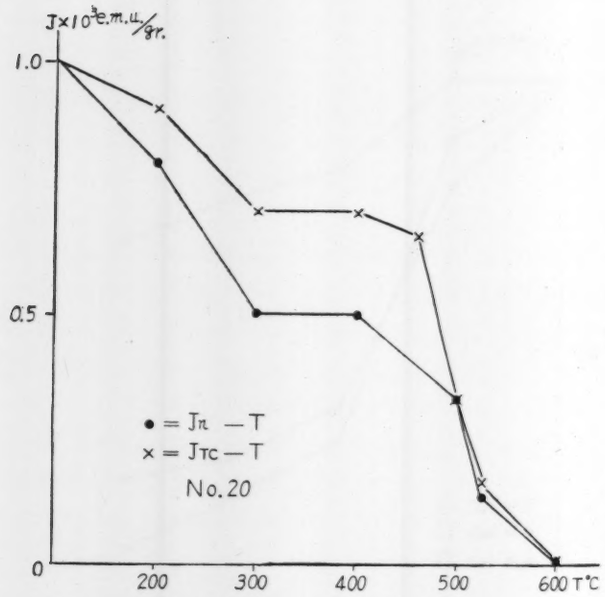

Fig. 4 A 2. Samples from Mt. Takao-san.

Fig. 4A 1-4 B 2. Curves of thermal demagnetization applied for both *Jn* and *Jrc*.

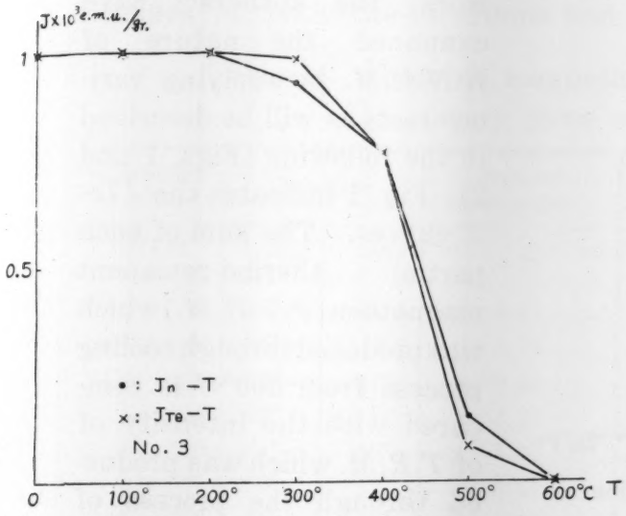

Fig. 4 B 1. Samples from Fukuzawa-yama.

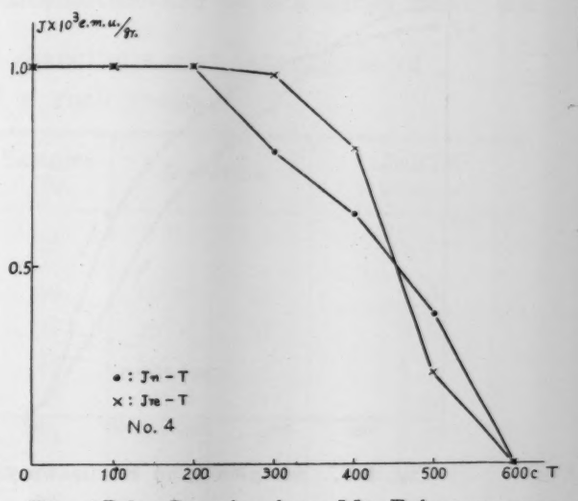

Fig. 4 B 2. Samples from Mt. Fukuzawa-yama.

Fig. 5A 1-5 B. Saturation magnetization (*Js*) curves through heating and cooling processes [*Js-T*]. (After Akimoto's measurements)

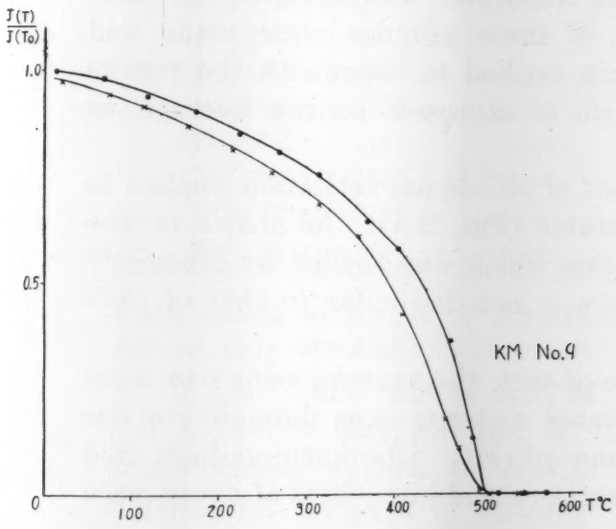

Fig. 5 A 1. Samples from Mt. Takao-san.

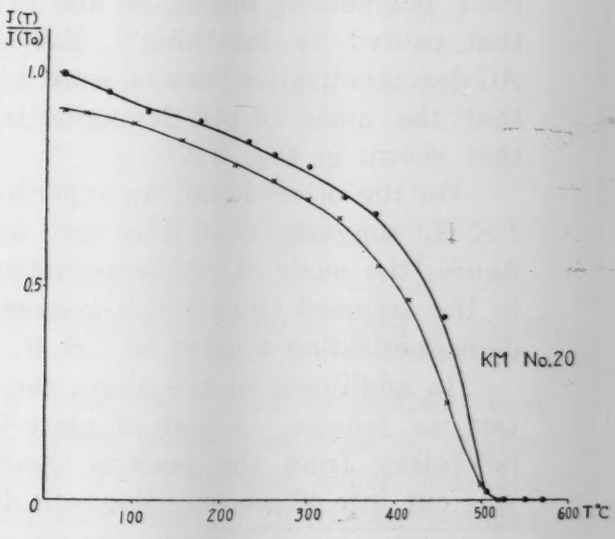

Fig. 5 A 2. Samples from Mt. Takao-san.

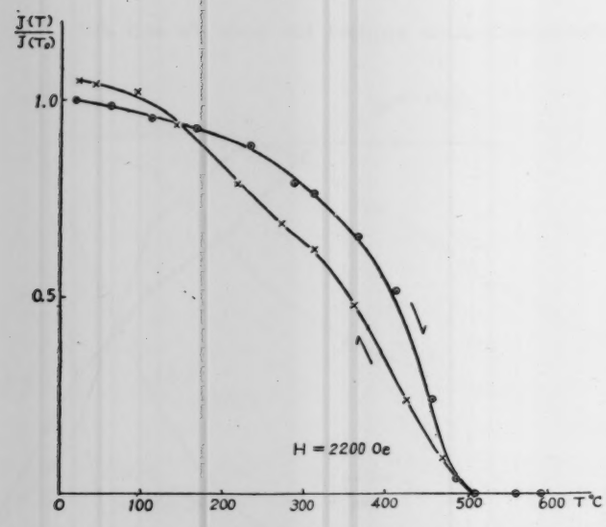

Fig. 5 B. Samples from Fukuzawa-yama.

basis for our succeeding work, the authors[14] have examined the nature of *R.N.R.M.* by applying various tests as will be described in the following (Figs. 1 and 2). Fig. 1 indicates the *JTc-T* curves. The sum of each partial thermo-remanent magnetism (*P.T.R.M.*) which was produced through cooling process from 600°*C* is compared with the intensity of of *T.R.M.* which was produced through the process of cooling from 600°*C* down to the room temperature as shown in Fig. 2.

3. *Magnetization caused by thunderbolts.*

Magnetic polarizations of samples taken from the summit region of Mt. Utsukushi-ga-hara are utterly scattered in direction, while the highest value of Jn/JTc was observed to be $122/4 = 30.5$. This sort of magnetism is different from usual "*N.R.M.*".

The result obtained from *AC*-demagnetization also suggests that their magnetism might be due to an abnormal magnetization perhaps that caused by lightning[15]. *T.R.M.* of these samples were made and *AC*-demagnetization assays were again applied to them with the results that the mode of *AC*-demagnetization is expressed on the average as that shown in Fig. 3 A.

On the other hand, an experiment of *AC*-demagnetization applied to *I.R.M.* suggests that it is very unstable (Fig. 3 A). As shown in the figure, the mode of *AC*-demagnetization which was applied by Momose[16] to the assumed thunderbolt-magnetism is not dissimilar to that of *AC*-demagnetization applied to *I.R.M.*.

In additional to the above series of test, the authors made one more test as follows. A slab of platy-jointed andesite was brought to our laboratory from the peak of Ogahana of Mt. Utsukushi-ga-hara and was cut into 48 pieces. Magnetic directions and intensities of every piece

14) T. NAGATA, *et al.*, *loc. cit.*, 2a).
15) H. MATSUZAKI, K. KOBAYASHI, & K. MOMOSE, *Jour. Geomagn. Geoelectr.*, **6** (1954), 53.
16) H. MATSUZAKI, *et al.*, *loc. cit.*, 15).

are enumerated in Table 1 and illustrated also in Fig. 6. The observed values of both the directions and intensities are so scattered that we

Table 1. Observed magnetic directions and intensities of every piece of a rock mass.

Samples No.	Direction		$Jn \times 10^2$ e.m.u./gr.	Samples No.	Direction		$Jn \times 10^2$ e.m.u./gr.
521120 1	62°W	17°	4.33	25			
2	59° 〃	21°	4.19	26	45°W	21°	5.00
3	56° 〃	8°	3.79	27	38° 〃	33°	0.43
4	55° 〃	7°	0.35	28	55° 〃	7°	4.32
5	59° 〃	7°	3.21	29	57° 〃	11°	3.98
6	64° 〃	15°	4.41	30	57° 〃	8°	3.94
7	56° 〃	12°	0.44	31			
8	51° 〃	13°	4.17	32			
9	54° 〃	12°	3.78	33	34° 〃	67°	0.45
10	54° 〃	8°	3.78	34	49° 〃	26°	4.36
11	54° 〃	5°	2.84	35	55° 〃	13°	3.94
12	55° 〃	4°	2.79	36	52° 〃	8°	4.14
13	54° 〃	14°	0.44	37			
14	51° 〃	10°	4.47	38	69° 〃	68°	4.99
15	54° 〃	10°	4.28	39	58° 〃	36°	4.22
16	51° 〃	5°	0.40	40	53° 〃	26°	4.27
17	52° 〃	3°	0.37	41	58° 〃	17°	0.43
18	54° 〃	7°	3.40	42	87° 〃	73°	6.89
19	61° 〃	16°	4.60	43	74° 〃	57°	0.45
20	48° 〃	27°	4.55	44	58° 〃	19°	4.17
21	50° 〃	18°	4.76	45	64° 〃	28°	
22	54° 〃	19°	4.27	46	89° 〃	56°	0.66
23	55° 〃	14°	0.39	47	84° 〃	84°	4.67
24	56° 〃	13°	0.38	48	58° 〃	7°	4.11

must admit existence of remarkable disturbance even in such a small slab of only 900 cm².

If the main part of *N.R.M.* of these rocks were originated from *T.R.M.* which they acquired in the former times, the mode of *AC*-demagnetization applied to *N.R.M.* (Fig. 3 A). Several stone idols are standing on the peak of Ogahana, altitude 1,998 m. They were brought up from a quarry at the foot of Mt. Utsukushi-ga-hara and are lithologically referred to the lower type of the Utsukushi-ga-hara lava. We found an anomalously strong magnetization in these idols which is likely

to have been caused by thunderbolts after they were brought up there. The fact would suggest that care should be taken of the magnetization

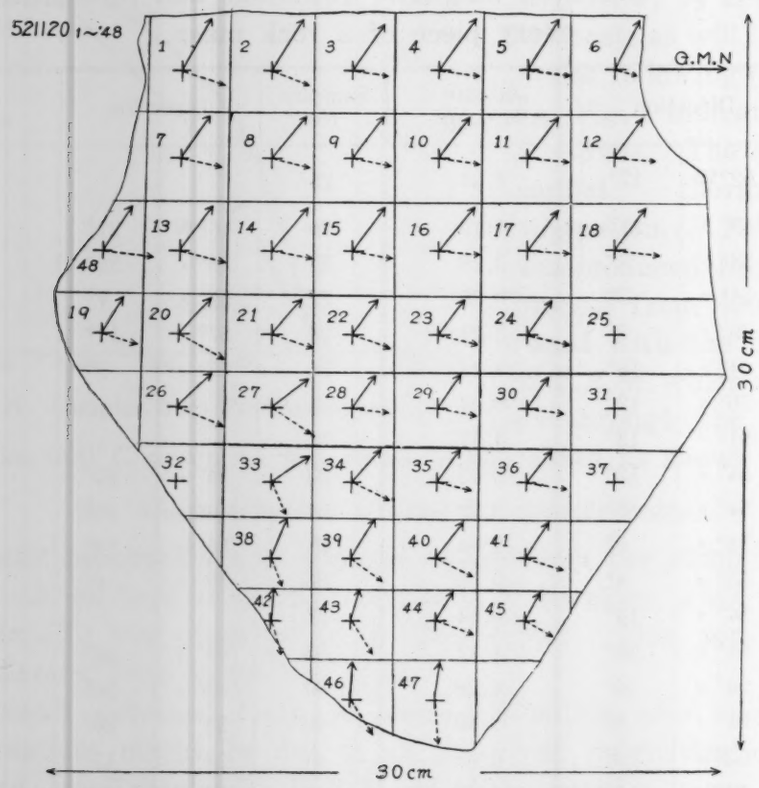

Fig. 6. Scattering magnetic polarizations measured from every piece of a rock mass. Arrow signs drawned by continuous line show the declination and those drawned by broken line show the inclination.

due to lightnings when rock samples are collected from the top of a mountain.

3. Measurements of Magnetic Directions

1. *Magnetic properties of Takaosan andesite.*

Among many samples, only a set of those from Mt. Takaosan have shown *N.N.R.M.* Since *N.N.R.M.* is seldom observed in our field, several tests in addition to *X*-ray analysis have been specially applied to the samples from Mt. Takaosan.

Mt. Takaosan is a type of volcanic neck and is capped by thin horizontal sediments, so that it is conceivable that remarkable dislocations have never taken place there since the formation of this rock bodies.

Fig. 7 illustrates the observed magnetic directions by means of stereographic projection.

Samples were collected from 3 localities each of which the altitudes are different from each other.

Unexpectedly, we observed scattered declinations ranging from N 11°E to N 74°E, whereas the inclinations took values around 70°. Such a random distribution of directions raises a doubt as to whether they were disturbed by thunderbolts. As shown in Fig. 3 B 1 and 3 B 2, however, the results obtained from application of *AC*-demagnetization as-

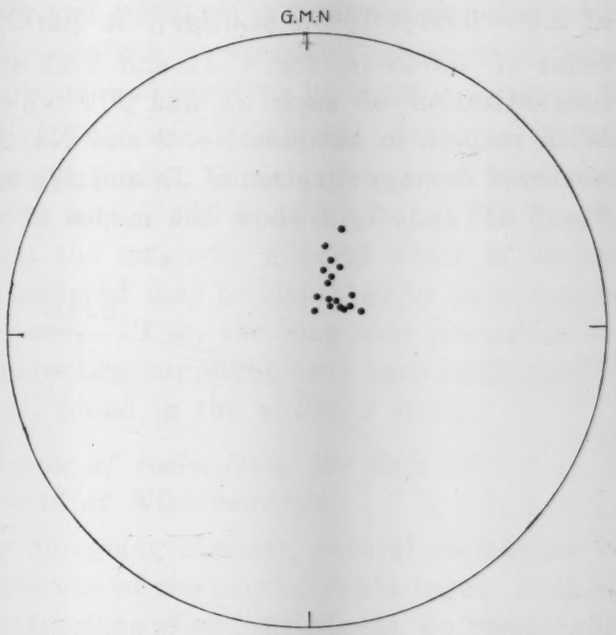

Fig. 7. Magnetic directions of the samples collected from Mt. Takaosan. (*N.N.R.M.*).

Table 2. Various magnetic properties of the samples taken from the pass of Wada-toge showing the directions, calculated directions of the centred dipoles, the intensities and the values of Jn/JTc.

Localities	Samples No.	Rock Names	Directions		Directions of the Centred Dipole		$Jn \times 10^3$ *e.m.u./gr.*	Jn/JTc
Wa 1a	2	(Ol.)-2-Py. And.	171°W	42°	30°S	124°E	0.20	0.154
	3		166°E	−49°	76°S	160°W	0.79	0.760
Wa 1b	Xenolith	(Ol.)-2-Py. And.	176°W	−38°	75°S	115°E	1.49	0.920
	4–6	Liparite	177°W	−36°	73°S	112°E		
Wa II	8–10	(Ho.)-2-Py. And.	151°W	53°	16°S	110°E	0.14	0.113
Wa III	11–13	(Ho.)-2-Py. And.	180°	− 2°	56°S	135°E	0.36	0.218
Wa V	17	2-Py.-And.	175°W	−41°	78°S	115°E	0.85	0.859
	18	2-Py.-And.	164°E	11°	46°S	160°E	0.43	0.476
Wa VI	20	obsidian	86°E	−60°			2	
WaVII	24–28	Liparite	164°W	−62°	76°S	5°E	0.24	0.50

says demonstrate that *N.R.M.* of the samples which are within a range of $2.0 - 0.85 \times 10^{-3}$ *e.m.u./gr.*, is hardly influenced by a field of the order of $100\,Oe\,\tilde{H}$. Fig. 4 A1 and 4 A2 show the modes of thermal demagnetization of each *Jn* and *JTc* which were applied to 2 samples. With respect to samples No. 3 and No. 20, it can be seen that both the modes of demagnetization of *Jn* and *JTc* are homologous with one another. Fig. 5 A1 and 5 A2 show the modes of saturation magnetization with

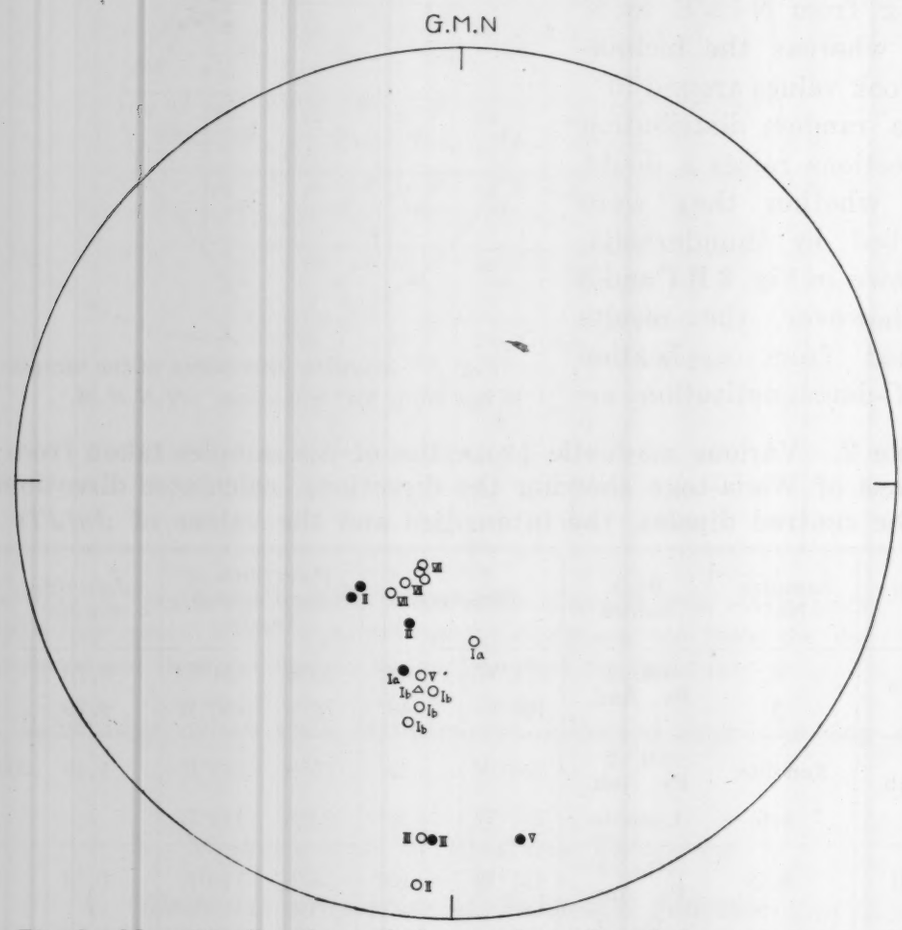

Fig. 8. Magnetic directions of the samples collected from the pass of Wada-toge (*R.N.R.M.*).

respect to changes in temperature. The modes of variation through both heating and cooling processes are also homologous with one another, so that no different mechanism of magnetization stands through both the processes.

In the samples No. 12 and No. 19[17], the values of *Jn/JTc* were observed to be 1.06/0.97 = 1.09 and 0.85/1.00 = 0.85 respectively.

In the application of *X*-ray analysis to magnetic minerals of these samples, the lattice constants were measured to be 8.396 ± 0.003 $\mathring{A}$ (in the case of the sample No. 9 of Takaosan) and 8.394 ± 0.002 $\mathring{A}$ (in the case of the sample No. 20) respectively. Curie points were also measured to be 505°C in the former and 510°C in the latter. The results thus obtained would imply that the magnetic mineral which is responsible for the magnetization considered may be identified to pure magnetite (Fe_3O_4) in $TiFe_2O_4$—Fe_3O_4 series. If so, the magnetic properties are highly stable. The observed magnetization might have been unchanged[18], though it is the only *N.N.R.M.* found in the author's study.

2. *Magnetic properties of rocks from the pass of Wada-toge and at Nishimochiya.*

As was mentioned in the foregoing chapter, several rock-types of volcanites are found in the environs of the pass of Wada-toge. Judging from the flow-structures and extensions of andesitic lavas, no remarkable dislocation is likely to have taken place in this area. The localities from which the samples were collected are all denoted in the geologic map.

Magnetic directions of samples collected from the pass of Wada-toge and from Nishimochiya are projected stereographically in Fig. 8 and the averages of each group of declinations and of inclinations are enumerated in Table 2.

As can be seen in Table 2 and Fig. 3 C, magnetic directions of most samples are reversed and point downwards except for those of obsidian samples No. 20 at the pass of Wada-toge.

Fig. 3 C shows the modes of *AC*-demagnetization applied to *N.R.M.* of samples collected from various localities. As the authors already examined[19] with respect of the results of *AC*-demagnetization applied to the assumed thunderbolts-magnetism, the modes shown in Fig. 3 C are analogous to those of *AC*-demagnetization applied to *T.R.M.* though there are a few exceptional instances.

The values of *Jn/JTc* are shown in Table 2. The directions of artificial mode *T.R.M.* produced during the cooling process 600°C to the

17) Both Samples No. 12 (here mentioned) and No. 9 (their result obtained from which is illustrated in Fig. 5 A1) were collected from the same rock mass; similarly, both samples No. 19 and No. 20 (Fig. 5 A2) were collected from the same rock mass.

18) S. UYEDA, *Jap. Jour. Geophys.*, **2** (1955) 1.

19) MATSUZAKI, *et al.*, *loc. cit.*, 15).

room temperature in the present geomagnetic field agree with the direction of the present geomagnetic field. The magnetic directions of the samples collected from one locality are centerized. Synthetizing the above-noted facts, the magnetism now under consideration may be due to that of *N.R.M.* different from those of the self-reversal and of *I.R.M.*, and is therefore stable.

Andesitic lava-flows of *Teppeiseki* type represented by the samples from Loc. Wa Ia is intruded by the Wada-toge liparite represented by the samples from Loc. Wa Ib and a contact spot is found at a locality near Nishimochiya. We can see several xenolithic blocks of andesite in the liparite body close to the contact plane. The average magnetic direction of liparite was measured to be N 171°W and −36°. Coinciding with this value, andesitic xenolith included in the former proved to be N 170°W and −38° in direction. Such a coincidence as noted above may imply that andesitic xenolith has acquired the *N.R.M.* after it was caught in the liparite.

Sample No. 3 is, however, located at a point only 2 m. distant from the contact plane and is doubtlessly a xenolithic block of andesitic host rock. The reason why such a peculiar direction was observed with respect to sample No. 3, might perhaps be attributed to the fact that it was affected by both the magnetic properties represented by those of samples from Loc. Wa Ia and Loc. Wa Ib. On the other hand, it is quite difficult to explain why the samples from Loc. Wa V are so scattered in direction. Moreover it is noteworthy that *Jn* of obsidian were observed to have particularly larger values, while it was never influenced by the application of the field of 400 *Oe* $\tilde{H}$ in *AC*-demagnetization assay.

Seeing the stableness proved by *AC*-demagnetization assays, Uyeda made an experimental test to examine if the obsidian might contain the minerals of the self-reversal type, with the result that he obtained a negative conclusion.

3. *Magnetism of Kawagishi Andesite.*

In those days preceding 1957, the authors were convinced that Kawagishi andesite would be reversed in magnetic direction because they are embedded in thick tuff-breccias which can be assigned lithologically to the so-called Enrei formation. The lavas are well-jointed and well-extended horizontally indicating that no dislocation has taken place since their extrusion.

Measured directions and corresponding pole position, the values of *Jn* and *Jn/JTc* are shown in Table 3, magnetic directions are also plotted in Fig. 9. All the observed directions are those that can be referred

Table 3. Various magnetic properties of the samples taken from Kawagishi showing the directions, calculated directions of the centred dipoles, the intensities and the values of Jn/JTc.

Localities	Samples No.	Rock Names	Directions		Directions of the Centred Dipole		$Jn \times 10^3$ *e.m.u./gr.*	Jn/JTc
Kw I	1-5	Ho.-2-Py. And.	160°W	−30°	64°S	85°E	0.410	0.640
Kw III A_1	10-12	Ho--2-Py. And.	160°W	−38°	67°S	78°E	0.240	0.462
Kw III A_2	13-14	Ho.-2-Py. And.	160°W	−35°	65°S	83°E	0.330	0.643
Kw III B	16-17	Ho.-2-Py. And.	168°E	−42°	74°S	174°W	0.920	0.726
Kw IV	19-20	(Ol.)-2-Py. And.	141°E	−27°	49°S	156°W	0.820	0.283
Kw V	23-27	(Ol.)-2-Py. And.	180°	−44°	81°S	135°E	0.640	0.515

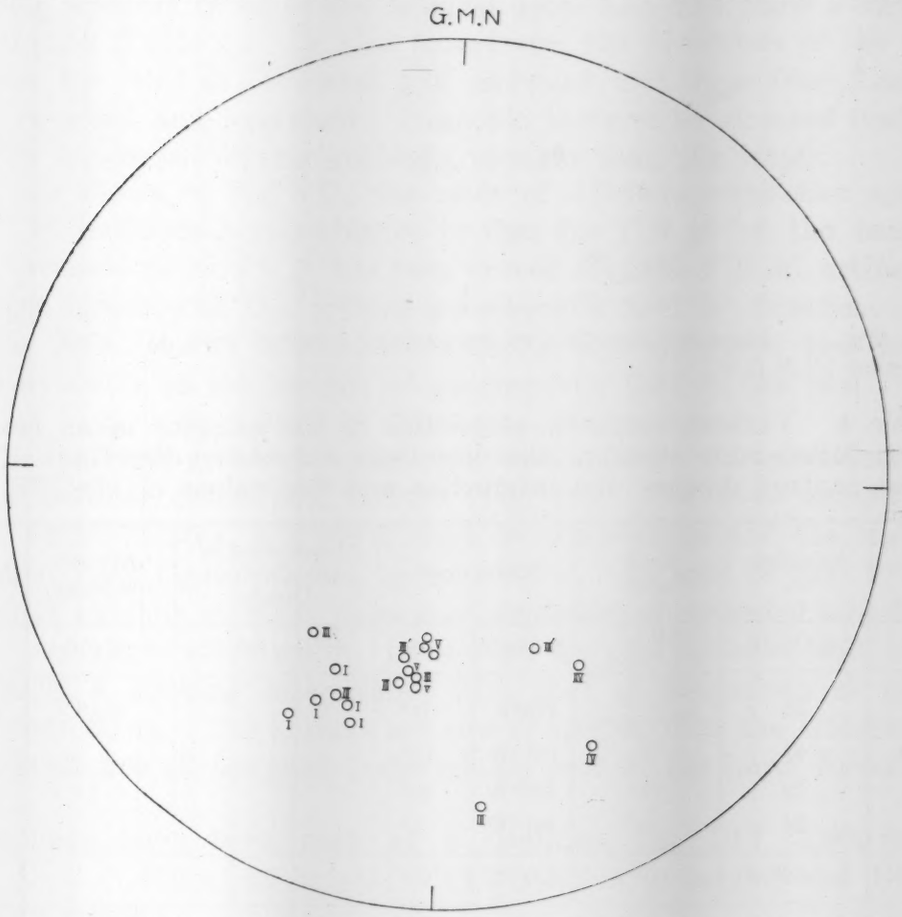

Fig 9. Magnetic directions of the samples collected from Kawagishi (*R.N.R.M.*).

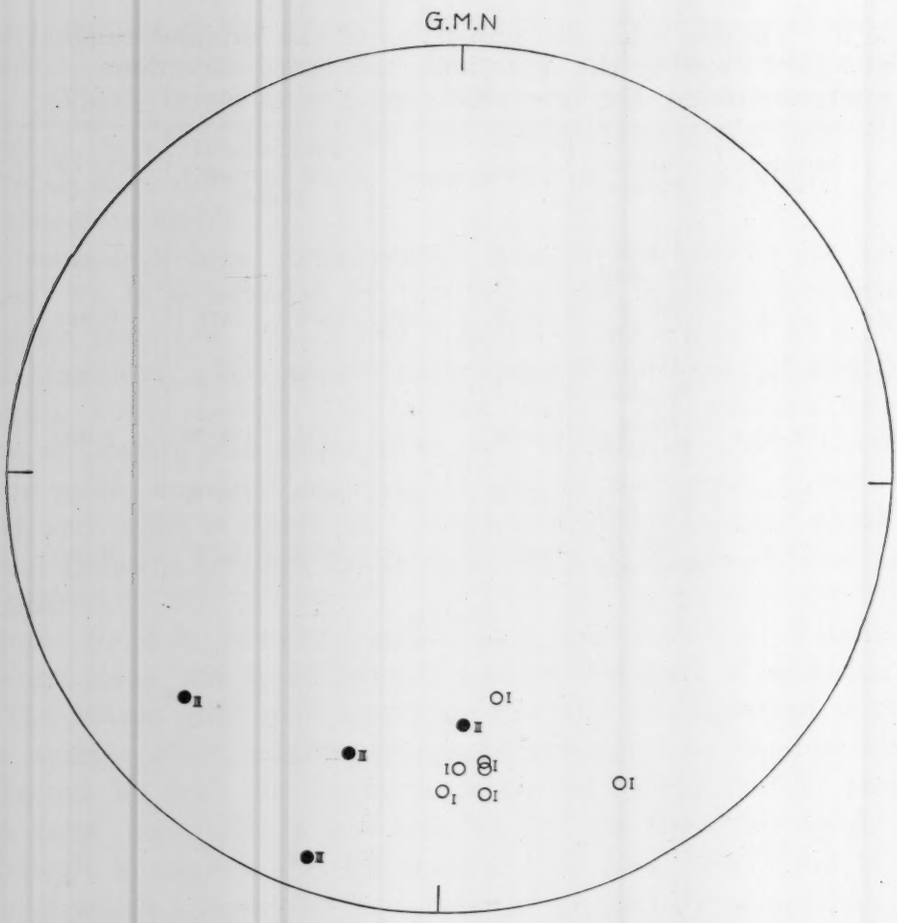

Fig. 10. Magnetic directions of the samples collected from Mt. Mitsu-mine (*R.N.R.M.*)

Table 4. Various magnetic properties of the samples taken from Mt. Mitsu-mine showing the directions, calculated directions of the centred dipoles, the intensities and the values of Jn/JTc.

Localities	Samples No.	Rock Names	Directions		Directions of the Centred Dipole		$Jn \times 10^3$ e.m.u./gr.	Jn/JTc
Mi I	9.11.-16	(Ol.)-2-Py. And.	N 168°E	−19°	64°S	161°E	0.810	0.750
Mi III	21	(Bl.)-ho.-2Py- And.	176°E	31°			0.19	0.24
	22	〃	131°W	15°				
	23	〃	162°W	23°			0.14	0.15
	24	〃	161°W	5°				
Mi III	22*	〃	133°W	16°				

* Direction obtained from the sample (Mi III 22) 2 months after the first measurement.

to *R.N.R.M.*, most of which are westward with a few exceptions.

As are shown in Fig. 3D, their stablenesses were warranted by the applications of *AC*-demagnetization assay. The directions of *T.R.M.* have also shown a marked coincidence with the present geomagnetic field.

Judging from the results thus obtained, we may conclude that the directions of *N.R.M.* can be regarded as the trustworthy records of geomagnetic field in the past.

4. *Magnetism of Mt. Mitsu-mine Andesite*

As noted proviously, Mitsu-mine andesites are referred to a member of the Enrei formation. The samples from Loc. Mi I are very platy-jointed and indicate lithologically the same rock facies as those in the environs of Suwa and Mt. Utsukushi-ga-hara.

In Table 4, magnetic directions, the pole positions calculated and the values of *Jn/JTc* are denoted, while their magnetic directions are plotted in Fig. 10. The observed directions of the samples from Loc. Mi III are scattered, whereas those of the samples from Loc. Mi I show a striking concentration (Table 4). As read from these, the directions of the samples from Loc. Mi I are reversed and eastward, and those from Loc. Mi III are reversed and westward. It should however be stressed that the former is considered stratigraphically younger than the latter.

As are shown in Fig. 3 E., the mode of *AC*-demagnetization applied to *N.R.M.* indicates a resemblance to that for *T.R.M.* of the samples from Utsukushi-ga-hara. It has been proved that the *T.R.M.* artificially made also agrees with the present geomagnetic field in direction. The magnetic directions of Mitsu-mine andesite thus measured and tested may be available as the records of geomagnetic field in the past.

5. *Magnetism of Utsukushi-ga-hara lavas*

Mt. Utsukushi-ga-hara, which has been called "Lava plateaus", shows a peculiar geomorphic feature (Fig. 16). The even summit as wide as 4 km^2. in area, is 2,000 m. high on the average and the highest peak called Peak Ogato reaches up to 2,034 m. As seen in Fig. 17 a,b, the summit exhibits in many parts good exposures of extended lava-flows dipping very slightly eastward. Lava-flows are platy-jointed and show lithologically a striking resemblance with that of *Teppeiseki* at type-locality near Suwa. The authors are now of opinion that the Utsukushi-ga-hara lavas are all assigned to the middle part of the Enrei formation in age.

Samplings have been made at 4 localities, i.e. Ut I (1,900 m in height), Ut II (1,450 m in height) Ut III (1,800 m in height) and Ut IV (1,900 m in height).

Table 5. Various magnetic properties of the samples taken from Mt. Utsukushi-ga-hara showing the directions, calculated directions of the centred dipoles, the intensities and the values of Jn/JTc.

Localities	Samples No.	Rock Names	Directions		Directions of the Centred Dipole		$Jn \times 10^3$ e.m.u./Jr.	Jn/JTc
Ut I_a	1-3	(Ol.)-2Py.-And.	142°E	−29°	56°S	156°W	1.07	0.79
Ut I_b	6-10	(Ol.)-2Py.-And.	157°E	−27°	61°S	175°W	0.65	0.41
Ut II	K1-8	(Ho.-Ol.)-2Py. And.	104°E	16°			0.67	0.24
Ut III	K3-10	(Ol.)-2Py.-And.	143°E	64°			5.70	1.30
Ut IV	1-4	(Ol.)-2Py.-And.	158°E	−20°	59°S	178°E	0.81	

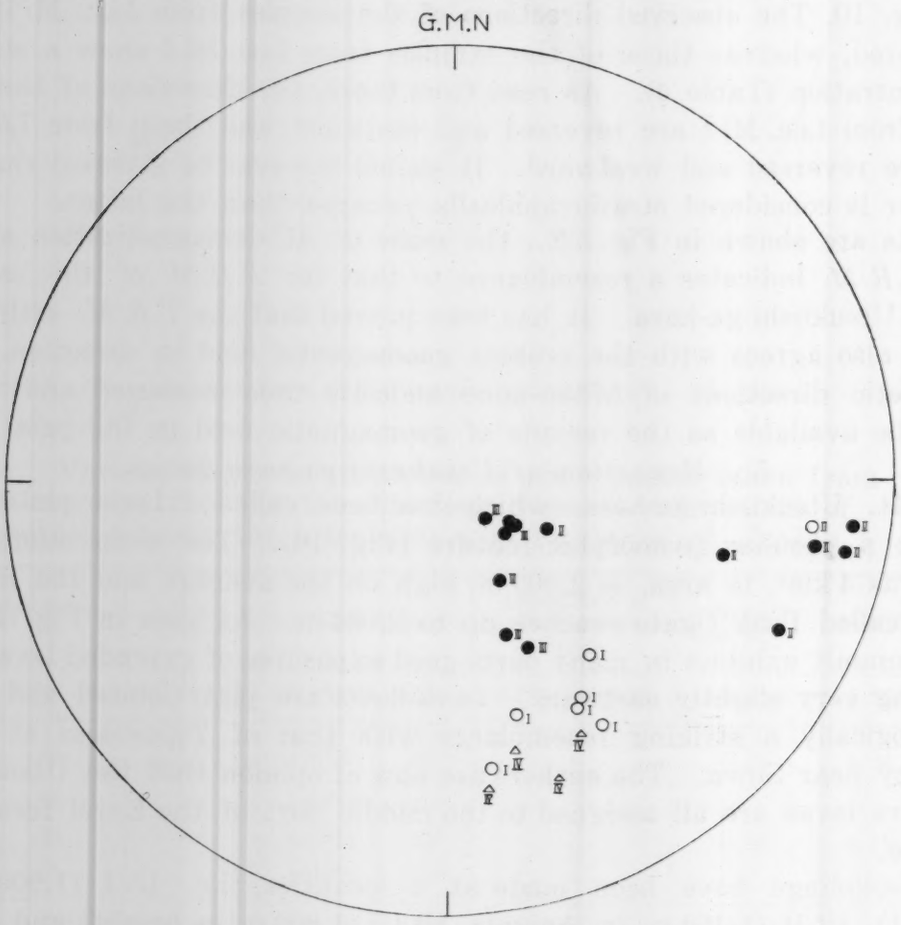

Fig. 11. Magnetic directions of the samples collected from Mt. Utsukushi-ga-hara. (*R.N.R.M.*).

Observed magnetic directions of the samples are shown in Table 5 and in Fig. 11. The directions indicate a good concentration and they are directed eastward. Fig. 3 F shows the results in the applications of *AC*-demagnetization to the samples from Ut I. The directions of artificially made *T.R.M.* also proved to be in parallel with the present geomagnetic field. Considering the distribution of observed direction, it seems likely that the obtained *R.N.R.M.* may be thought as stable.

6. *Magnetism of the samples collected in the environs of Suwa.*

Table 6. Magnetic directions and calculated directions of the centred dipoles of various samples in the environs of Suwa.

A) Suwa Kanko-doro group

Localities	Samples No.	Rock Names	Directions		Directions of the Centred Dipole	
Su VII	K 7	Ho.-2-Py. And.	177°E	−54°	86°S	140°W
Su VI	K22-25	2-Py.-And.	168°E	−40°	73°S	78°W
Su V	K29-34	(Ol.)-2-Py. And.	147°W	2°	34°S	87°E
Su II	K 1-6	2-Py.-And.	150°W	−25°	55°S	75°E
Su III	K 7-10	2-Py.-And.	132°W	−42°	46°S	45°E
Su IV	K11-16	2-Py.-And.	177°W	−25°	67°S	127°E
Su I	K 9-12	2-Py.-And.	121°E	35°	12°S	168°W

B) Fukuzawa-yama group

Ks II	Y 20-23	Ol.-2Py.-And.	142°E	−56°	59°S	120°W
Fu V	Y 17-19	Ol.-2Py.-And.	137°E	−45°	52°S	137°W
Fu IV	Y 15	Ol.-2Py.-And.	144°E	13°	37°S	178°E
Ks I	KK 12-19	Ol.-2Py.-And.	127°E	−44°	44°S	127°W
Fu III	531281-6 544101-5	Ol.-2Py.-And.	128°E	−72°	49°S	90°W
Fu II	Y 8-9	Ol.-2Py.-And.	120°W	−51°	40°S	61°E

Detailed descriptions of the geology of Suwa district will be made in the following chapter. Several flows of andesite lavas mainly of *Tep-*

peiseki type are embeded in thick tuff-breccias. Samplings were made at several places on Fukuzawa-yama—a type-locality of andesite of *Tep-peiseki* type (Loc. Fu Ks) and at several places (Loc. Su) along the so-called "Sight-seeing Road" (Kanko Doro).

These two groups of localities have ascertained that they belong to the lower and middle members of the Enrei formation.

Observed directions and calculated pole positions of the samples are shown in Table 6. It was clearly indicated that the samples from the lower member of the Enrei formation were reversed and westward in direction whereas those from the middle member were reversed and eastward. The results of our tests made for the samples from Loc. Fu III at Fukuzawa-yama quarry (Fig. 18 a, b) will be mentioned in the following. The modes of thermal demagnetization applied to *Jn* and *Jtc* are alike as are illustrated in Fig. 4 B1 and 4 B2. Akimoto[20] measured the changes in *Js* in relation to changes in temperature, and the curves thus obtained are shown Fig. 5 B. The results also indicate that the curves through both process of heating and cooling are similar to each other and that the Curie point is estimated to be 490°C. The lattice constant of the magnetic minerals contained was calculated to be 8.382 Å for sample No. 4. This implies that the mineral belongs to Titano-spinel-Magnetite series.

Fig. 3 G shows the modes of *AC*-demagnetization of *Jn*, *JTc* and *I.R.M.*. The values of *Jn*/*JTc* of samples No. 4 and No. 3 were calculated respectively to be $1.29/2.45 = 0.52$ and $1.3/2.05 = 0.63$.

Summarizing all the experimental results, it may be said that the *N.R.M.* retained in all the samples from Loc. Fu III may be normal and very stable[21]. As all the samples from Loc. Fu-Ks group are lithologically quite similar to those from Loc. Fu III, the former is supposed to be consisted of the mineral stable in magnetic characters. Although the test considered may not always be sufficient to provide a decisive basis for our conclusions, the results above mentioned, will support, to some extent, the view that most of the *N.R.M.* of rock samples studied by the authors can be used for tracing the directions of the geomagnetic field in the past.

IV. Geological Settings

1. *General geology of the Enrei formation*

Various volcanic ejecta which consist chiefly of andesite lava-flows

20) S. AKIMOTO, *loc. cit.*, 18).

21) T. NAGATA, *loc. cit.*, 2a).

and tuff-breccias are distributed over a wide area around Lake Suwa. They extend northward to the vicinity of Utsukushi-ga-hara which is located east of Matsumoto City. The main part of these pyroclastic formations seems to have originated through a sort of volcanic depression accompanied by intensive volcanism, the thickness of the formation may attain to at least more than 400 m. Their wide distribution is shown in our geologic map. In some parts of the formation well stratified facies of sedimentary deposition are found, especially in the lowermost and the uppermost parts. Their depositional surfaces are fairly well-preserved as seen in an even summit-levels and shown in Figs. 20 and 21. These volcanic deposits were named the Enrei formation by one of the authors[22].

The oldest formations in our area are represented by the rocks of palaeozoic formation and those of metamorphics of the Sambagawa type; the former occupies small area in the south-western part of our geologic map, whereas the latter consisting of crystalline shists and phyllites of the Sambagawa type occur along the upper course of the Yokokawa-gawa.

The metamorphic groups of the Moriya and the Uchimura formations of the middle or early Miocene in age are exposed in some parts near Shimosuwa, Utsukushi-ga-hara and Hachibuse-yama. The metamorphics[23] called usually "Green-tuff" are intruded by quartz-diorite which is exposed in certain places near Omegura and Wada, and in another area very near to Lake Suwa.

The heights of the unconformity at which the Enrei formation overlies these basement rocks are at the level of 1,000 m. (above *M.S.L.*) in the north of Shimosuwa; 1,400 m. (the boundary between both formations is now in tectonic contact) in the east of Mt. Higashi-yama; 1,500 m. at the pass of Tobira-toge; 1,300～1,900 m. at Utsukushi-ga-hara, and 1,100 m. along the Yokokawa-gawa. The lowest level of exposure of the Enrei formation, on the other hand, is about 700m. above *M.S.L*, though the basement rocks are not found there.

The area where the basal unconformities are conceived to be located below the ground surface is interpreted to correspond with the sunken area introduced by volcanic depression.

2. *Stratigraphy and lithologic features of the Enrei formation*

The Enrei formation is generally characterized by large amounts of

22) Fossa-Magna Research Group, *Earth Science* (*Chikyukagaku*), **37** (1958), 46.

23) They consist mainly of altered volcanic pyroclastics with less sediments and altered porphyrite. The Tobira formations are similar to the Uchimura group lithologically, but the stratigraphic relation between the both, have not yet been sufficiently known.

tuff-breccias intercalating many sheets of lava-flows, much less conglomeratic and mud beds. Excepting local area of intense dislocation, the Enrei formation is represented by horizontal or gently inclined strata, although most parts of the formation do not show any remarkable stratification. Flat-lying and thin lava-flows are embedded at various horizons and show no crater-like landforms over there. Therefore it seems likely that very fluidal lava of lower-viscosity has extruded in many places from craters and flowed downwards over the gently-sloped surface of the tuff-breccias. The lava-flows are composed mainly of two-pyroxene andesite being accompanied by local occupation of liparite lava. Several intrusive bodies of hornblende andesite and basalt, though much less in amount, are also found locally. But they are undoubtedly of post-Enrei volcanic origin.

The liparitic bodies at the pass of Wada-toge have long been famous for the accompanying of glassy parts—obsidian and for that of large crystals of garnet. The obsidian has been used by our ancient ancestors for making stone implements since Palaeolithic times.

The basal part of the Enrei formation has not yet been ascertained but the area in the upper course of the Yosawa-gawa seems likely to represent the lower part. In this area conglomeratic beds are seen to underlie the main part of tuff-breccias suggesting that the bed might represent the pre-volcanic environments.

The name of *Teppeiseki* or *Hira*-ishi has been popularly used for the andesite which shows a remarkable appearance of well-developed jointing. The thickness of each flagstone separated by joint-planes is ranging from 1 to 3 cm. Flagstones, therefore, have been used for tiling over the roof of farm-houses in the environs of Suwa. The lavas of *Teppeiseki* are characterized by not only platy-joints but also by remakable lateral extension. The lavas which show the appearance of the *Teppeiseki*, comprise not only the special rock-type as seen at Fukuzawa-yama—a type-locality, but also several other rock-types being somehow varied in lithology as seen in many places of the Enrei formation.

Well-jointed feature of lavas dominates in the rocks of olivine-two-pyroxene-andesite which are quarried at several places now. The Fukuzawa-yama quarry is the largest and most famous one. Besides these, the quarries at Nyukai and Kakuma-shinden which are located north of the former are referrable to the same lava-flow. Making use of the perfect platy-joint and the vertical columnar-joints, large amounts of the flagstone are quarried at these places and sent to central cities for the buildingstone.

The quarries producing excellent plates are chiefly limited to these located at the exposures of olivine-two-pyroxene andesite distributed north of Kamisuwa. The thinner platy-joints are developed generally in the lower parts of lava-flow, whereas the upper part is less perfectly jointed and each flag is thicker. Sometimes intercrosses of joint-planes are observed in the uppermost part as shown in Fig. 19 a.

Tateishi quarry is located on the ridge opposite to Fukuzawa-yama quarry, and the altitudes of both quarries are almost equal to each other, although magnetic directions of both *Teppeiseki* lavas are different i.e. Tateishi andesite exhibits *Rw* but Fukuzawa-yama andesite is *Re*. That fact indicates that both lava-flows belong to different horizons respectively.

Another lava-flow of *Teppeiseki* type is found in the environs of Kawagishi and Tatsuno along the Tenryu-gawa. Its magnetic direction is *Rw* indicating that it represents the lowest member of the Enrei formation.

Well-jointed andesite lava of different rock-type is hornblende-bearing-two-pyroxene andesite of Nishimochiya. All of hornblende-bearing andesite are not invariably characterized by well-developed joints. For convenience of description, the area of the Enrei formation is to be divided into the following seven major units from geological and geographical stand points.

i) *Yosawa District*

A lithologic facies representing the basal members of the Enrei formation is found along the upper stream of the Yosawa-gawa in the western part of the map. In this district, the formation consists of the basal conglomerate, volcanic conglomerate and volcanic detritus, and they seem to cover uncomformably the older basement.[24]

The lower part of the conglomerate contains pebbles derived from the basal Miocene sandy and conglomeratic rocks that are highly silicified, whereas the upper part of the conglomerate comprises numerous cobbles and boulders consist of crystalline schists and phyllites of the Sambagawa type (Fig. 23). Overlying the conglomerate, are tuff-breccias which show in some parts the signes of water-deposition. It is designated the Yosawa conglomerate and the thickness is estimated to be more than 30 m. In the overlying tuffaceous beds fragmentary trunks of trees are found (Fig. 25). At Yuno-sawa, for instance, general strikes of the beds are variable from N 40°E to N 70°E and their dips

24) K. KOBAYASHI, *Rep. Geol. Survey. Nagano Pref.* (1955), 155.

are steep to the south, sometimes they are even vertical or partly reversal (Fig. 23). As a matter of course the steep dip of the bed is considered to have been caused by the transposition after the sedimentation. It seems that this transposition of strata might be affected by the faulting in the trend of NW-SE. The Yosawa conglomerate is accordingly, supposed to convert southwards to the tuff-breccia around Mt. Higashi-yama. A lava-flow is found in the lower part of tuff-breccias, but its magnetic direction has not been observed.

ii) *Yokokawa-gawa District*

Through the whole area of the Enrei formation, the Yokokawa-gawa and Utsukushi-ga-hara districts are characterized by the development of a thick assemblage of lava-flows.

Thick lava-flows of several kinds are exposed along both sides of the Yokokawa-gawa running down along the eastern foot of Mts. Higashi-yama and Takabotchi-yama. Although remarkably dislocated in many parts, a southward dip of about 60° has been observed in the lava-flow along the Yokokawa-gawa, and the magnetic directions of each of these lava-flows were measured. The obtained data of the magnetic direction of these lavas are satisfactory as compared with these of the equivalents in other places. But there is a little doubt as to whether we are able to make correct restorations of geologic displacements as we fear that too intense a displacement to be detected might have taken place.

The groups of lava-flows exposed along the Yokokawa-gawa are geologically referring to the lower and the middle members of the Enrei formation.

iii) *Shiojiri-toge District.*

The vicinity of the pass of Shiojiri-toge has been considered as the type-locality of the tuff-breccia facies of the Enrei formation. The thick tuff-breccia developed here overlies the above-noted part developed in the neighbourhood of the Yosawa. The exposures of lava-flows are found on the banks of a pond at Katturu and of Midoriko (a storage dam) in the southwestern part of the map. Both lava-flows show similar thin platy-joints to those developed in *Teppeiseki*, and are petrographically two-pyroxene andesite.

The sedimentary beddings in this region are much less inclined than those of Yosawa and Yokokawa-gawa districts, and in reality almost horizontal.

Blocks contained in the tuff-breccia which developed in the vicinity of the pass of Misawa-toge often carry hornblende and the member may

therefore lithologically correspond to the upper member of the Enrei formation. At the top of the formation, conglomeratic facies and intercalated mud-seams are recognised at the pass of Misawa-toge. Such a sedimentary facies might undoubtedly have been water-deposited.

Two domes of Mt. Takao-san and east of Enrei park are necks of hornblende andesite[25] intruded into the Enrei formation in the later stage.

iv) *Kawagishi District*

In the east of Kawagishi, thick tuff-breccias which intercalated several lava-flows indicate also that they have been water-deposited as suggested by the occurrence of thin mud-seams at various horizons. Inclinations of the formation indicated by these intercalated sediments are averagely 10° toward the southwest.

A lava-flow of olivine-bearing-two-pyroxene andesite at Komazawa-shinden is found to be at the lowest level of the formation in the south of Kawagishi (Fig. 17 C). The lava-flow is not only characterized by remarkable platy-joints similar to *Teppeiseki* but also petrographically identical with that of the type-locality of Fukuzawa-yama and Kakuma-shinden quarries.

Three layers of lavas of two-pyroxene-hornblende andesite exposing at Doda and Karakasa-daira, are interbeded in the tuff-breccia which overlies the lava of *Teppeiseki*. Platy-joints are also developed in these lavas, whereas each joint-plane is more apart than that of *Teppeiseki*.

Magnetic directions of all lavas of Kawagishi district are observed to be *Rw* (reverse and westwards) as shown in Fig. 12. The fact may suggest, therefore, that tuff-breccias and lavas of this district represent the lower member of the Enrei formation. When we are to consider only the petrographic features, the *Teppeiseki* lavas at Komazawa-shinden may be correlated to those at the quarry of Fukuzawa-yama and the hornblende-bearing andesite lavas at Doda and Karakasa-daira are correlated to those at Kowashimizu and Mt. Kuruma-yama of Kirigamine district respectively[26].

v) *Wada-toge District.*

Another type-locality of the lower member of the Enrei formation

---

25) It is one of the volcanics showing the normal magnetization in the volcanic rocks developed around Lake Suwa and it seems to indicate the volcanic activity in the latest Pliocene or the earliest Pleistocene from the paleomagnetic points of view.

26) In the Suwa Sheet of Geological Survey (1/50,000), the tuff-breccia of the east of Kawagishi are named S 4 which was referred to the overlying members of the *Teppeiseki* lava in Suwa-Kirigamine district, the misunderstanding of this kind might be due to the correlation basing upon only the petrographic point of views.

is found in the district of Nishimochiya and Wada-toge along Nakasendo. At Nishimochiya, along the Nakasendo road olivine-bearing-two-pyroxene andesite which is demonstrated by the well-developed platy-joint as seen in the *Teppeiseki* lies unconformably above the altered porphyrites of the Tobira formation intruded by quartz-diorite.

In the west of Nishimochiya, a branched body of the well-known liparite main-mass which is typically exposed at the pass of Wada-toge, shows the relation in which the liparite intrudes into the lowest lava (Fig. 24). Up to the present day, most researchers[27),28),29)] understood that this outcrop indicated the fault relation between both rocks, and the liparite was the basement rock under the andesite lavas of this region. A block of the host rock (andesite lava) is caught in the liparite and the trend of flow-structure of the liparite is nearly vertical. The intrusive relation of liparite to andesite was also confirmed by means of geomagnetic consideration as already discussed (see p. 448). Hornblende-bearing-two-pyroxene andesite lava-flows overlying the olivine-bearing-two-pyroxene andesite lava, in the environ of Nishimochiya and the former exhibits as well-developed platy-joint as *Teppeiseki*-lava (Fig. 17 d).

The olivine-basalt exposes at one spot north of Nishimochiya and at higher altitude beside the Nakasendo road. The exposure of the rock is small but is traced vertically along the slope. It has often been discussed by the researchers who studied the geology of this district whether the basalt is dike or lava-flow. The authors have concluded on the geologic and geomagnetic evidence that the basalt is a dike which was injected in the later Pliocene age. A similar kind of basalt also outcrops at Horoku-zawa, beneath the ridge from Mt. Mitsu-mine to the pass of Wada-toge.

The uppermost flow of the andesite occupying the vicinity of the pass of Wada-toge is one of the biotite-bearing-hornblende-two-pyroxene andesite and it occurs along the ridge from Mt. Mitsu-mine to the pass of Wada-toge.

Intruding these andesite lavas, the liparite is exposed in the vicinity of Wada-toge indicating, however, certain varied facies in lithology. The liparite carries fine crystals of garnet. It can also be divided megascopically into several rock-types by the abundance and magnitude of the

27) F. HOMMA, *loc. cit.*, 5).
28) S. KOZU, *et al.*, *Jour. Jap. Min. Petro. Econ. Geol.*, **24** (1940), 165.
29) K. SAWAMURA and E. OWA, *loc. cit.*, 6).

phenocrysts of quartz and feldspars and by amount of gas-pore, and sometimes it intercalates belts of black glass (obsidian) showing the appearance as if obsidian has injected in parallel with flow-structure of the liparite. Although the obsidian shows a much more intense remanent magnetism, the presence of the magnetic minerals is not recognized under the microscope.

The magnetic direction of the series from the andesite lava-flows of Nishimochiya to the liparite mass are all *Rw*, the facts suggest also that the volcanic complex of Nishimochiya～Wada-toge district represents the lower member of the Enrei formation.

In the east of Wada-toge, the lava of hornblende andesite is exposed around the summit of Mt. Washiga-mine covering unconformably the liparite. The hornblende andesite of Mt. Washiga-mine is scarcely accompanied by tuff-breccia. Natural remanent magnetism of the andesite lava seems to have been disturbed by thunderbolts. The geomagnetic field when the magnetism was acquired would, therefore, be impossible to determine. The petrographic characters of the lava, however, are identical with those of the lavas at Kowashimizu and also Mt. Kurumayama of Kiriga-mine volcano. The lava-flow at Mt. Washiga-mine may, accordingly, represent the upper member of the Enrei formation.

vi) *Mitsu-mine～Utsukushi-ga-hara District*

The andesite lava occurs in a rather limited area of the summit of Mt. Mitsu-mine. The lava indicated the *Re* (reverse and eastwards) magnetisation, and is petrographically identical with *Teppeiseki* (olivine-bearing-two-pyroxene andesite) of the Fukuzawa-yama quarry, and the lava is one of the representative types of the middle member of the Enrei formation. Though the lava of the summit of Mt. Mitsu-mine overlies directly biotite-bearing-hornblende-two-pyroxene andesite lava exposed along the ridge from Mt. Mitsu-mine to the pass of Wada-toge. A certain time-interval might be placed between the extrusions of both lava-flows, because it is concluded from the interpretation of the geomagnetic variation that the liparite of Wada-toge has intruded after the extrusion of the biotite-bearing-hornblende-two-pyroxene andesite and before the olivine-bearing-two-pyroxene andesite.

The similar type of andesite lava distributes in the environs of Mt. Utsukushi-ga-hara, north of the pass of Tobira-toge. As already stated, the Enrei formation here consists merely of thick andesite lava-flow covering directly the basement-rocks of the green-tuff, the sediments of the Hongo formation and quartz-diorite.

The thickness of the lava-flow attains in one place to at least 600

m. The surface of lava-flow as a whole forms a flat-topped summit of Mt. Utsukushi-ga-hara (Fig. 16).

Despite the striking thickness, the lava seems to show an uniform magnetic directions form bottom to top. There is a little doubt as to the magnetic direction of the lava of the highest part of Mt. Utsukushi-ga-hara, because the disturbances are markedly recorded in these rocks[30]. Excepting that the specimens obtained near the bottom carry a small amount of hornblende and their groundmass crystals are coarser-grained as compared with the specimens from the upper part, the andesite as a whole is very homogeneous in their petrographic characters, showing also the perfect platy-joints as seen in *Teppeiseki* (Fig. 17 a, b).

The same lava is distributed separately in the vicinity of Mts. Monomi-ishi-yama and Mizunotatsusawa-no-atama, north-eastward of Utsukushi-ga-hara.

The facts suggest that the fluidal lava-flow extruded at the same time has filled up the hollow part of the surface of the basement-rocks as if the water had filled up a pond, and partly overflowed to the north-east and the other direction. The extensive platform of Mt. Utsukushi-ga-hara having an altitude of about 2,000 m. may indicate the surface of a pond of extruded magma.

vii) *Kamisuwa-Kirigamine District.*

In the Enrei formation of the Kamisuwa-Kirigamine district, the lava-flows at the same altitudes may not always correspond to each other between the west and the east sides of the valley of the Kakuma-gawa. The formation of the west side of the valley of the Kakuma-gawa, namely that exposed along Kanko-doro (the sight-seeing road) from Jizo-ji to Tadeno-umi is recognized to intercalate the five flows of lavas as shown in our geologic map. The lowest flow of these lava is two-pyroxene andesite exposed at Jizo-ji. Though it can hardly be thought that the lava has been displaced, its magnetic direction is rather peculiar in this district as already stated (see p. 454).

At higher levels than Tate-ishi along Kanko-doro thin mud-seams and volcanic conglomerate beds which recorded marked signs of water-deposition are commonly found in the tuff-breccia.

The inclinations of the strata indicated by these mud-seams are about 30° south-westwards. Accordingly, it is thought that the higher the level we go up, the lower the strata we meet with in the vicinity of Tate-ishi. All of these three lava-flows (altitudes of their exposures are

30) K. KOBAYASHI, *et al.*, *Science* (*Kagaku*), **19** (1949), 284.

1,020 m., 1,050 m. and 1,050 m. above *M.S.L.* respectively.) are the two-pyroxene andesite and show the perfect platy-joints of the *Teppeiseki* type.

The olivine-two-pyroxene andesite exposed in the vicinity of Tateno-umi overlies the groups of Tate-ishi lava-flows. Except for the lava at Jizo-ji, all of these andesite lava-flows show the magnetic direction of *Rw*, and may represent the lower member of the Enrei formation.

At the east side of the valley of the Kakuma-gawa, on the other hand, olivine-two-pyroxene andesite lava is exposed at the lower level ($h = 980$ m. above *M.S.L.*), and another lava-flow of the same kind is also found below the Fukuzawa-yama quarry ($h = 1075$ m). Both these flows of the andesite lava show the magnetic direction of *Rw*, and may therefore correspond to the lower member of the Enrei formation. Marked platy-joints develop also in these lavas, although the thickness of each flag is somewhat larger than that of the typical *Teppeiseki* (Fig. 19 b). From the standpoints concerning magnetic directions and petrographic characters, it may be concluded that the lava-flow located beneath the Fukuzawa-yama quarry is correlated to the lava at Tateno-umi.

Above these lower members, the famous *Teppeiseki* lava quarried at such various places as Fukuzawa-yama (1,130 m. above *M.S.L*, Fig. 18 a, b), Nyukai (1,260 m.) and Kakuma-shinden (1,230 m.) is developed in wide extension as shown in our map.

The lava as a whole is identified with olivine-bearing-two-pyroxene andesite and is more than 30 m. in maximal thickness. The lateral extension of the lava-flow is traced southwards for a long distance and forms an continuous cliff as can be viewed from the opposite bank of Lake Suwa (Fig. 13 a). The magnetic directions of the lavas are observed to be *Re* (reverse and eastwards) and seem to indicate that they represent the middle member of the Enrei formation as supposed from the consideration due to petrographic studies.

Two flows of two-pyroxene andesite lava are found at higher levels above that at Tateno-umi. Tough their magnetic directions have not yet been measured, the flows may be referred petrographically to the middle member including the *Teppeiseki* lava.

The upper member of the Enrei formation is Kiriga-mine volcano and consists mainly of hornblende andesite lavas and associating tuff-breccias exposed between the area from Kowashimizu to Mt. Kuruma-yama and overlies all the middle member stated before. The hornblende andesite lava is characterized by the features in which it carries only

hornblende as phenocrystic minerals and exhibits fairly glassy groundmass and remarkable flow-structure (Fig. 22), hence they are easily distinguished from the other rock members. So, they are discriminated from the lower and middle member as shown in our map.

The magnetic directions of this member were determined only from the specimens obtained from Kowashimizu because the specimens collected from the localities around Mt. Kuruma-yama have shown a distrubance influenced by thunderbolts. The observed magnetic directions of the lava are all *Re* too.

It seems however that a significant time-interval is not expected to intervene between the hornblende andesite at Kowashimizu and the *Teppeiseki* lavas at the Fukuzawa-yama and Kakuma-shinden quarries basing upon our considerations on the magnetic variation as will later be stated. Hence, hornblende andesite lavas of Kirigamine might have extruded succesively after the *Teppeiseki* and allied lavas which are assigned to the middle member of the Enrei formation.

As already mentioned, both the hornblende andesite at Washiga-mine and that at Kiriga-mine might therefore have extruded at the same stage.

3. *Petrographic notes*

Late Pliocene～early Pleistocene rocks around Lake Suwa may be classified as follows;

(1) two-pyroxene andesites and some varieties carrying olivine, hornblende and the least amount of biotite.

(2) liparite with obsidian.

(3) glassy hornblende andesite (lava-flow).

(4) hornblende andesite (neck).

(5) olivine basalt (dike).

Their petrographic characters will be described one by one concerning the specimens collected from type-localities.

i) *Hornblende-bearing-two-pyroxene andesite* (*Nishimochiya, Wadatoge*)

They contain phenocrysts of plagioclase, hypersthene, augite, magnetite and opathitized hornblende.

Large tabular phenocryst of plagioclase (up to 3 mm., idiomorphic) shows honeycomb structure due to the presence of glass inclusions and oscillatory zonal-structure ranging from acidic labradorite to andesite. Turbid core crowding with many minute inclusions is often observed. Sometimes plagioclase flocks together with pyroxene and forms large

glomeroporphyritic aggregates. Clear prismatic and weakly zoned plagioclase (up to 1.5 mm. in length) is also scattered.

Prismatic hypersthene (up to 2.5 mm., sometimes fragmental) is common, sometimes it includes minute rounded inclusions and parallel intergrowth in which a small ill-formed hypersthene core usually enveloped by a thick augite mantle is often observed. Augite is smaller and less idiomorphic than hypersthene. Twinning on (100) is common in augite. Many small fragments of augite are arranged in the same optic orientation in a certain area under the microscopic field. The latter fact suggests that the previous large augite crystal has been replaced by later plagioclase crystal (Fig. 26 a). Small rounded or sphenoid grains of opathitized hornblende are often found, the pleochroism is as follows; X = pale brownish yellow, Y = light brown, Z = light blackish brown to reddish brown. Besides brownish hornblende, comparatively large crystal of greenish hornblende is rarely observed being surrounded by narrow opathite margin. Pleochroism is X = pale green, $Y \fallingdotseq Z$ = pale brownish green.

Xenoliths of two-pyroxene andesite characterized by higher crystallinity, coarser-grained and more basic groundmass are rarely found under the microscope.

Groundmass consists essentially of plagioclase, hypersthene, augite, magnetite and a little amount of tridymite and glass. Crystallinity of groundmass is lower than that of olivine-bearing-two-pyroxene andesite (*Teppeiseki*), though magascopic characters are similar to *Teppeiseki* especially in respect of well-developed thin platy-joints. Texture of the rock is pilotaxitic. Brownish glass fills sometimes large cavity of groundmass.

Biotite-bearing variety occurs west of the pass of Wada-toge, biotite flake is found as both phenocryst- and groundmass-minerals. This rock-type is characterized by low-crystallinity of groundmass and the predominant presence of tabular plagioclase. Plagioclase phenocryst encloses rarely hornblende and pyroxene grains. No brownish hornblende is found.

ii) *Olivine-bearing-two-pyroxene andesite* (*Teppeiseki*) (*Fukuzawa-yama*)

They contain phenocrysts of tabular plagioclase, hypersthene, augite magnetite, and olivine. Large tabular plagioclase (3～5 mm. long) is rarely found, groundmass is coarse-grained, sometimes the rock looks non-porphyritic under the microscope. Tabular plagioclase is dominant and

usually oscillatory zoned from labradorite to andesine and its central part is often charged with glass inclusions. A smaller prismatic phenocryst of plagioclase is also found, but it is generally clearer and more acidic than tabular phenocrysts. Polysymmetrical and penetrating twins are common.

Prisms of hypersthene and augite are also dominant. Hypersthene is generally larger and better-formed than augite. Parallel intergrowth in which irregular hypersthene core is enveloped by augite mantle is often observed. Both sorts of pyroxenes flock together with plagioclase forming glomerophorphyry.

Skeleton crystals of magnetite are common, and sometimes include minute inclusions of anisotropic minerals.

Olivine is usually corroded, often crushed and rimmed by small augite grains, it is sometimes recognized only as serpentinous pseudomorph after olivine.

Groundmass consists mainly of acicular plagioclase, hypersthene, granular augite, magnetite and subordinate amount of anorthoclase with a small amount of glass, and is characterized by pilotaxitic texture. Crystallinity of groundmass is considerably high.

iii) *Liparite* (*Wada-toge*)

They are purplish grey or white colored rocks and often spotted by iron rusts showing a frosty pattern. A striped pattern due to the repeat of dark and light colored bands may be a sign of flow-structure.

They contain rounded phenocrysts of quartz, oligoclase, alkali-feldspar and flaky biotite. The voluminal proportion of these phenocrysts to groundmass is less than 5 % of the bulk of rock.

Corroded quartz (sometimes fragmental and up to 2 mm. in diameter) occupies one half of the total amount of phenocrysts, is often remarkably cracked and has usually many minute inclusions. Plagioclase crystal exhibits rounded form due to corrosion, zonal structure is not recognized, and it often shows honeycomb structure due to the presence of glass inclusions. Alkali-feldspar is rarely found.

Sometimes biotite is found as slender flakes (up to 2 mm. in length). Judging from its form, it seems to be pseudomorph after hornblende. Pleochroism is X = pale yellow, $Y \fallingdotseq Z$ = dark yellowish brown.

Groundmass is microfelsitic due to devitrification, often spherulitic and by minute grains of magnetite is scattered universally.

Obsidian. Black or brownish belts of obsidian sandwiched between light-colored liparite with 1～0.1 m. in width are often observed, and they

show dike- or vein-like appearances as if obsidian might intrude into liparite in parallel with their flow-structure. In black belts of obsidian, small, purplish grey and opaque spherulites are scattered. Sometimes they are in directional arrangement producing bands of spherulites.

Phenocryst is usually not found. Groundmass consists mainly of small anisotropic crystals (possibly quartz) and glass (colorless in thin section) enclosing minute hair-like crystallites. These trichites are in remarkable parallel arrangement.

Spherulites mentioned above are radial aggregates of devitrified glass and are brownish in color under the microscope.

iv) *Glassy hornblende-two-pyroxene andesite* (*Kowashimizu*)

They contain phenocrysts of plagioclase, hornblende, hypersthene, augite and magnetite, and characterized by marked flow-structure and vitric appearances. Idiomorphic prisms of plagioclase (up to 3 mm. in diameter) are common and oscilatory zoned from sodic labradorite to calcic andesine. The central part of such crystal is often charged with glass inclusions.

Hornblende is commonly small and prismatic crystals (1∼3 mm. in length). Most of the hornblende is either rimmed by opathite-margin or replaced wholly by opathitic aggregates, the central part of which consists of augite grains and is surrounded by magnetite grains. Pleochroism is X = pale yellow to light brown, Y = brownish yellow, Z = brown to reddish brown.

In pyroxenes, monoclinic pyroxene is subordinate to orthorhombic pyroxene in amount. Sometimes both kinds of pyroxenes flock together and form glomeroporphyry. Large poikilitic phenocryst of hypersthene is common. Corroded hypersthene crystal is rarely enveloped by hornblende crystals.

Groundmass is hypohyalline and rarely pilotaxitic, and exhibits remarkable flow-structure. It consists of plagioclase, hornblende, biotite, hypersthene, magnetite, alkali-feldspar and tridymite with considerably devitrified glass. Sometimes the groundmass is porous, and fine crystals of tridymite and other minerals are found in these druses.

In some varieties, biotite is found as a small anhedral phenocryst.

v) *Hornblende andesite* (*intrusive neck*) (*Takao-san*)

They contain phenocrysts of plagioclase, hornblende, magnetite, hypersthene and augite.

Plagioclase is as large as 3 mm. in length, hypidiomorphic and tabu-

lar andesine, and is often crushed. Usually it exhibits oscilatory zoning, and its core is charged with glass inclusions.

Hornblende is hypidiomorphic prism in form and encloses often augite grains poikilitically. It has altered partially to biotite with or without narrow opathite-margin. Sometimes it flocks together with pyroxene grains, plagioclase and magnetite. Pleochroism is X = light green, Y= pale brownish green, Z = brownish green.

Skeleton crystal of magnetite is common and often rimmed by biotite flakes.

Hypersthene and augite are found as phenocrysts but are less in amount.

Groundmass is very compact and hypohyalline and consists of plagioclase, hypersthene, biotite and tridymite. Glass fills the interspace.

vi) *Olivine-two-pyroxene basalt* (*Nishimochiya*)

They contain phenocrysts of skeleton crystals of olivine, hypersthene, prismatic augite and labradorite. The amount of phenocrysts is less than only 10 % of the bulk. Often glomeroporphyritic aggregate of small augite with plagioclase is found. Sometimes plagioclase bears turbid and more calcic core (bytownite) and shows rarely oscillatory zoning. Parallel intergrowth of rhombic and monoclinic pyroxenes, zonal structure and hourglass structure or wave extinction of augite are commonly observed.

Groundmass exhibits hyalo-ophitic texture and consists of plagioclase, monoclinic pyroxene (pigionitic pyroxene), magnetite and subordinate amount of colorless glass.

4. *Correlation*

As the volcanic area is scarce of fossils, it is very difficult to establish the mutual relation between each separate volcanic mass and strata and search stratigraphically for the age of the explosion of the volcano.

However, the role of paleomagnetic research in our studies concerned with the geologic survey in Central Japan has propounded that the magnetic directions of rocks are very effective as a new type of fossil for stratigraphic work of the volcanic area. Based on geologic and paleomagnetic research, the volcanic rocks around Lake Suwa are divided into four units as follows.

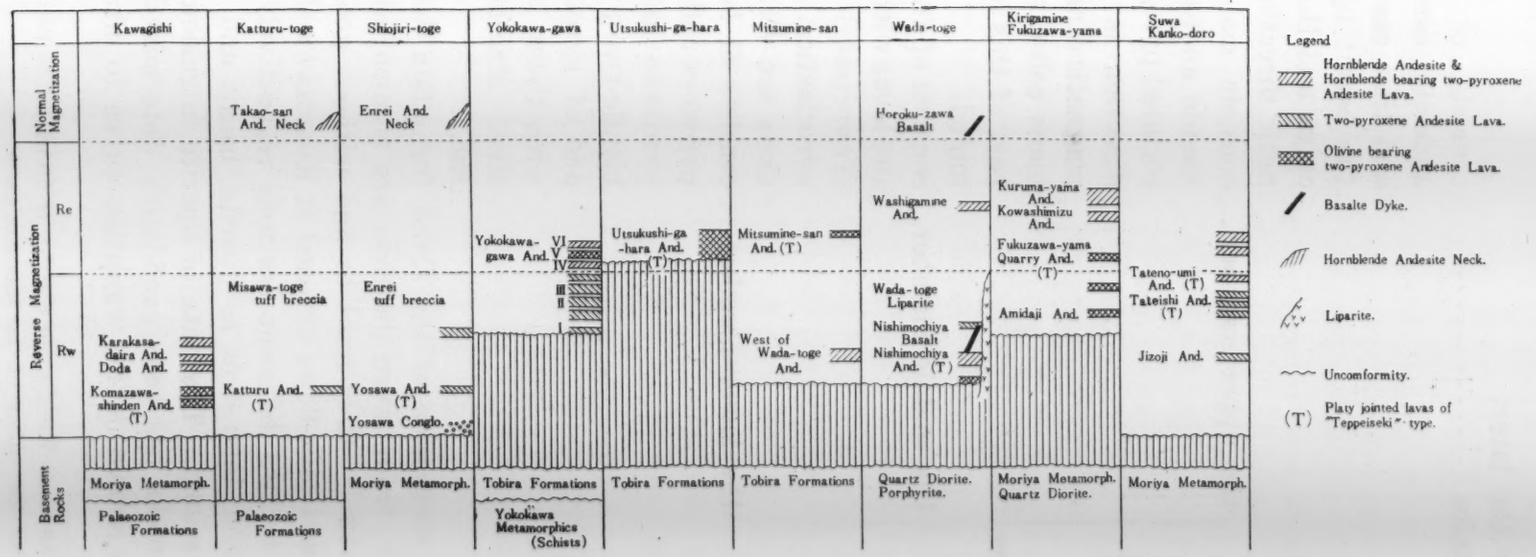

Fig. 12. Correlation chart basing upon geomagnetic and geologic studies of the Enrei formation.

Pleistocene or the latest
Pliocene volcanics ..... consists of the hornblende andesite necks of Takao-san and that east of Enrei Park, the basalt bykes of Nishimochiya and Horoku-zawa. Magnetic directions are *Ne*.

Enrei Formation (Late Pliocene)

- the upper member ... consists mainly of the hornblende andesite lavas and associated pyroclastics. Magnetic direction is *Re* so far as the magnetic direction of the specimens collected from the lower part of this member are determined.
- the middle member... consists of two-pyroxene andesite lavas with or without olivine (*Teppeiseki*) and associated pyroclastics. Magnetic directions are *Re*.
- the lower member ... consists of lava-flows of two-pyroxene andesite, olivine-two-pyroxene andesite and hornblende-two-pyroxene andesite and of pyroclastics associated with them, and liparite intrusive. Magnetic directions are *Rw*.

The stratigraphic succession of the Enrei formation that have been described individually from seven districts are summarized and correlated as shown in Fig. 12[31]. It is hard to find without geomagnetic criteria that both *Teppeiseki* lava-flows exposed at Komazawa-shinden and Fukuzawa-yama refer to two different horizons respectively. Similarly, the ages of such volcanic intrusives as liparite, basalt and hornblende andesite are not determined. The data of liparite intrusion of Wada-toge in relation to other rocks has been confidently determined by its magnetic direction which is shown on the variation curve to situate just near to

31) In Fig. 12, Kamisuwa-Kirigamine district is divided into two column, i.e. the eastern and western sides of the valley of the Kakuma-gawa.

the critical point at which magnetic direction have turned from *Rw* to *Re* as will later be demonstrated in Fig. 13. Because such a type of lava as the *Teppeiseki* of Fukuzawa-yama and Mt. Mitsu-mine is absent around the liparite body, the relation of liparite to the *Teppeiseki* lava can not be clarified in such a traditional method as has been used in geology.

Correlations by means of paleomagnetic researches for various Pliocene volcanics of the Fossa-magna region in Central Japan was already supplied by the senior author[32]. A remarkable coincidence with geologic data has been accepted to stand in all of the Shigarami, Komoro and the Enrei formations.

5. Discussion

1. *Summarized results of observed magnetic directions of samples collected from various localities.*

Geologic surveys made by us have supplied many conclusions concerning the geologic structures of the Enrei formation. In the light of the magnetic studies hitherto made, the change of geomagnetic field during late Pliocene times is supposed to be that which will be discussed in the following:

The observed magnetic directions of samples from the Enrei formation are all assigned to *R.N.R.M.* and it moreover is said that those in the lower part are westward and those in the upper part are eastward in direction.

All the lava-flows distributed over a wide area are accordingly conceived to be roughly contemporaneous with one another from the standpoints of geology and rock magnetism.

According to our measurements, only two examples which are represented by the andesite from Mt. Takao-san and the basalt from Horoku indicate their directions are normal. Both bodies are recognized as the postdated intrusives into the Enrei formation.

The fact will not provide a decisive evidence for considering that the whole range of the Enrei formation might be characterized by only geomagnetic reversal. We can suspect within the range of the Enrei formation that there has intervened a time when the geomagnetic field was normal. If such is the case, it is likely that we ought to have made a finding of *N.N.R.M.* in some of the samples collected from the Enrei formation.

The observed *N.N.R.M.* of the samples from Takao-san and Horoku,

32) K. Momose, *loc. cit.*, 1).

therefore, seems to indicate their age of intrusion to be close to the Plio-Pleistocene boundary.

2. *Late Pliocene variations of geomagnetic dipole suggested by the obtained results.*

Pole positions calculated from the average magnetic directions with

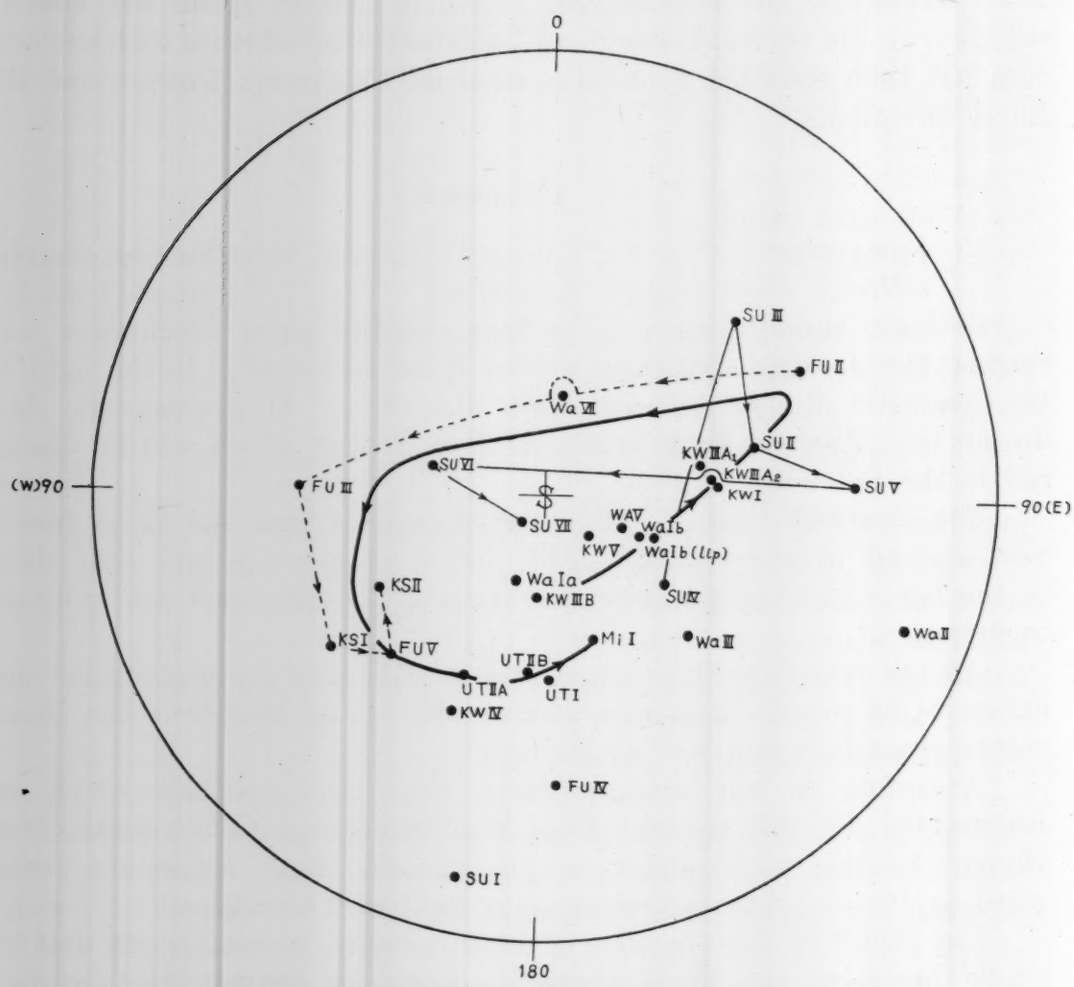

Fig. 13. Modes of the variation of pole positions which might have taken place during the time range of the Enrei formation. Pole positions calculated from measured magnetic directions of the samples taken from every locality are all plotted in this figure. Pole positions can be considered to have shifted along two slender lines with arrow signs basing upon stratigraphic succession in two areas. Taking advantages of other data obtained from the samples of the Enrei formation, we can conceive that pole positions might have shifted along the thick line drawned in the figure during the whole range of the Enrei formation.

respect to every locality are projected in Fig. 13 in relation to their stratigraphic situations. The shifting of pole position through late Pliocene times have thus been established by us.

The continuous and broken lines in Fig. 13 indicate respectively the shiftings of pole position inferred from the results obtained from the samples from Loc. Fu (called Fu group) and from Loc. Su (Su group) respectively. The mass of Su group marks in some parts certain dislocations influenced by faulting. As regards such dislocated beds, original values obtained, therefore, were corrected by making restoration for actual geologic dip of the bed. Although both modes of shifting of pole positions with regard to above-mentioned groups, do not show a complete coincidence with one another, they can be comparable as to the tendency in which pole positions might have shifted from east to west.

In addition to these, numerous instances have supplied a basis for considering that pole position might have shifted from east encircling the present position of the rotation axis westward through the whole time range of the Enrei formation (Fig. 13).

It can not easily be estimated how long the time range of polar variation of this sort lasted, it can, however, easily be inferred that the mode cited above does signify a continuous feature of polar variation during the late Pliocene.

3. *Pliocene chronology inferred by means of geomagnetic variation.*

As seen in the correlation chart which the senior author previously published[33], the whole range of Pliocene is thought to be represented by Shigarami, Komoro and Enrei formations, and he propounded in the paper his opinion that the geomagnetic polarization might have reversed in a continuous way through the span of middle Pliocene times. During the late Pliocene which is represented mainly by the Enrei formation, the pole position might be located close to the rotation axis of the earth.

According to publications hitherto made, many instances of inferred pole positions during the geologic past, even if they were those of either *N.N.R.M.* or *R.N.R.M.*, have been known to be located close to the rotation axis.

The senior author would like to believe that such affairs might be due to the actual existence of the fact that the time range when pole positions were close to the rotation axis might have lasted long.

He would also like to infer that the pole position might rather be

33) K. MOMOSE, *loc. cit.*, 1).

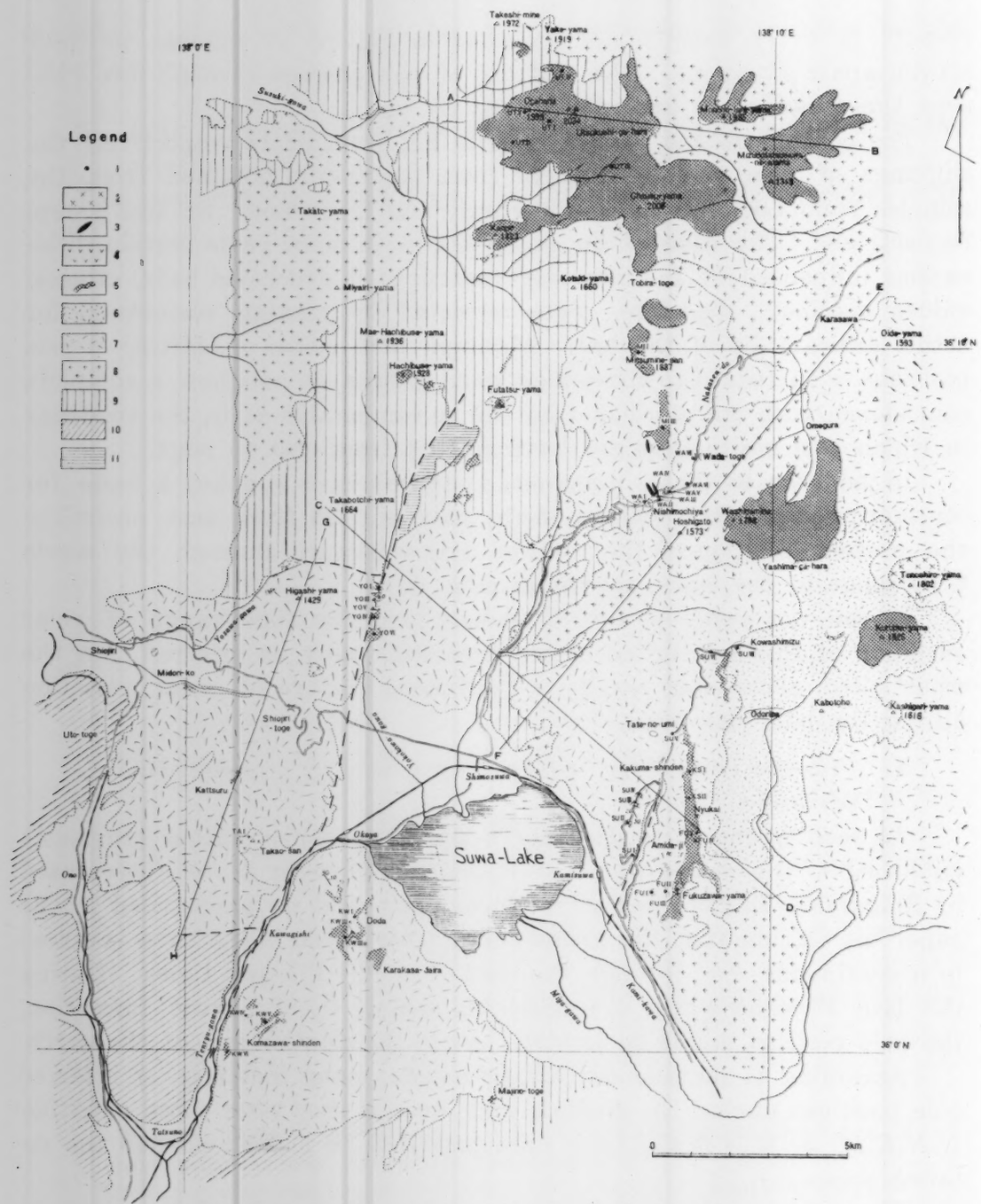

Fig. 14. Geologic map of the area around Lake Suwa.

1. Localities of the collected samples
2. Hornblende Andesite
3. Basalt
4. Liparite ..... } Enrei formation
5. Lava-flow ..... } Enrei formation
6. Upper part of tuff-brecia } Enrei formation
7. Lower part of tuff-brecia } Enrei formation
8. Quartz-diorite
9. Pre-Pliocene Tertiary
10. Palaeozoic
11. Yokokawa Metamorphics

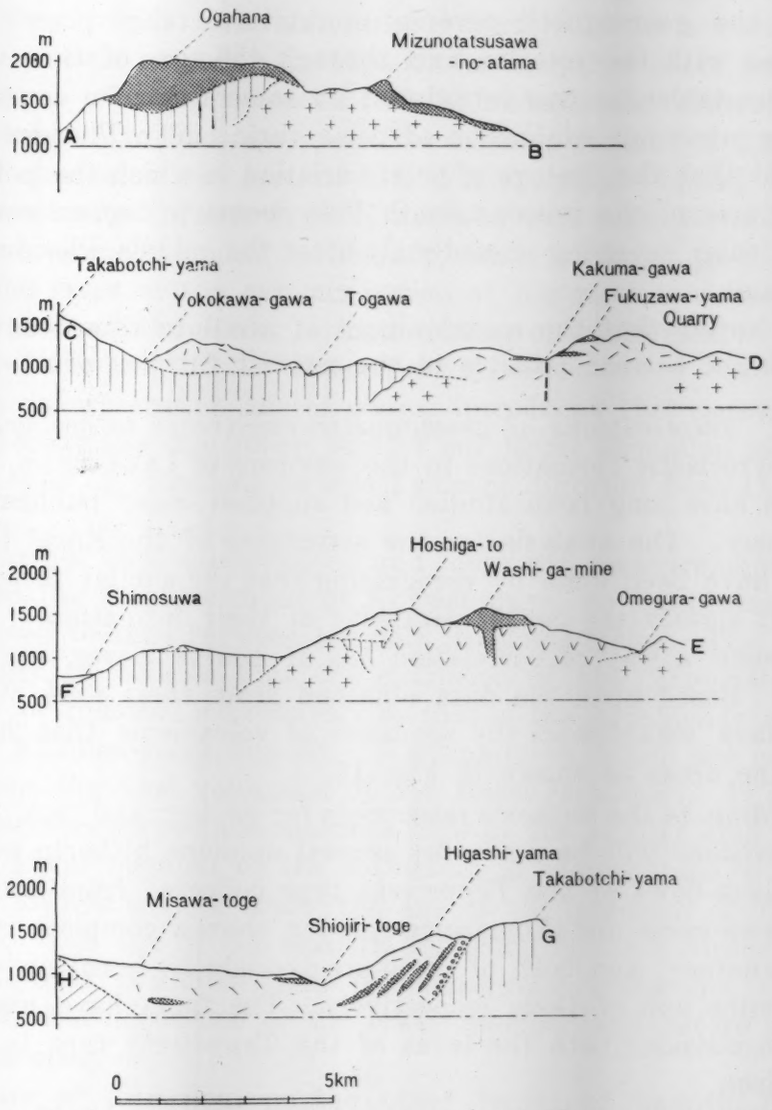

Fig. 15. Geologic profiles along lines $A-B$, $C-D$, $E-F$, and $G-H$ on map in Fig. 14.

stable only in the case when the dipole axis was close to the rotation axis, and the geomagnetic reversal might have taken place in a way unconnected with the rotation axis through the span of time when geomagnetic unstableness was introduced by some unknown causes.

Basing upon our evaluation of polar variation in Pliocene times, it can be said that the feature of polar variation in which the pole position has swing around the present South Pole seems to demonstrate the existence of polar swinging immediately after the middle Pliocene reversal of dipole axis.

It is hoped that the measurement of absolute time length of the Pliocene might become possible in the nearest future.

4. *Implications of geomagnetic researches to geology.*

The pyroclastic formations in the environs of Lake Suwa, the Enrei formations have long been studied and supplied many publications as to their geology. The analysis for the structures of the Enrei formations, however, have been done by recognizing that the similar facies in lithology might signify the contemporaneity of their formation.

But such a way of correlation has of course never warranted its adequacy. Based upon the data obtained from their field studies, the authors have established the sequence of volcanisms that have taken place in the areas as shown in Fig. 12.

According to the author's researches for geology and rock magnetism, certain revisions will be made for several opinions hitherto published.

Two lava-flows of the *Teppeiseki* type collected from both localities at Fukuzawa-yama and Komazawa-shinden show a complete resemblance with one another, and both of these are overlain by hornblende andesites of Kirigamine and of Doda respectively. The facts have made various authors to consider both the lavas of the *Teppeiseki* type to be at the same horizon.

The lava-flows at Komazawa-shinden, however, should be referred from the geomagnetic points of views to those of the lower part of the Enrei formation and those of Fukuzawa-yama should as well be referred to those of the middle.

The fact will imply that the extrusion of the similar kind of olivine-bearing-two-pyroxene andesite has twice taken place. The lava of olivine-bearing-two-pyroxene andesites at Mt. Utsukushi-ga-hara and Mt. Mitsumine (*Teppeiseki*-type) each of which locates apart, have been confirmed to be at the similar horizon to that of Fukuzawa-yama. Although a slight difference in the lithologic characters is recognized between the

upper and the lower lavas of Utsukushi-ga-hara, they suggest in particular that they might have accumulated locally up to a considerable thickness in a basin or valley perhaps during a rather short period.

The horizon of the *Teppeiseki* lava is undoubtedly situated below the lava forming Mt. Kuruma-yama—the highest summit of Kirigamine Volcano and also below the lava of Mt. Washigamine. Seeing that the latters are markedly vitreous type of andesite and characterized by the occurrence of phenocrysts of hornblende, most authors have hitherto dealt with the lavas of the summit region of Kirigamine Volcano separately from those of the Enrei formation being characterized by the accompanying of the lava of the *Teppeiseki* type.

Such an interpretation has of course introduced the conception in which they recognized the upper part of our Enrei formation as one of the peculiar type of volcanoes—a shield volcano different from the Enrei formation.

So far as our field observations and magnetic measurements have been made in the neighbourhood of Kowashimizu, no significant hiatus can be expected to exist between the both lithologic facies. The authors are accordingly to believe that the extrusion of the *Teppeiseki* lava might surely be followed successively by that of the hornblende andesite lavas of Mt. Kuruma-yama and Mt. Washiga-mine, which are considered to represent the final volcanism of the Enrei formation. It is quite noticeable that the hornblende andesite lava of the similar kind is also found in the lower member of the formation in the environs of Doda.

It is not always easy to know the age of the intrusion of dike and volcanic neck. The age of the liparitic intrusion in the environs of the pass of Wada-toge is known from palaeomagnetic researches to have happened after the deposition of the lower member and before that of the middle member.

Both times of intrusion, on the other hand, of basaltic dike at Nishimochiya and volcanic neck at Mt. Takaosan have been clarified in the sense that they might have intruded a certain while after the final deposition of the Enrei formation.

Our estimation of the ages of intrusions of these special rock-types located in the area mainly of two-pyroxene andesite will surely be significant. It will also be useful for the considerations of the volcanism within the periods from the late Pliocene to the early Pleistocene.

5. *Implications to Geomorphology*

(i) *Mt. Utsukushi-ga-hara—a volcanic mesa.*

Mt. Utsukushi-ga-hara has long been discussed by various authors[34),35),36)] among whom were several authors who considered the mountain as a lava plateau. It exhibits a peculiar appearance in which a rather wide and level summit of more than 4 km^2 stands at a level of about 1,900m above the sea-level. On the southern slope of the upland where a good exposure of rocks as high as 500 m is displayed, there is found no pyroclastic materials interbedded with lavas. These facts are likely to have introduced an opinion that Mt. Utsukushi-ga-hara is sure to be a lava plateau. If the present geomorphic feature of the upland might be due to the primary volcanic froms, the origination of the steep cliff above-mentioned can hardly be explained. The level surface of Mt. Utsukushi-ga-hara is composed of lava and in parts of basement of quartz-diorite, marine sediments of middle Miocene times.

In the summit region, there can not be detected any marked discontinuity in topographical relief between the lava and the basement rocks. In the summit region consisting of lava-flows, the even surface dipping imperceptively eastward seems to represent the primary surface of lava-flows. On the marginal part of the main area of lava-flows, the lavas occupy in many places the upper part of mountain ridges and the basement rocks therefore are exposed up to the higher part of the valley sides. These facts will imply that Mt. Utsukushi-ga-hara which was built up during late Pliocene times would have been moderately dissected and its topographic feature should therefore be referred to "volcanic mesa".

(ii) *Geological age of the highest erosion surface.*

Two remarkable erosion surfaces are recognized along the western border of the Enrei formation, each of which is at the level of 1,900 m and at that of 1,500 m respectively. The erosion surface which truncates the basal rocks just at the level of the even summit of Mt. Utsukushi-ga-hara and the even crest of Mt. Hachibuse altitude 1,928 m consisting of middle Miocene sedimentary rocks are at the some level indicating the past development of the former erosion surfaces at the highest level in our district.

As was previously mentioned, the altitudes of surface of the basement over which the Enrei formation lies are variously at the lowest level of 1,300 m. and at the highest level of 1,900 m. or more. The

34) F. HOMMA, *loc. cit*,. 5).
35) T. YAGI, *Jour. Geol. Soc. Jap.*, **27** (1920), 125.
36) K. KOBAYASHI, *Geogr. Rev. Jap.*, **26** (1953), 291.

lavas might flood filling the tract of former valley or basin-like lower part introducing perhaps no distinguished volcanic inversion of relief, because the lavas are not exhibited so thickly on the highest erosion surfaces. The extruded lavas of Mt. Utsukushi-ga-hara might have piled up to the level of about 1,900 m filling up the former valleys whose bottoms are now at the level of about 1,300 m.

The highest erosion surface might therefore be formed before the time of deposition of the Enrei formation and after that of the middle Miocene formations. It is usually difficult in any district to know the time of origination of erosion surfaces at higher altitudes. The present studies have made without fail a contribution to a problem of geomorphological significances.

(iii) *Kirigamine Volcano—a shield volcano.*

The so-called Kirigamine whose summit region exhibits a low relief topography with rather flat cones here and there, has been referred to a shield volcano. However, no remarkable hiatus is considered to be placed between the middle part of the Enrei formation and the lava-flows forming the summit region of Kirigamine volcano. Although lithologic features of both members are discriminated, both members can not be discriminated perfectly by means of palaeomagnetic considerations. This is the reason why the authors have dealt with the hornblende andesite in the summit region as the upper member of the Enrei formation.

The lava flows of the *Teppeiseki* type as well as many flows of other types of andesite are generally less than 30 m in thickness and indicate a nature in which remarbable lateral extensions of lavas took place covering the even surface of tuff-breccia which in many places shows more or less signs of water-deposition.

It is easily understood that the striking platy-jointed structures might be originated from the striking lateral extension of lava-flows. The lava-flows in the summit region also suggest the fluidal nature of extruded lavas being indicated by dominant existence of flow structures of glassy groundmass.

Even the highest summit Peak Kuruma altitude 1,925 m. is only 300 m. higher above the middle horizon of the Enrei formation.

The so-called Kirigamine volcano as a whole is composed mainly of the pyroclastic material with interbedded lava-flows, but a sort of volcanic depression took place in the early stage of volcanism and several flat cones were formed in the later stage. These facts seem likely to have produced a volcanic form with the appearance of volcanic upland.

It may be said that Kirigamine volcano would be a shield volcano, but the necessary conditions in which such a peculiar type of landform might be resulted, should be explained in the way as mentioned above.

Acknowledgements

It was in 1940 when one of the authors made a finding that the andesite of Mt. Utsukushi-ga-hara indicated anomalously strong magnetism. Our palaeomagnetic researches that were commenced at that time have long been developed in order to decipher the geomagnetic chronology of late Cenozoic times. The present paper has discussed the palaeomagnetic and geologic problems concerning the volcanic area around Lake Suwa.

The authors are indebted in particular to Prof. T. Nagata and to Dr. T. Rikitake in Tokyo University for their kind guidance. Dr. S. Akimoto, Dr. S. Uyeda and Mr. Y. Shimizu have offered many facilities and cordial co-operation, and we are also greatly indebted to them.

Prof. M. Suzuki in the Medical School of Shinshu University afforded facilities for our field work, Mr. Y. Hino prepared many rock slices for our microscopic observations, and Miss M. Momose and Miss C. Nakamura prepared the typescript of our manuscript for publication.

The authors wish to record here their sincere gratitude to all these persons.

---

29. 諏訪湖周辺の火山岩類の古地磁気学的および地質学的研究 — 中部地方における鮮新世火山岩の古地磁気学的研究（2）—

地震研究所 百瀬寛一
信州大学文理学部地学教室 小林国夫
信州大学文理学部地学教室 山田哲雄

（1） 諏訪湖周辺には，鉄平石とよばれる板状節理のよく発達した安山岩やそれに類似する安山岩の熔岩が何枚もある．全体的にこれらの熔岩は塩嶺累層とよばれる凝灰角礫岩を主とする火砕質岩属のなかに含まれている．

塩嶺累層中の火山岩のしめす磁化方位を利用して，地質時代における地球磁場の変動の模様，火山岩相互の時代の対比，地質年代，いわゆる霧ヶ峯火山の地質学および地形学的意義，さらにすすんで地形面の形成時代などについて研究した．

（2） 塩嶺累層の火山岩のうち，次の各グループ和田峠，川岸，三峯，美ガ原，諏訪地方より岩石を採取し，磁化方位の測定および安定性のテストを行つた．塩嶺累層の下部層の岩石の磁化方位は Reverse の西偏，上部層の岩石は Reverse 東偏をしめした．また，この累層のすべての岩石の磁化方位は Reverse N.R.M. であつた．高雄山安山岩は塩嶺累層を貫く岩頸であることと，磁化方

Fig. 16. Flat-topped summit of Mt. Utsukushi-ga-hara — a volcanic mesa, as seen from the south-west. The summit level is averagely at the height of approximately 2,000 m.

（震研彙報 第三十七号 図版 百瀬・小林・山田）

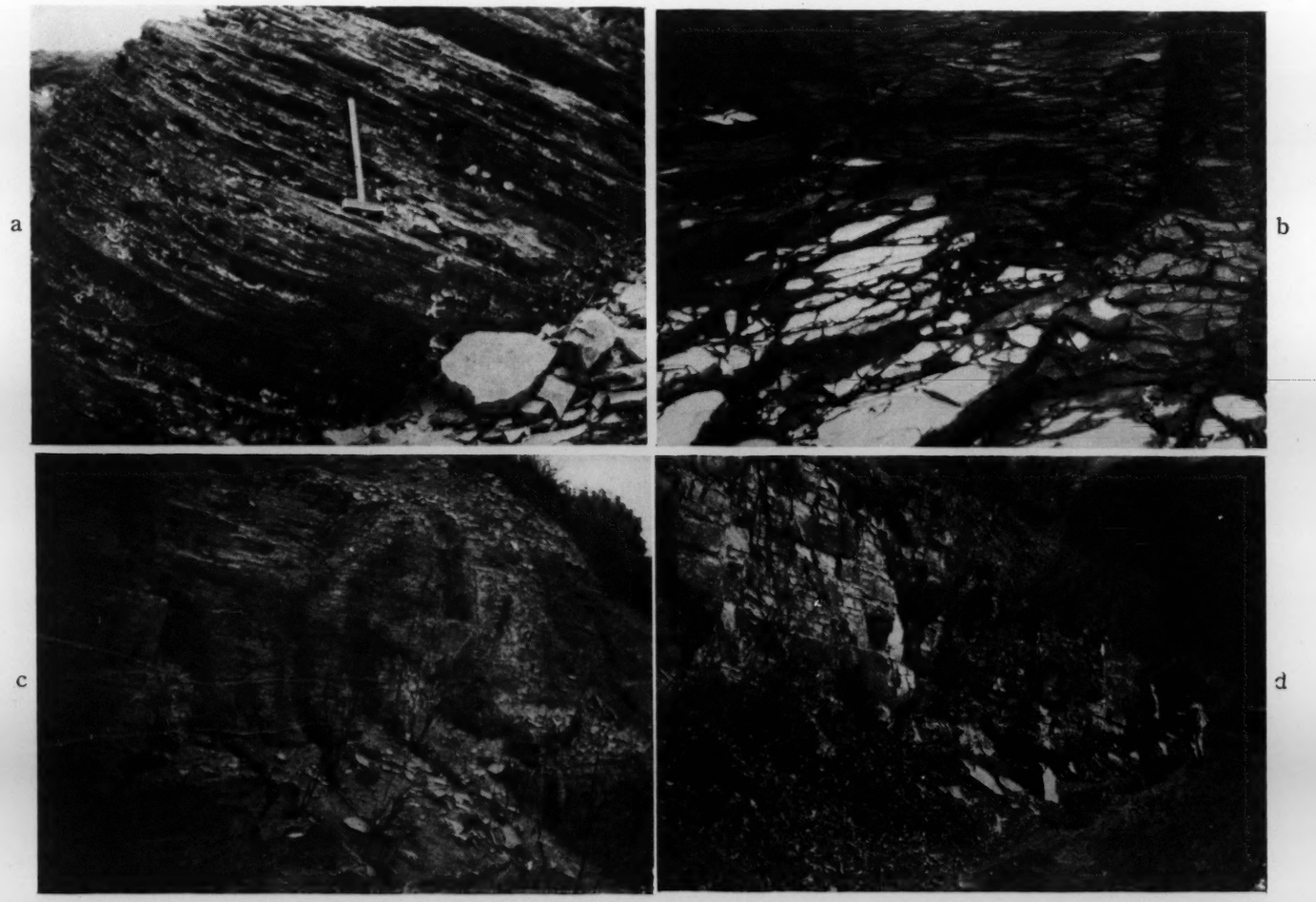

Fig. 17. Jointed andesite (Teppeiseki) at Loc. UT III (a) [Hyaku-magari on the southern part of Mt. Utsukushi-ga-hara], at Loc. UT IV (b) [north of Peak Ogahana], at Loc. Kw V (c) [Komazawa-shinden near Kawagishi]; and at Loc. Wa III (d) [Nishimochiya near the pass of Wada-toge] (hornblende-bearing-two-pyroxene andesite).

（震研彙報 第三十七号 図版 百瀬・小林・山田）

a

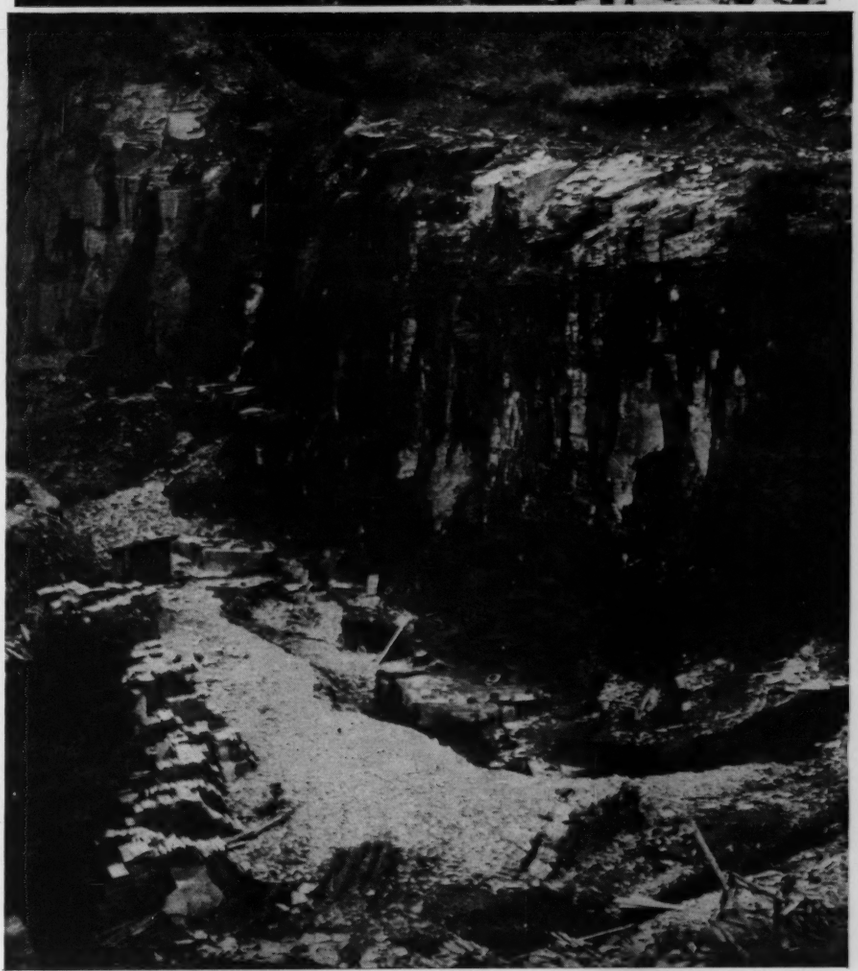

b

Fig. 18. Jointed andesite at Fukuzawa-yama quarry (a) and the whole view of the locality Fu III (b).

（震研彙報 第三十七号 図版 百瀬・小林・山田）

a

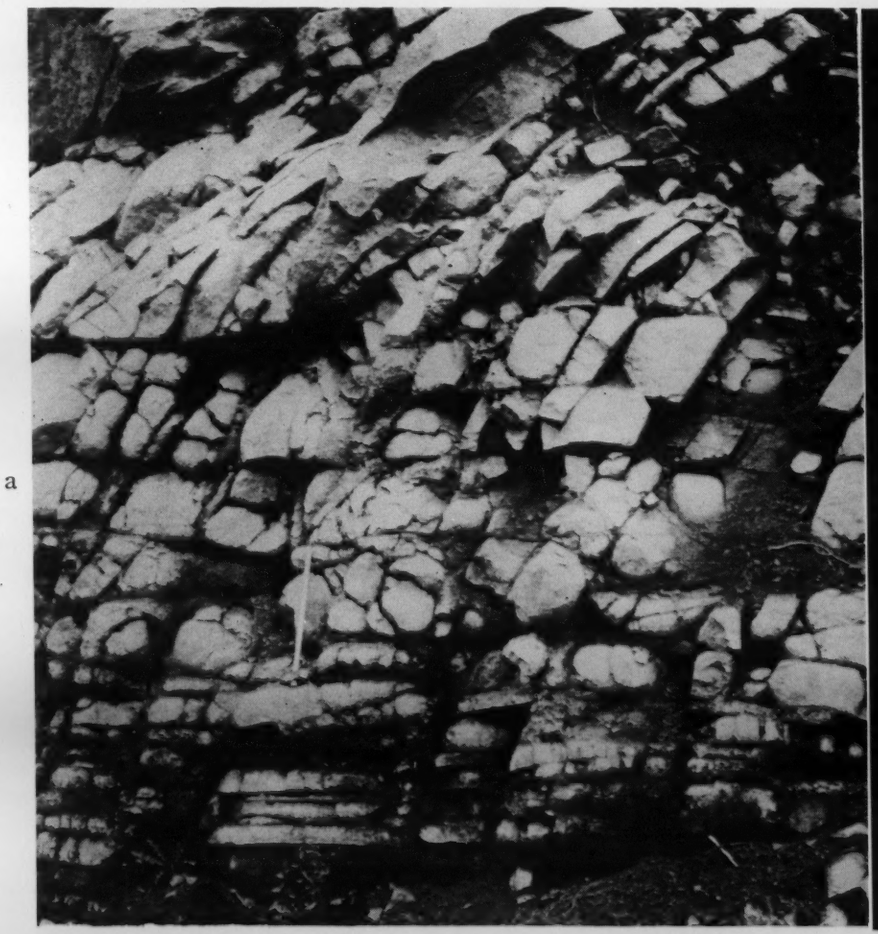

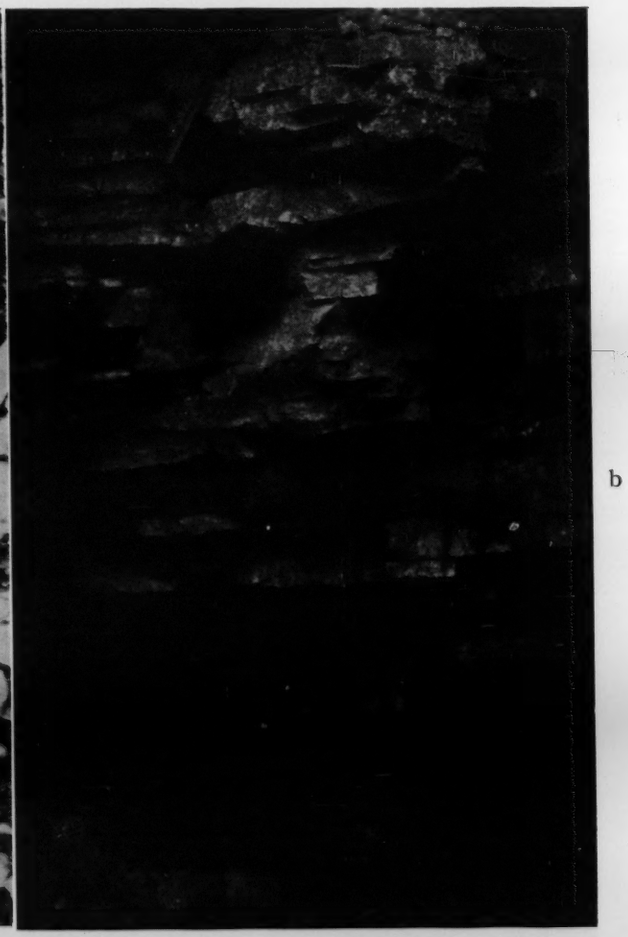

b

Fig. 19. Jointed andesite at Loc. Fu IV (a) below Nyukai showing the intercrossed joints of the upper part of the flow, and that (Oliv.-bearing-two-pyroxene andesite) at Loc. Fu II (b) below the Fukuzawa-yama quarry.

Fig. 20.

Fig. 21.

Fig. 22.

Fig. 23.

Fig. 20. View from south-west showing quarrys at Fukuzawa-yama and the summit level of the Enrei formation.

Fig. 21. The summit region of Mt. Kirigamine showing hilly but rather monotonous landscape of low relief.

Fig. 22. The upper lava exposed near Peak Kurumayama of Kirigamine Volcano showing its remarkable flow structure.

Fig. 23. Basal conglomerate of the Enrei formation at the uppermost part of the Yosawa.

（震研彙報 第三十七号 図版 百瀬・小林・山田）

Fig. 24.

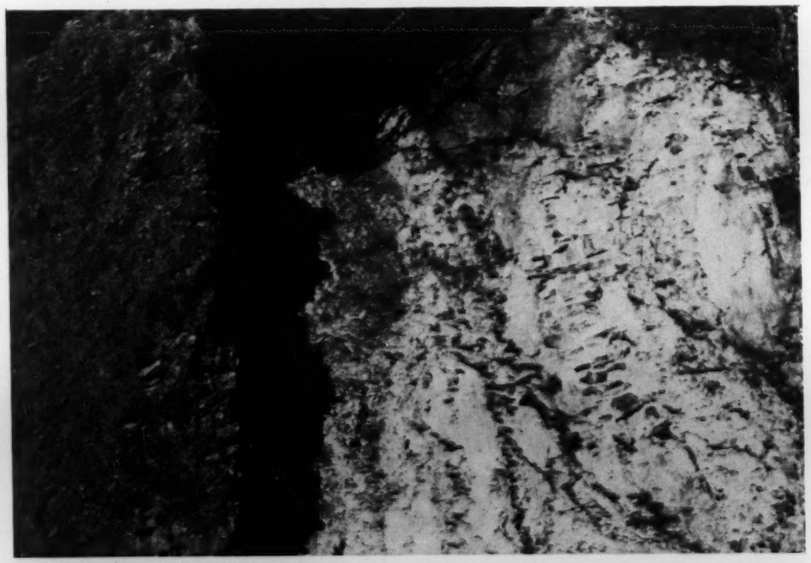

Fig. 25.

Fig. 26 a

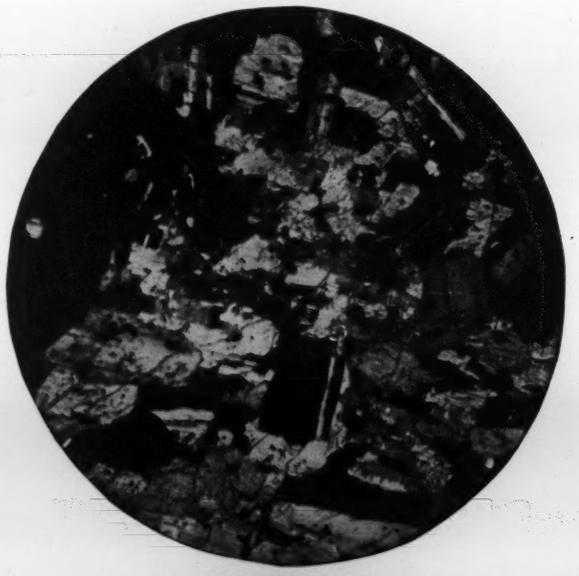

Fig. 26 b

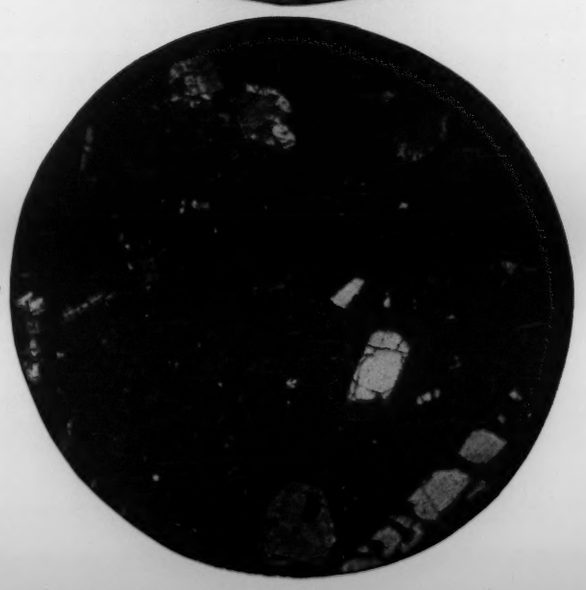

Fig. 24. Wada-toge liparite on the right in contact with andesite mass on the left.
Fig. 25. Tree fragments enclosed in the lower part of tuff-breccia at the uppermost part of the Yosawa.
Fig. 26. Microscopic photos of andesite of the Teppeiseki type at Nishimochiya (hornblende-bearing-two-pyroxene andesite a), and at Komazawa-shinden (olivine-bearing-two-pyroxene andesite b).

位が Normal N.R.M. を示す事実からみて，Plio.—Pleistocene にちかい Normal N.R.M. であろうと思われる．

（3） 各グループの磁化方位よりもとめた Dipole の位置を投影したのが Fig. 13 である．そこに示されるように Dipole の変動は累層の下部より上部になるにしたがつて，東から西へ変化している．すなわち，あたかも地球の回転軸を中心にして，一回転したようにみられる．この間の時間の長さを知ることはできないが，しかしうえにのべた変動形式は一種の極移動の連続的変化といつたものではないかと推察する．

（4） 百瀬 (J.G.G. Vol. 10, No. 1, 1958) はさきに柵累層および小諸層群と塩嶺累層との対比表で，この三層をつみかさねたものは，鮮新世全般にわたること，このうち鮮新世の中間にあたる部分の Dipole の軌跡は，地球磁場が連続的に比較的短時間のうちに極性を変えたごとくであることを報告した．

塩嶺累層の岩石より求めた Dipole の位置は，現在の地球回転軸の近傍にある．このことはまた柵累層上部や小諸層群上部（これらは塩嶺累層の下部にあたる）についても同様である．多くの研究者によつて従来発見された資料の大部分のものは，Normal N.R.M. と Reverse N.R.M. とをとわずそれらの Dipole が地球回転軸の近傍にあつたことを示している．このことはつぎのような事実が存在したことによるものではないであろうか? すなわち，地質時代において Dipole が回転軸近傍に存在した時間は，それが連続的に極性をかえるために要した時間にくらべてはるかに長いものであること，さらに前者は地球磁場の比較的安定していた時代—たとえば現在の地球磁場のような安定度のものではなかつたかと臆測する．地球磁場の逆転について漠然とした考えではあるが，地球磁場は Dipole の軸方向が回転軸の方向にある場合には安定しているが，何らかの理由によつて磁場に不安定な状態がおこると，比較的短時間に連続的に極性を変えるのではないかと考える．

BULLETIN OF THE EARTHQUAKE
RESEARCH INSTITUTE
Vol. 37 (1959), pp. 483-494

30. *Investigations into Microseisms by the Observational Data of Many Stations (Part II).* —*Further Considerations on the Origin of Microseisms.*—

By Tetsuo A. SANTÔ,

Earthquake Research Institute.

(Read Feb. 24, 1959.—Received June 1, 1959)

1. Introduction

In the previous paper,[1] the writer investigated the features of occurrence of microseismic storms in the Japan Islands due to the passing of cyclones, typhoons and strong cold fronts. One of the most important features we found was that when a cyclone passed off the eastern coast of Japan with high speed, microseismic amplitudes at a certain district became maximum considerably later than the passing of the cyclonic center.

From this observational fact, and further, by comparing the data of microseisms and swells recorded at the two stations in the same district, the writer made a suggestion that the origin of microseisms* (the area where the energy of swell changes into that of microseismic waves) exists somewhere near the coast.

This suggestion is quite important in the study of microseisms. Therefore, the writer will, in this paper, try to re-examine this suggestion by using additional data of microseismic storms due to the passing of typhoons.

The data of microseisms being used in this paper were, as before, all obtained at many stations in the Japan Islands during I.G.Y. period.

2. Additional data of microseismic storms due to the passing of typhoons.

After the first paper was written, the writer was able to get plenty of data on microseismic storms due to the passing of typhoons. In September 1958 especially, three typhoons T5819, T5821 and T5822 pas-

1) T. A. SANTÔ, *Bull. Earthq. Res. Inst.*, **37** (1959), 307.

*) The microseisms treated in this paper are restricted to those which have the periods of approximately 3~7 seconds.

sed near and across the Japan Islands. Fig. 1 shows the feature of the occurrence of microseismic storms at thirteen observation stations due to the passing of these typhoons.

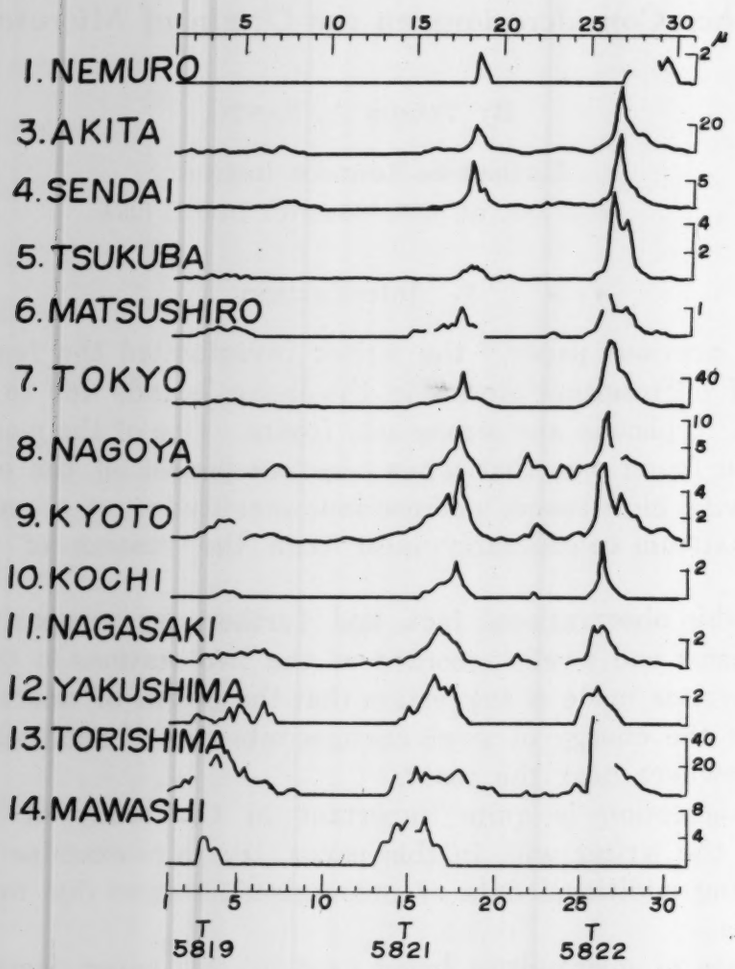

Fig. 1. Time variations of microseismic amplitudes (in μ) at many stations due to the passing of three typhoons on September 1958.

As was reported in the previous paper, it is clearly seen that the microseismic storms shift from the southern to northeastern stations. The relation between the positions of the centers of typhoons and the relative strengths of microseismic storms at many stations at given times are, for the case of T5821 and T5822, represented in Fig. 2. These two very strong ones passed across the central part of the Japan Islands and caused severe damage on their landing districts. In these cases, as can be seen in Fig. 2, the appearance of the microseismic storm is

not after the passing of the centers of these typhoons but rather before it. Fig. 3 shows the time variations concerning the periods of microseismic storms due to the passing of these three typhoons given above. Except

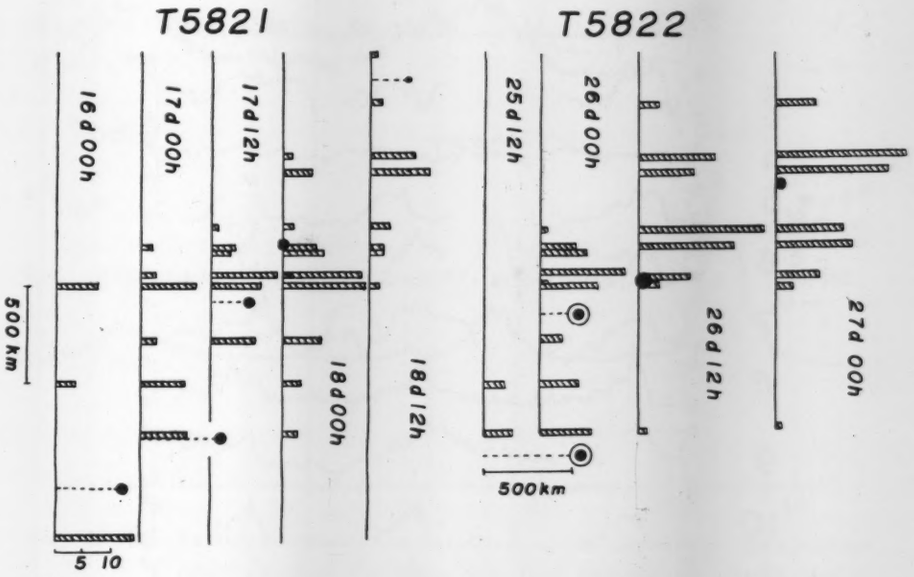

Fig. 2. Shifts of the region of microseismic storms due to the passing of two strong typhoons. The positions of the observation stations are taken along the ordinate. Station 1 and 14 correspond to the uppermost and lowermost edge. In the case of T5822, the data of station 14 was missed. The length of the hatched column at every station is the amplitude ratio of microseismic storm at a given time to the ordinary ones. Diameters of black (for $p>970$ mb) and inner black (for $p<970$ mb) circles are inversely proportional to the central pressures of typhoons.

a few stations on which the responses of seismographs were not good for long periods, the periods of microseisms remarkably increased up to six or seven seconds due to the passing of these typhoons. Comparing one of these curves, for instance that of observation station 5 (Tsukuba), with the curve of the half periods of swells recorded at Naarai (about 80 km south-east of Tsukuba), a noticeable phenomenon can be found, i.e., these two curves coincide very well at around the time of the passing of these typhoons (See Fig. 4(a)). This phenomenon has also been

found by J. E. Dinger and G. H. Fisher.[2] We cannot say, however, that the standing wave theory does not hold in the other ordinary case. For, in calm times, the wave form of microseisms recorded at Tsukuba

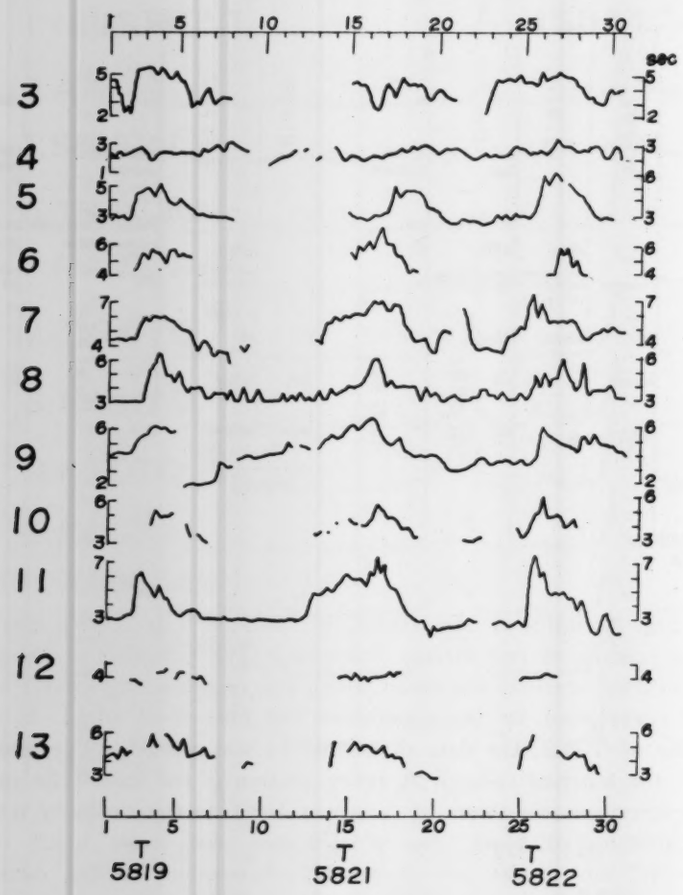

Fig. 3. Time variations of microseismic periods at many stations due to the passing of the same typhoons as in Fig. 1.

at least is irregular (Fig. 5), having many components with nearly equal amplitudes, therefore, in calm times, we are apt to measure the periods for different waves which do not correspond to each other from these two kinds of records. Correspondence between the amplitude variation

2) J. E. DINGER and G. H. FISHER, *Trans. Amer. Geophys. Union*, **36** (1955), 262.

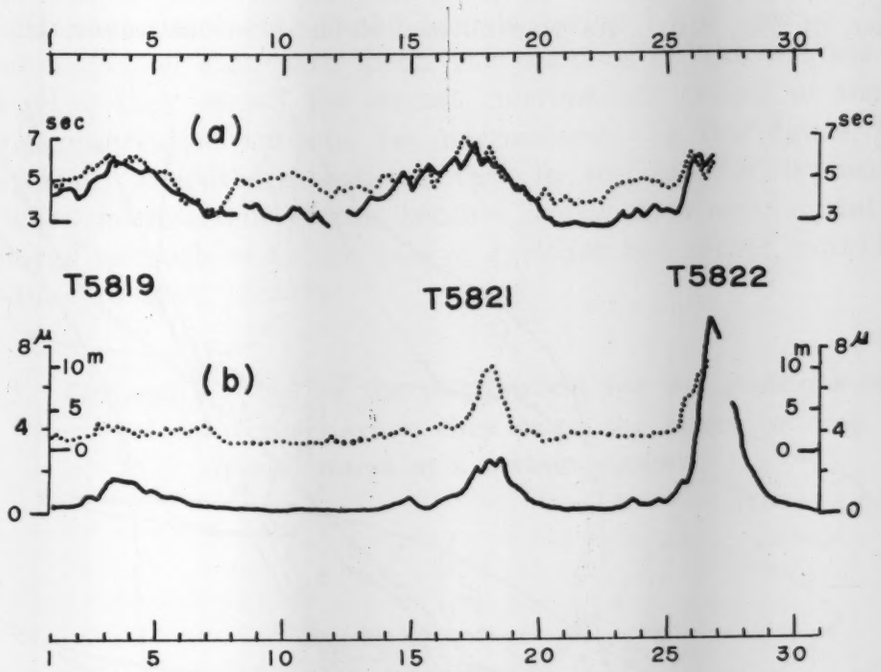

Fig. 4. (a) Relation between the variations of the periods of microseisms (solid line) at Tsukuba and half periods of swells (dotted line) at Naarai on September 1958.
(b) Relation between the variations of the amplitudes of microseisms (solid line) at Tsukuba and of swells (dotted line) at Naarai. Inside scale of ordinate is for the heights of swells.

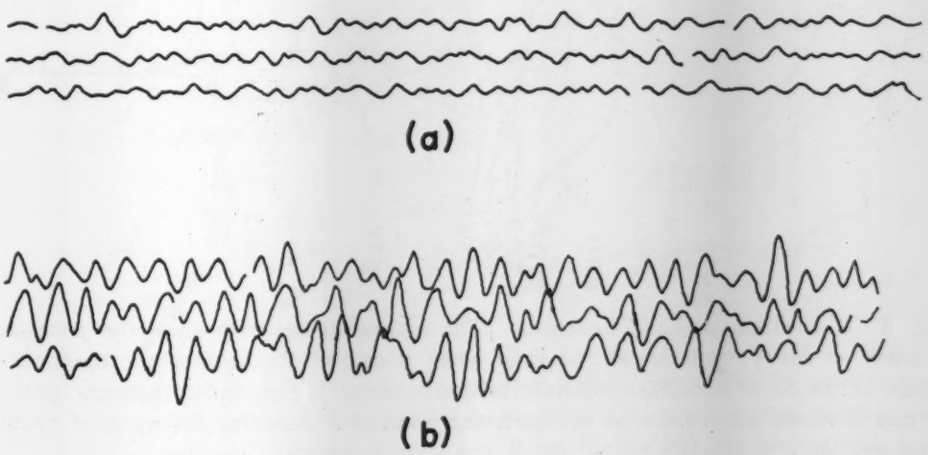

Fig. 5. Examples of microseismic wave forms recorded at Tsukuba in two cases. (a) Calm. (b) Stormy.

of microseisms recorded at Tsukuba and that of the swells at Naarai is shown in Fig. 4(b). As was noticed in the previous paper, the maxi-

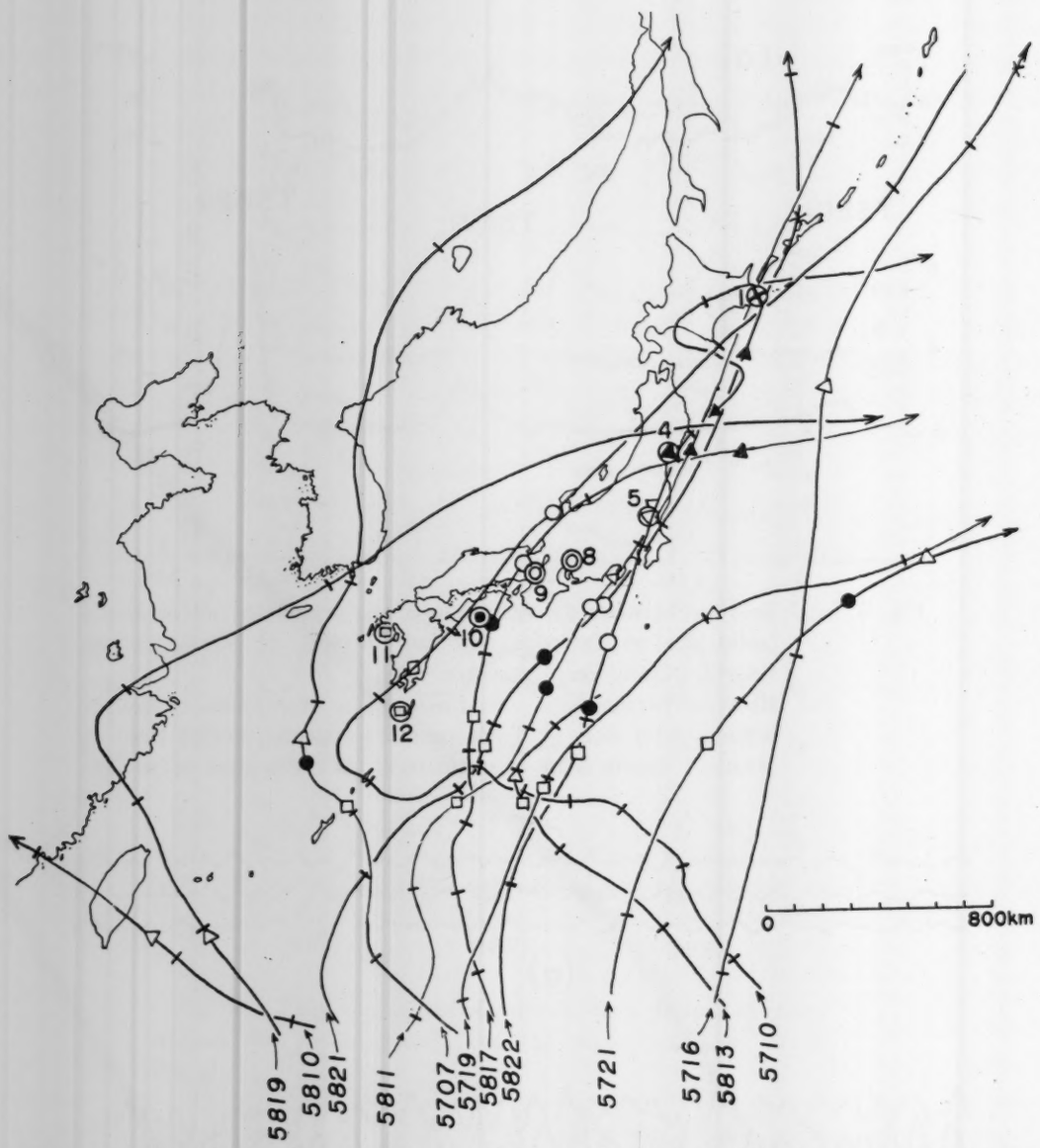

Fig. 6. Travelling paths of typhoons. The marks on the path show the positions of the center of every typhoon at the time when it caused the largest microseismic amplitudes at the corresponding stations (circles are added to the marks of center position). Intervals between short bars on the path represent the travelling distances of typhoons during one day.

mum amplitude of microseisms never occurs before that of swells which arrived at the coast in the same district.

Fig. 6 represents the travelling paths of typhoons which caused microseismic storms in the Japan Islands during I.G.Y. period. Several kinds of marks on each path mean the positions of the centers of typhoons when they caused the largest microseismic storms at the corresponding observation stations for microseisms. In this figure, we can see, especially at southern stations, that in the case of typhoons, the times when microseismic storms become largest at a certain station are not delayed so much as in the case of cyclones but rather coincide with the passing of their centers.

3. General features of the distribution for the positions of cyclonic centers when they cause the largest microseismic storm at a certain station.

Fig. 7. Positions and travelling velocities of cyclonic centers when they caused the largest microseismic storms at a few observation stations. Double marks are those for $p<990$ mb and others are for $p>990$ mb.

Black and white circles, and triangles are those positions of cyclonic centers correspond to the station 5, 10 and 12 respectively.

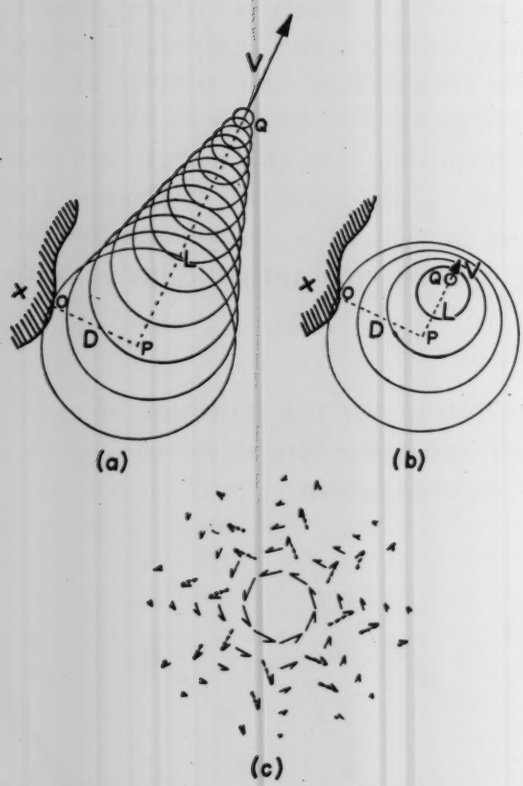

Fig. 8 (a and b). Schematical figures of wave distributions around and behind the center of a running point source. (a) When $V>v$. (b) When $V<v$. (c) Schematical figure of the directions of winds (solid arrows) and swells (dotted arrows) around a stationary cyclone.

In the previous paper, we found that microseismic storms at a certain station became largest remarkably later than the passing of a cyclonic center. As we have seen in the previous section of this paper, however, this phenomenon is not so noticeable in the case of typhoons. Furthermore, just the opposite relation could be found for the case of T5821 and T5822 which passed just above the observation station Tsukuba. Getting together, the positions of the centers of cyclones and typhoons when they caused the largest microseismic storm at a station were shown in Fig. 7 for a few representative stations (Tsukuba, Kochi and Yakushima).

Consider now a simple case when a vibrating point source is travelling straight with the velocity V on the water surface. In this case, when the wave front originated at P reaches a position O with a distance $D(=OP)$ from the travelling path, the wave source has covered the distance $L(=PQ)$. (Fig. 8(a) and 8(b)). In other words, the wave always arrives at the point O later than the passing of the wave source. In this case, the following relations must be satisfied.

$$D=vt, \qquad L=Vt,$$

in which, v is the wave velocity and t is the travel time of the wave covered the distance D. From these, the next relation easily follows.

$$V=vL/D\,. \tag{1}$$

Of course, in the actual case of a cyclone or a typhoon, the mechanism of wave generation around the center is much more complicated than this case of a point source (Fig. 8(c)). Winds and swells are be-

ing sent away in counter-clockwise directions around the center and their strength distributions depend upon those of the atmospheric pressure gradients around the center. Furthermore, when the center moves, the wind becomes stronger in the first and weaker in the third quadrant for the travelling direction of the center, and as a result so does the swell.

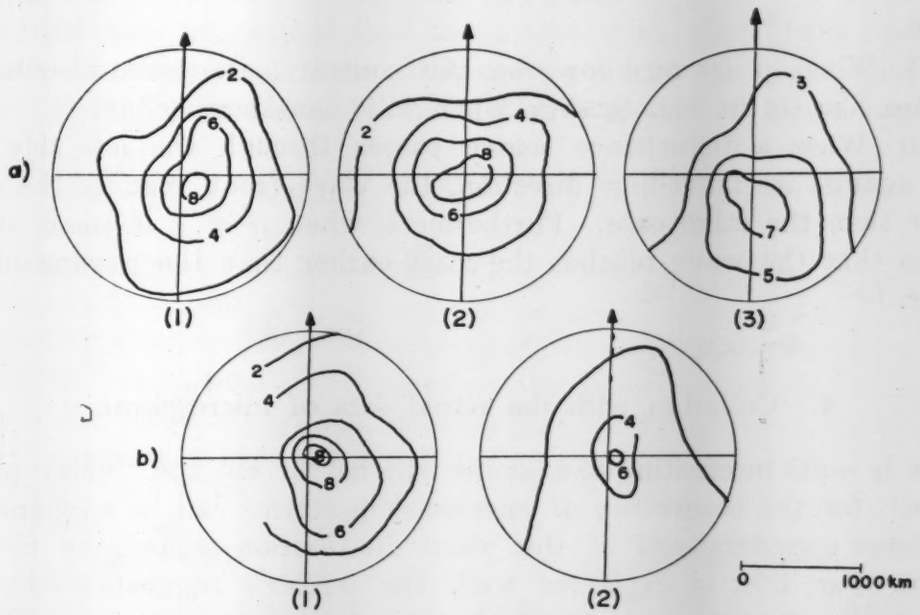

Fig. 9. (a) Mean distribution maps of wave heights (in meter) due to the typhoons with the same central pressures 960~980 mb, but different travelling speeds. (1) $V<20$ km/hr. (2) 20 km/hr$<V<$40 km/hr. (3) $V>40$ km/hr.

(b) Mean distribution maps of wave heights (in meter) due to the typhoons with the same speed but different central pressures. (1) $p<940$ mb. (2) $p>980$ mb.

(After S. Unoki)

It is, as a matter of fact, very difficult to observe the distribution of swell height around the center of a cyclone or a typhoon. There is, however, a laborious work on this problem done by S. Unoki.[3] He collected the data of swell heights due to forty seven typhoons being observed during 1949~1956 at the Ocean Weather Station "Tango" (29°N, 135°E), and made the averaged distribution maps concerning the heights of swells around the center of typhoon within a certain range of central pressure p and travelling speed V. His results are shown in Fig. 9(a) and 9(b). Regrettable to say, as the travelling speeds of typhoon are, in general, still low on the southern ocean around this ob-

3) S. UNOKI, *Journ. of Met. Soc. Japan*, [ii], **35** (1957), 297.

servation point, he could not know the actual heights of wave distribution around the center of the typhoon with such high travelling speeds as 60~80 km/hr, which is needed for the present case. However, the following general tendency can be imagined by these maps concerning the distributions of swell heights:

i) When p or V becomes high, the wave distribution around the cyclonic center becomes similar to those due to a single running point source.

ii) When p is very low, on the contrary, the wave distribution becomes like (b) in Fig. 8, even when V is considerably high.

iii) When a disturbance source passes through the left side of a coast against its travelling direction, the wave front reaches the coast earlier than the other case. Furthermore, when p or V is small, it can happen that the wave reaches the coast earlier than the passing of the center.

4. Collation with the actual data of microseisms.

It is quite interesting to examine whether or not the "delay phenomenon" for the occurrence of microseismic storms can be explained by the above considerations of the wave distribution around the cyclonic center. For, if it is explained well, the writer's suggestion that the energy transformation from swells to microseisms occurs somewhere near the coast will be powerfully verified.

Based upon considerations i), ii) and iii) in the previous section, a test was made if the actual data satisfy the relation (1) in section 3. For this purpose, V, L and D were measured on maps only for those cyclones and typhoons which run approximately straight. The actual relation between V and L/D thus obtained are shown in Fig. 10, in which the marks of points have the same meaning as in Fig. 7. Further, in this figure, the two cases when the observation station is located on left or right side of a running cyclonic center are distinguished by the location of a short bar on every mark.

This result satisfies very well, beyond the writer's expectation, the relation between V and L/D which holds for waves generated around the running point source. That is:

i) Two kinds of marks (for $p>990$ mb and for $p<990$ mb) are scattered separately around two straight lines with different inclinations. From these inclinations, we can find two different travelling velocities

of the swells due to the cyclones or typhoons. The results are: for $p>990$ mb, $v \fallingdotseq 17$ km/hr and for $p<990$ mb, $v \fallingdotseq 30$ km/hr. As almost all the central pressures of cyclones belong to the first class here used were higher than 1010 mb (only one of them were 990 mb) and those belong to the second class lower than 965 mb (only one of them were 985 mb), these values of v are quite reasonable ones as the velocity of swells due to the cyclones with such strengths.

It must also be noticed that the marks with short bars on their right side (meaning that these data correspond to the cases when the cyclones or typhoons passed through the left side of these stations)

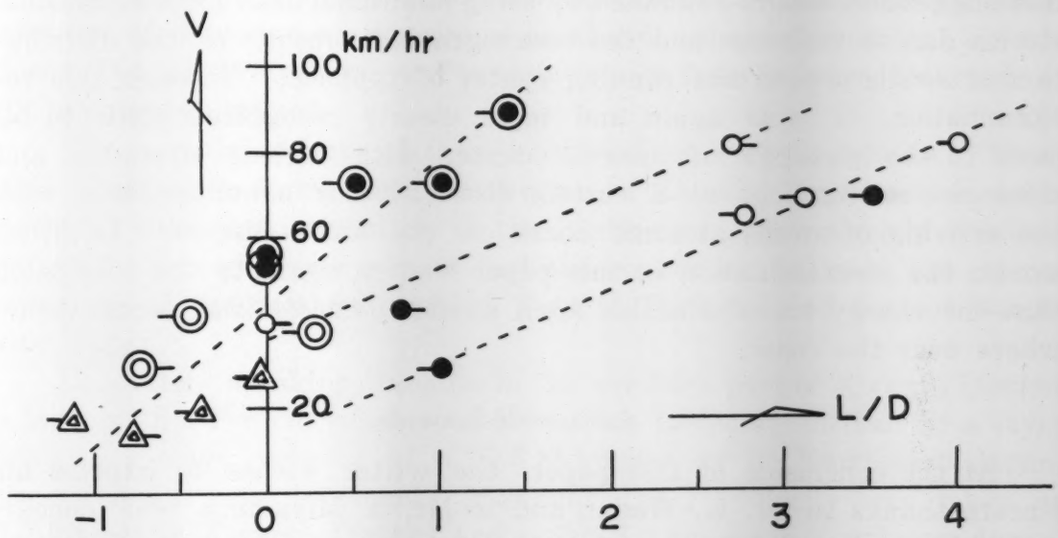

Fig. 10. Relation between V and L/D. V is the travelling speed of the center of cyclone or typhoon. L and D are the travel distances of wave source and wave itself respectively as are shown in Fig. 8 (a) or 8 (b).

make another straight line approximately parallel to the line for $v \fallingdotseq 17$ km/hr. This fact can also satisfy the circumstances given in the third item of the previous section.

ii) If the running wave source is a point, the straight line of $V \sim L/D$ must point to the origin of the coordinate. In the case of actual cyclones or typhoons, as we have found in section 3, the wave distribution becomes circular around the center only when V reaches a certain value V_0. In this case, the wave can reach the coast almost simultaneously at the time of the cyclone passing. The value of V_0 satisfying the above condition will become larger for the lower value of p. Seeing the cutting point of two straight lines in Fig. 10, the circumstance can also be very well recognized.

iii) When V is lower than V_0, wave pattern projects to the front of the running cyclonic center. In this case, it can happen that the wave reaches the coast earlier than the passing of the cyclonic center. Several points in Fig. 10 on minus side of the ordinate show the above circumstances.

5. Conclusions.

In the previous paper, the writer made an important suggestion for the origin of microseisms that the microseisms with periods of 3～7 seconds are caused somewhere near the coast. In this second paper, this suggestion was re-examined by using additional data on microseismic storms due to typhoons and the oceanographical results on the distribution of swells around the running center of typhoons. Through this re-examination, it was again and more clearly recognized that, in all cases of the passings of cyclonic center with various strengths and distances, microseisms at a certain district occur simultaneously with the arriving of swells at some coast on the same district. In other words, the re-examination in this paper lead us again to the conclusion that the energy transformation from swells to microseisms occurs somewhere near the coast.

6. Acknowledgments.

At the conclusion of this paper, the writer wishes to express his sincere thanks to Dr. K. Wadati and to Mr. S. Miyamura who encouraged him during the course of his investigations. The writer's hearty thanks are also due to Mr. T. Kizawa who gave him much help in collecting the data on swells.

---

30. 多くの観測点の資料に基づく脈動の研究 (その二)
—脈動源に関する前推論への再検討—

地震研究所　三　東　哲　夫

前論文で，3 秒から 7～8 秒の周期をもつた脈動の発生源は，台風や低気圧の中心附近にはなくて，陸地のすぐ近くにある．という考え方を提出した．この推論は，大変重要なことと思われるので，更にその後の台風による脈動嵐の資料を加え，また台風の中心周囲の波高分布に関する海洋学上の観測事実をも考慮に入れた上で，この点をもう一度追究して見た．その結果，台風の通過に際して，脈動嵐はやはり波浪が陸地に到達した頃に起ることが示され，前論文の推論通り，波浪のエネルギーは陸地のすぐそばで脈動のエネルギーに変ると考えて差支えないことが分つた．

BULLETIN OF THE EARTHQUAKE
RESEARCH INSTITUTE
Vol. 37 (1959), pp. 495-508

31. *Observations of Seismic Waves from the Second Hokoda Explosion.*

By The Research Group for Explosion Seismology.

(Read May 27, 1958.—Received June 30, 1959.)

1. Introduction

At midnight on August 26, 1957 the Research Group blasted about one ton of explosive at the site of an abandoned aerodrome near Hokoda town, Ibaragi Prefecture, and seismic waves from it were observed at 18 temporary stations.

The essential objects of these observations were as follows: First, this observation forms a profile reverse to Kamaisi Explosions in order to verify the crustal structure of the North-east Japan already obtained by us.[1] Secondly, we aim to find the connection between the crustal structure of the northern part of Kwantô District[2] and that of North-east Japan.

Concretely speaking, because in the northern part of Kwantô District a layer with a P-wave velocity of 5.5 km/sec is found, instead of a layer with a P-wave velocity of 5.75-5.85 km/sec as in North-east Japan, their relation must be found. Moreover, the P_n velocity was taken as 7.7 km/sec in Kwantô District and as 7.5-8.0 km/sec in North-east Japan. For their unified interpretation, more accurate determination of the P_n velocity and of the depth of the Mohorovičić discontinuity were aimed at. For the latter purpose accurate observations are necessary in a region, where the crustal structure in the shallow part is well known. From this view point observation points were spread in a profile nearly reverse to the Kamaisi and Isibuti explosions.

2. Observations

The shot point was shifted by 188 m in the S57°W direction from

1) The Research Group for Explosion Seismology (Japan), *Pub. Bur. Cent. Séism. Intern.*, Sér. A. Trav. Sci., **19** (1954), 229-242.
T. MATUZAWA, *Bull. Earthq. Res. Inst.*, **37** (1959).

2) The Research Group for Explosion Seismology (Japan), *Bull. Earthq. Res. Inst.*, **36** (1958), 329-348; T. USAMI et al., *Bull. Earthq. Res. Inst.*, **36** (1958), 349-357.

Table 1.

Station	λ	φ	H m	Θ	Δ km	Apparatus	Observer
1. Shot Point (Hokoda)	140°33′34.5″E	36°08′16.3″N	41	N 8°30.0′W	0-0.55	S.S.C.	Matuzawa, Kaneko, Tateishi, Ôtaki, Kamata, Kawashima
2. Ôya	30 48.2	14 4.1	29	21 11.1	11.496	15V1, 30H1, 3V1, 3H1	Wada, Kumazawa
3. Mito A	32 29.0	20 2.2	14	4 17.9	21.817	2V1, 2H2	Mikumo, Okamoto
4. Mito B	31 46.8	21 37.4	6	6 12.9	24.836	2V1, 2H2	Otsuka,
5. Sano	30 12.4	26 24.9	34	8 39.2	33.928	E.T.L.M-3	Murauchi, Honda, Asanuma
6. Hitati	35 47.4	38 2.8	357	3 26.5 E	55.161	2V1, 7V1, 4H1	Tanaka, T. Suzuki
7. Daigo	21 6.3	46 27.4	111	14 46.7 W	73.030	3V1, 2H2	Tamaki, Kitamura
8. Tanakura	23 36.6	37 01 9.8	243	8 38.4	98.935	N.D. 3V1, 3V1, 3H1	Muramatu, Takeda
9. Tamagawa	25 2.0	12 30.4	279	6 6.8	119.472	N.D. 3V1, 3V2	Takahashi, Watanabe
10. Tamura	25 11.8	19 12.8	246	5 25.8	131.789	N.D. 3V1	Utsu, Usami
11. Siroiwa	28 53.2	29 28.3	344	2 39.5	150.331	N.D. 3V1, 3V1	T. Matumoto, Karakama
12. Kawamata	36 49.8	41 5.2	176	1 36.8 E	171.720	3V2, N.D. 3V1	Onda, Takeuti, H. Okada
13. Isida	38 11.7	46 5.8	163	2 10.2	181.049	N.D. 3V1	Shima, Sibano
14. Kaneyama	47 52.3	53 45.9	22	6 12.1	196.252	N.D. 3V1, T.A. 4V1	Asano, Yanagisawa
15. Watari	51 19.6	38 01 30.0	10	7 8.6	211.056	N.D. 3V1, 4V1, 1V1	Santo, Terashima
16. Mukaiyama	51 20.7	14 32.9		6 25.4	235.022	N.D. 3V3, 5H1	Mine, Ishigaki
17. Miyatoko	51 0.3	24 0.6	49	5 51.2	252.368	N.D. 3V1, 3V1, 4V1	Z. Suzuki, Emura
18. Matusiro	138 12 23.6	36 32 22.4	383	78 5.1 W	215.870	N.D. 3V1	Suyehiro
Surveyor	A. Okada						

the first shot point. It consisted of six holes as before. Each hole was 5″ in diameter and 60–70 m deep. They were situated at the five angular points of a regular pentagon inscribed in a circle of 7 m redius and at its centre.

About one ton of dynamite was almost equally distributed to these six holes. The depth of the dynamite head in each hole was about 35 m from the ground level in the mean. The rest of the hole was tamped

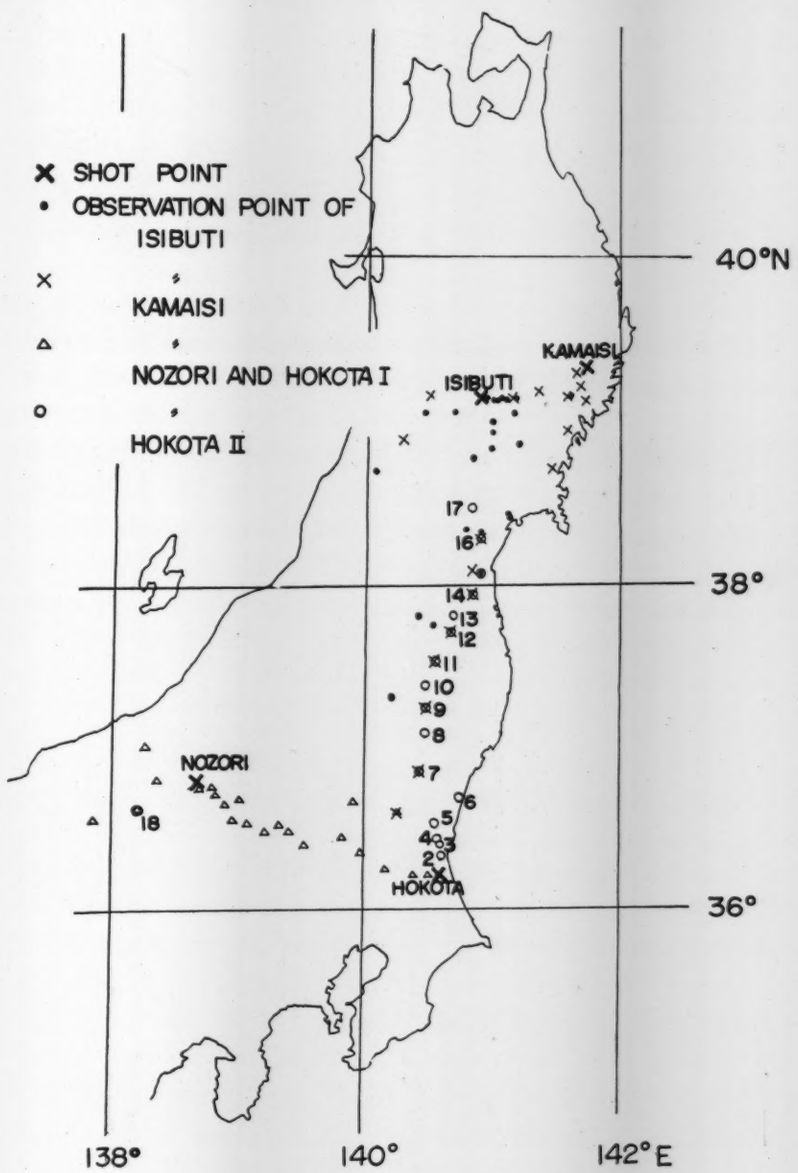

Fig. 1. Shot and observation points

with water. The number of observation points was 7 in the northern part of the Kwantô District, 10 in North-east Japan and one at Matusiro, i.e., 18 points in total. Among these points 7 are common (Siroiwa, Kaneyama, and Mukaiyama) or near (Hitati, Tamagawa, Kawamata and

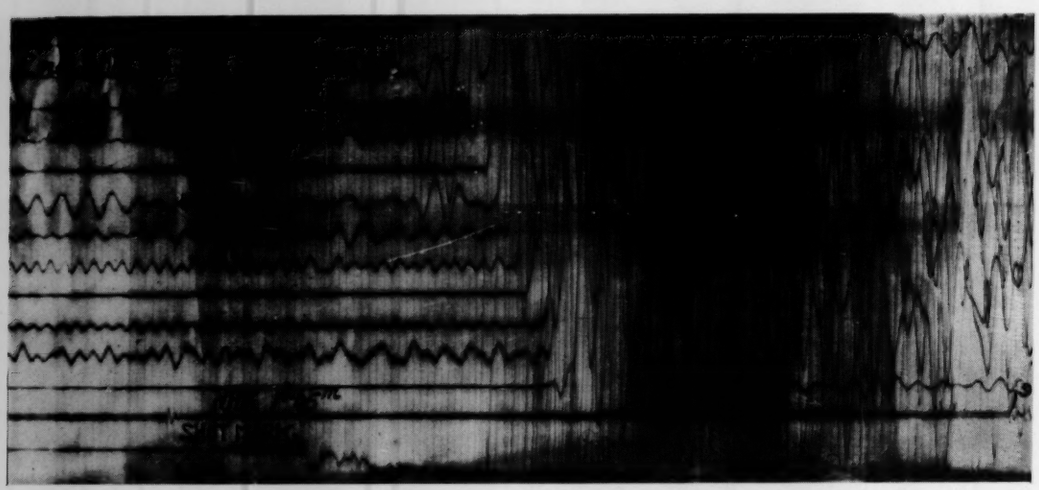

Fig. 2. Seismogram obtained at Hokoda.

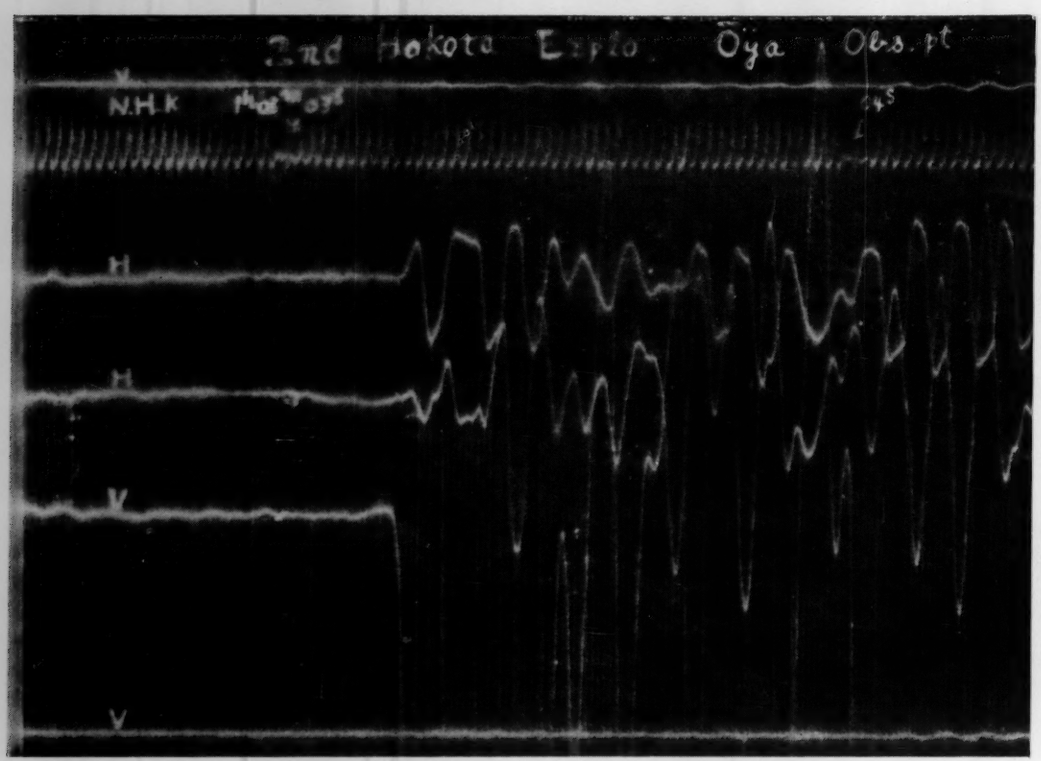

Fig. 3. Seismogram obtained at Ôya.

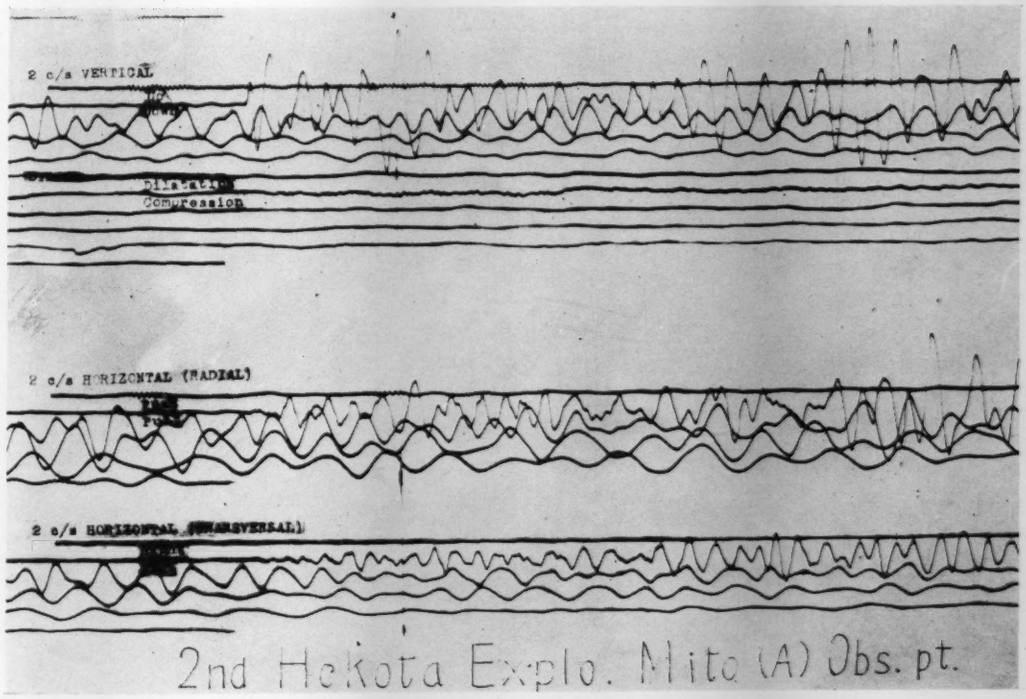

Fig. 4. Seismogram obtained at Mito A.

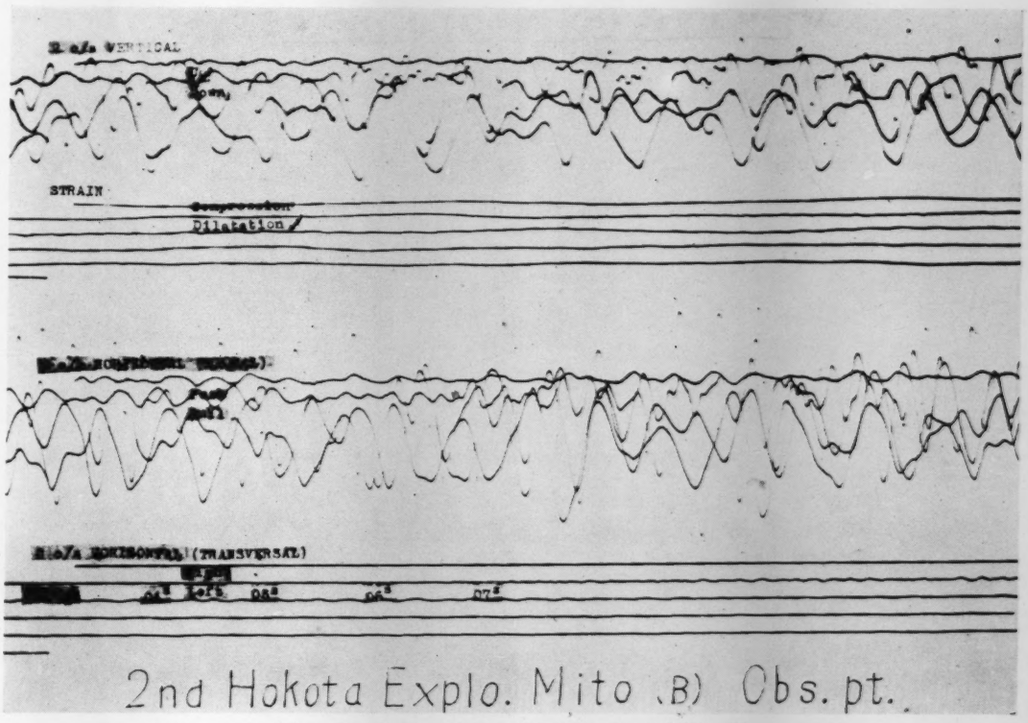

Fig. 5. Seismogram obtained at Mito B.

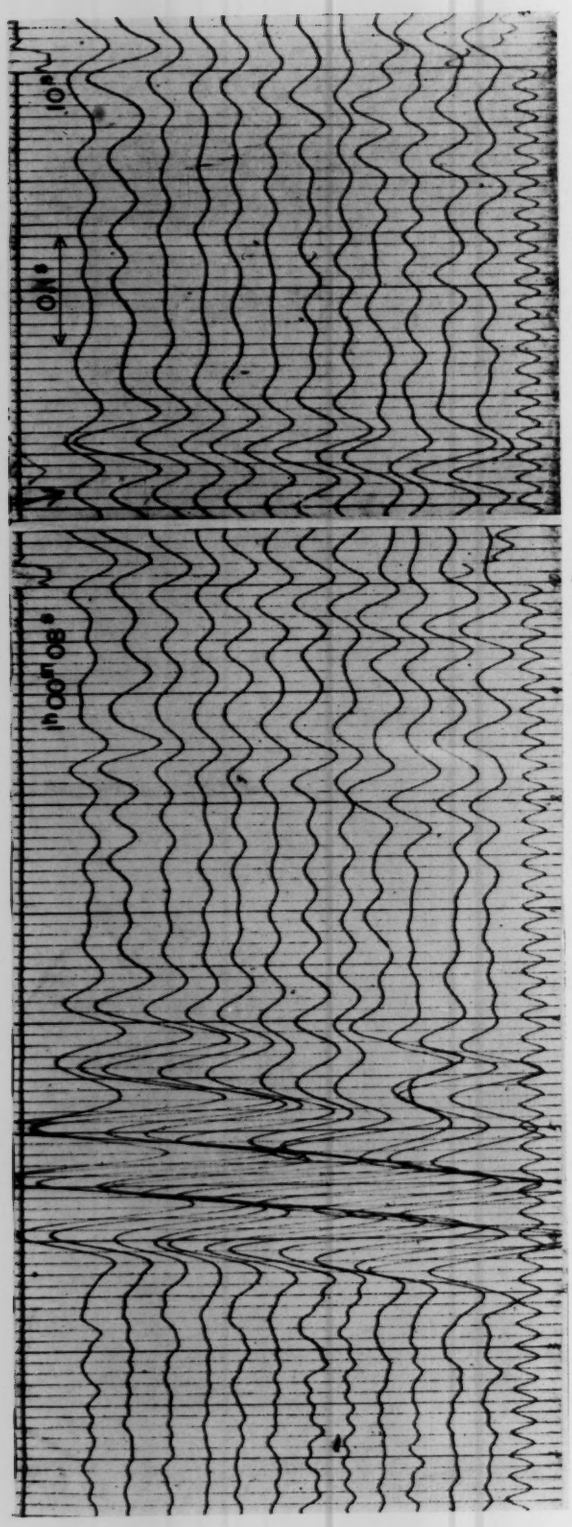

Fig. 6-a. Seismogram obtained at Sano.

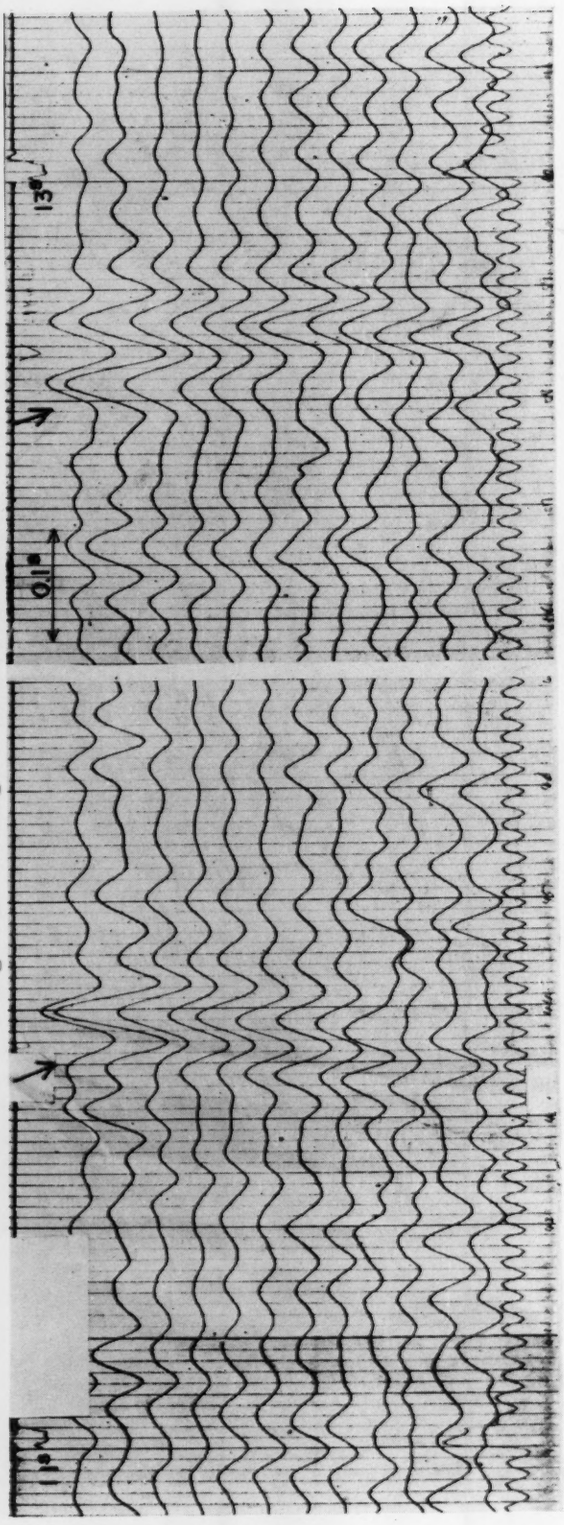

Fig. 6-b. Seismogram obtained at Sano.

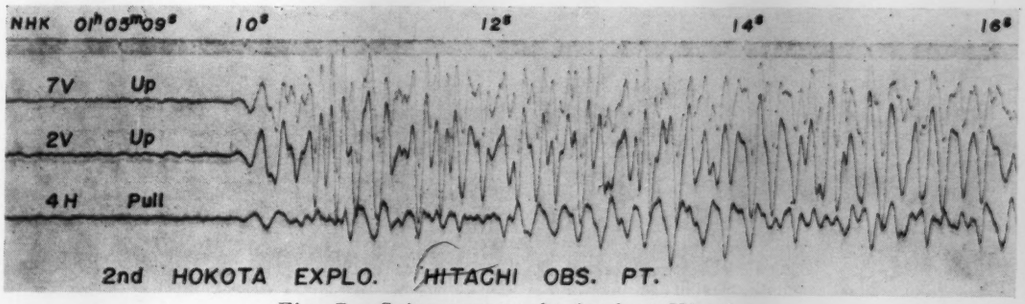

Fig. 7. Seismogram obtained at Hitati.

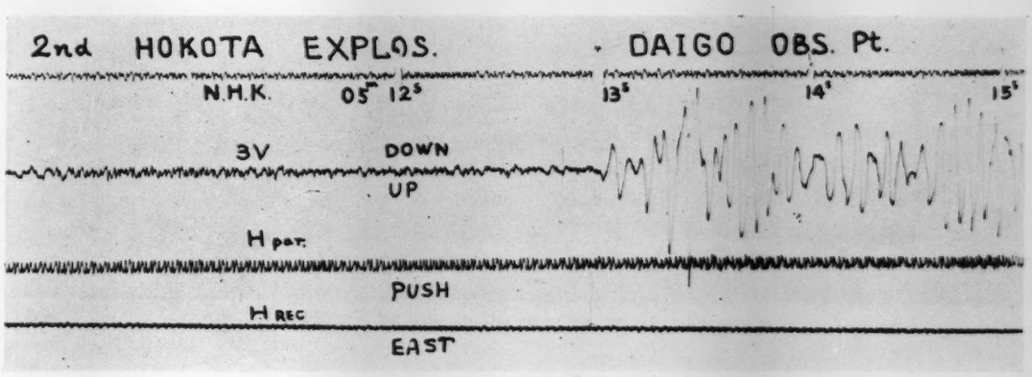

Fig. 8. Seismogram obtained at Daigo.

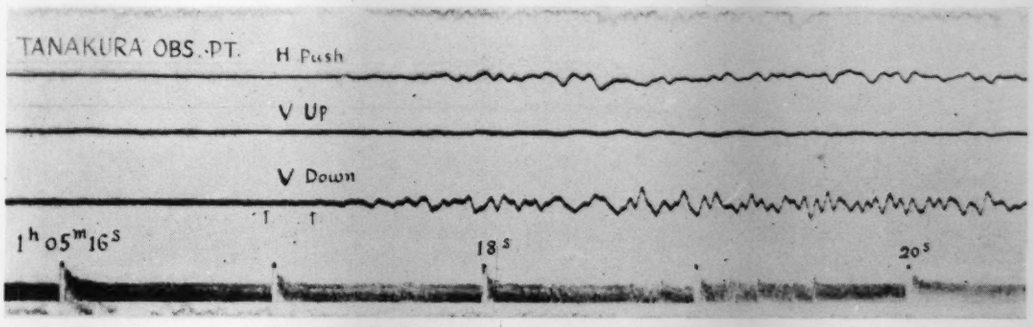

Fig. 9. Seismogram obtained at Tanakura.

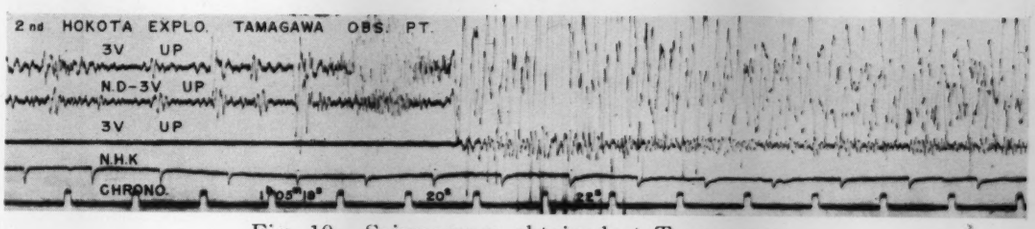

Fig. 10. Seismogram obtained at Tamagawa.

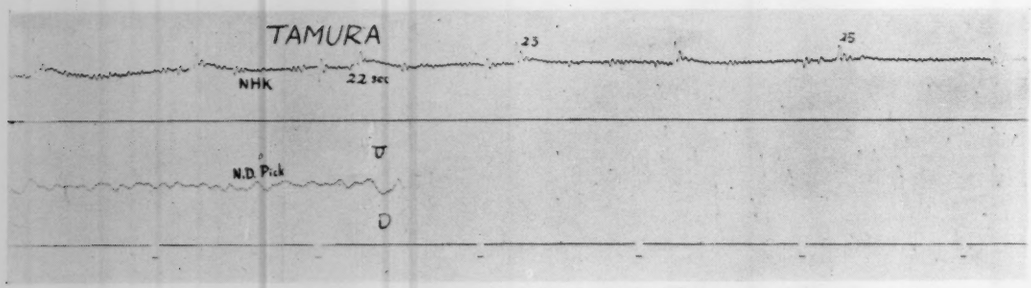

Fig. 11. Seismogram obtained at Tamura.

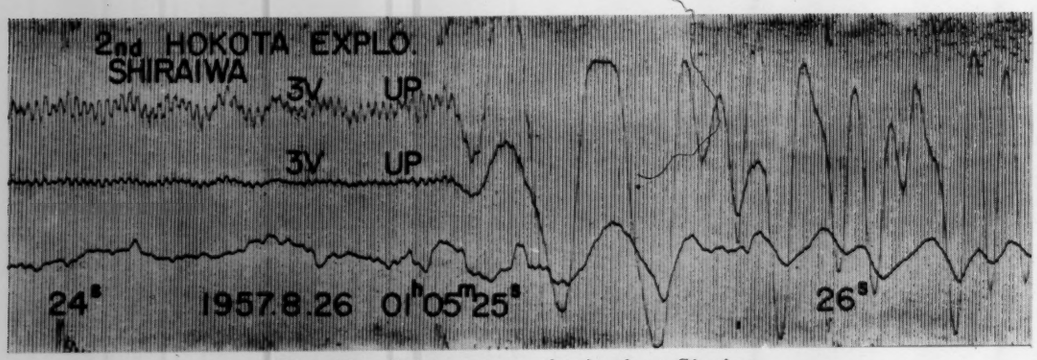

Fig. 12. Seismogram obtained at Siroiwa.

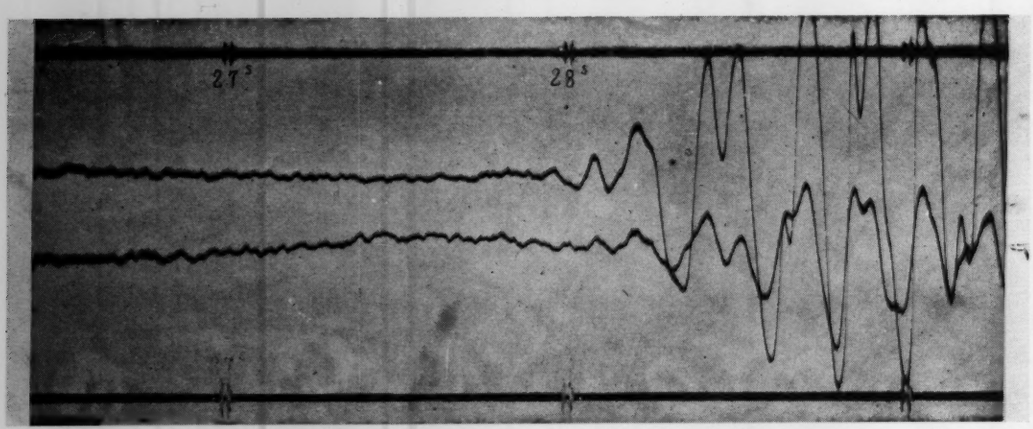

Fig. 13. Seismogram obtained at Kawamata.

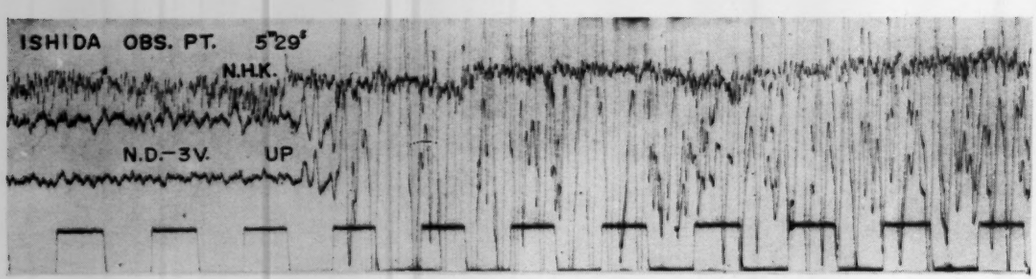

Fig. 14. Seismogram obtained at Isida.

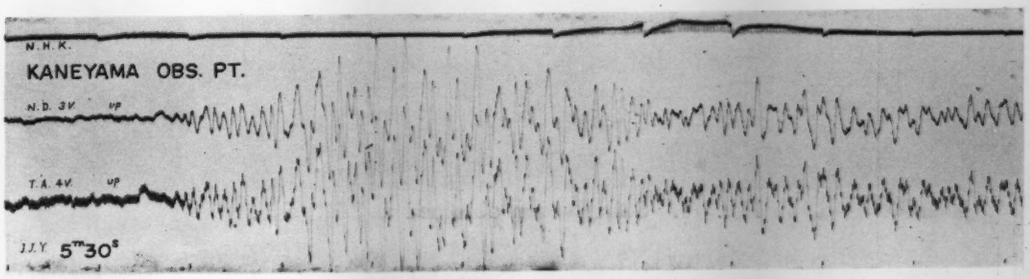

Fig. 15. Seismogram obtained at Kaneyama.

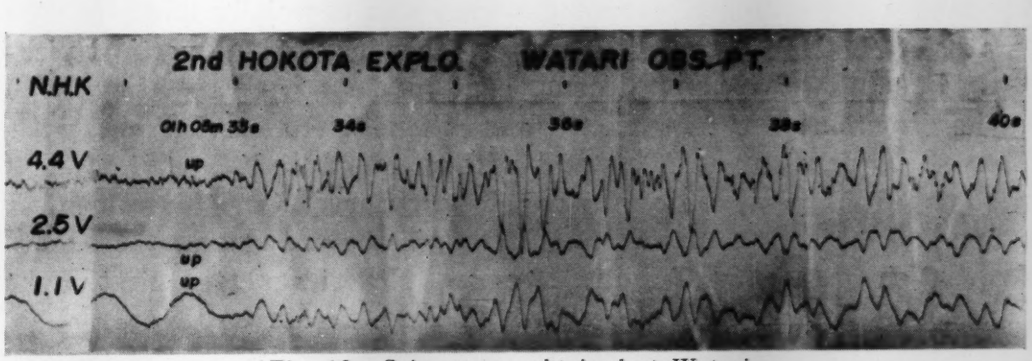

Fig. 16. Seismogram obtained at Watari.

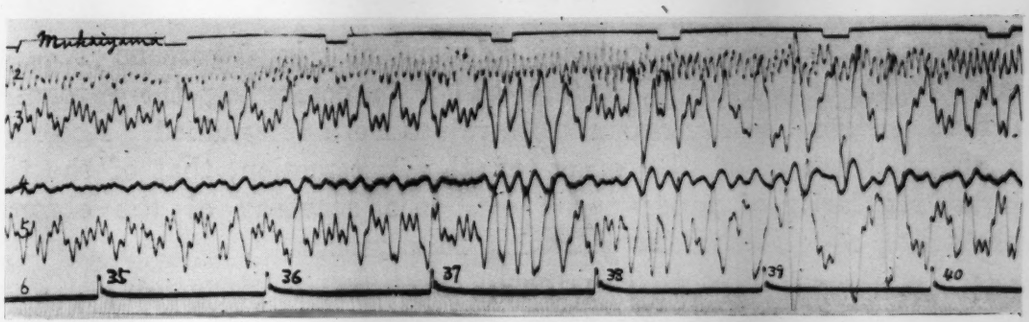

Fig. 17. Seismogram obtained at Mukaiyama.

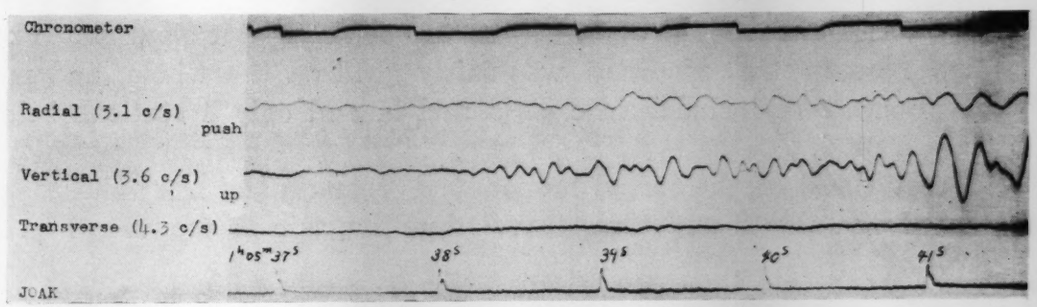

Fig. 18. Seismogram obtained at Miyatoko.

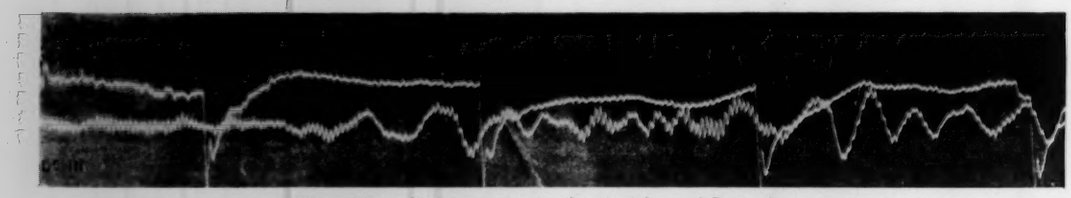

Fig. 19. Seismogram obtained at Matusiro.

Watari) to those of the Isibuti or Kamaisi explosions. At most stations pick-ups with a proper frequency of 3 c/s were connected to amplifiers. At Sano observation of reflected waves was especially tried by an apparatus of E.T.L.M-3 type, the proper frequency of the vertical pick-up being 7 c/s. Twelve vertical component pick-ups were set at every 20 m in the direction of the profile. Observations were carried out with a filter of high-cut above 20 c/s and without suppressor.

The shot point, observation points, observers and instruments are shown in Table 1 and in Fig. 1. In Fig. 1 are added also the shot and observation points for Isibuti, Kamaisi, Nozori and the first Hokoda explosions. Seismograms are shown in Figs. 2～19.

3. Measurement of seismograms

First, seismograms were read independently by 3 persons (T. Matuzawa, T. Matumoto and S. Asano) and then comparing them together with the original seismograms, final values were determined. According to the distinction of the onset of the first motion, that of the time marks, regularity of paper speed etc., the accuracy of the observed values was classified in the following four groups;

class a : $\Delta t \leqq 1/100$ sec
class b : $1/100 < \Delta t \leqq 3/100$ 〃
class c : $3/100 < \Delta t \leqq 1/10$ 〃
class d : $1/10 < \Delta t$

where Δt is the expected error of the travel time determination. From various reasons the accuracy was fairly good on the whole, and most observations were included in class a and b, and only 4 stations belong to class c or d.

Onset times of the initial motion and remarkable late phases are tabulated in Table 2 and their travel time diagram is shown in Fig. 20.

Table 2. Travel time for the second Hokoda Explosion Shot time : 1 h 05 m 0.006 s

Station	Δ km	P_1 class	L (late phase) in sec	$\Delta/6$ in sec	$P_1-O-\frac{\Delta}{6}$	$L-O-\Delta/6$ in sec	Remark
		sec			sec		
Hokoda	0.00	0.006		0	0		
Ôya	11.50	3.18 a	3.37, 3.66, 28.82	1.92	1.25	1.44, 1.73, 26.89	
Mito A	21.82	5.05 c		3.64	1.40		
Mito B	24.84	5.52 b	6.76	4.14	1.37	2.61	
Sano	33.93	7.35 b		5.66	1.68		
Hitati	55.16	9.89 a	10.54, 10.80, 11.33 12.08	9.19	0.69	1.34, 1.60, 2.13, 2.88	
Daigo	73.03	13.02 b	13.20	12.17	0.84	1.02	
Tanakura	98.94	17.17 c	17.80, 18.27	16.49	0.67	1.30, 1.77	May be earlier, owing to the small initial motion.
Tamagawa	119.47	20.23 b	20.84, 35.22	19.91	0.31	0.92, 15.30	
Tamura	131.79	22.28 a	22.55, 40.20, 41.55	21.97	0.30	0.57, 18.22, 19.57	
Siroiwa	150.33	25.01 a	44.30	25.06	−0.06	19.23	
Kawamata	171.72	27.92 b	28.24	28.62	−0.71	−0.39	
Isida	181.05	29.16 a	29.59, 52.80, 71.6, 111.5	30.18	−1.03	−0.60, 22.61	
Kaneyama	196.25	30.77 b	31.90, 32.47, 37.21	32.71	−1.95	−0.82, −0.25, 4.49	
Watari	211.06	32.92 b	33.14, 35.32	35.18	−2.27	−2.05, 0.13	
Mukaiyama	235.02		37.30(d), 38.16 39.00, 40.50, 42.25	39.17		−1.88, −1.02, −0.18 1.32, 3.07	
Miyatoko	252.37	38.15 c	38.90, 40.77	42.06	−3.92	−3.17, −1.30	The initial motion is small.
Matusiro	215.87	34.28 d	36.25	35.98	−1.71	0.26	

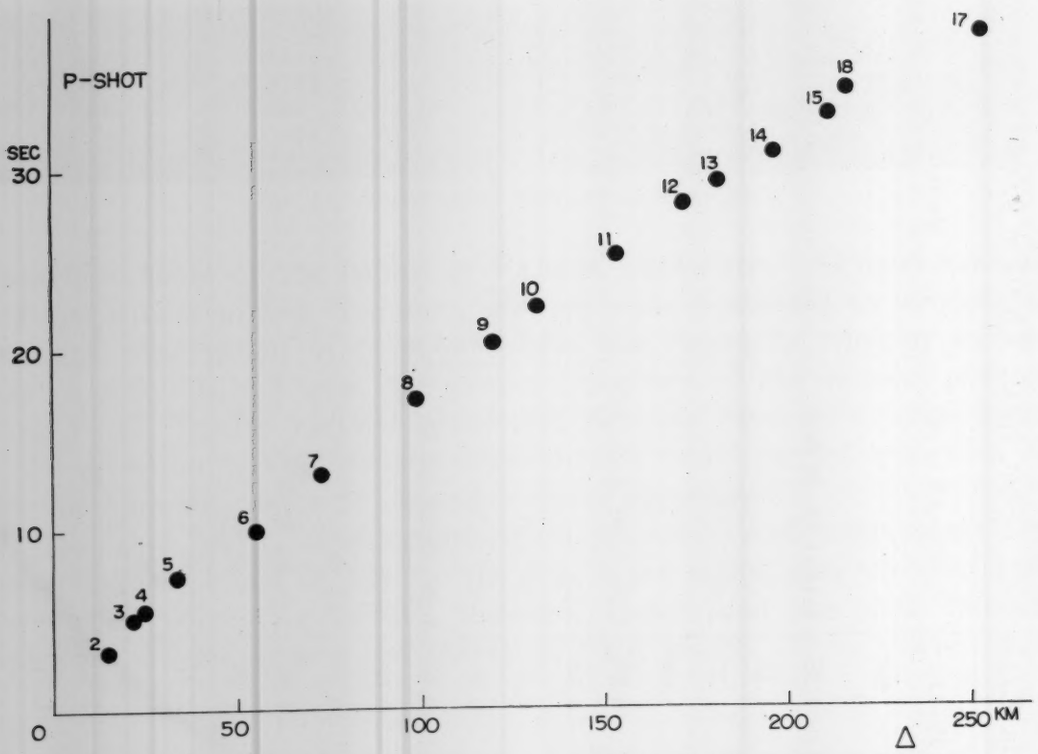

Fig. 20. Travel time diagram of the waves from the Second Hokoda Explosion.

Table 3. Travel times near the shot point

Hokoda I			Hokoda II			
Station	Δ m	$P-O$	Station	Δ m	P	$P-O$
		ms			ms	ms
1	0	0	1	150	120	114
2	188	160	2	300	212	206
3	471	318	3	325	226	220
4	676	432	4	350	238	232
5	840	519	5	375	252	246
6	1090	634	6	400	269	263
7	1240	767	7	425	282	276
			8	450	295	289
			9	475	308	302
			10	500	333	327
			11	525	340	334
			12	550	?	?

4. Observations near the shot point

Seismic waves at 12 points in a profile 550 m long from the shot point were observed. Their travel times are tabulated in Table 3 together with those of the first Hokoda explosion and plotted in Fig. 21.

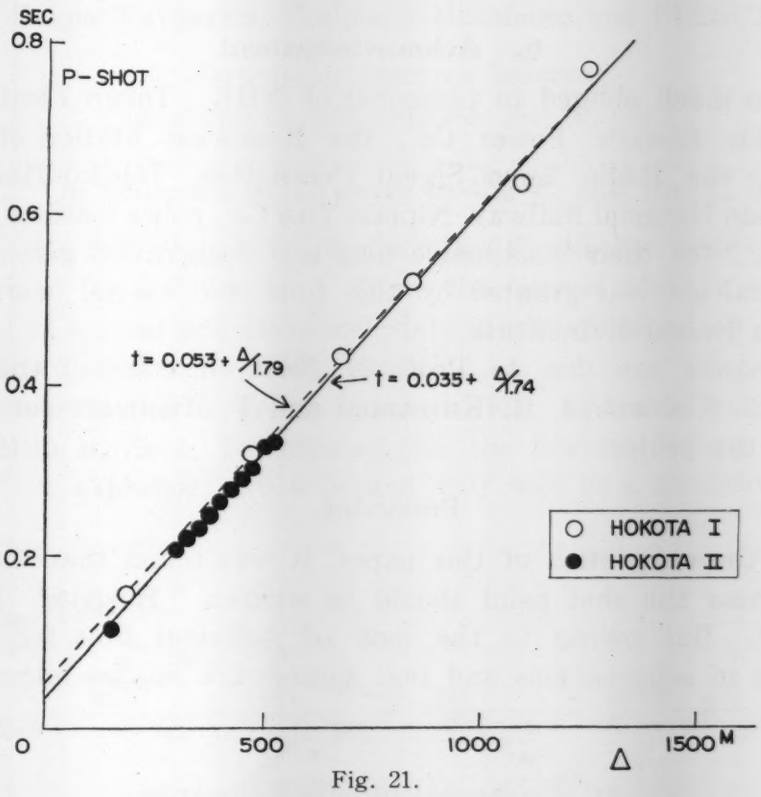

Fig. 21.

From observations exclusively of the second explosion the P velocity turns out as 1.71 km/sec with the intercept time of 0.028 sec. This value is somewhat different from 1.79 km/sec for the first explosion, but this difference can be explained by the difference of the shot points about 200 m apart.

Adding both observations, the following equation is obtained,

$$t=0.035+\Delta/1.74$$

with t in sec and Δ in km.

5. Observation of reflected waves at Sano

Seismograms obtained were excellent (refer to Fig. 6), and predom-

inant phases were read as follows:

1 h 05 m 9.61 sec ; 11.35 sec ; 12.85 sec.

These three phases are especially distinct among other phases.

Discussions of the observed travel times from the standpoint of the crustal structure are given in a separate paper.[3)]

6. Acknowledgement

We are much obliged to personnel of NHK., Tôkyô Electric Power Co., Tôhoku Electric Power Co., the Broadcast Station of Standard Frequency, the Radio Time Signal Committee, Tôhoku-Tihô-Kensetu-Kyoku, Japan National Railway, Nippon-Yusi Co., police stations, provincial bureaus etc., for their inestimable help and cooperation given to us.

Financial aid was granted by the fund for special works of the Earthquake Research Institute.

Our thanks are due to Prof. N. Nasu, director of the institute, Professors F. Kishinouye, H. Kawasumi and T. Hagiwara for their kind advices in the project.

Postscript

After the completion of this paper, it was found that the name of the town near the shot point should be written "Hokoda" instead of "Hokota". But owing to the lack of sufficient time for correction, inscriptions in seismograms and text figures are left as hitherto used.

---

31. 第2回鉾田爆破地震動の観測

爆破地震動研究グループ

1957年8月26日午前1時5分，茨城県鹿島郡大洋村の旧飛行場跡で約1屯の火薬の大爆破が行われ，その地震動を Fig. 1, Table 1 に与えられている 18 ケ所で観測した．爆破点は第1回の場所から S 57° W の方向に 188 m移つた点で前回同様の方法で行つた．

今回の観測の目的は，第1には，既に得られている東北地方の地殻構造を検討する逆測線であり，第2には，関東地方北部と東北地方の地殻構造の関係を求めることである．得られた観測値は Table 2 及び Table 3 に与えられている．

なお，今回の実験についても，日本放送協会，東京電力株式会社，東北電力株式会社，電波研究所，学術会議報時委員会，東北地方建設局，日本国有鉄道，日本油脂株式会社，観測点所在の各県警察本部，市町村役場などの非常な御協力を得たので心から感謝の意を表します．

また本観測は地震研究所特別事業費により実施し，那須所長，岸上，河角，萩原各教授には大変お骨折りいただいたので，記して感謝致します．

3) T. MATUZAWA, T. MATUMOTO and S. ASANO, *Bull. Earthq. Res. Inst.*, **37** (1959).

BULLETIN OF THE EARTHQUAKE
RESEARCH INSTITUTE
Vol. 37 (1959), pp. 509-524

32. *On the Crustal Structure Derived from Observations of the Second Hokoda Explosion.*

By Takeo Matuzawa, Tosimatu Matumoto and Shûzô Asano,

Earthquake Research Institute.

(Read May 27, 1958.—Received June 30, 1959.)

1. On velocities of P waves in the P_1 and the P_2 layer

From the first Hokoda explosion[1] the P velocity near the surface was obtained as 1.79 km/sec. From the second Hokoda explosion we obtained 1.71 km/sec and from both data it was obtained as 1.74 km/sec, as was shown in the preceding paper.[2]

As to the second layer, as shown in Fig. 1, travel times at Ôya, Mito A, Mito B, Sano, Tomoegawa (for the first explosion) and Tamari (for the first explosion) are arranged very well on a straight line show-

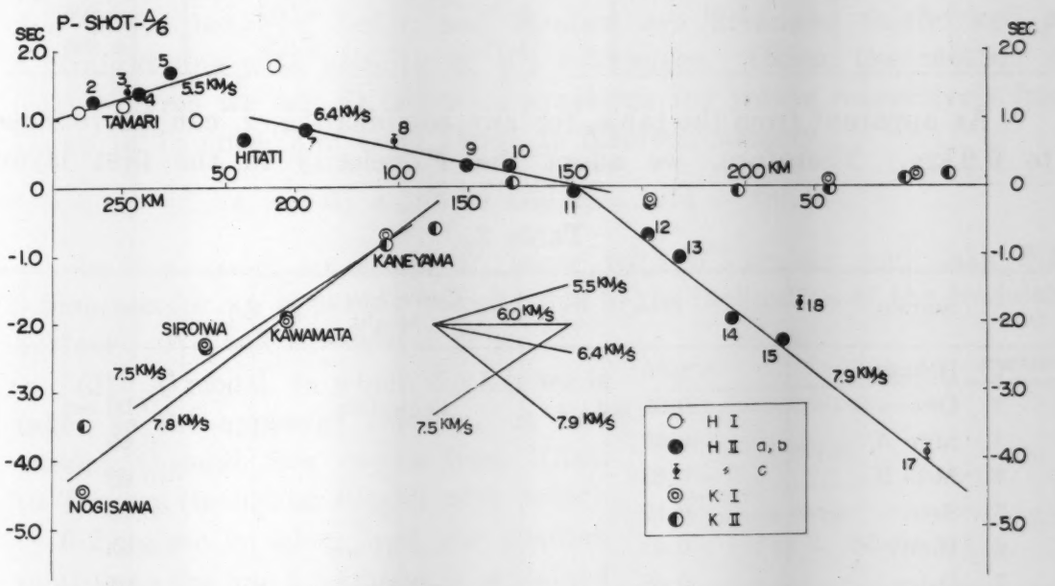

Fig. 1. Travel time curves of the waves from the second Hokoda Explosion. HI, HII, KI and KII mean observed travel times of the first, second Hokoda Explosion, the first and second Kamaisi Explosion respectively.

1) The Research Group for Explosion Seismology, *Bull. Earthq. Res. Inst.*, **36** (1958) 529-548.

2) The Research Group for Explosion Seismology, *Bull. Earthq. Res. Inst.*, **37** (1959).

ing velocity of 5.5 km/sec with intercept time of 1.02 sec. If we use exclusively the values for the second explosion, i.e., values at 4 stations between Ôya and Sano, and deduce a straight line by the method of least squares, putting weights 4, 3, 2 and 1 corresponding to its classes of accuracy a, b, c and d given in the former paper,[3] then we get

$$t = 1.01 + \Delta/5.40 ,$$

where t in sec and Δ in km.

We have two sets of velocity V_2 and intercept time τ_2 for the second layer and three sets of them for the first layer. For some combinations of them the depth of the P_1 layer, z_1, is calculated as shown in Table 1.

Table 1. Thickness of the P_1 layer

V_2 km/sec	τ_2 sec	V_1 km/sec	τ_1 sec	z_1 km
5.5	1.02	1.74	0.035	0.92
5.4	1.01	1.74	0.035	0.895
		1.79	0.053	0.906
		1.71	0.028	0.885

As apparent from the table, for any combination, z_1 can be rounded to 0.9 km. Therefore, we adopt the P velocity in the first layer,

Table 2.

Station	$O-C$	Correction for height	$(O-C)_H$*
1. Hokoda			
2. Ôya	0.06 sec	negligible	0.06 sec
3. Mito A	0.05	〃	0.05
4. Mito B	−0.03	〃	−0.03
5. Sano	0.15	〃	0.15
6. Hitati	−0.03	−0.05 sec	−0.08
7. Daigo	0.05	−0.01	0.04
8. Tanakura	0.16	−0.02	0.14
9. Tamagawa	0.01	−0.02	−0.01
10. Tamura	0.12	−0.04	0.08

* $(O-C)_H$ means $(O-C)$ in which correction for height is taken into account.

3) The Research Group for Explosion Seismology, *loc. cit.*, 2).

1.74 km/sec, the thickness of the layer, 0.92 km, the P velocity in the second layer, 5.5 km/sec, and the intercept time, 1.02 sec.

$O-C$ values at stations between Ôya and Sano calculated from these assumptions are tabulated in Table 2, together with other values.

The value at Sano, 0.15 sec, is rather large, however, it may be explained from a reasonable supposition that the thickness of the P_1 layer is larger at Sano than at other stations.

2. Probable models of the crustal structure

As apparent from Fig. 1, travel times between Hitati and Tamura or Hitati and Siroiwa belong to a line with velocity, nearly 6 km/sec, however, owing to the abnormally small value at Hitati, according to various ways of its interpretation, some different values of velocity can be taken. Namely, various models as follows can be at least assumed, without paying any attention to the crustal structure in neighbouring areas.

(1) A model, in which 6.4–6.5 km/sec is adopted as the apparent velocity, i.e., the travel time at Hitati is excluded as a singularity. Then, five points between Daigo and Siroiwa are arranged fairly well on a straight line with velocity of 6.4 6.5 km/sec. Using the method of least squares we can fit following equations for points respectively from Daigo to Tamura, and from Daigo to Siroiwa, namely,

$$t_3 = 1.61 + \Delta/6.39 \text{ and } t_3 = 1.74 + \Delta/6.44 \ .$$

In this model, we adopt P_2 layer with 5.5 km/sec and take 6.4–6.5km/sec for an apparent velocity due to the inclination of the boundary surface. We call it model 1 (Fig. 2).

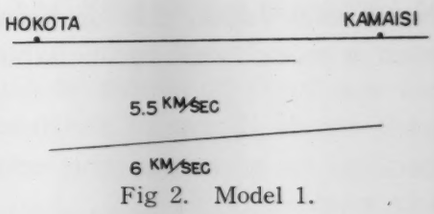

Fig 2. Model 1.

(2) A model, in which 6.2 km/sec is taken as the apparent velocity. A line passing through five points from Hitati to Tamura (including Hitati) with velocity 6.2 km/sec is taken and its position relative to the line 5.5 km/sec is explained by putting a fault under the ground.

In this case two further subdivisions are possible.

(a) A layer with velocity 5.5 km/sec exists really: model 2a.

(b) The velocity 5.5 km/sec is only an apparent one and explained by inclination of the boundary surface: model 2b.

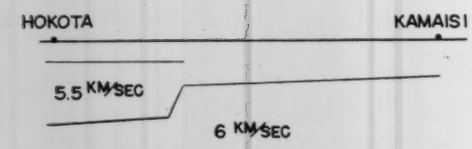

Fig. 3(a). Model 2a.

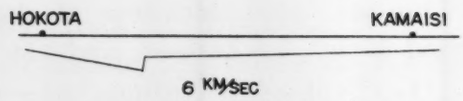

Fig. 3(b). Model 2b.

(3) A model in which an apparent velocity of 6.3 km/sec is assumed (model 3).

The large travel time at Sano is excluded as a singularity owing to a supposed large thickness of a surface layer[4], and a line passing through seven points from Ôya to Tamura (excluding Sano) with velocity of 6.3 km/sec is adopted. As a consequence a line with velocity of 5.5 km/sec is discarded. This model is somewhat akin to model 2b, however, an underground fault is not necessary. (Fig. 4).

(4) A model in which the velocity of 5.8 km/sec in the second layer is adopted. (model 4).

In models 1, 2 and 3, different assumptions of apparent velocities near 6 km/sec were due to differences in the way of grouping the observed travel times. In this model we adopt 5.8 km/sec in the P_2 layer which was already obtained for North-east Japan[5] and try to explain the apparent velocity of 5.5 km/sec by the inclination of the layer boundary (Fig. 5).

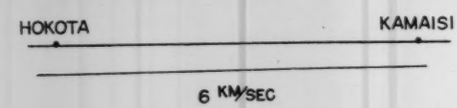

Fig. 4. Model 3.

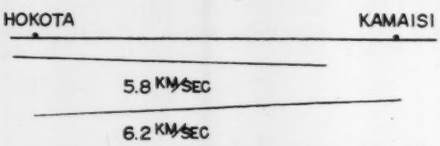

Fig. 5. Model 4.

In investigating these four models we take the crustal structure of North-east Japan and of Kwantô District into consideration and select such a model well reconcilable with them.

3. Form of the lower boundary of the P_2 layer and the velocity in the P_3 layer

First, model 1 is investigated. The true velocity in the P_3 layer 6.1 km/sec, which was obtained in the northern part of Kwantô District,[6]

4) "A surface layer" in this paper stands for an unidentified surface layer with a low velocity, for example, a weathered layer in common use.

5) The Research Group for Explosion Seismology, *Pub. Bureau Central Séism. Intern. Série A. Trav. Sc.*, **19** (1954), 229-242; T. MATUZAWA, *Bull. Earthq. Res. Inst.*, **37** (1959).

6) T. USAMI *et al.*, *Bull. Earthq. Res. Inst.*, **36** (1957), 349-357.

is tentatively adopted, because the area concerned is a direct continuation to it.

As for the allowance of the residue $O-C$, we take it ± 0.1 sec, as in the case of North-east Japan.[7]

Now, in order to produce an apparent velocity of 6.4–6.5 km/sec instead of the true velocity of 6.1 km/sec, the layer boundary must be shallower in the north with a dip of 5°14′–6°32′. Its depth at the shot point is calculated as 5.3 km, using $\Delta = 30$ km of the intersection point of lines for 5.5 km/sec and for 6.4–6.5 km/sec. If we assume a uniform inclination, the P_3 layer should be exposed to the earth surface at $\Delta = 46.3$–57.9 km. Even if we use the depth of 6 km of the P_3 layer obtained in the northern part of Kwantô District, the said distance should be 52.4–65.5 km. On the other hand, the line belonging to the apparent velocity of 6.4–6.5 km/sec is extended to 73–132 km (from Daigo to Tamura) or 73–150 km (from Daigo to Siroiwa). This is contradictory to the alleged short distance of the exposure.

In order to avoid this contradiction, taking a mode of stratification similar to model 2a, we assume a model as shown in Fig. 6.

Namely, until a certain distance Δ_0 km, the layer boundary is horizontal and then may be shallower toward the north. If we take 30–50 km as the break distance of the travel time lines (between Sano and Hitati), then the depth of the lower boundary of the P_2 layer turns out as 3.4–5.7 km. Thus we adopt tentatively the value of 6 km for the northern Kwantô District. Taking Δ_0 as a parameter, $(O-C)$ values for stations between Hitati and Siroiwa are calculated as shown in Table 3.

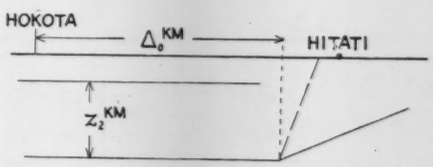

Fig. 6.

As is apparent from the table the absolute values of $O-C$ are too large in general. The absolute values of $O-C$ are still larger than 0.1 sec even if the bottom surface of P_2 layer is assumed to be inclined without changing its depth under the shot point. The next step to make the absolute values of $O-C$ smaller is to take the bottom shallower. This procedure does not induce any contradictions against the value of depth of bottom surface of P_2 layer obtained before for the Kwantô

7) The Research Group for Explosion Seismology, *loc. cit.*, 4). T. MATUZAWA, *loc. cit.*, 5).

8) T. USAMI *et al.*, *loc. cit.*, 6).

Table 3.

Station	Δ km	T_0 sec	$O-C$ sec	
			$\Delta_0=20$ km	$\Delta_0=30$ km
Hitati	55.16	9.88	−0.25	−0.29
Daigo	73.03	13.01	−0.02	−0.03
Tanakura	98.94	17.16	−0.07	−0.09
Tamagawa	119.47	20.22	−0.37	−0.40
Tamura	131.79	22.27	−0.31	−0.37
Siroiwa	150.33	25.00	−0.71	−0.70

District, because the seismic ray concerned did not pass through this part of the bottom under the shot point. Taking the value of the depth of the P_2 layer and Δ_0 as parameters, the $O-C$ value at Hitati is calculated as shown in Table 4.

Table 4. $O-C$ in sec at Hitati

z_2 km \ Δ_0 km	20	30	35	40
3.8	—	−0.04	−0.05	−0.08
4.0	−0.04	−0.06	−0.08	−0.11
4.5	−0.09	—	—	—

As the travel time of the first wave at Sano should be associated with waves through the P_2 layer, z_2 value must be at least 4 km.

Thus tentatively adopting $z_2=4$ km and $\Delta_0=30$ km, the $O-C$ values at Tamagawa and Tamura are again −0.21 sec and −0.17 sec respectively, even if the waves pass through the P_3 layer only. These very small values suggest that the adopted velocity 6.1 km/sec in the P_3 layer be too small.

As an another piece of evidence, taking velocity V_3 of the P_3 layer as a parameter, for a few combinations of the apparent velocity V_3' and the true velocity of P_2 layer V_2, and assuming that the P_3 layer be exposed to the earth surface at a distance $\Delta=150$ km (near Siroiwa), the depth d of the bottom surface of the P_2 layer under Hokoda is calculated as shown in Table 5.

As apparent from the table, d values for $V_3 \leq 6.1$ km/sec are too large.

Table 5. Depth d km of the bottom surface of the P_2 layer under Hokoda

V_3'km/sec	6.3			6.4				6.3			6.4			
V_2 〃	5.4			5.4				5.5			5.5			
V_3 〃	6.0	6.1	6.2	6.0	6.1	6.2	6.3	6.0	6.1	6.2	6.0	6.1	6.2	6.3
d km	11.4	7.2	3.4	17.5	12.7	8.3	4.4	14.8	9.6	4.4	19.3	14.0	8.7	4.8

Thus, assuming 6.2 km/sec as the true velocity in the P_3 layer, similar examinations are repeated.

At first, the depth z_2 of the P_2 layer corresponding to the break distance of 35-50 km (between Sano and Hitati) turns out 4.3-6.2 km. $O-C$ values of Hitati for some combinations of Δ_0 and z_2 are calculated as shown in Table 6.

Table 6. $O-C$ at Hitati (in 0.01 sec)

z_2 km \ Δ_0 km	30	35	40	45
4.3	4	1	−3	−8
4.5	—	—	−5	—
4.9	−5	—	—	—

As the correction for the height of Hitati is −0.05 sec, $O-C$ for Hitati is −0.08 sec for $z_2=4.3$ km and $\Delta_0=40$ km. This value is also compatible with the interpretation that the first motion at Sano is due to waves through the P_2 layer.

The first waves at Tamagawa and Tamura are supposed to be propagated exclusively in the P_3 layer after refraction into this layer. The dip of the line connecting Tamagawa and the point at $\Delta_0=40$ km on the bottom plane is 3°46′ and that for Tamura is 3°15′. On the other hand, the dip of the bottom plane giving the apparent velocity of 6.4 km/sec must be 3°18′.

$O-C$ values at Daigo, Tamura and Tamagawa for both values of inclinations are given in Table 7.

Table 7. Inclination and $O-C$ in sec

Inclination \ Station	Daigo	Tanakura	Tamagawa	Tamura
3°46′	0.05	0.19	0.05	0.12
3°15′	0.05	0.16	0.01	0.12

As apparent from the table, differences between the two cases are trivial. We adopt the latter value 3°15′ of the dip.

5. On P_n

As stated in § 1, the main object of the present investigation has been to increase the knowledge of the P_n layer, together with the data obtained in North-east Japan. Among all observation points, stations at which the first motion is expected to be due to waves passing through the P_n layer are those beyond Siroiwa, and as apparent from Fig. 1 they are arranged fairly well on a straight line with apparent velocity of 7.9 km/sec.

Comparing it with the value obtained in North-east Japan, we take for granted that this value corresponds to the P_n layer. In calculating the travel time for P_n waves, it is necessary to know the crustal structure above the P_n layer, however, the structure near Siroiwa and Kawamata is still obscure. Therefore, we must assume a probable one there. On the other hand we obtained in North-east Japan that the boundary between the layer of 5.75–5.85 km/sec and that of 6.1–6.2 km/sec has a dip of 6–11° nearly westward and a strike of 200–210° from the north over the east and its depth under the Kamaisi shot point is 0.5–2.0 km, while as apparent in Fig. 1 of the former paper[9] the observation points beyond Siroiwa are spread nearly along a line parallel to the strike direction. The distance of this line from the strike line passing through the Kamaisi shot point is about 30 km. The depth to the boundary, z_2', under this line (Fig. 7) is calculated for some combinations of inclination θ and depth under Kamaisi shot point h as shown in Table 8.

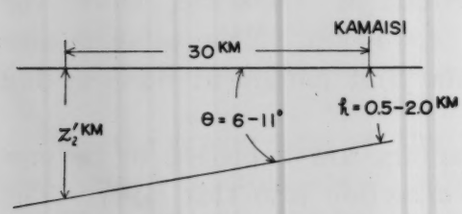

Fig. 7.

As apparent from the table, the thickness of the layer 5.8 km/sec under this line is confined between 4–8 km.

In the next place, the approximate depth of the Mohorovičić discontinuity is calculated as 25 km from the distance, 145 km, of the intersection point of lines

Table 8. z_2' km

θ \ h	0.5 km	2.0 km
6°	3.7	5.2
11°	6.3	7.9

9) *loc. cit.*, 2).

with 6.2 km/sec and with 7.9 km/sec. The relation between the inclination θ of the Mohorovičić discontinuity and the true velocity V_4 in the P_n layer, which should give the apparent velocity of 7.9 km/sec is shown in Table 9.

Table 9. V_4 and θ which give 7.9 km/sec (The negative sign of θ means the dip toward the north.)

V_4 km/sec	7.5	7.6	7.7	7.8	7.9	8.0	8.1	8.2
θ	4°04′	2°58′	1°56′	57′	0°	−54′	−1°45′	−2°35′

6. Case of the horizontal Mohorovičić surface

For the assumption of the horizontal Mohorovičić discontinuity, i.e., $\theta=0°$ and $V_4=7.9$ km/sec, $O-C$ values corresponding to several values of z'_2 are calculated as shown in Table 10.

Table 10. $O-C$ (in sec) for various z'_2 (in km) ($V_4=7.9$ km/sec, and $d_3=27.5$ km)

Station \ z'_2	0	2	4	5	6	8
Siroiwa	−0.09	−0.12	−0.15	−0.17	−0.18	−0.22
Kawamata	0.11	0.08	−0.05	0.03	0.02	0.00
Isida	0.17	0.14	0.11	0.09	0.08	0.05
Kaneyama	−0.14	−0.18	−0.21	−0.23	−0.23	−0.27
Watari	0.13	0.10	0.07	0.05	0.04	0.01
Miyatoko	0.13	0.10	0.07	0.05	0.04	0.01

We find from the table that travel times at Siroiwa and Kaneyama are too early compared with other stations, and moreover, the variation of $O-C$ value of each station in the range of $z'_2=4$-8 km is trivial. These very large absolute values of $O-C$ for Siroiwa and Kaneyama are not explained by the assumption that the thickness of the 5.8 km/sec layer would be smaller than those under other stations, because, even if we take $z'_2=0$ km, $O-C$ values for Siroiwa and Kaneyama are calculated as −0.09 sec and −0.14 sec respectively. As for the effect of a surface layer, we know from the investigation of North-east Japan that at almost all stations in the area, which is adjacent to the area here concerned, the 5.8 km/sec layer is nearly exposed to the surface.

There are a few possible ways of explanation. First, we resort to an explanation that the Mohorovičić discontinuity under these stations might be shallow in such a way that the $O-C$ values at other stations would not be affected. The result is shown in Fig. 8. As for Siroiwa station, the inclination of 5° of the Mohorovičić surface begins at a refracting point of the wave arriving at Tamura, 52.44 km to Siroiwa and continues to a point 26.08 km to Siroiwa, which is a point where waves arriving at Siroiwa refracted into the upper layer with a critical angle. Further north the upheaval ceases to exist and turns back to the original level. As for Kaneyama, similarly, the inclination of 5° begins at a point 49.10 km south to Kaneyama and ends at a point 26.42 km south to Kaneyama and turns back quickly to the original level. In this way $O-C$ values at Siroiwa and Kaneyama become respectively -0.02 and -0.05 sec.

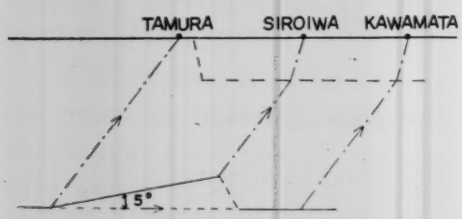

Fig. 8.

As this procedure introduces two local independent assumptions, it is somewhat arbitrary.

The second alternative is as follows. The small $O-C$ values (absolute values are large) at Siroiwa and Kaneyama are supposed to be due to the lack of a surface layer, while positive $O-C$ values at other stations are assumed to be due to a thick surface layer. From this standpoint, as shown in Table 11, $z'_2=5$ km and $d_3=26.5$ km are adequate.

The third alternative is that at Siroiwa and Kaneyama the 5.8 km/sec layer is lacking and other stations are covered by a thick surface layer. In this case $d_3=27$–27.5 km is adequate.

7. Case of the inclined Mohorovičić surface

In the case of the inclined Mohorovičić surface also, for the explanation of travel times at Siroiwa and Kaneyame we can take three standpoints similar to the case of the horizontal Mohorovičić surface.

If we assume $V_4=7.7$ km/sec obtained in the northern part of Kwantô District, from the first standpoint it is found adequate that its depth under Hokoda shot point d_3 is equal to 29 km and its inclination is 1°56′, becoming shallower in the north. (Refer to Table 9 and Table 11). As for the explanation of the small travel times of Siroiwa and

Kaneyama, upheaval of the Mohorovičić surface, i.e., increase of its dip under each station is taken. Namely, for Siroiwa dip of 6°56′ (i.e., 1°56′+5°) begins at a point 51 km south from Siroiwa and ends at a point 22.9 km south to Siroiwa and in the further north it takes sharply its original trend with inclination of 1°56′. For Kaneyama corresponding points are at 55 km and 20.8 km south from there, the dips being the same. (Fig. 9) $O-C$ values are given in Table 11.

From the second standpoint, in which large values of $O-C$ at other stations are attributed to a thick surface layer, the adequate value of d_3 is 27.5 km, and $O-C$ values for this case are given in Table 11.

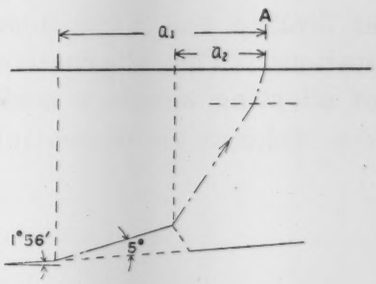

Fig. 9.

The third standpoint is omitted, because it is easily inferred from these results.

From investigations stated above, we see that observed data are equally well explained for both values of V_4, 7.7 km/sec and 7.9 km/sec and thus the unique determination of V_4 is not possible. In order to put a limit to the variable range of V_4, we added in Table 11 $O-C$ values corresponding to $V_4=7.5$ km/sec and 8.2 km/sec, which have been both limits hitherto appearing in publications. As far as the data here concerned, no contradictions occur.

8. Reference to the data of Kamaisi explosions

As the second Hokoda explosion forms a reverse profile to the Kamaisi shots,[10] their data must be taken into account. In Fig. 1 travel times for two Kamaisi shots are plotted. Among P_n travel times, accurate ones are those of Kaneyama for the first and second Kamaisi shot and those of Kawamata and Siroiwa for the second Kamaisi shot. At farther stations sometimes amplitudes were too small and sometimes natural earthquakes disturbed the record. These four travel times of three stations are fairly well arranged on a straight line with an apparent velocity of 7.5 km/sec. If we add the travel time at Nogisawa for the first shot (that for the second shot was disturbed by a natural earthquake), a straight line with velocity of 7.8 km/sec is obtained.

Combination of the apparent velocity of 7.9 km/sec for the Hokoda

10) The Research Group for Explosion Seismology, *Bull. Earthq. Res. Inst.*, **32** (1954), 79; **33** (1955), 699.

shot and 7.5 km/sec for the Kamaisi shot gives 7.7 km/sec as the true value and an inclination of 1°56′, and another combination of 7.9 km/sec and 7.8 km/sec gives 7.8 km/sec as the true velocity and an inclination of 29′. In both cases the dip is from the north to the south.

We are inclined to adopt $V_4=7.7$ km/sec and $\theta=1°56'$, because the data at Nogisawa were somewhat dubious.

As for the alternative models explained in § 6 and § 7, we are inclined to adopt the second alternative, i.e., relatively small $O-C$ values at Siroiwa and Kaneyama are attributed to thick surface layers at other stations. This alternative is more consistent with our guiding principle of adopting simple a model as possible. Thus we adopt the depth of the Mohorovičić discontinuity at Hokoda $d_3=27.5$ km.

9. Final Model

Summarizing examinations stated above we obtain a crustal model as shown in Fig. 10 as a final one.

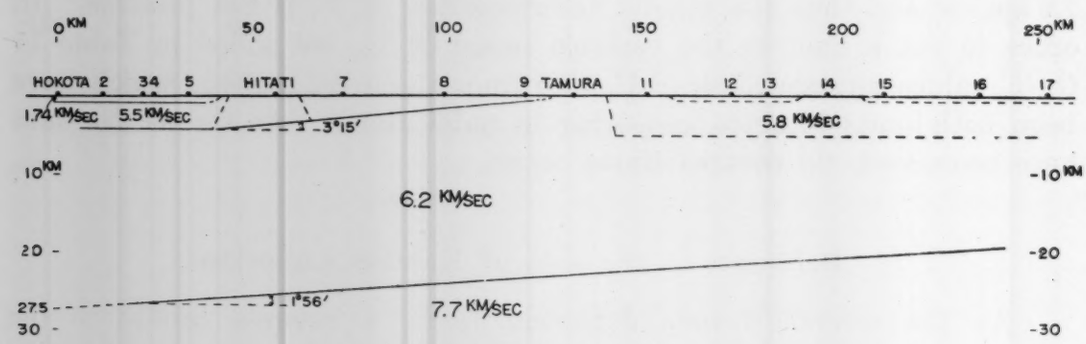

Fig. 10. Final model

The P_1 layer has a velocity of P waves of 1.74 km/sec and is 0.92 km thick. It is somewhat thicker near Sano and ceases to exist beyond Hitati. The P_2 layer has a velocity of 5.5 km/sec and is 4.3 km thick under the Kwantô area and tapers northward with inclination of 3°15′ of the bottom surface from a point $\Delta=40$ km from Hokoda and the P_3 layer is nearly exposed to the earth surface near Tamura. Station Hitati, being a point with much deviation from the profile, is an exceptional point, and the P_3 layer is supposed to be almost exposed to the surface as shown by conical dotted lines in the figure.

Beyond Siroiwa the P'_2 layer has a velocity of 5.8 km/sec and a thickness of 4–8 km. Excluding Siroiwa and Kaneyama, it is supposed that

the surface is covered by a certain thin surface layer.

The P_3 layer has a velocity of 6.2 km/sec, and the depth of its lower surface, i.e., the Mohorovičić surface, is 27.5 km under Hokoda and tapers northward with an inclination of 1°56′.

The velocity of the P_n wave is 7.7 km/sec. $O-C$ values for this model are shown as far as Tamura in Table 2. As for P_n waves, they are given in Table 11 for some combinations of V_4 and d_3.

Table 11.

Station	Correction for height	$V_4=7.7$, $z_2'=5$, $\theta=1°56'$		$V_4=7.9$, $z_2'=5$, $\theta=0°$		$V_4=7.5$, $z_2'=5$, $\theta=4°04'$	$V_4=8.2$, $z_2'=5$, $\theta=-2°35'$
		$d_3=27.5$	$d_3=29.0$	$d_3=26.5$	$d_3=27.5$	$d_3=30.0$	$d_3=26.0$
	sec	sec	sec	sec	sec	sec	sec
11. Siroiwa	−0.04	0.04	−0.06	−0.01	−0.02	−0.19	−0.18
12. Kawamata	−0.02	0.25	−0.05	0.21	0.01	0.04	0.04
13. Isida	−0.02	0.32	0.01	0.27	0.07	0.10	0.10
14. Kaneyama	negligible	0.02	−0.05	−0.03	−0.05	−0.20	−0.19
15. Watari	〃	0.29	0.00	0.25	0.05	0.07	0.09
17. Miyatoko	〃	0.29	0.00	0.25	0.05	0.07	0.09

(V_4 in km/sec, z_2' and d_3 in km.)

Speaking of correction for height, it was not necessary for the shot point, because its height above sea level is 41 m and the head of explosives was 35 m deep below the surface of the ground.

As is apparent from the tables, except for a few stations all $O-C$ absolute values are less than 0.1 sec and can be regarded as random errors.

In Table 2, $O-C$ values at Sano and Tanakura are larger than 0.1 sec. It is supposed that at Sano the surface layer is thick and at Tanakura the travel time of the first motion was read too late, owing to its small amplitude.

In Table 11, for the most adequate values of $V_4=7.7$ km/sec and $d_3=27.5$ km, $O-C$ values attain 0.2–0.3 sec, except Siroiwa and Kaneyama. This is explained by the existence of a certain surface layer. If we assume a layer with velocity of 1.74 km/sec, as found at Hokoda shot point, thickness of 0.4 km is sufficient to explain them, which is supposed to be very probable.

10. Remarks to reflected waves

As stated in the former paper[11] at Sano a seismograph of the E. T. L.—M3 type for seismic exploration was used, in order to catch reflected waves from the Mohorovičić discontinuity. Three distinct phases obtained were 1 h 05 m 9.61 sec, 11.35 sec and 12.85 sec. On the other hand, travel times of reflected waves expected from calculations are 19.56 sec from the bottom of the P_1 layer and 7.38 sec from that of the P_2 layer. No phase corresponding to the former was observed and none corresponding to the latter identified, its time being nearly coincident with the commencement of the first refracted wave.

As for the reflected waves from the Mohorovičić discontinuity, the travel time calculated from the model in Fig. 10 is 11.27 sec. The difference from the observed value 11.35 sec is only 0.08 sec and the coincidence is very good. If we adopt the horizontal Mohorovičić discontinuity with $V_4=7.9$ km/sec and $d_3=27.5$ km, the coincidence is better.

A further remark should be added, because at this time a refracted S-waves are expected to set in. But as the apparent velocity of the phase due to these 12 components is 7.7 km/sec, where the apparent velocity of the initial phase is 5.9 km/sec, we can very probably conclude that this phase be due to P-waves reflected at the Mohorovičić discontinuity.

11. Remarks to gravity anomaly and the surface geology

The Bouguer anomaly of gravity near Hitati is very large in positive.[12] This fact corresponds very well to the supposed upheaval of the P_3 layer. In Fig. 11 the Bouguer anomaly in the profile Hokoda-Hitati is shown.

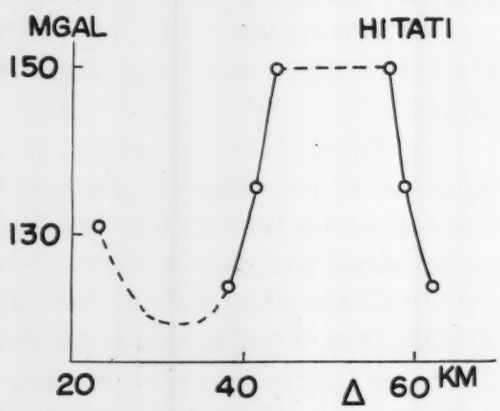

Fig. 11. Bouguer Anomaly in the Section of Hokoda-Hitati.

As for the surface geology near Hitati, a detouched layer called Hitati Palaeozoic layer is exposed.

One more characteristic feature shown in Fig. 10 is the structure near Tamagawa, Tamura and Siroiwa. Of course, as it is not necessary that the P_3 layer is literally exposed to the surface, the exact correspondence to the surface geology is not indispensable. This area belongs geologically

11) *loc. cit.*, 2).

12) C. TSUBOI *et al.*, *Bull. Earthq. Res. Inst., Suppl. Vol.*, **4**, Part 7 (1956).

to the Abukuma mountain land and has not such a remarkable characteristic as the Hitati area and no visible fault was found. However, some geologists seem to suppose existence of faults in this area.

At any rate, the direct correspondence is not so good as in the Hitati area.

12. Conclusion

As often stated elsewhere, the principal objects of this observation were precise determination of several quantities concerning the Mohorovicić discontinuity and to find out the connection between the crustal structure in North-east Japan and in the northern part of Kwantô District. Results of analysis are shown in Fig. 10, and we could consistently connect the latter and get values about P_n more precise than hitherto obtained.

In summary, in the Kwantô area the first layer has a velocity of 1.74 km/sec with a thickness of 0.92 km and ceases to exist in the farther north of Hitati. The second layer has a velocity of 5.5 km/sec with a thickness of 4.3 km, however, its bottom surface begins to taper northward at a distance of $\Delta=40$ km from Hokoda, and near Tamura the third layer with velocity of 6.2 km/sec comes near to the earth surface.

In North-east Japan, except Siroiwa and Kaneyama the surface is covered by a certain thin layer and the second layer, corresponding to that of Kwantô area with velocity of 5.5 km/sec, has a velocity of 5.8 km/sec with thickness 4–8 km.

The velocity of P_n waves is 7.7 km/sec and the depth of the Mohorovičić discontinuity is 27.5 km under Hokoda and tapers northward with inclination of about 2°. The depth of the Mohorovičić discontinuity is verified by reflected waves observed at Sano.

From observations of the Nozori explosions and the first Hokoda explosion,[13] we derived velocity of 6.1 km/sec of the third layer and the depth of the Mohorovičić surface 25 km for the northern part of Kwantô District.

In the present case we have 6.2 km/sec instead of 6.1 km/sec and the depth of the Mohorovičić surface under Hokoda, 27.5 km, instead of 25 km. Therefore, a small correction to the structure of the northern part of Kwantô District may be necessary, but we think it trivial.

13) *loc cit.*, 1).

Hitati is a singular point and the third layer is supposed to be upheaved near to the surface of the ground.[1]

13. Acknowledgement

In conclusion, we wish to express our hearty thanks to the Research Group for Explosion Seismology who placed the data at our disposal. Also we are much obliged to Miss Yoriko Utida who prepared many text figures in a short time.

Postscript

After the completion of this paper, it was found that the name of the town near the shot point should be written "Hokoda" instead of "Hokota." But owing to the lack of sufficient time for correction, inscriptions in text figures are left as hitherto used.

---

32. 第2回鉾田爆破観測から得られた地殻構造について

地震研究所 松沢武雄・松本利松・浅野周三

第2回鉾田爆破の観測資料を解析した結果，Fig. 10に示されるような，東北地方，関東地方北部を結びつける地殻構造を得た．すなわち，関東地方では，第一層は速度，1.74 km/s，厚さ 0.92 kmで，この層は日立以北ではなくなる．第2層は速度 5.5 km/s，厚さ 4.3 km，底面は Δ=40 km の所から 3°15′ で傾き，田村付近では速度 6.2 km/s の第3層が地表近くまで来ている．東北地方では，白岩，金山以外ではうすい未知の表面層があり，関東北部の 5.5 km/s の速度に相当するのは，東北地方の結果を考えあわせると 5.8 km/s であり，厚さ 4～8 km の程度と仮定した．P_n 波の速度は 7.7 km/s，Moho. 面の深さは鉾田直下で 27.5 km であり，約 2° の傾斜で東北地方では浅くなつている．この Moho. 面の値は，また，佐野で得られた反射波の走時からも妥当性を裏付けされた．日立の方向だけは構造が別で，日立では第3層が地表近くまで来ている．これは，重力や，地質の資料とも極めてよく調和する．

---

[1] According to K. Kanai, Bull. Earthq. Res. Inst., **29** (1951), 505-509, at the depth of 440m 5.65 km/sec was found.

地震研究所彙報
第37号(1959) 525-530頁

33. 地震計用トランジスター前置増幅器

地震研究所　松本英照

(昭和 34 年4月 28 日発表——昭和 34 年6月 30 日受理)

§1.

自然地震および爆破地震の高感度観測を臨時あるいは経常的に任意の地点でおこなう目的で筆者はこれまでに数種の電子管式地震計を試作し実用に供してきた.

しかし，真空管回路は消費電力がおおいのでその電源として蓄電池を長期観測に使用することは施設・要員の整備された保守の完全な固定観測所以外ではのぞめない.

一方，商用交流電源から電力を供給すれば電源の安定化と雑音制禦の制約から増幅器の感度は 0.1 mm/μV 以下に制限をうけ，われわれの要求する 1 mm/μV 以上の感度を安定で無雑音な状態では保持することができない.

そこで，われわれは地震計の感度をあげる手段として換振器の感度をあげることに努力してきた. あたらしく地震研究所技術部において設計製作された可動線輪型動電換振器*は出力約 6 V/kine で従来の爆破グループ型大型換振器よりさらに出力はおおきく初期の小型換振器の感度にくらべ 10 倍以上の感度になつたが，このばあい換振器は形状・重量ともに増大し，設置・運搬の簡易さをうしなう傾向を招来し，その意味で，このような可搬型換振器の感度をあげることは限界に達したとおもわれる.

ところで，形状・重量が増大したことは観測の性質によつては非常に都合のわるいことであるので，感度をあげるのにほかによい方法があれば採用したいとおもい，その方法を検討してみた.

ひとつの方法は変成器を使用して換振器の出力を昇圧する方法であるが，最近の発達した電子工業においても，われわれの対象とする周波数帯で周波数特性や能率のよい変成器の製作は困難だし，自己 inductance も充分おおきくすることができないので，換振器の制動に作用をおよぼし，特定の換振器とくみあわせて使用する場合をのぞいては実用にならないし，利得もあげられない.

もうひとつの方法は transistor を使用して前置増幅器をつくり換振器の出力を増幅して主増幅器に供給する方法である.

変成器は受動回路であるから，電力消費はなく雑音発生や安定度の心配なしに昇圧できることが特長であるが，前置増幅器は能動回路で電力を消費するから，電源をふくめての

---

* 地震研究所技術部製動線輪型動電換振器上下動 3 c/s II型，形状 159 mm × 190 mm × 164mm (高×縦×横)，重量 8.55 kg, Coil 2800 Turns 1.6 KΩ，磁石 MK-5 (三菱) 内磁型 7400 gauss，出力約 6 V/kine.

安定度や雑音発生の level が主増幅器のそれらよりもわるくないことが必要条件となる．

元来 transitor は温度特性がわるく雑音の発生もはげしいものであつたが，ここ数年で transistor 工業はめざましい発達をとげ，雑音発生もすくなく利得のおおきな製品が量産されるようになつたので，これを使用し利得の一部を温度補償や安定度の増加にふりむけるような回路を採用し，電流を制限して雑音の発生を最小限にとどめるように回路を設計試作したところ予期以上に良好な結果をえたので報告する．

§ 2.

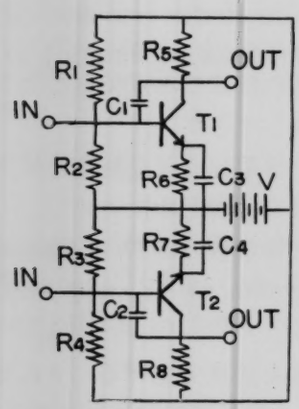

Fig. 1. Circuit of the pre-amplifier.
R1, R4, 200 KΩ.
R2, R3, 100 KΩ.
R5, R6, R7, R8, 50 KΩ.
T1, T2, 2T65 (SONY).
C1, C2, 0.1 μF.
C3, C4, 200 μF.
V, UM-3A ×4 (6V).

最初に前置増幅器の必要条件としてかんがえられることは，つぎのとおりである．

1. 入力換算の発生雑音 level がひくい．
2. 小型軽量しかも安定で取扱い簡単である．
3. 製品の特性が均一で調整が簡単である．
4. 主増幅器あるいはその電源から作用をうけず，また作用をあたえない．
5. 換振器に作用をあたえず，また作用をうけない．そのために装置の入力 impedance が充分にたかい．
6. 利得周波数特性が 1～30 c/s の範囲で平坦である．
7. 消費電力がすくなく乾電池で長期使用ができる．

今回試作した装置は入力 impedance が充分たかくとれず，しかも周波数特性をもつため，換振器によつては制動作用が影響をうける欠点があり 5) の条件において不満足であるが，その他の条件はすべてみたすことができた．

第1図にこの transistor 前置増幅器の配線図をしめす．この回路はごく平凡な emitter 接地の回路に，高域遮断の負帰還をかけたものである．雑音発生をおさえるために諸抵抗値をたかくとり，偏倚電流は非常にひくくとつている．

第2図，第3図に利得周波数特性と入力

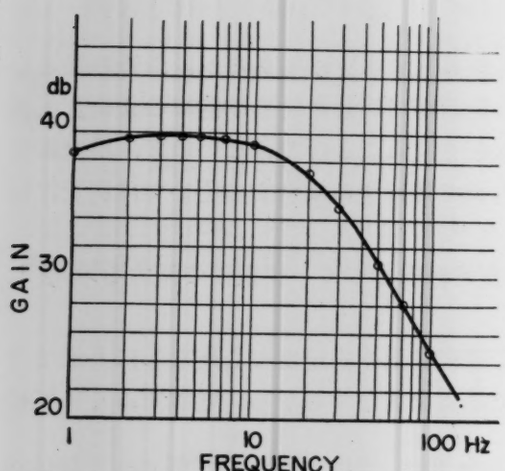

Fig. 2. Gain-frequency characteristic of the pre-amplifier at 20°C.

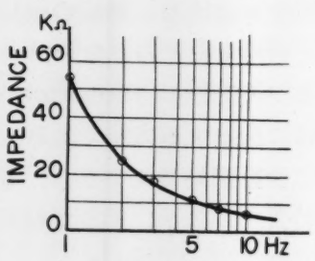

Fig. 3. Input impedance-frequency characteristic of the pre-amplifier at 20°C.

impedance 周波数特性をしめす．入力 impedance の周波数特性は emitter に挿入してある 200 μF の側路 condenser によるもので，利得の周波数特性はこの condenser と 0.1 μF の負帰還 condenser の双方の作用で高域，低域の利得低下をしめす．

勿論これらの周波数特性は観測のためには平坦であることがのぞましいが，利得をたかくとり，しかも温度特性や安定度のよいことの利益がこの欠点による損失よりもおおきいのでこの回路を採用した．

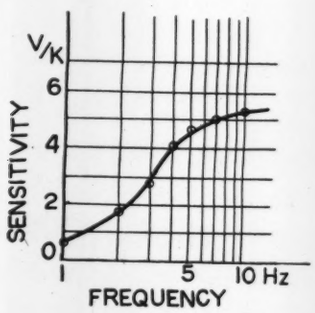

Fig. 4. Velocity sensitivity-frequency characteristic of the transducer when the output is terminated with 60 kilo-ohms.

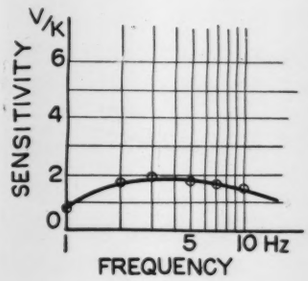

Fig. 5. Velocity sensitivity-frequency characteristic of the transducer when the output is terminated with the pre-amplifier.

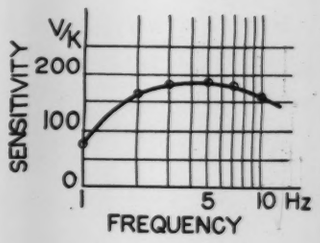

Fig. 6. Velocity sensitivity-frequency of the pre-ampilfier output when the input is supplied with the transducer used.

第4図，第5図に負荷抵抗 60 KΩ を結合したとき，またはこの増幅器を結合したときの，すでにのべた本所技術部製作の新型換振器の出力周波数特性，第6図にそのときの増幅器出力周波数特性をしめす．目的によつては速度感度特性の平坦部が換振器単独の場合よりもひろいから便利でもある．しかし，これは特性を実験からもとめる場合はよいが，計算で算出することは複雑になる．

この回路はいわゆる安定指数を，良好なあたいにとるよう設計してあるから，製法上均一性ののぞめない transistor を使用しても，一応均一の特性の装置をうることができるし，温度による動作点の移動もすくないので温度特性も比較的よい．

試作した装置と前記換振器の外観写真を第7図にしめす．この試作に際しては形態を特に小型化することに努力しなかつたので，散漫で，ややおおきな容積のものになつているが，空間をもつと上手に利用すればこの 1/3 程度にはおさまるはずであるから，取扱いは便利であり，換振器の一部と

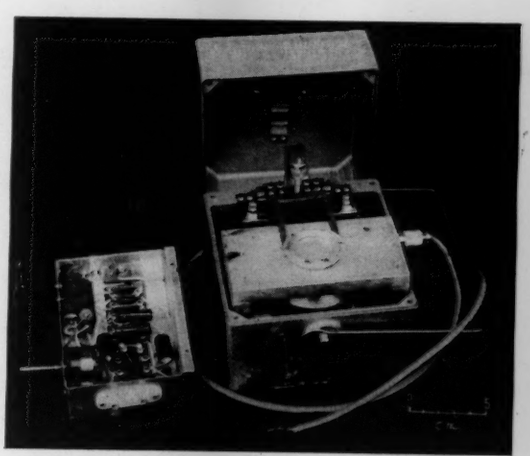

Fig. 7. Appearance of the amplifier and the transducer used.

してあつかつてもよいとおもわれる.

§ 3.

この装置の使用電力は 6 V 200 μA. この消費状況では単3乾電池4本を 6 V で使用して電池寿命は6ヶ月以上になる. 発生雑音は入力換算値で 0.1 μV 以下の低雑音で, 非常にすぐれた性能といえる. 同程度の低雑音を真空管増幅器でうることはほとんど不可能である. かかる意味を総合して, 今日試作した前置増幅器は現在まで実施することができなかつた程度の高感度で, 極微小地震動の観測を, 装置の雑音にわずらわされることなく安定な状態でおこなうことを可能ならしめたことで意義をもつている.

このほか, この装置を使用してえられる利点は入力 impedance をなるべくたかくし, 換振器に直流をながしたり, あるいは換振器を結合することによつて, 回路の動作点がかわらないように対称型に回路が構成されているので, 同相の雑音入力が消去されていることである.

このことは換振器と主増幅器との距離がはなれていたりするときにおきる, 交流静電誘導による観測妨害をすくなくするのに有効で, このため換振器の設置ならびにそのための野外配線作業は非常にらくになつた.

また, この装置は利得が充分たかくとつているので, 換振器を小型化したり, 主増幅器の利得をさげ安定度を増加させたり, 電源を簡略化したりすることに利得をふりむけることができるから, 地震計としての安定度やとりあつかいの点, あるいは装置の簡易化にやくだち, 安定した電子地震計による経常的観測をおこなうことができ, また臨時的にその利得をおおきくあげて超微小地震動の観測をこころみることができるなど地震観測法の向上に資するところがおおきいものと確信する.

第8図に感度 2 mm/mV の主増幅器にこの装置を結合し, 筑波地方の微小地震を観測した例を H.E.S. 短周期 ($T_0 = 1$ s, $T_g = 0.1$ s) によつてえられた記録とならべしめす.

おわりにこの装置を試作するにあたり, 研究室主任宮村助教授の御指導御援助ならびに技術部後藤健一技官の御助力をえたことを感謝する.

---

33. Transistor Pre-amplifier for a Seismograph.

By Hideteru MATUMOTO,
Earthquake Research Institute.

In order to construct a high sensitive electronic seismograph, the author designed a transistor pre-amplifier.

At present, we have only low sensitive seismographs, source power for which is supplied exclusively by commercial A.C. mains, owing to the restriction of practical operating conditions in observations.

There are two kinds of troubles in the multi-stage high gain E.L.F amplifier which is supplied with eliminated D.C. source. One of the troubles comes from high

level noise which is generated in a head vacuum tube or included primarily in the source, and the quality of amplifier is limited by it. The other trouble is poor stability of the eliminated D. C. source itself, and the quality of amplifier is also limited by the disturbances coming from motorboating or other fluctuation in the source.

Of course, these defects can be removed by making use of D.C. source from a secondary battery, using it in a condition of lower voltage than usual, but this will be only possible in well-equipped stations.

In higher frequencies we can easily get a higher gain amplifier with high stability, putting a transformer between transducer and amplifier in order to step up voltage or current and to take matching between transducer and amplifier. But we can not design such a transformer that can serve satisfactorily in our frequency band, 1～30 Hz.

Thus the author decided to adopt transistor pre-amplifier which can serve in satisfactory condition without any restrict of main amplifier or its eliminated D. C. source, and shows excellent characteristics in noise, frequency, gain and temperature effect, with a low consumption of small dry cell D.C. source. Total consumption of source is 6 V, 200 μA, and in this condition life of dry cell (4 units of UM-3A 1.5 V) is about 6 months.

Circuit noise of the pre-amplifier is less than 10 μV, which is equivalent to the input voltage less than 0.1 μV, and consequently, the limit of amplifier sensitivity due to the generated noise is 10 mm/μV, which cannot be obtained easily by vacuum tube amplifier.

In general, the characteristics of transistor are deviated by temperature fluctuation but the author succeeded to stabilize temperature characteristic in gain by a choice of circuit construction. Deviation of gain is restricted within $\pm$ 2 db in 0～40°C temperature range.

The circuit of the pre-amplifier is shown in Fig. 1.

In order to decrease noise generation and to increase input impedance, all resistances were chosen as large as possible, and the current flowing in each part of the circuit is limited in the smallest condition for the transistor 2T-65 (Sony).

Fig. 2 and Fig. 3 show the characteristics of gain-frequency and input impedance-frequency. They are not sufficient for our purpose, but we can only get satisfactory stability, high gain and low noise in sacrificing their characteristics. Fig. 4, 5 and 6 are frequency characteristics of the transducer and amplifier outputs. Fig. 5 shows an effect of the input impedance, but in case of using other low sensitive transducer, this effect does not appear so clearly.

In our observations we put transducers a good distance off from the main-amplifiers to keep out of the artificial ground motions or to set up a small tripartite station, and consequently, we had to stretch several hundred meters of wire between the transducer and the main-amplifier, which circumstance, hereto-fore, often gave us much trouble by disturbances of A.C. influence induced from the wire and transducer itself. But now the disturbances of A.C. influence was decreased by push-pull phase composition in the circuit and suppression by the high level output resulting from amplification of weak signals by the pre-amplifier, and thus we have not to care about in the operation of wire stretch.

Moreover, the delicacy in practical operation of a high gain amplifier owing to the complex adjustment required was removed by using this pre-amplifier to make up deficit gain for higher sensitivity which had to be lowered to increase stability of main-amplifier and its power source.

Fig. 7 shows the appearance of the pre-amplifier and the transducer, the character-

istics of which are shown on the preceding page.

Reproductions in Fig. 8 indicate the seismograms obtained by the two kinds of seismographs. One is recorded by H.E.S. short period, and the other is obtained by an electronic seismograph which consists of the transducer, the pre-amplifier and a main-amplifier with lowered sensitivity of 2 mm/mV.

Thus we conclude that, by introducing the pre-amplifier, the stability and sensitivity for minor shock observations would become higher than those which have been so far attained by ordinary electronic seismographs.

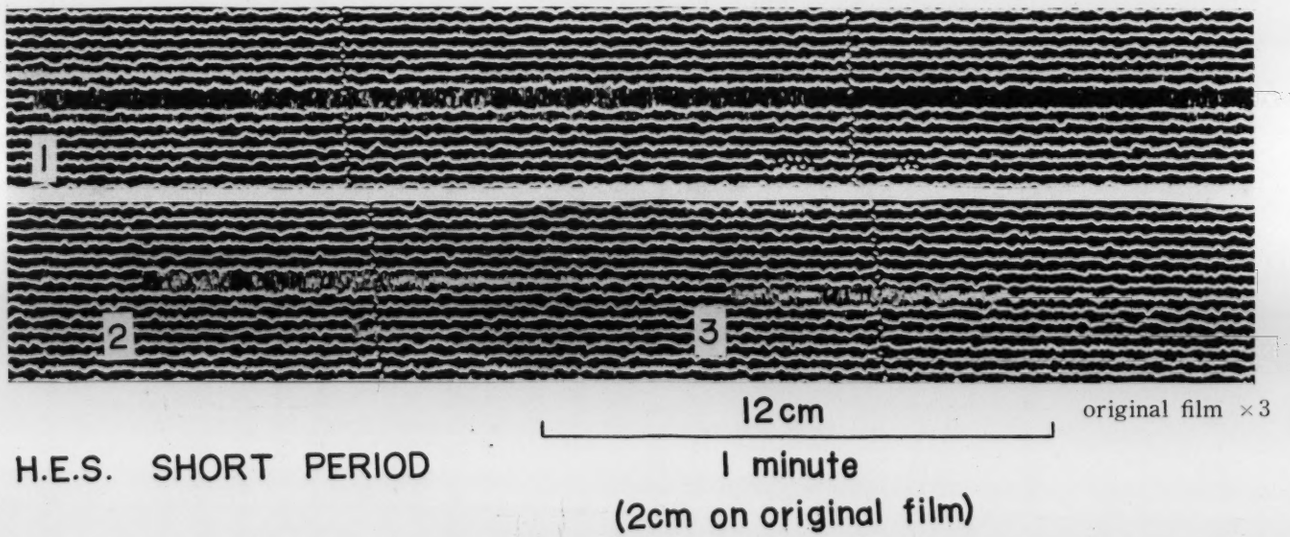

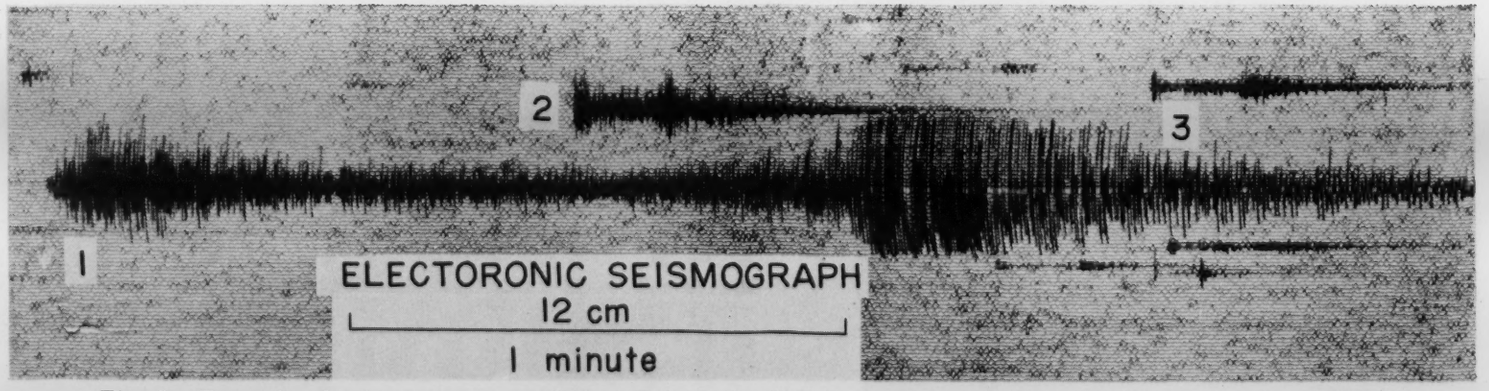

Fig. 8. Example of seismograms recorded at Tukuba by H.E.S. short period ($T_0 = 1$ s, $T_g = 0.1$ s, $V_{max} = 21{,}250$ on original film) and by the electronic seismograph with transistor pre-amplifier.

地震研究所彙報
第37号(1959)531-544頁

34. 1959年1月31日北海道弟子屈(てしかが)地震の余震観測報告

地震研究所　松本利松

(昭和34年4月28日発表——昭和34年6月30日受理)

§1. はしがき

1959年1月31日5時39分，北海道川上郡弟子屈町附近に，最大震度5ないし6におよぶ地震が発生し，附近一帯に若干の被害を与えた．

弟子屈は阿寒・屈斜路から知床半島にかけて分布する一連の第4紀の火山列の外縁に近く位置し，雄大な屈斜路カルデラを間近に仰ぎ見る火山砕屑岩台地上の町である．

5時39分の地震に引続き，同日7時17分にも，ほとんど同じ規模の地震が発生した．これらのマグニチュードはともに約6.2と推定される．

これらの地震に引続いて多数の余震が発生した．我々はこの余震群を観測するために，弟子屈町郊外の弟子屈高等学校に臨時の観測点を設け，2月14日より3月1日迄の期間観測を行つた．更に，北大観測班の協力を受け，2月24日より20日の期間には，震央により近いと考えられた奥春別小学校にも観測点を設けた．

余震観測開始の時期が遅れたのは，最初地震の規模が余震観測を実施するには小さすぎると考えられたのであるが，余震群が中々減少せず，住民の不安が容易に解消しないと伝えられたのが，我々出動の動機となつたためである．この地方は活溌な活動を続ける火山列に接近しているため，あるいはこの地震群は，火山活動と直接の関連を持つような原因に基くものではないかという疑いも最初には持たれた．

この地方には，1938年5月29日に今回の弟子屈地震の発生したよりも約20 km北寄りの地域で屈斜路湖地震が発生している．この地震についてはくわしい踏査報告[1)-4)]がある．

§2. 弟子屈地震の概況

今回の弟子屈地方に発生した地震群の内の主な地震をTable 1に示した．

1月31日5時39分と7時17分の二つの地震のマグニチュードは特に大きく，後者

1) 津屋弘達　地震 [i] **10** (1938), 283–313.
2) 加藤愛雄　地震 [i] **10** (1938), 321–333.
3) 田中館秀三　地震 [i] **11** (1939), 16–26.
4) 田中館秀三　地震 [i] **11** (1939), 16–26.

Table 1. 弟子屈地震と主な前震および余震の表（釧路気象台の観測による）
Fore- and after-shocks accompanied by the Tesikaga Earthquake.

Date	h	m	s	$P\sim S$	Maximum motion NS	Maximum motion EW	Remarks
1959				sec.	μ	μ	
Jan. 22	16	33	27.5	7.8	1150	1600	43.45°N, 144.2°E, d=0–10 km, $M=5.7$
22	17	57	09.6	8.4	—	—	
31	05	39	08.6	8.0	3600	5600	Tesikaga Earthquake, 43.35°N, 144.4°E, d=20 km, $M=6.2$.
	05	51	32.1	7.0	125	138	
	06	04	12.3	7.5	74	54	
	07	01	24.7	7.6	184	245	
	07	17	00.0	8.7	3500	7300	43.45°N, 144.4°E, $d=0$ km, $M=6.2$.
	07	25	20.4	8.1	—	—	
	07	26	05.2	8.0	—	—	
	07	31	53.9	7.2	100	83	
	07	35	45.4	7.6	—	—	
	07	40	47.9	7.4	249	545	
	08	03	47.0	7.6	65	85	
	08	15	08.6	7.5	—	—	
	20	55	59.4	7.7	63	30	
Feb. 01	00	56	32.2	7.3	75	75	
	01	48	35.9	7.1	—	—	
	02	08	28.5	7.8	46	35	
	02	26	48.0	7.9			
	02	32	47.3	7.5			
	06	52	46.6	7.8			
	08	59	27.1	7.7			
	10	54	54.5	7.7			
	13	47	08.7	7.8			
	14	09	49.3	8.3			
02	03	35	49.7	11.1			
	11	30	20.5	—			
	12	59	57.9	8.0			
03	00	16	05.8	7.6	136	17	
	05	51	27.6	7.8			
	16	47	23.6	7.4			
04	01	01	33.9	9.1			
05	03	07	22.9	7.6			
	09	23	23.0	7.8	160	179	
06	16	14	40.4	7.7	404	382	
	21	44	56.1	7.6			
07	10	59	23.0	8.2			
	21	13	49.3	7.3			
	00	29	14.9	8.4			
	04	37	23.5	8.8			
10	09	56	15.4	7.6			
12	03	06	30.8	7.7	89	83	
15	06	27	40.2	8.4			
	17	53	30.5	8.2			
18	01	43	00.1	8.1			
19	20	29	22.9	8.0			
23	12	30	07.3	7.6			
24	01	57	59.9	7.5			
28	05	45	45.1	7.9			
	06	17	41.9	14.0			

（つづく）

(Table 1 つづき)

Date	h m s	P～S	Maximum motion NS	Maximum motion EW	Remarks
		sec.	μ	μ	
Mar. 01	04 49 33.9	7.2			
02	13 47 22.2	10.7			
	18 06 26.9	7.8			
20	14 52 31.2	8.5			
	20 48 21.4	9.2			
25	14 50 10.6	8.8			
Apr. 01	17 47 33.0	7.7			
11	23 05 01.4	8.5			
12	09 25 13.9	8.1	81	89	
	08 42 04.5	7.8			

を前者の余震と考えるならば，ほとんど本震と同じ規模を持つ余震の起つた例として注目される．気象庁に依つて求められたこれらの地震のマグニチュードはそれぞれ6.2および6.1であるが，震度分布から M_K を求め，M_K と M との関係を示す河角の公式[5]

$$M = 0.5\,M_K + 4.85 \qquad (1)$$

に依つて定められた M は 6.1 および 6.2 であり，むしろ7時 17 分の地震の方が大きい．この傾向は筑波山で観測を行つている，アンダーソン・ウツド捩れ地震計の振幅により求められた M がそれぞれ 6.2 および 6.3 であることとも一致している．Table 1 に

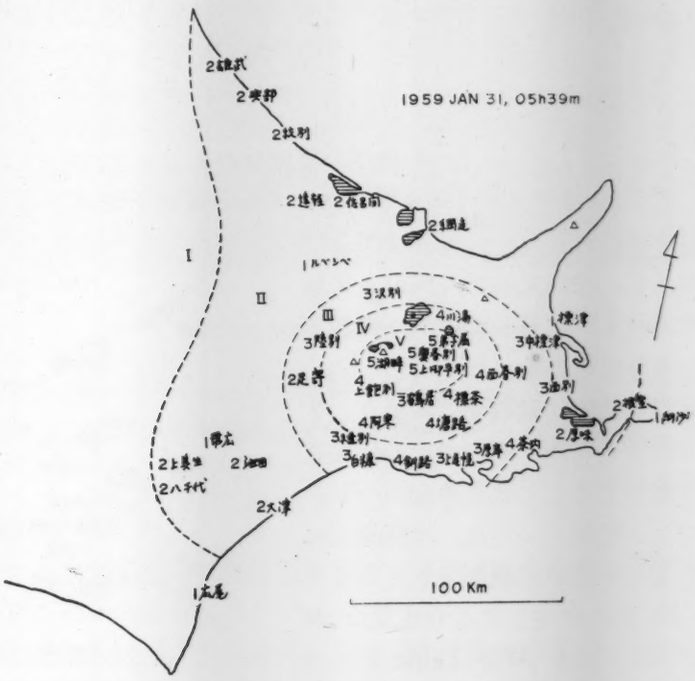

Fig. 1. 1959 Jan. 31, 05^h39^m 震度分布図
Isoseismal map.

5) H. KAWASUMI, *Bull. Earthq. Res. Inst.*, **30** (1952), 319–323.

Fig. 2. 1959 Jan. 31, 07^h17^m 震度分布図
Isoseismal map. (釧路気象台による)

用いた M はこれらの値の平均値をとつてある.

Fig. 1 および Fig. 2 にはこの二つの地震の震度分布を示した.

この地震により生じた,炭ガマ・サイロ・畜舎などの被害を Fig. 4 に示した. これらの被害情況の地理的分布から見ると, 奥春別部落附近が最も被害が大きく, 従つて本震の震央も気象庁の発表した位置よりも, 北寄りになり, 奥春別部落附近にあつたと考えられる.

余震観測を実施した期間は積雪期にあたり, 2メートル余に及ぶ積雪のため, 断層やその他地変の有無をその当時確認することは出きなかつた.

弟子屈地震の著しい特徴の一つは, 本震発生に先立つて, かなり著しい前震が観測されていることである. 1月 22 日に発生したこの地震の M は 5.7 に及んでいる. この Mは Table 1 に示すように, 1月 31 日5時 39 分および7時 17 分の二つの地震に次ぐものである. この地震の震央が, 気象庁の報告及び Fig. 3 に示した震度分

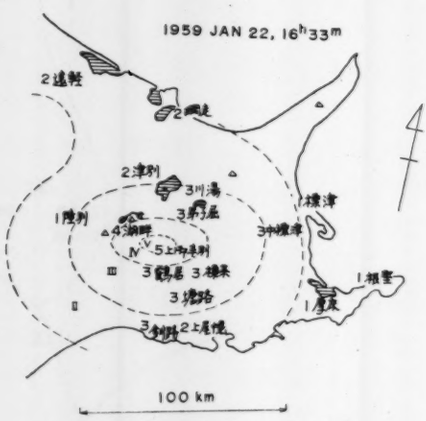

Fig. 3. 1959 Jan. 22, 16^h33^m 震度分布(釧路気象台に依る)
Isoseismal map.

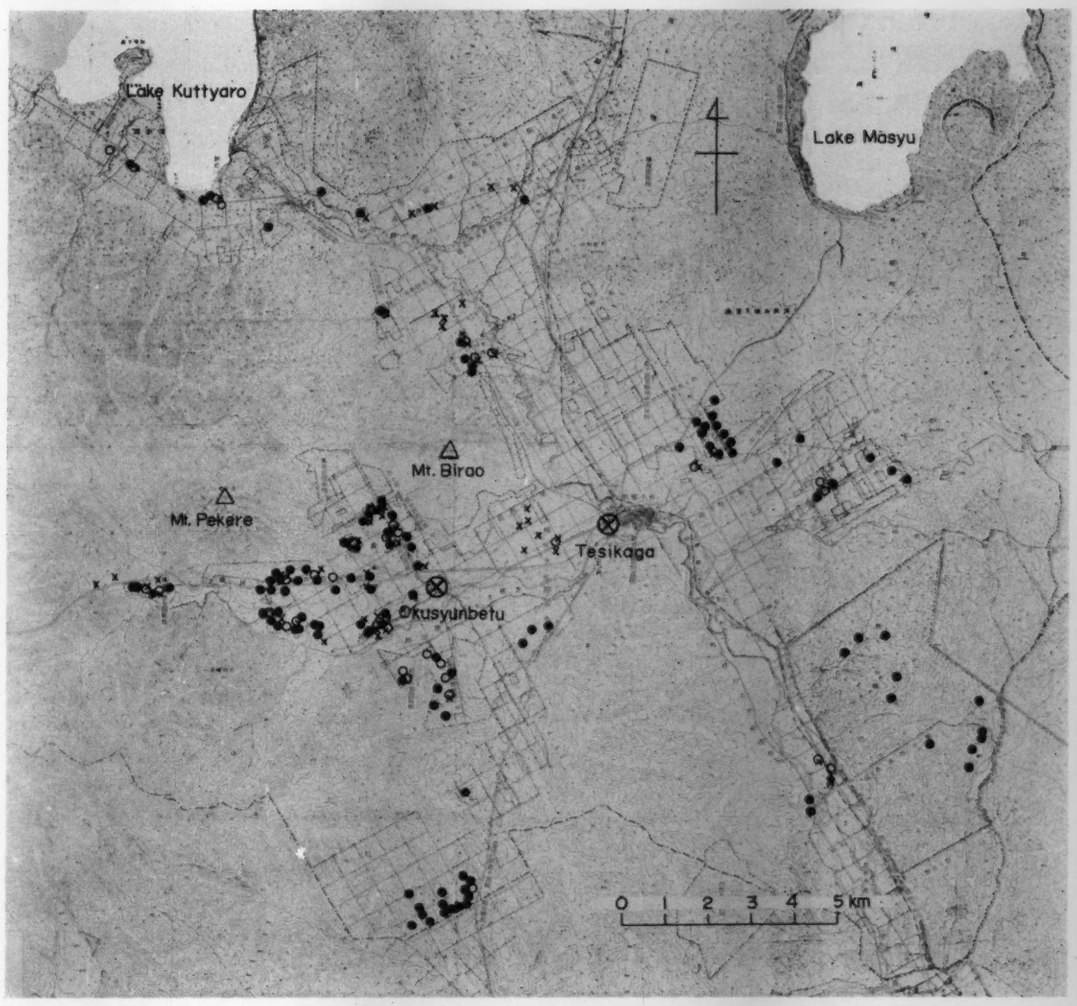

Fig. 4. 被害分布図（● 炭ガマ，○ 畜舎，× サイロ）
The distribution of damages.

布から見て，1月 31 日早朝の二つの地震とはなはだ近接している事はほとんど疑いのない事実である。この前震の余震と思われる地震は釧路気象台の観測では2回だけ観測されている．

§ 3. 余震観測の情況

諸般の情勢から多数の班の出動は困難であつたので，今回の余震観測は2名の人員で，2点の観測を行う程度に限られた．

従つて観測の目標を次のように定め，その目的に沿つてなるべく有効な情報を求るめように努めた．

1) 高感度の地震計による連続観測

本震の規模が小さく，また観測開始の時期が遅れたので，なるべくマグニチュードの

小さい地震までを連続記録して，統計的処理に充分な数の地震を得ること．

2) 広い振幅帯域にわたつての観測

振幅の広い範囲での石本・飯田の統計式における係数 m の変化を調べること，並びに特性が同じで倍率のみ異るような地震計で記録された地震の記録でマグニチュードによるスペクトル構造の変化を調べること．

3) Tripartite Method による観測

波面の入射方向ならびに見掛けの速度を求め，余震群の震源の位置並びに地殻構造を推定すること．

4) 周波数特性の異つた地震計による観測

これらの地震計によつて記録された地震群の波形の比較．

これらの目的に応じて；我々の準備した地震計は Table 2 の通りである．

Table 2. 余震観測に用いた地震計 (Instrument used for our observation.)

Name		Remarks
Hagiwara Electromagnetic Seismograph (HES)		
HES film recorder (4 channels) with 1 c/s and 4 c/s galvanometers	2	running speed: 2.7 mm/sec. (on the film reader)
Horizontal transducer (1 c/s)	2	
Vertical transducer (1 c/s)	1	
RGES-type Electromagnetic Seismometer		
MG-IV amplifier	5	
ND 3 c/s pick up	2	
ERI 3 c/s pick up	3	
Oscillograph	1	running speed: 10 and 30 mm/sec
Chronometer and other accessories		

連続観測に用いた地震計は，直結型フィルムレコーディング方式の萩原式電磁地震計 (HES) で送りの速さはフィルムリーダー上で 2.7 mm/sec にとつた．この送り速度では

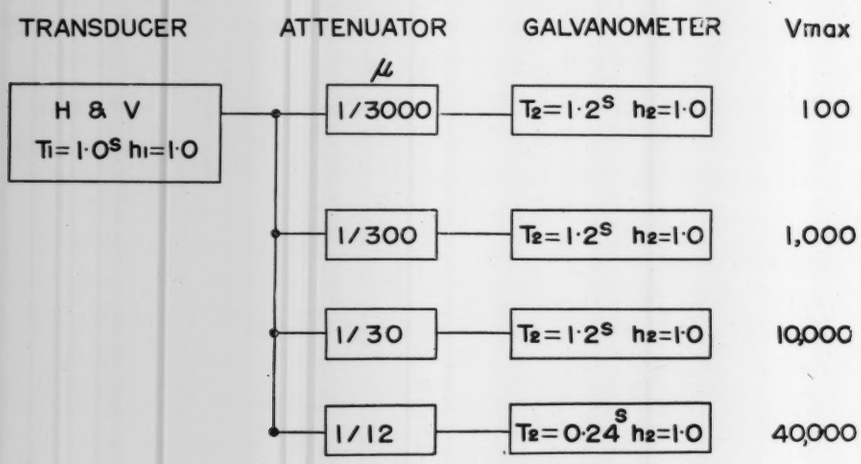

Fig. 5. H E S 観 測 系 統 図
Block diagram of HES observation system.

1日2回のフィルム交換を必要とする．常時微動のために換振器1.0秒，検流計1.2秒の系（以下これを HES 1—1 と書く）で，最高倍率は 10,000 倍，HES 1—0.2 で 40,000 倍にとつた．弟子屈観測点においては（2）の目的のために，Fig. 5 に示すように1個の換振器に4個の検流計を並列につなぎ，それぞれのアテニュエーション μ を変えて観測を行つた．普通の地震計においては記録し得る最大—最小の振幅比は 50 ないし 100 程度であるがこのような方式を用いることによつて，HES 1—1 では相対的な特性を変更することなく最大—最小振幅比が 5000 に達することができた．勿論この地動振幅の範囲に関しては換振器の出力は直線性を保つている．

当時は戸外の積雪量は 1～2 米に達していたので，積雪を除き，露出した氷結層の上に底板を敷き，換振器をその上に設置した．この換振器を上から木箱で覆い，雪で埋没した状態で使用したが，日中の融氷や低温（最低 −27°C に達した）による障碍は殆んど見られなかつた．

3点観測は2月24日から27日迄の夜間に弟子屈観測点において実施された．3c/s 換

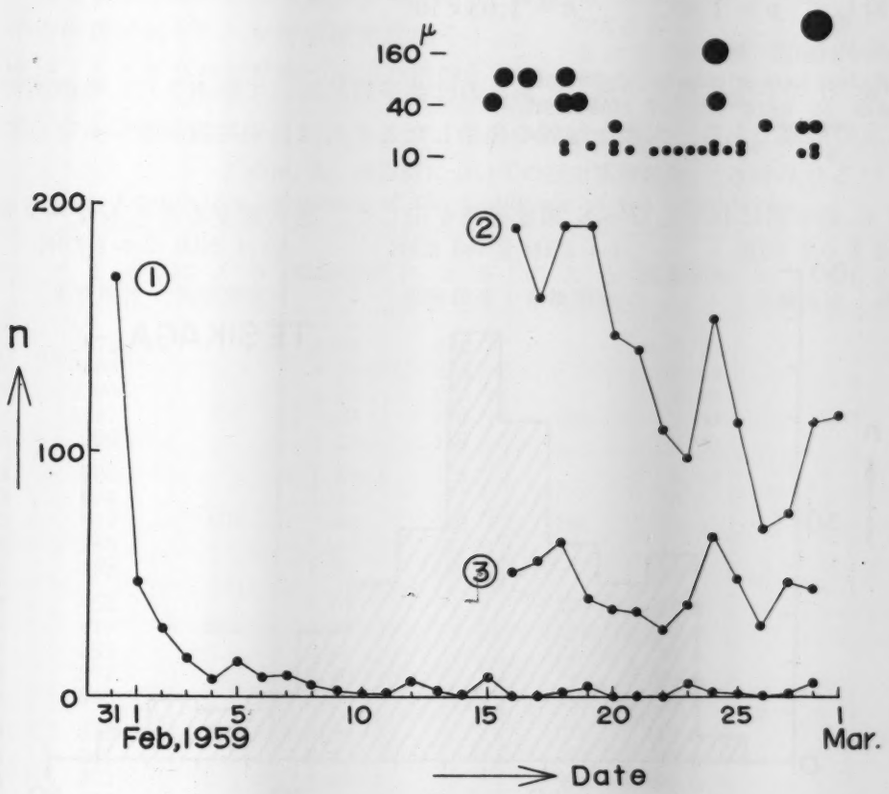

Fig. 6. 日別余震回数
Daily frequency of aftershocks.

① 釧路における観測（釧路気象台による）
② HES 1—0.2 による観測（$V_{max} = 40,000$）
③ HES 1—1 による観測（$V_{max} = 10,000$）
図の上部の黒丸は主な余震と弟子屈におけるその振巾とを示す．

振器を増幅器につなぎ，電磁オツシロに依る記録方式を用いた．基線長をなるべく大きくとりブロマイド送りの速さは 10 mm/sec または 30 mm/sec とした．総観測時間 10 時間に対して 99 個の地震が記録されたが，その内 28 個の地震について入射方向ならびに初動の見かけの速度 V_p とがかなり明瞭に求められた．

§ 4. 日別地震回数と *PS* 頻度分布

Fig. 6 には日別地震回数を示した．図中①の曲線で示してあるのは釧路気象台で観測された地震回数[6]である．②及び③で示されているのは HES 1—0.2 および HES 1—1 による回数である．振幅はリーダー上でおよそ 0.5 ミリまでの地震をとつてある．

余震の減少の傾向は次式で示される．

①及び②の曲線から (2) の式における k および p を求めれば

$$n(t) = k/(t + C)^p \quad \cdots\cdots (2)$$

①に対して $p = 1.49$, $k = 1.31 \times 10^2$

②に対して $p = 1.40$, $k = 1.03 \times 10^4$

の値が得られる．

なお Fig. 6 で右上に黒丸で示してあるのは弟子屈において観測された地動振幅 10 ミクロン以上の地震である．大きな地震の発生したときには日別地震回数がかなりに明瞭に増加しているのが判る．

Fig. 7 に弟子屈における P～S 頻度分布を示した．最大頻度を与える P～S 時間は

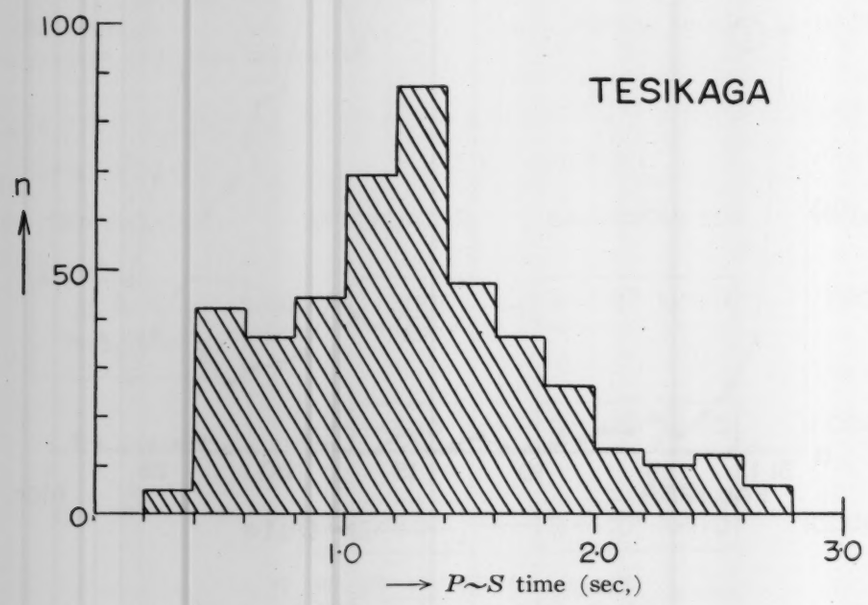

Fig. 7. *PS* 頻度分布
Frequency distribution of P～S duration time.

6) 簡単微動計 (40 倍) による．

1.3 秒附近であり，下限および上限はそれぞれ0.2秒，2.8 秒となつている．

PS 時間の上限と下限の差に大森常数 k (ここでは 8 km/sec とする) をかけてこれを余震域の直径 (D) と考えれば，Fig. 8 に示すように本震のマグニチュード M と $\log D$ の関係は宇津[7]の求めた直線に良く一致する，

§ 5. 石本・飯田の関係について

前に求めたように今回の余震観測においては，振幅の広い帯域にわたつての観測を実施するのが目的の一つであつた．Table 3 及び Fig. 9 には地動振幅に対する累積頻度 (N) を示す．但し便宜上記録振幅を最大倍率で除したものを地動振幅とし，また累積頻度はその級代表値より大きな振幅を持つ地震の総数をとるものとする．

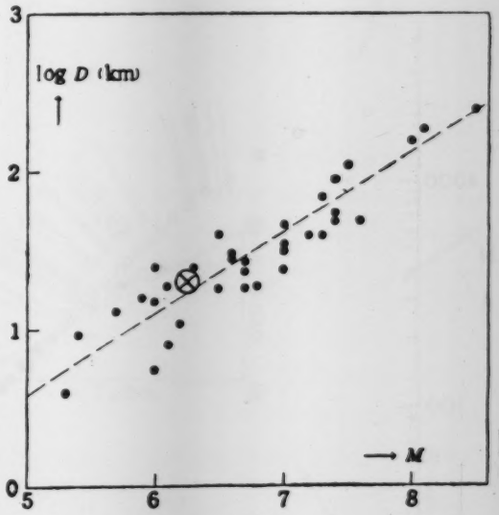

Fig. 8. 本震のマグニチュードを余震域の大きさ
⊛ は弟子屈地震（原図は宇津による）
Magnitude of earthquake and the linear dimension of the area of aftershock occurrence.

Table. 3. 余震群についての振巾累積頻度
Cumulative frequency of the amplitude of the aftershocks.

地動振幅	HES 1–0.2 による累積頻度	HES 1–1 による累積頻度	地動振幅	HES 1–0.2 による累積頻度	HES 1–1 による累積頻度	地動振幅	HES 1–0.2 による累積頻度	HES 1–1 による累積頻度
μ			μ			μ		
0.05	2072		1.05	242		5.20		53
0.10	1662		1.10	226		5.60		50
0.15	1300		1.15	206		6.00		44
0.20	1041	470	1.20	190	215	7.00		40
0.25	906		1.25	186		8.00		35
0.30	786		1.30	178		9.00		33
0.35	684		1.35	172		10.0		30
0.40	612	410	1.40	166	184	11.0		27
0.45	550		1.45	163		12.0		23
0.50	498		1.50	168		13.0		20
0.55	452		1.60		156	14.0		18
0.60	416	353	1.80		136	16.0		18
0.65	392		2.00		127	18.0		16
0.70	372		2.40		95	20.0		14
0.75	348		2.80		80	30.0		13
0.80	332	289	3.20		71	40.0		11
0.85	308		3.60		68	50.0		8
0.90	292		4.00		64	60.0		5
0.95	274		4.40		58	80.0		4
1.00	262	247	4.80		55	100.0		3
						200.0		2
						340.0		1

7) 宇津徳治　地震 [ii] **10** (1957), 35–45.

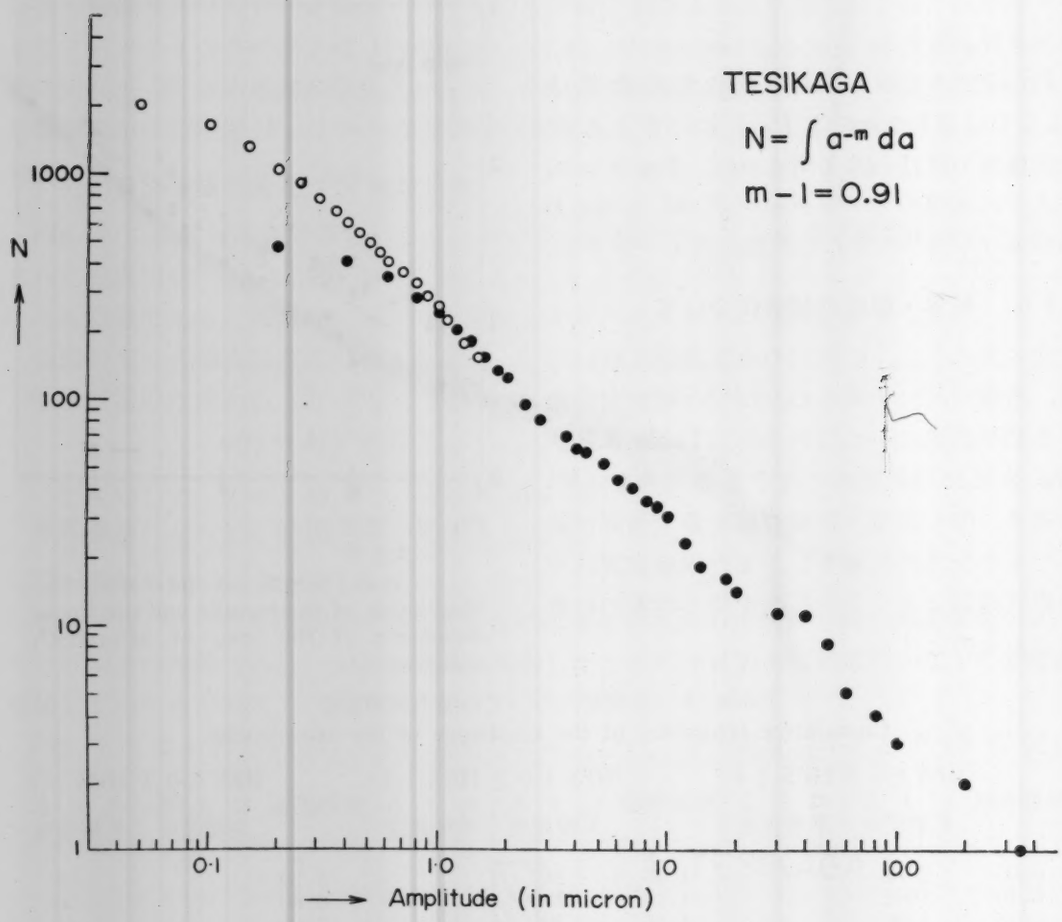

Fig. 9. 振 幅—頻 度 曲 線
Amplitude–Cumulative frequency relation of the aftershocks.

Fig. 9 に示すように地動振幅 300 ミクロンから 0.1 ミクロンの帯域に対してかなり直線的な関係が見られる.

微分形式の石本・飯田の関係

$$n(A)dA = kA^{-m}dA$$

を積分して求められる式

$$N(A) = \int_A^{\infty} n(A')dA' = \frac{-k}{m-1} A^{-(m-1)}$$

から判るように $\log N$–$\log A$ 図表の傾斜は $-(m-1)$ に相当する. 弟子屈の観測から m を求めて次のような値を得た.

$$m = 1.909 \pm 0.013$$

今回の余震群のように，同一の母集団から抽出されたと考えられる標本では m の値が一定であることはむしろ当然の事であるが，振幅帯域のかなり広い範囲についてもこの事が実証された訳である．

なお観測期間をいくつかに区分してそれぞれの期間について m の値を求めたが，有意な差は認められなかつた．

§ 6. 3点観測の結果

Fig. 10 に3点観測の基線ならびに波面の入射方向を示した．殆んどの地震は北西の象限に集中している．同時に初動の見かけの速度 V_p が求められるが，Fig. 11 には $P\sim S$ 時間を横軸に，V_p を縦軸にとつて示した，V_p の下限は略 4.5 km/sec であり，$P\sim S$ 時間が1.5

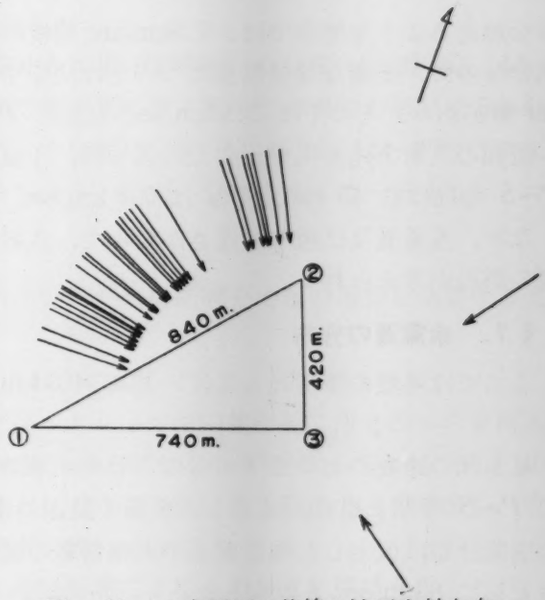

Fig. 10. 3点観測の基線と波面入射方向
The base line of tripartite observation. Arrow lines show the direction of the incidence of P-wave front.

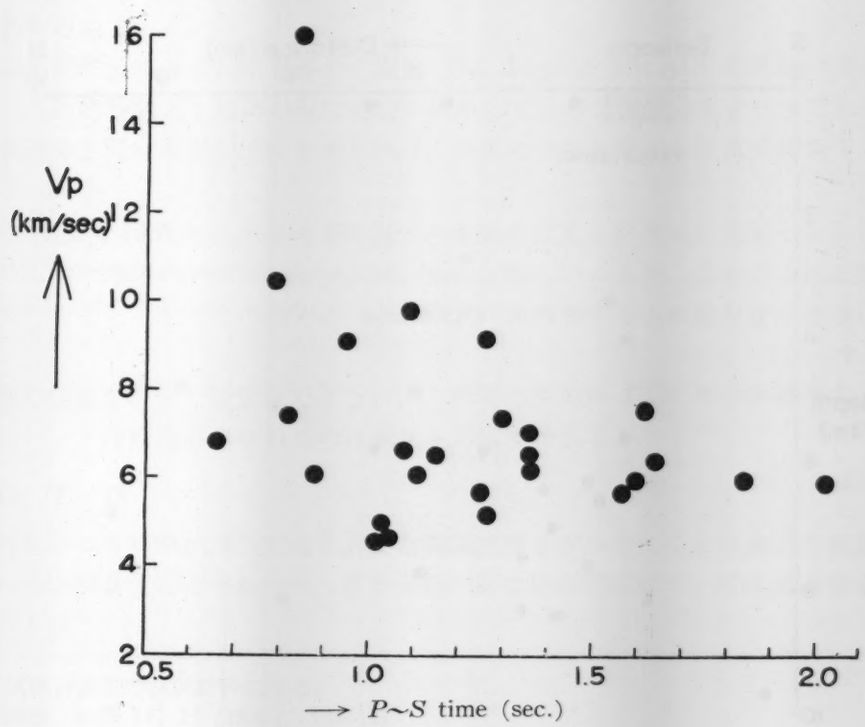

Fig. 11. $P\sim S$ 時間と見かけの初動速度
$P\sim S$ time versus apparent velocity of the initial motion.

秒を越えるような部分では，5.5km/sec 程度になるようである．観測された地震の数が不充分なので，正確な地殻構造については決定できないが，厚さ 1.90 km 程度の 4.5 km/sec 層があり，その下は 5.5 km/sec 程度の P 波速度をもつと考えてよいようである．

波面の入射方向を決定出来た地震の内，1 個は南東から入射しているが，この地震の $P\sim S$ 時間は約 45 秒で，V_p は 7.8 km/sec であつた．

なお，基線長及び送りの速さからみて，入射方向には 10 度，V_p には 0.3 km/sec 程度の誤差が考えられる．

§ 7. 余震源の分布

ここでは地殻の模型として，一様に 4.5 km/sec の P 波速度をもつ均質な構造を考える．

見かけの速度によつて下からの入射角が求められ，前にのべた平面上の入射方向ならびに $P\sim S$ 時間と組合わせると，余震の震源の空間分布を決定することが出来る．勿論この空間分布は仮定した地殻構造や大森常数の値に依つて影響される．ここでは大森常数の値として 8 km/sec と仮定した．

Fig. 12 に南北方向に置いた鉛直面にこれらの余震源を投影した位置を示した．

余震は比較的浅い部分に発生し，たかだか 10 km までの範囲に収まつている．

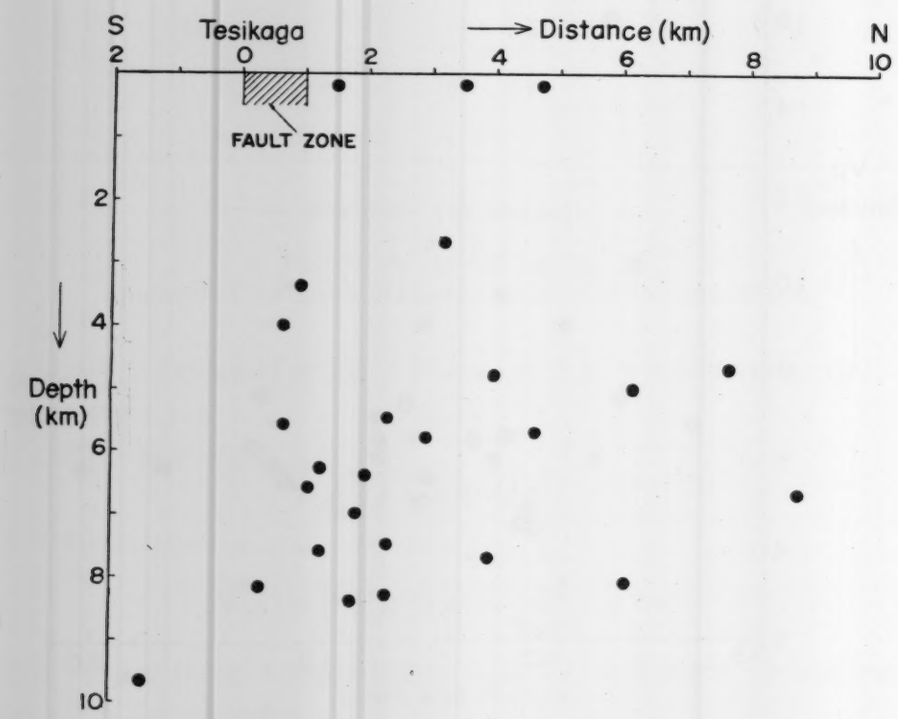

Fig. 12. 余震源の深さの分布
Distribution of the hypocenter projected to the vertical plane.

また Fig. 13 には余震源の平面的分布を示した.

余震の分布する区域にくらべて気象庁の定めた本震 (05^h39^m) の位置 (43.35°N, 144.4°E) は，10 km あまり南に寄つている．気象庁観測網に依る震央位置決定の誤差は 5～10 km 程度あると考えられるので，7^h17^m の最大の余震の位置 (43.45°N, 144.4°E) と同じ附近に本震の位置を考えることが適当のようであり，被害の分布ともよく一致する.

§ 8. 断層について

我々の滞在中は地表は積雪によつて覆われていたために断層その他の地変を発見することが出来なかつた.

融雪後発見された地変は釧路気象台[8]によれば次の如くである.

“弟子屈地震に伴い弟子屈町奥春別第四部落ペケレ山南東山麓附近に西北西から東南東に延長約 2 キロにわたり地割れを生じた．地割れの大きなものは幅 25～30 cm，深さ 40 cm，垂直のづれは約 10 cm であるが，全体としては幅の狭い電光形に小さく屈曲し，或る部分では分岐し，また合一し，奥春別西岸まで達している.”

この地割れが地すべりによるものかまたは地震断層によるものかは疑問の点もあるが，その附近では地形的には傾斜が極めて緩やかであること，2 キロの長さにわたり生じていることから一応地震断層と考えてもよいのであろう.

この他に弟子屈—阿寒湖畔間の横断道路の崩壊が報ぜられているが，これは単なる地崩れとして解釈される.

この奥別部落附近に生じた断層線の位置は Fig. 12 及び Fig. 13 に斜線の部分で示されている．この断層線より北側のみに余震が集中していることは注目すべきであろう.

この断層線の位置を本震の位置と考えれば，余震の分布に関する松沢の理論[9]と良く一致する.

Fig. 13 にはまた 1938 年の屈斜路湖地震[10]の本震の位置と断層域の位置[11]を示した.

これらの二つの地震のマグニチュードは，殆んど等しいことや，このように近接した位置に生じていることなどはこの地方の seismicity を理解する上に注目すべき事実であろう.

また観測の精度からみて断定はできないが，余震の震央が 1938 年の断層帯の上には分布していないような傾向がみられるのは興味ある事実である.

§ 9. むすび

余震観測を行つた時期が適当でなく，また観測点数も少かつたことは余震の性質の全貌を知るためには残念なことであつた．波形解析やその他の問題については後日稿を改めて報告したいと思う.

---

8) 釧路気象台よりの提供資料に依る.
9) 松沢武雄　地震 [i] **11** (1936), 124–127.
10) 43.6°N, 144.3°E　$d = 20$ km, $M = 6.0$　J.M.A Seismological catalogue (1957) による.
11) 文献 1) による.

種々の指導と援助をいただいた津屋弘達教授，萩原尊禮教授，田治米鏡二教授に感謝する．

今回の観測にあたつて多くの厚意を寄せていただいた北海道庁釧路支庁三村敏晴氏ならびに社会福祉課の方々，弟子屈町長今泉秀雄氏ならびに弟子屈町の多くの方々，弟子屈高等学校長脇本正路氏ならびに諸先生に感謝の意をささげる．

観測に協力いただいた北海道大学村瀬　勉，岡田　広，清野善明の諸氏に感謝する．

また今回の報告を草するにあたつて貴重な資料を提供していただいた釧路気象台長柴田章吾氏に厚く御礼の言葉を述べる次第である．

---

34. Tesikaga Earthquake of Jan. 31, 1959.

By Tosimatsu MATUMOTO,
Earthquake Research Institute.

An earthquake having a magnitude of 6.2 occurred in the neighbourhood of Tesikaga-town, Hokkaido, at 5h 39m (G.M.T.) on January 31, 1959. The location of the hypocenter of this shock is determined as 43°26′ N, 144°23′ E, and 20 km depth by Japan Meteorological Agency.

The aftershocks were observed at Tesikaga and Okusyunbetu wich the electromagnetic seismographs during the period of Feb. 14 to Mar. 1.

The main results are summerized as follows:

(1) As shown in Fig. 3, a foreshock having a magnitude of 5.6 had occurred at the same region at 16 h 33 m of January 22, 1959.

(2) About 100 minutes later than the main shock, the strongest aftershock occurred of which the magnitude was almost the same as that of the main shock.

(3) Daily frequency of aftershocks observed at Kusiro decreased according to the formula as: $n(t)=k/(t+c)^P$

(4) The most frequent $P\sim S$ duration time was 1.3 sec., and the upper and the lower limit was 0.2 and 2.9 sec. respectively.

(5) Ishimoto-Iida's formula $nA^{-m}=k$ held good over the wide range of the amplitude for the shocks observed from Feb. 14 to Mar. 1. The value of m was 1.91 at Tesikaga.

(6) By means of the tripartite method, the apparent P-wave velocities of 24 shocks were measured. Using the $P\sim S$ time and the assumption of the true P-wave velocity, the hypocenters of these shocks were determined.

(7) It is reported by Kusiro Local Meteorological Observatory that the zig-zag shaped cracks were found at the east foot of Mt. Pekere, which continued 2 km long towards WNW to ESE with 10 cm vertical crossing and 25–30 cm width. It may be natural to consider that these cracks were not regarded as mere landsliding but as earthquake faults.

(8) The epicenters of aftershocks were distributed only on the north side of the faults, earthquake and none of them were found on the south side of the faults.

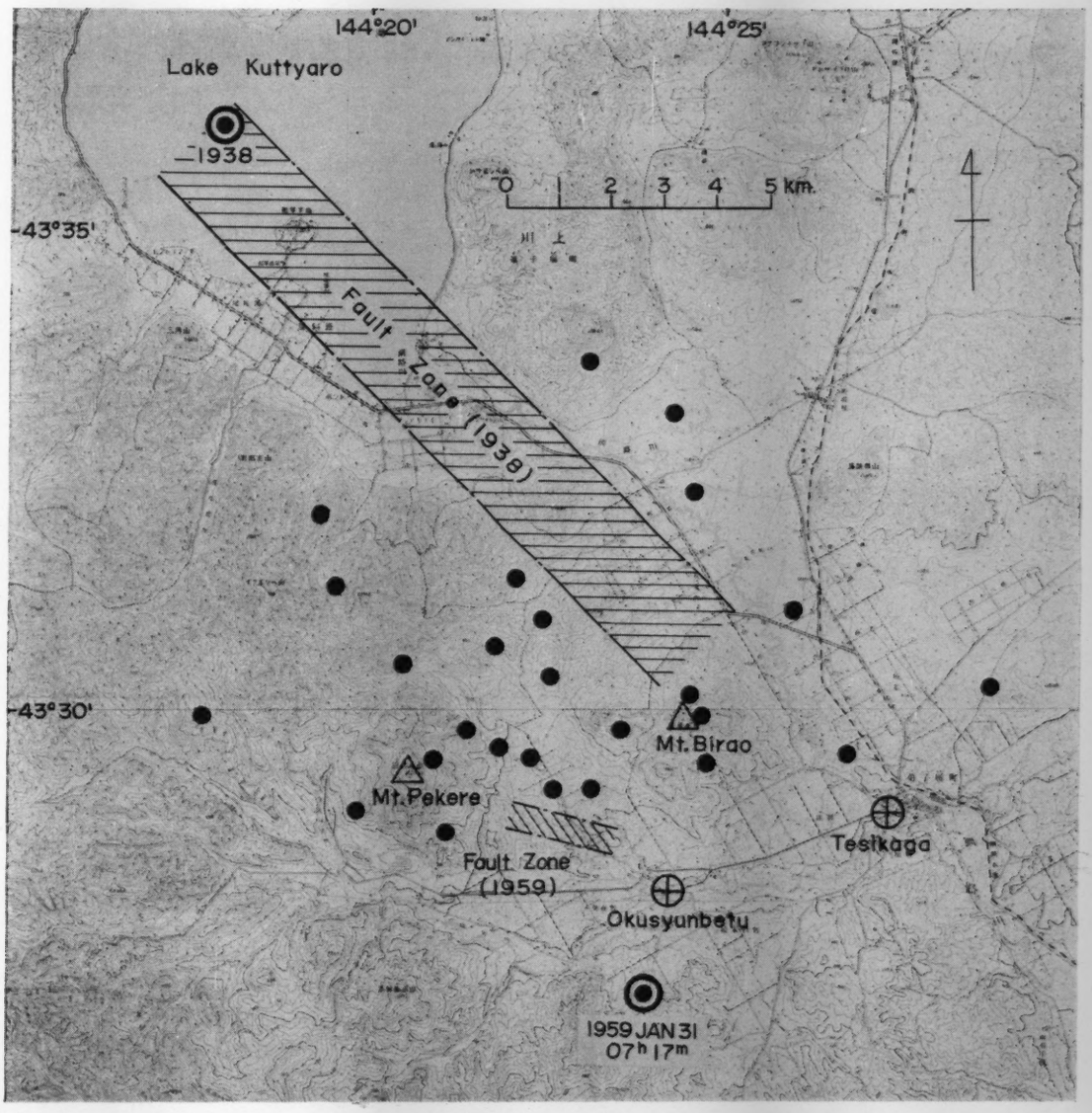

Fig. 13. 弟子屈地震余震の震央の分布
斜線の部分は屈斜路湖地震 (1938). ならびに弟子屈地震 (1959) によつ生じた断層域の存在を示す.
Distribution of the epicenter of the aftershocks and fault zone.

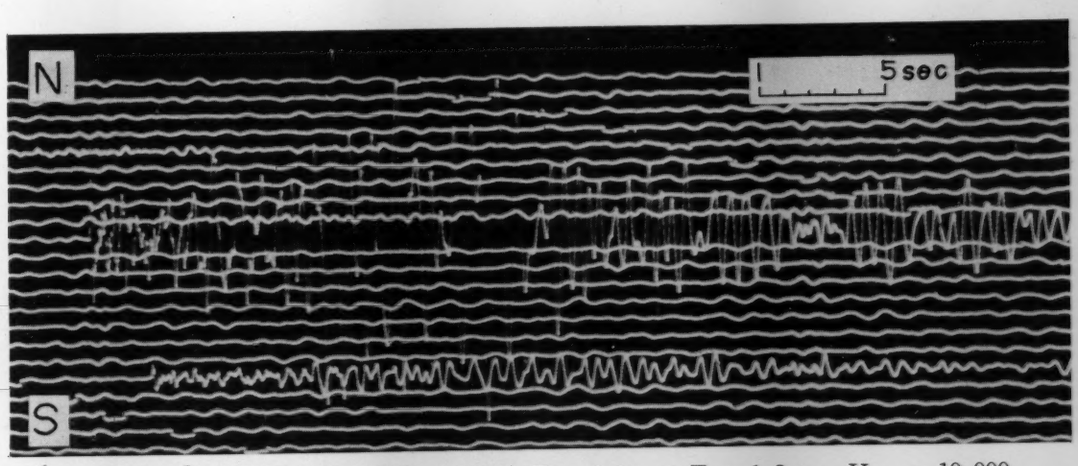

Fig. 14-a. 弟子屈地震の余震，奥春別 $T_1 = 1.0$ sec, $T_2 = 1.2$ sec, $V_{max} = 10{,}000$

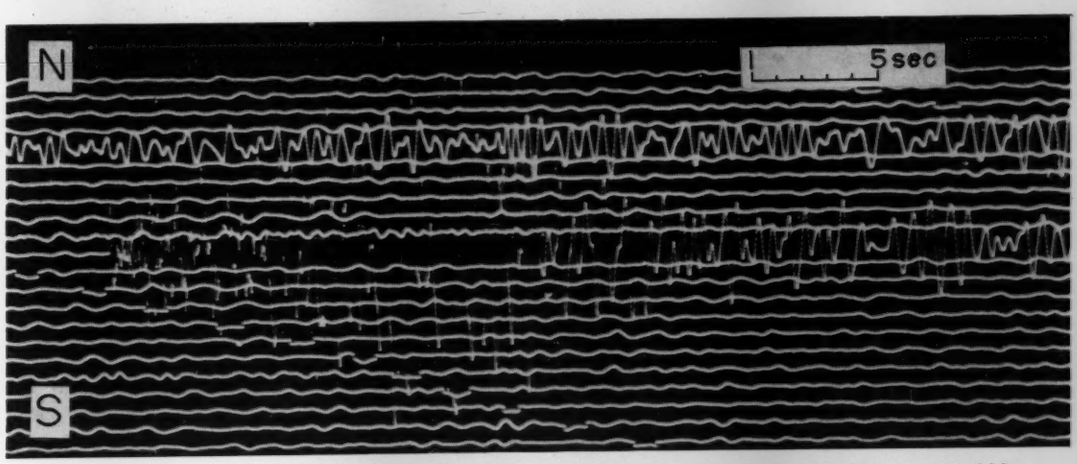

Fig. 14-b. 弟子屈地震の余震，奥春別 $T_1 = 1.0$ sec, $T_2 = 1.2$ sec, $V_{max} = 10{,}000$

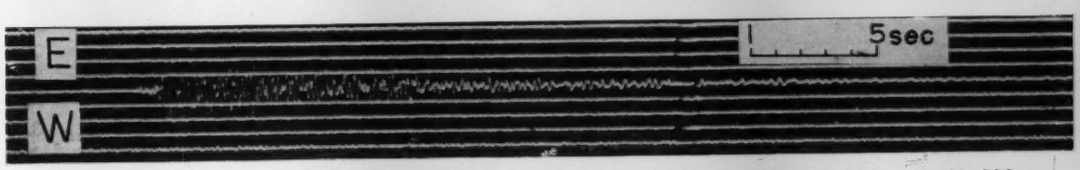

Fig. 14-c. 弟子屈地震の余震，弟子屈 $T_1 = 1.0$ sec, $T_2 = 0.24$ sec, $V_{max} = 40{,}000$

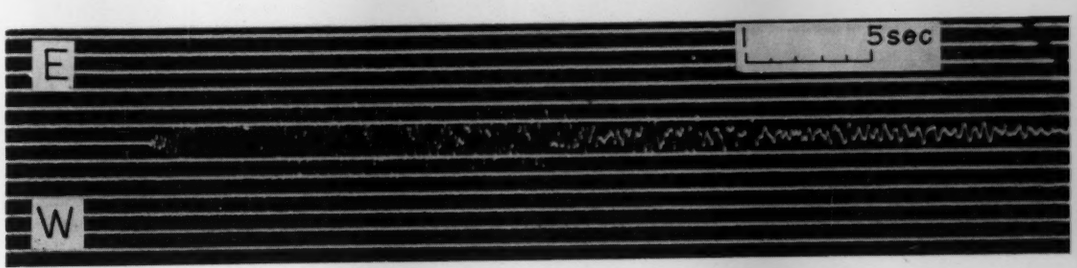

Fig. 14-d. 弟子屈地震の余震，弟子屈 $T_1 = 1.0$ sec, $T_2 = 0.24$ sec, $V_{max} = 40{,}000$

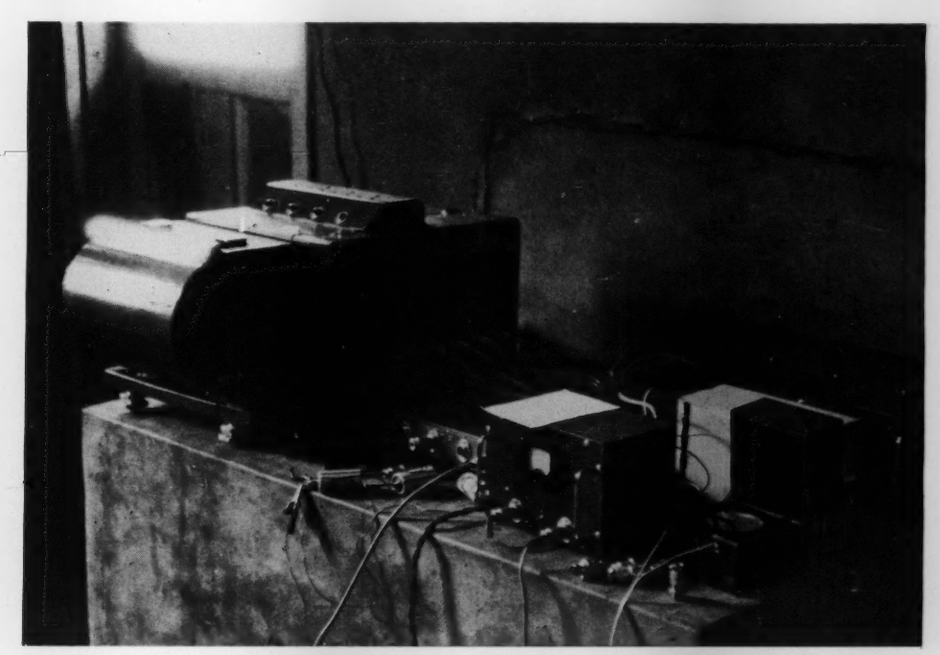

Fig. 15. HES (Hagiwara Electromagnetic Seismograph) 記録部分設置情況

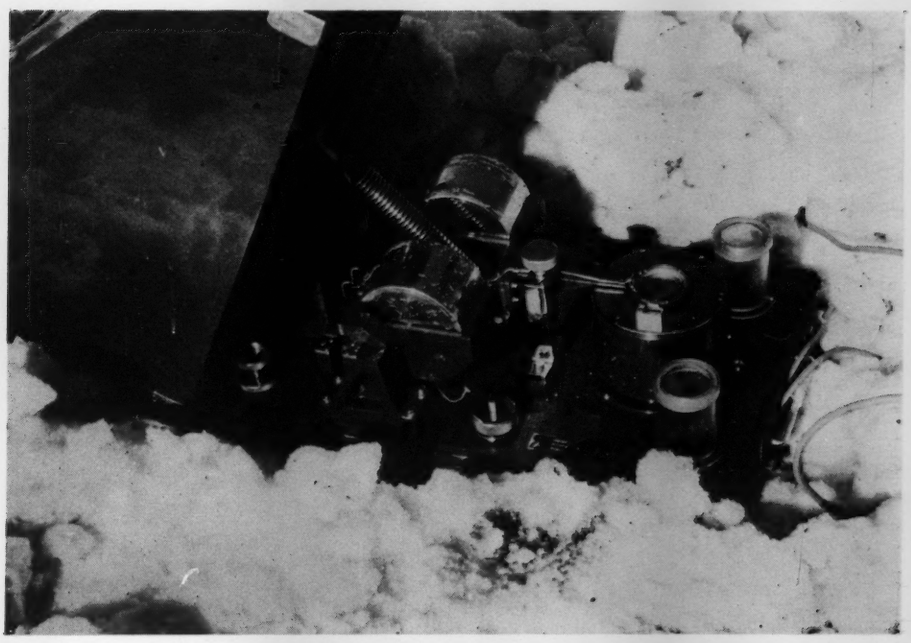

Fig. 16. HES 上下動換振器 ($T_1 = 1.0$ sec)
(凍土層に氷着した板の上に設置されている)

Fig. 17. 換振器設置情況

Fig. 18　畜舎の被害（奥春別部落）
（北海タイムス社の提供による）

Fig. 19. サイロの被害（奥春別部落）
（北海タイムスの提供による）

Fig 20. 弟子屈阿寒横断道路の夕映橋橋脚の破損
（北海タイムス社の提供による）

（震研彙報 第三十七号 図版 松本）

(a)

(b)

Fig. 21-a-b. 弟子屈—阿寒湖畑間横断道路の欠潰
(釧路開発建設部撮影)

(震研彙報 第三十七号 図版 松本)

Fig. 22-a. 奥春別第部落における地割れ（釧路地方気象台撮影）

Fig. 22-b. a に同じ

（震研彙報 第三十七号 図版 松本）

Fig. 22-c. a に同じ

Fig. 22-d. a に同じ

Fig. 22–e. a に同じ

（震研彙報 第三十七号 図版 松本）

昭和34年10月15日印刷
昭和34年10月20日発行

東京都文京区本富士町一番地
東京大学構内
編纂兼
発行者　東京大学地震研究所

東京都新宿区山吹町一八四番地
印刷者　笠井康頼

東京都新宿区山吹町一八四番地
印刷所　株式会社国際文献印刷社

売捌所
東京都中央区日本橋通二丁目六番地
丸善株式会社

Sold by Maruzen Co., Ltd., Nihonbashi-dôri, Chûô-ku, Tôkyô.
Price of this copy: 533 Yen. (Postage exclusive.)